# Hybrid Frequency-Time Analysis and Numerical Methods for Time-Dependent Wave Propagation

Thesis by
Thomas Geoffrey Anderson

In Partial Fulfillment of the Requirements for the
Degree of
Doctor of Philosophy


CALIFORNIA INSTITUTE OF TECHNOLOGY
Pasadena, California

2020
Defended August 17, 2020

Thomas Geoffrey Anderson
ORCID: 0000–0002–0643–2571

# ACKNOWLEDGEMENTS

"Heaven ain't bad but you don't get nothing done."
—Townes Van Zandt (1971)

First and foremost I must thank my mentor Oscar Bruno for his support and guidance these past years. His dedication to excellence in technical communication and in true scientific understanding and progress will always inspire me, while his readiness to teach, patience for, encouragement of, and willingness to draw ideas from those with whom he works will always be a model for me in academic professionalism. I also want to thank those past mentors and colleagues who have shaped my academic life. In particular, I acknowledge David Horntrop for his encouragement to embark on a serious pursuit of mathematics, as well as Catalin Turc and Peter Petropoulos to whom I owe both my introduction to and love for numerical approximation generally and for PDEs specifically. Their encouragement, support, and advice are deeply appreciated. I want to thank Agustin Fernandez-Lado in particular, but also Carlos Pérez-Arancibia, Emmanuel Garza, Christoph Bauinger, Daniel Leibovici, and Florian Schäfer for being the very best of graduate school colleagues and friends.

I would not have been able to complete the work in this thesis and succeed in graduate school, nor successfully navigate challenging periods of life without some remarkable individuals who have enriched my personal life. In particular in these regards, I want to thank my friends Cameron Voloshin and Jessica Wang. To Cameron I owe an introduction to what all of life is about as well as how to live it; I want to thank him for the loyal friendship that I trust will last many years. Jessica, I have to acknowledge and be thankful for our many long conversations that were immeasurably helpful. I am grateful to Terry Gdoutos and Desiree de Vries for treating me like family, both at home in Pasadena and on our many travels and adventures, and for our discussions of philosophy, values, and purpose. Further thanks to my friends Alex Turzillo and Armeen Taeb for always approaching our lives and work with a wry sense of humor, to Nadia Heninger for her friendship, advice and perspective at some critical times in my life and career, and to Song, Andreea, Joanna, Olga, Olivia, Rie, and Roberta. My sincerest gratitude to all for believing in me and helping me achieve the best version of myself: I am forever in your debt.

Finally, I am continually thankful to my parents not only for teaching me how to learn but also for instilling in me a love of the pursuit of knowledge for its own sake.

# ABSTRACT

This thesis focuses on the solution of causal, time-dependent wave propagation and scattering problems, in two- and three-dimensional spatial domains. This important and long-lasting problem has attracted a great deal of interest reflecting not only its use as a model problem but also the prevalence of wave phenomena in diverse areas of modern science, technology and engineering. Essentially all prior methods rely on "time-stepping" in one form or another, which involves local-in-time approximation of the evolution of the solution of the partial differential equation (PDE) based on the immediate time history and temporal finite-difference approximation. In addition to the need to manage the accumulation of (dispersion) error and the burdensome increase in computational cost over time, there are additionally difficult issues of stability, time-domain boundary conditions, and absorbing boundary conditions which often need to be addressed.

To sidestep many of these problems, this thesis develops a novel highly-efficient approach for time-dependent wave scattering problems employing the global-in-time techniques of Fourier transformation and leading to a frequency/time hybrid method for the time-dependent wave equation. Thus, relying on Fourier Transformation in time and utilizing a fixed (time-independent) number of frequency-domain solutions, the method evaluates the desired time-domain evolution with errors that both, decay faster than any negative power of the temporal sampling rate, and that, for a given sampling rate, are additionally uniform in time for all time. The fast error decay guarantees that high accuracies can be attained on the basis of relatively coarse temporal and frequency discretizations. The uniformity of the error for all time with fixed sampling rate, a property known as dispersionlessness, plays a crucial role, together with other properties of the Fourier transform, in enabling the evaluation of solutions for long times at $O(1)$ cost. In particular, this thesis demonstrates the significant advantages enjoyed by the proposed methods over alternative approaches based on volumetric discretizations, time-domain integral equations, and convolution-quadrature.

The approach relies on two main elements, namely, 1) A smooth time-windowing methodology that enables accurate band-limited representations for arbitrarily-long time signals, and 2) A novel Fourier transform approach which, in a time-parallel manner and without causing spurious periodicity effects, delivers numerically dispersionless spectrally-accurate solutions. A similar hybrid technique can be obtained on the basis of Laplace transforms instead of Fourier transforms, but we do not con-

sider in detail the Laplace-based method, and only briefly point out its essential features and associated challenges.

The proposed frequency/time Fourier-transform methods for obstacle scattering problems are easily generalizable to any linear partial differential equation in the time domain for which frequency-domain solutions can readily be obtained, including e.g. the time-domain Maxwell equations, the linear elasticity equations, inhomogeneous and/or frequency-dependent dispersive media, etc. Further, the proposed approach can tackle complex physical structures, it enables parallelization in time in a straightforward manner, and it allows for time leaping—that is, solution sampling at any given time $T$ at $O(1)$-bounded sampling cost, for arbitrarily large values of $T$, and without requirement of evaluation of the solution at intermediate times. In particular, effective algorithms are introduced that, relying on use of time-asymptotics, compute two-dimensional solutions at $O(1)$ cost despite the very slow time-decay that takes place in the two-dimensional case.

A significant portion of this thesis is devoted to a theoretical study of the validity of a certain stopping criterion used by the algorithm, which guarantees that certain field contributions can safely be neglected after certain stopping times. Roughly speaking, the theoretical results guarantee that, after the incident field is turned off, the magnitude of the future scattering density (and thus the magnitudes of the fields) can be estimated by the magnitude of the integral density *over a time period comparable to the time required by a wave to travel a distance equal to the diameter of the scatterer*. The criterion, which is crucial in ensuring the $O(1)$ computational cost of the algorithm, is closely related to the well-known scattering theory developed in the 1960s and '70s by Lax, Morawetz, Phillips, Strauss and others. Our approach to the decay problem is based on use of frequency-domain estimates (developed previously in the context of numerical analysis of frequency-domain problems) on integral operators in the high-frequency regime for obstacles of various trapping classes. In particular, our theory yields, for the first time, decay estimates for a class of connected trapping obstacles: all previous estimates of scattered-field decay for connected obstacles are restricted to nontrapping structures.

In all, the proposed approach leverages the power of the Fourier transformation together with a range of newly developed spectrally convergent numerical methods in both the frequency and time domain and a variety of novel theoretical results in the general area of scattering theory to produce a radically-new framework for the solution of time-dependent wave propagation and scattering problems.

# PUBLISHED CONTENT AND CONTRIBUTIONS

[1] T. G. Anderson and O. P. Bruno. *On the decay of time-dependent solutions to the wave equation and finite-time analysis of their boundary integral densities*. 2020, in preparation.
T.G.A. participated in the conception of the project, performed the literature review, developed the proofs, and led the writing of the manuscript.

[2] T. G. Anderson, O. P. Bruno, and M. Lyon. *High-order, Dispersionless "Fast-Hybrid" Wave Equation Solver. Part II: Window Tracking, Spatio-Temporal Parallelism, General Incident Fields*. 2020, in preparation.
T.G.A. participated in the conception of the project, performed the literature review, implemented the algorithms (with the exception of Chapter III), and led the writing of the manuscript.

[3] T. G. Anderson, O. P. Bruno, and M. Lyon. "High-order, Dispersionless "Fast-Hybrid" Wave Equation Solver. Part I: O(1) Sampling Cost via Incident-Field Windowing and Recentering". In: *SIAM Journal on Scientific Computing* 42.2 (Apr. 2020), A1348–A1379. DOI: 10.1137/19m1251953.
T.G.A. participated in the conception of the project, performed the literature review, implemented the algorithms, and led the writing of the manuscript.

# TABLE OF CONTENTS

# LIST OF ILLUSTRATIONS

# LIST OF TABLES

*Chapter 1*

# INTRODUCTION

"Sound is nought but air y-broken"
—Geoffrey Chaucer (c. 1380, see also [72])

**Overview**

This chapter provides in Section 1 a brief introduction to the physical context of this thesis and the broad applicability of research in waves; introduces in Section 2 long-standing mathematical formulations for questions of wave scattering in the form of partial differential equations boundary-value problems, both in time- and frequency-domain and both in volumetric regions and in terms of integral equations posed on the boundary of obstacles; and finally in Section 3 gives a thorough overview of the predominant methods used to numerically approximate the solution of time-dependent wave propagation and scattering problems while contrasting each of these methods with the methodology proposed in this thesis.

## 1 Background on wave propagation, acoustics, and electromagnetics

A wave is a deviation of a scalar or vector field from an equilibrium, and occurs when there are forces pulling a perturbed system toward that equilibrium. They can be categorized broadly into standing and traveling waves, the former referring to those waves which remain in a stationary physical position while the latter describes waves where the relative amplitudes of the deviation from equilibrium at distinct physical locations may change as time progresses. Many physical media are capable of supporting waves of various types and at disparate physical length scales; for example, fluids can support gravity waves in the ocean at the scale of meters, acoustic sound waves in quiescent or convected air (audible to humans at the scale of centimeters to several meters) or more generally any compressible fluid, and seismic

---

[1] T. G. Anderson, O. P. Bruno, and M. Lyon. "High-order, Dispersionless "Fast-Hybrid" Wave Equation Solver. Part I: O(1) Sampling Cost via Incident-Field Windowing and Recentering". In: *SIAM Journal on Scientific Computing* 42.2 (Apr. 2020), A1348–A1379. DOI: 10.1137/19m1251953.

waves in the Earth's crust. Indeed, consideration of electromagnetic radiation leads to the conclusion that waves can even travel in a vacuum. Owing to the wide variety of settings in which wave theory is applicable and the transferability of understanding across these settings, the study of waves leads to fundamental understanding and development of technology in application areas as diverse as telecommunications and computing, imaging, seismic prediction and resilience, and acoustics.

A brief overview of the history and setting of acoustic and electromagnetic wave phenomena is provided in what follows. Firstly, acoustics (a term coined by the French mathematician Sauveur who worked in the area), the study of vibrations propagating in a background medium, has a suitably long history befitting its import. Dating at least to Pythagoras who studied the production of sound due to standing waves on stretched strings, it attracted such familiar names as Hooke (the eponymous creator of certain laws of elasticity and vibration), D'Alembert (who indeed formulated the first description of wave motion as obeying a partial differential equation), Poisson (who studied compressional waves in fluids in three dimensions), Helmholtz, and Lord Rayleigh. Indeed Rayleigh published widely in acoustics throughout his life and in 1877 published an expansive two-volume work, *The Theory of Sound* [106]. Rayleigh points out that the propagation of sound has long been known to not be instantaneous, but rather instead to proceed at a finite speed $c$, and that in fact this speed in still air at standard conditions had been first accurately measured (with a measured value of $c = 337$ m/s versus a true value of $c \approx 332$ m/s) by the French Academy using time-retarded reports of the firing of cannons at measured distances. Acoustic waves of a small amplitude are understood to obey the acoustic wave equation, a time-dependent linear partial differential equation which in three dimensions carries this time-retarded character. Secondly, electromagnetics as a discipline is usually attributed to Ampere, Faraday and Maxwell, and is concerned with the propagation of electromagnetic radiation, including light and radio waves. The Maxwell equations are a model for the physics of electromagneticism; in certain situations in the absence of charges and currents they can be reduced to homogeneous wave equations for the electric and magnetic vector field quantities. The acoustic wave equation is thus not only of interest in its own right for describing the physics of acoustic waves, but, as we shall see, serves also as an avenue to understanding more complex wave phenomena in electromagnetism. Development of numerical simulation techniques for the former is typically fruitful for the latter.

## 1.1 The acoustic wave equation

The acoustic wave equation was earlier mentioned to describe the propagation of disturbances of small amplitude. We show here a commonly-given brief derivation of the equation from first physical principles, though much more detailed discussion can be found in the comprehensive review [89]. The equations for the disturbance of any scale of a compressible inviscid fluid follow from conservation of mass and linear momentum. Conservation of mass gives the continuity equation which can be written using the convective (or total) derivative $\frac{D}{Dt} = \frac{\partial}{\partial t} + \mathbf{v} \cdot \nabla$ as

$$\frac{1}{\rho}\frac{D\rho}{Dt} = -\nabla \cdot \mathbf{v},$$

with $\nabla \cdot \mathbf{v}$ giving the change in fluid density of a infinitesimal fluid particle with fluid density $\rho$ and fluid velocity $v$. In differential form, we have

$$\frac{\partial \rho}{\partial t} + \nabla \cdot (\rho \mathbf{v}) = 0, \tag{1.1}$$

and we see that at rest, that is, when $\mathbf{v} = 0$, the fluid density is time-invariant. The momentum equation or inviscid Euler equation is

$$\rho \frac{D\mathbf{v}}{Dt} = -\nabla p,$$

or in differential form,

$$\rho \frac{\partial \mathbf{v}}{\partial t} + \rho(\mathbf{v} \cdot \nabla)\mathbf{v} + \nabla p = 0, \tag{1.2}$$

and describes linear momentum conservation in an infinitesimal spatial region with pressure $p$. When the fluid is at rest, the momentum equation implies that the pressure is constant. The system is completed through an equation of state $p = p(\rho)$ for the fluid medium. A small-parameter perturbation analysis about steady state ($\mathbf{v} = 0$) substitutes the expansions $p = p_0 + \varepsilon p_1 + O(\varepsilon^2)$, $\rho = \rho_0 + \varepsilon \rho_1 + O(\varepsilon^2)$, $\mathbf{v} = \varepsilon \mathbf{v}_1 + O(\varepsilon^2)$, into Equations (1.1)–(1.2) and yields a partial differential equation relating the fluid density deviation $\rho_1$ to the pressure deviation $p_1$,

$$\frac{\partial^2 \rho_1}{\partial t^2} = \nabla^2 p_1.$$

These quantities are already related through the equation of state, whose linearization (about the equilibrium $\rho = \rho_0$) gives the approximation $p_1 = \left(\frac{\mathrm{d}p}{\mathrm{d}\rho}(\rho_0)\right)\rho_1 =: c^2 \rho_1$, from which it follows that the acoustic pressure deviation obeys the *acoustic wave equation*

$$\frac{\partial^2 p_1}{\partial t^2} = c^2 \nabla^2 p_1. \tag{1.3}$$

The quantity $c$ is the acoustic sound speed in the fluid. It can also be shown that the velocity $\mathbf{v}$ is the gradient of a potential $u$, which also obeys Equation (1.3).

## 1.2 Maxwell's and electromagnetic wave equations

Electromagnetic fields are understood to be physically caused by a spatial density of electric current and charge. Maxwell's equations [75]

$$\nabla \times E + \frac{\partial \mathbf{B}}{\partial t} = 0, \tag{1.4a}$$

$$\nabla \times H - \frac{\partial \mathbf{D}}{\partial t} = \mathbf{J}, \tag{1.4b}$$

$$\nabla \cdot \mathbf{D} = \varrho, \tag{1.4c}$$

$$\nabla \cdot \mathbf{B} = 0, \tag{1.4d}$$

are a hyperbolic system of PDEs in three dimensions that describe the dynamics of vector field quantities **E**, the electric intensity, **B**, the magnetic flux density, **D**, the electric flux density, and **H**, the magnetic intensity. Physically, the instantaneous electric intensity field **E** and magnetic flux density **B** due to a point charge $Q_1$ result in a force on the particle $Q$ moving at velocity **v** in the amount of $Q\mathbf{E} + Q\mathbf{v} \wedge B$. Maxwell's equations govern how the field quantities evolve in response to time-dependent electric and magnetic fields.

Under the conditions of a linear homogeneous and isotropic medium (with electric and magnetic permeability constants $\epsilon$ and $\mu$, respectively), in which case the constitutive relations

$$\mathbf{D} = \epsilon\mathbf{E}, \quad \mathbf{B} = \mu\mathbf{H},$$

hold, Jones [75] lays out an argument whereby the vector potential **A** and scalar potential $V$ solving the wave equations

$$\nabla^2\mathbf{A} - \mu\epsilon\frac{\partial^2\mathbf{A}}{\partial t^2} = -\mu\mathbf{J}, \tag{1.5a}$$

$$\nabla^2 V - \mu\epsilon\frac{\partial^2 V}{\partial t^2} = -\varrho/\epsilon, \tag{1.5b}$$

yield an expression for the electric field **E** by

$$\mathbf{E} = -\frac{\partial \mathbf{A}}{\partial t} - \nabla V.$$

Each of the (four!) time-dependent partial differential equations in Equation (1.5) can be easily identified as forced wave equations with sources **J** and $\varrho$. In the absence of sources, they are the familiar homogeneous wave equations encountered before in the acoustic case, motivating a study of time-dependent wave phenomena generally and in particular identifying the wave equation as a worthy problem of

study. Equation (1.5) is not the only means of formulating Maxwell's equations as vector wave equations; indeed reference [71] formulates Maxwell's equations as wave equations for the **E** and **H** fields (for which boundary conditions typically are more readily posed).

## 2 Time- and frequency-dependent PDEs and scattering problems

This thesis is primarily concerned with the solution of wave *scattering* problems posed in complex geometries, problems which describe the interaction of an incident traveling wave with an obstacle with physically-informed boundary conditions; the boundary values of the incident wave become the boundary data for the PDE. Much of this thesis focuses on the initial boundary value problem

$$\frac{\partial^2 u}{\partial t^2}(\mathbf{r}, t) - c^2 \Delta u(\mathbf{r}, t) = 0, \quad \mathbf{r} \in \Omega, \tag{1.6a}$$

$$u(\mathbf{r}, 0) = \frac{\partial u}{\partial t}(\mathbf{r}, 0) = 0, \quad \mathbf{r} \in \Omega, \tag{1.6b}$$

$$u(\mathbf{r}, t) = b(\mathbf{r}, t) \quad \text{for} \quad (\mathbf{r}, t) \in \Gamma \times [0, T^{inc}], \tag{1.6c}$$

for the time domain wave equation in the exterior domain $\Omega \subset \mathbb{R}^d$ (the complement of a bounded set) for $d = 2, 3$. The boundary of $\Omega$, which we will denote by $\Gamma$, is an arbitrary Lipschitz surface for which an adequate frequency domain integral-equation solver on $\Gamma$, or some alternative frequency-domain method in the exterior of $\Gamma$, can be used to solve the required frequency domain problems in the domain $\Omega$. For definiteness, throughout this thesis we assume a boundary condition of the form (1.6c), but similar treatments apply in presence of boundary conditions of other types. Given an incident field $u^{inc}$, the selection $b = -u^{inc}$ corresponds to a sound-soft boundary condition for the total field $u + u^{inc}$ on the boundary of the scatterer,

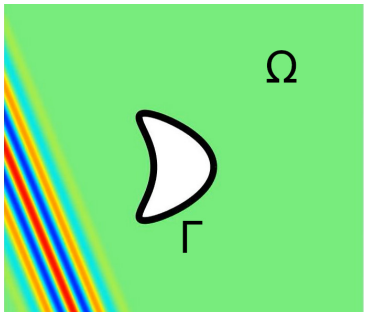


Figure 1.1: A schematic of a typical time-domain surface scattering configuration.

$$u^{tot}(\mathbf{r}, t) = u^{inc}(\mathbf{r}, t) + u(\mathbf{r}, t) = 0, \quad \mathbf{r} \in \Gamma,$$

which expresses the physical requirement of zero pressure deviation (see Section 1.1) at a material boundary. The Fourier transforms (see (1.23) below) $U^t$ and $B^t$ of the solutions $u$ and $b$ of the wave equation (1.6) satisfy the Helmholtz problem with

linear dispersion relation $\kappa = \kappa(\omega) = \omega/c$,

$$\Delta U^t(\mathbf{r},\omega) + \kappa^2(\omega) U^t(\mathbf{r},\omega) = 0, \quad \mathbf{r} \in \Omega \tag{1.7a}$$

$$U^t(\mathbf{r},\omega) = B^t(\mathbf{r},\omega), \quad \mathbf{r} \in \Gamma. \tag{1.7b}$$

This is the fundamental relationship underpinning the proposals in this thesis.

**Remark 1.** *For definiteness, in Chapter* 2 *we restrict most of our discussion to one of the most common incident-field functions $b = b(\mathbf{r},t)$ arising in applications, namely, incident fields impinging along a single direction* $\mathbf{p}$*:*

$$b(\mathbf{r},t) = \frac{1}{2\pi}\int_{-\infty}^{\infty} B^t(\omega) \mathrm{e}^{\mathrm{i}\frac{\omega}{c}(\mathbf{p}\cdot\mathbf{r}-ct)}\,\mathrm{d}\omega \quad \textit{and} \quad B^t(\omega) = \int_{-\infty}^{\infty} a(t)\mathrm{e}^{\mathrm{i}\omega t}\,\mathrm{d}t, \tag{1.8}$$

*for some compactly supported function $a(t)$ (consistent with the time interval of interest in* (1.6c)*). Note that in particular, $b(\mathbf{r},t) = -u^{inc}(\mathbf{r},t) = a(t - \mathbf{p}\cdot\mathbf{r}/c)$. In order to ensure the re-usability of the required set of frequency-domain solutions (see Section 5.2), arbitrary-incidence fields could either be treated by means of source- or scatterer-centered spherical expansions; or synthesis relying on principal-component analysis, etc. Such methodologies are proposed in Chapter* 3*, though see also Section* 9.2 *for asymptotic cost comparisons with other methods.*

**Remark 2.** *The super-index $t$ in $B^t(\omega)$ (Equation* (1.8)*), indicates that the variable $\omega$ in this function's argument is the Fourier variable corresponding to $t$. In general, for any given function $f(\mathbf{r},t)$ (resp. $f(t)$), $F^t(\mathbf{r},\omega)$ (resp. $F^t(\omega)$) will be used to denote the partial (resp. full) temporal Fourier transform of $f$ with respect to $t$, as indicated e.g. in Equation* (1.34)*. Although only partial Fourier transforms in time are used in Chapter* 2*, the notation is adopted here to preserve consistency with Chapter* 3*—in which partial- or full-transforms with respect to both temporal and spatial variables are considered.*

### 2.1 Integral equation methods for scattering problems

Much of this thesis involves the treatment of surface scattering problems using integral equation techniques. We collect here some relevant facts concerning the acoustic wave and Helmholtz equations. The Green's function for Equation (1.6a) is

$$G(\mathbf{r},t;\mathbf{r}',t') = \begin{cases} \frac{H(c(t-t')-|\mathbf{r}-\mathbf{r}'|)}{2\pi\sqrt{c^2(t-t')^2-|\mathbf{r}-\mathbf{r}'|^2}} & \text{for} \quad d=2 \quad \text{and} \\ \frac{\delta(c(t-t')-|\mathbf{r}-\mathbf{r}'|)}{4\pi|\mathbf{r}-\mathbf{r}'|} & \text{for} \quad d=3, \end{cases} \tag{1.9}$$

which gives the fundamental response at position $\mathbf{r}$, time $t$ induced by an impulse at position $\mathbf{r}'$, time $t'$, while the Green's function for Equation (1.7a) is

$$G_\omega(\mathbf{r},\mathbf{r}') = \begin{cases} \frac{\mathrm{i}}{4}H_0^{(1)}(\frac{\omega}{c}|\mathbf{r}-\mathbf{r}'|) & \text{for} \quad d=2 \quad \text{and} \\ \frac{\mathrm{e}^{\mathrm{i}\frac{\omega}{c}|\mathbf{r}-\mathbf{r}'|}}{4\pi|\mathbf{r}-\mathbf{r}'|} & \text{for} \quad d=3. \end{cases} \tag{1.10}$$

and gives the fundamental response at position $\mathbf{r}$ induced by a monochromatic (time-harmonic) source of frequency $\omega/c$ at position $\mathbf{r}'$. It is crucial to observe that just as the Fourier transform of the wave equation (1.6) is the Helmholtz equation (1.7), so too the fundamental solutions are related, with the temporal Fourier transform of (1.9) equalling (1.10). This observation is the theoretical underpinning of the numerical methods proposed in this thesis and the efforts to make numerical versions of such global-in-time transformations efficient.

It will be useful to introduce some integral operators making use of these Green's functions. The time-domain single-layer operator

$$(S\mu)(\mathbf{r},t) = \int_{-\infty}^{t}\int_\Gamma G(\mathbf{r},t;\mathbf{r}',t')\mu(\mathbf{r}',t')\,\mathrm{d}\sigma(\mathbf{r}')\,\mathrm{d}t', \tag{1.11}$$

is useful in time-domain integral equations, as it can be observed that the single-layer potential $u(\mathbf{r},t) = (S\mu)(\mathbf{r},t)$ is a solution to the wave equation (1.6a) for each "density" $\mu$. In the frequency-domain, it will be useful to refer to the single-layer operator

$$(S_\omega\mu)(\mathbf{r}) = \int_\Gamma G_\omega(\mathbf{r},\mathbf{r}')\mu(\mathbf{r}')\,\mathrm{d}\sigma(\mathbf{r}'), \tag{1.12}$$

and we note that as a superposition of fundamental responses due to the continuous density $\mu$ the single-layer potential $u(\mathbf{r}) = (S_\omega\mu)(\mathbf{r})$ is a solution to the Helmholtz equation (1.7a). It is also useful to introduce the double-layer operator

$$(K_\omega\mu)(\mathbf{r}) = \int_\Gamma \frac{\partial G_\omega(\mathbf{r},\mathbf{r}')}{\partial n(\mathbf{r}')}\mu(\mathbf{r}')\,\mathrm{d}\sigma(\mathbf{r}'), \tag{1.13}$$

and the adjoint double-layer operator

$$(K_\omega^*\mu)(\mathbf{r}) = \int_\Gamma \frac{\partial G_\omega(\mathbf{r},\mathbf{r}')}{\partial n(\mathbf{r})}\mu(\mathbf{r}')\,\mathrm{d}\sigma(\mathbf{r}'), \quad \mathbf{r}\in\Gamma. \tag{1.14}$$

Green's third identity in the time-domain leads to Kirchhoff's formula for the sound-soft scattering problem (1.6),

$$u(\mathbf{r},t) = (S\psi)\,(\mathbf{r},t) \tag{1.15}$$

where $\psi = \frac{\partial u^{tot}}{\partial \mathbf{n}}$ and by use of the jump relations in the time-domain, results in the time-domain single-layer integral equation

$$(S\psi)(\mathbf{r}, t) = b(\mathbf{r}, t) \quad \text{for} \quad (\mathbf{r}, t) \in \Gamma \times [0, T]. \tag{1.16}$$

Use of the Green's function $G_\omega$ and Green's third identity yields the frequency domain field representation

$$U^t(\mathbf{r}, \omega) = \int_\Gamma \psi^t(\mathbf{r}', \omega) G_\omega(\mathbf{r}, \mathbf{r}') \, \mathrm{d}\sigma(\mathbf{r}'), \quad \mathbf{r} \in \mathcal{R} \subset \Omega, \tag{1.17}$$

where $\psi^t$, which equals the boundary values of the normal derivative of the total field ($\psi^t(\mathbf{r}, \omega) = \frac{\partial U^{t,tot}(\mathbf{r},\omega)}{\partial \mathbf{n}}$), may be obtained as the solution of the direct integral equation

$$(S_\omega \psi^t)(\mathbf{r}, \omega) = B^t(\mathbf{r}, \omega), \quad \mathbf{r} \in \Gamma. \tag{1.18}$$

Note that the time- and frequency-domain integral equations (1.16) and (1.18) and representation formulas (1.15) and (1.17) are Fourier transforms of each other. Further discussion of the connections between hybrid frequency/time formulations and time-domain integral representations will be presented in Chapter 3.

Unfortunately, equation (1.18) is not uniquely solvable for certain values of $\omega$ and in any case would result in linear systems that are poorly-conditioned. Making use of the auxiliary adjoint double-layer operator, we obtain the *uniquely solvable* direct combined field integral equation formulation (see e.g. [38]):

$$\frac{1}{2}\psi^t(\mathbf{r}, \omega) + (K^*_\omega \psi^t)(\mathbf{r}, \omega) - \mathrm{i}\eta (S_\omega \psi^t)(\mathbf{r}, \omega) = \frac{\partial B^t(\mathbf{r}, \omega)}{\partial n(\mathbf{r})} - \mathrm{i}\eta B^t(\mathbf{r}, \omega), \quad \mathbf{r} \in \Gamma, \tag{1.19}$$

which is a Fredholm integral equation of the second kind. An alternative approach in the frequency-domain that may in some cases prove useful proceeds via the representation formula

$$U^t(\mathbf{r}, \omega) = \left(K_\omega \varphi^t - i\eta S_\omega \varphi^t\right)(\mathbf{r}, \omega), \quad \mathbf{r} \in \mathcal{R} \subset \Omega, \tag{1.20}$$

for which the density $\varphi^t$ can be found as the solution of the (indirect) boundary integral equation (see [25])

$$\frac{1}{2}\varphi^t(\mathbf{r}, \omega) + (K_\omega \varphi^t)(\mathbf{r}, \omega) - \mathrm{i}\eta (S_\omega \varphi^t)(\mathbf{r}, \omega) = B^t(\mathbf{r}, \omega), \quad \mathbf{r} \in \Gamma. \tag{1.21}$$

A wide literature exists for the numerical solution of boundary integral equations of the form (1.19) and (1.21). This thesis uses Nyström methods to discretize and solve the integral equations (1.19) for all desired frequencies. Unless stated otherwise, in the case $d = 2$ (resp. $d = 3$) the Nyström method described in [45, §3.5] (resp. in [30]) is used.

## 2.2 Notation for Fourier transforms

We outline here the notation we use in this thesis for Fourier transformation. In all cases, unless otherwise stated, functions with upper-case symbols indicate a transform. To facilitate transformations in only a single variable for functions of several variables, "partial transforms," we use super-index notation for the original time variable ($t \in \mathbb{R}$) and sub-index notation for the original spatial variable ($\mathbf{r} \in \mathbb{R}^d$) in which the partial (or, indeed, complete) transform is performed. The word "*slow*" appearing in a super-index also indicates a temporal transform, of a quantity shifted in time through the time partitioning strategy outlined in Chapter 2. In general, for any given function $v(\mathbf{r}, t)$ (resp. $v(t)$), $V^t(\mathbf{r}, \omega)$ (resp. $V^t(\omega)$) will be used to denote the partial (resp. full) temporal Fourier transform of $v$ with respect to $t$, as indicated e.g. in Equation (1.23). For a transform in all variables, we use the pair

$$v(\mathbf{r}, t) = \frac{1}{(2\pi)^{d+1}} \int_{-\infty}^{\infty} \int_{\mathbb{R}^d} V^{t,\mathbf{r}}(\mathbf{p}, \omega) \mathrm{e}^{\mathrm{i}(\mathbf{p}\cdot\mathbf{r} - \omega t)} \, \mathrm{d}\mathbf{p} \, \mathrm{d}\omega \tag{1.22a}$$

$$V^{t,\mathbf{r}}(\mathbf{p}, \omega) = \int_{-\infty}^{\infty} \int_{\mathbb{R}^d} v(\mathbf{r}, t) \mathrm{e}^{-\mathrm{i}(\mathbf{r}\cdot\mathbf{p} - \omega t)} \, \mathrm{d}\mathbf{r} \, \mathrm{d}t \tag{1.22b}$$

Transformation in only one variable is possible, with the following pair resulting from partial transformation in the time $t$ variable,

$$v(\mathbf{r}, t) = \frac{1}{2\pi} \int_{-\infty}^{\infty} V^t(\mathbf{r}, \omega) \mathrm{e}^{-\mathrm{i}\omega t} \, d\omega, \quad V^t(\mathbf{r}, \omega) = \int_{-\infty}^{\infty} v(\mathbf{r}, t) \mathrm{e}^{\mathrm{i}\omega t} \, \mathrm{d}t, \tag{1.23}$$

and the pair for partial transform in the spatial coordinate

$$v(\mathbf{r}, t) = \frac{1}{(2\pi)^d} \int_{\mathbb{R}^d} V^{\mathbf{r}}(\mathbf{p}, t) \mathrm{e}^{\mathrm{i}\mathbf{p}\cdot\mathbf{r}} \, d\mathbf{p}, \quad V^{\mathbf{r}}(\mathbf{p}, t) = \int_{\mathbb{R}^d} v(\mathbf{r}, t) \mathrm{e}^{-\mathrm{i}\mathbf{p}\cdot\mathbf{r}} \, \mathrm{d}\mathbf{r}. \tag{1.24}$$

For a solution $v$ to the wave equation (1.6a), we have the plane-wave representation form [51, 121]

$$v(\mathbf{r}, t) = \frac{1}{(2\pi)^{d+1}} \int_{-\infty}^{\infty} \int_{S^{d-1}} \lambda^t(\mathbf{p}, \omega) \mathrm{e}^{\mathrm{i}(\kappa(\omega)\mathbf{p}\cdot\mathbf{r} - \omega t)} \, \mathrm{d}\mathbf{p} \, d\omega, \tag{1.25}$$

in terms of the directional intensity $\lambda$. If propagation exist in only a single direction $\mathbf{p}$, then (1.25) takes the simpler form

$$v_{\mathbf{p}}(\mathbf{r}, t) = \frac{1}{2\pi} \int_{-\infty}^{\infty} \lambda^t_{\mathbf{p}}(\omega) \mathrm{e}^{\mathrm{i}(\kappa(\omega)\mathbf{p}\cdot\mathbf{r} - \omega t)} \, \mathrm{d}\omega. \tag{1.26}$$

# 3 Numerical Methods for linear time-dependent PDEs

This thesis proposes a fast hybrid frequency-time method for the solution of the time domain acoustic wave equation in two- and three-dimensional spatial domains;

typically, frequency-domain scattering problems are treated with integral equation formulations of the corresponding Helmholtz equations, though this is not strictly required by the methodology.

A wide literature exists, of course, for the treatment of the classical wave equation problem. Among the many approaches utilized in this context, we find finite-difference and finite-element time domain methods [84, 113] (FDTD and FETD, respectively), retarded potential boundary integral equation methods [8, 55, 57, 123], Huygens-preserving treatments for odd-dimensional spatial domains [102], and, most closely related to the present work, two hybrid frequency-time methodologies, namely, the Laplace-transform/finite-difference convolution quadrature method [9–13, 20, 87], and the Fourier-transform/operator-expansion method [91]. A brief discussion of the character of these methodologies is presented in what follows.

### 3.1 Volumetric finite-difference-in-time methods

The FDTD approach and related finite-difference methods underlie most of the wave-equation solvers used in practice. In these approaches, the solution on the entire spatial domain is obtained via finite difference discretization of the PDE in both space and time. It should be noted that finite-difference time-marching schemes are more general than many of the other methods discussed or proposed in this thesis, in that they can be applied to nonlinear problems (that is, partial differential equations that are nonlinear in the dependent variable, denoted $u$ in this thesis) with ease; we do not discuss such problems in this thesis, and we restrict our attention to linear wave-type scattering problems. (Note that certain problems in media with nonlinear frequency-response properties can also be straightforwardly-treated with the proposed methodology.) For the ubiquitous exterior-domain problems, volumetric methods require use of absorbing boundary conditions to render the problem computationally feasible—which has in fact been an important and challenging problem in itself [17, 18, 56, 69]. Most importantly, however, finite-difference methods suffer from numerical dispersion, and they therefore require the use of fine spatial meshes (and, thus, fine temporal meshes, for stability) to produce accurate solutions. Numerical dispersion errors therefore present a significant obstacle for high frequency and/or long time simulations via methods based on finite-difference spatial discretizations. FETD methods provide an additional element of geometric generality, but they require creation of high-quality finite element meshes (which can be challenging for complex three-dimensional structures). Further, like FDTD methods, they entail use of absorbing boundary conditions, and they also gener-

ally give rise to detrimental dispersion errors (also called "pollution errors" in this context [5]).

In order to present the essential character of finite-difference time-domain methods, we consider a one-dimensional version of the problem (1.6) on the computational domain $\Omega = [0, 1]$,

$$\frac{\partial^2 u}{\partial t^2}(x,t) - c^2 \frac{\partial^2 u}{\partial x^2}(x,t) = 0, \quad x \in \Omega, \tag{1.27a}$$

$$u(x,0) = \frac{\partial u}{\partial t}(x,0) = 0, \quad x \in \Omega, \tag{1.27b}$$

$$u(x,t) = b(x,t) \quad \text{for} \quad (x,t) \in \{0\} \times [0, T^{inc}], \tag{1.27c}$$

leaving aside challenging issues of the treatment of complex geometry and enforcement of absorbing boundary conditions in multiple dimensions. Exact solutions to Equation (1.27a) take the form

$$u(x,t) = \mathrm{e}^{\mathrm{i}(\omega t - \kappa(\omega) x)}, \quad \kappa(\omega) = \pm\omega/c. \tag{1.28}$$

The function $\kappa(\omega)$ is known as the dispersion relation, and the error a numerical method commits in propagating a monochromatic wave with frequency $\omega$ is called dispersion error [116].

Now, a second-order accurate approximation to (1.27a) is defined on a spatial grid with $M + 1$ points ($\Delta x = \frac{1}{M}$) and a temporal grid with $N$ points ($\Delta t = \frac{T}{N-1}$) defined by $x_j = j\Delta x$, $t_n = n\Delta t$, and is given by the iteration scheme

$$v_j^{n+1} = (c\Delta t)^2 \left( \frac{v_{j+1}^n - 2v_j^n + v_{j-1}^n}{(\Delta x)^2} \right) + 2v_j^n - v_j^{n-1}, \quad 1 \le j \le M - 1 \tag{1.29}$$

where $v_j^n \approx u(x_j, t_n)$. This is the FDTD method in 1D [113], and 1.29 demonstrates the local-in-time nature of approximation, whereby approximations to future time-levels $t_n$ are made on the basis of previous approximations. Note that at every time-step, the solution at all points in the computational domain must be computed and updated, a requirement that can carry significant costs in large computational domains and in multiple dimensions. A boundary condition at $x = x_{M-1} = 1$ is required for completeness of the scheme, and for illustrative purposes, one such condition is

$$v_M^{n+1} = v_{M-1}^n + \frac{c\Delta t - \Delta x}{c\Delta t + \Delta x} \left( v_{M-1}^{n+1} - v_M^n \right),$$

which is a discretization of the 1-way wave equation and is known as the Mur perfectly-absorbing boundary condition [97]. We ignore, however, the absorbing

layer in what follows, and focus on the effect of the finite difference approximation in (1.29), in the interior of the domain.

Motivated by the exact plane-wave solution Equation (1.28), we consider the numerical propagation of such a wave, $v_j^n = \mathrm{e}^{\mathrm{i}(\omega n\Delta t - \kappa_* j\Delta x)}$, and substitution of this expression into (1.27a) yields [113, Ch. 2] the expression for $\kappa_*$,

$$\kappa_* = \frac{1}{\Delta x}\arccos\left(1 + \left(\frac{\Delta x}{c\Delta t}\right)(\cos(\omega\Delta t) - 1)\right), \tag{1.30}$$

known as the numerical dispersion relation for the finite-difference time-domain numerical method, and which is clearly not generically equal to the correct dispersion relation $\kappa(\omega)$. Dispersion relations such as this are typical with any finite-difference-in-time approximation to a PDE, and carry important information concerning the error committed in propagating waves over distances of several wavelengths $\lambda = 2\pi/\kappa$ since they show that there is error in the speed of propagation of the wave. As it is required that $\Delta t \propto \Delta x$ for stability reasons, the numerical dispersion relation shows that for a desired limited level of error in the speed of propagation of a wave with frequency $\omega$, the time- and space-steps must both be kept correspondingly small, increasing the computational burden. Clearly, as longer- and longer-propagation times are required, this burden can become prohibitive. Higher-order finite-difference methods do reduce this burden, but the overall feature of error increasing with propagation distance remains. One motivation of this thesis is to design methods for time-dependent wave propagation without this limitation.

### 3.2 Time-domain retarded-potential integral equation methods

Time domain integral-equation (TDIE) formulations for surface scattering problems based on direct discretization of the time-domain retarded-potential Green's function (1.9) require treatment of the Dirac delta function and thus give rise to integration domains given by the intersection of the light cone with the overall scattering surface [8, 55]. (Loosely related to this class of methods is recent work on discretizations which are Huygens-preserving—that is, treatments of the retarded potential operators with the advantage that they do not entail an increasing amount of computational work for increasing time, at least in odd dimensions [102].) These approaches generally result in relatively complex overall schemes for which it has proven rather challenging to ensure stability [57, 60] (let alone proof guarantees thereof), and which have typically been implemented in low-order accuracy setups and, thus, with significant numerical dispersion error. Accelerated versions of these methods have also been proposed [123]. Motivated by the work in [57], temporally

and spatially high-order time domain integral equation schemes have recently been proposed [14].

A popular formulation involves the single-layer representation formula, which, given a density $\mu(\mathbf{r}, t)$ defined on $\Gamma \times \mathbb{R}^+$ uses the time-domain single-layer operator (1.11) to yield

$$u(\mathbf{r}, t) = (S\mu)(\mathbf{r}, t), \tag{1.31}$$

a solution to the wave equation (1.6a). Ensuring the boundary condition (1.6c) is satisfied leads, via jump relations for the single-layer operator, to the TDIE (1.16)

$$(S\mu)(\mathbf{r}, t) = b(\mathbf{r}, t) \quad \text{for} \quad (\mathbf{r}, t) \in \Gamma \times [0, T].$$

The methods with well-established stability theory are the space-time Galerkin methods [8]. Such TDIE methods proceed by use of a quadrature method for the integrals arising from a weak formulation for (1.16), for which, as mentioned previously, care must be taken due to the role the Dirac delta plays in determining the quadrature domain, a non-polytopal subset of $\Gamma \times \Gamma \times [0, T]$, compounded by the need to approximate singular integrals over this region. Collocation methods are simpler to implement, but for the most part lack a rigorous underlying stability theory [50]. See also, though, the recent work on convolution-splines [48, 49]). All of these methods are based on local-in-time marching and so, like the volumetric FDTD/FETD methods, these methods do incur dispersion error, errors most significant in the low-order implementations which have characterized most reported stable solvers.

### 3.3 Hybrid frequency-time methods

Hybrid time-frequency methods rely on transform techniques to evaluate time domain solutions by synthesis from sets of frequency domain solutions; clearly the necessary solutions of (decoupled) frequency-domain problems can be obtained via parallel computation. The Convolution Quadrature (CQ) method [87] is a prominent example of this class of approaches. This method relies on the combination of a finite-difference time discretization and a Laplace transformation to effectively reduce the time domain wave equation to a set of modified Helmholtz equations over a range of frequencies. There has additionally been some interest in the direct use of Fourier transformations in time [53, 91] to decouple the time-domain problem into frequency-domain sub-problems. In detail, assuming a Gaussian-modulated incident time-pulse, the approach [91] evaluates Fourier integrals on the basis of a Gauss-Hermite quadrature rule, and it obtains the necessary frequency-domain

solutions by means of a certain "operator expansion method"; earlier efforts in a single spatial dimension [53] recognized the advantages of hybrid methods for simulating wave phenomena in complex, and specifically attenuating media, but relied on a low-order accurate midpoint quadrature rule for Fourier integrals. In all cases, however, the number of frequency-domain solutions required, and hence the associated computing and memory costs, grow linearly with the number $N$ of time steps used to evolve the solution to a given final time $T$. (A more detailed discussion of previous hybrid methods, including CQ and direct-transform methods, is presented in Sections 3.3.1 and 3.3.2.)

As mentioned before, two hybrid time-domain methods (i.e., methods that rely on transformation of the time variable by means of Fourier or Laplace transforms) have previously been proposed, namely, the Convolution Quadrature method [9–13, 20, 87] and the direct Fourier transform method [91]. The Convolution Quadrature method employs a discrete convolution that is obtained as temporal finite-difference schemes are solved by transform methods. Like the method introduced in this thesis, in turn, the direct Fourier transform method is based on direct Fourier synthesis of time-harmonic solutions. The following two sections briefly review these two methodologies.

### 3.3.1 Previous hybrid methods: convolution quadrature [87]

The CQ algorithms result as the $Z$-transform is applied to the forward recurrence relation arising from finite-difference temporal semi-discretizations of the problem (1.6). A key point is that the resulting time domain solution is *itself an approximation of the chosen temporal finite-difference approximation of the solution*. In brief, utilizing the $Z$-transform, a finite-difference time discretization of the wave equation can be reformulated as a set of modified Helmholtz problems. The discrete time domain solution is then obtained by evaluation of the inverse $Z$-transform of the frequency domain solutions by means of trapezoidal-rule quadrature. (References [20, 87] provide further elaboration on the connections of the CQ method to $Z$-transforms and convolutions, respectively.) As a result, the solutions produced by this method accumulate temporal and spatial discretizations errors at each timestep as well as overall inversion errors arising from the approximate quadrature used in the inversion of the $Z$-transform. The reliance of the CQ algorithm on a certain "infinite-tail" in the time-history presents certain difficulties also. Furthermore, approximation errors in FFT-accelerated evaluation of the Cauchy integral formula for

required weights in the $Z$-transform inversion typically imply [13, §3.3] a maximum achievable overall accuracy of $\sqrt{\varepsilon_{\text{mach}}} \approx 10^{-8}$, where $\varepsilon_{\text{mach}}$ denotes double precision machine epsilon. Finally, reduction of order of *temporal* convergence is observed at points in the near-field as an observation point approaches the scatterer [12]. A more detailed discussion of the character of CQ numerical methods is presented in what follows.

The characteristics of a particular implementation of the CQ algorithm are determined by the choice made for time-domain finite-difference discretization, the spectral character of the discrete frequency-domain solver used [20], and the methods utilized for numerical inversion of the $Z$-transform. Existing CQ approaches have primarily utilized the second-order accurate BDF2 time discretization [10], but recent work [9] proposes the use of higher-order $m$-stage Runge-Kutta schemes. In all cases, the number of required frequency-domain solutions (which equals $N_f$ for single-stage methods and $mN_f$ for $m$-stage methods, where $N_f$ denotes the number of frequencies used to invert the $Z$-transform) grows in a roughly linear fashion with the size of the time interval for which the solution is to be produced. Thus, the cost of the $m$-stage CQ approaches is $O(mN_t)$, where $N_t$ denotes the number of time-steps taken. Stability and accuracy considerations presented in [20] further suggest that the stability of the CQ algorithm may be linked to certain "scattering poles" of the spatial solution operator which depend on both the geometry of the spatial domain and the choice of the frequency-domain formulation used. Reference [20] further suggests that the error of the contour integral discretization in the CQ method (which is typically effected via the trapezoidal rule) can dominate the error in the overall CQ time-stepping algorithm (even under the well established $N_f = N_t$ setup), and that this difficulty can be mitigated by over-resolving the problem in frequency domain—that is, using $N_f > N_t$. This is elaborated on and justified in what follows, following the presentation in [20] to demonstrate these important characteristics and to discuss their implications.

As pointed out above, there are two main sources of error in CQ methods; following [20], here we only consider errors of the first kind, namely the errors solely due to $Z$-transform-inversion. For these purposes, it suffices to consider as exact the discrete finite-difference time-stepped solutions $u_d(\mathbf{r}, t_n) \approx u(\mathbf{r}, t_n)$, forming the sequence $\{u_d(\mathbf{r}, t_n\}_{n=0}^{\infty}$. The $Z$-transform of this sequence is

$$U_d(\mathbf{r}, z) = \sum_{n=0}^{\infty} u_d(\mathbf{r}, t_n) z^n.$$

If the quantity $U_d$ could be determined for adequate $z$, then an inversion would yield the desired time-marching values $u_d$; the details can be found in [20] and are beyond the present scope. However, it suffices to note that $U_d$ are solutions of certain modified Helmholtz problems, for a certain choice of a certain parameter $\lambda \in \mathbb{R}$ (typically $\lambda < 1$), at certain complex frequencies related to the time-stepping scheme used. A $Z$-transform inversion can be achieved by evaluating the contour integral

$$u_d(\mathbf{r}, t_n) = \frac{1}{2\pi \mathrm{i}} \int_{|z|=\lambda} \frac{U_d(\mathbf{r}, z)}{z^{n+1}} \, \mathrm{d}z, \quad n = 0, \ldots, N_t,$$

and the CQ method prescribes an approximation of this integral via a trapezoidal rule quadrature with $N_f$ points. Letting $\lambda_U$ be the maximum radius of analyticity of $U_d$, it follows that use of the contour $|z| = \lambda$ requires $\lambda < \lambda_U$. Further, analysis of the CQ method shows that the approximate solution $u_d^{N_f}$ using $N_f$ frequency points satisfies

$$u_d^{N_f}(\mathbf{r}, t_n) - u_d(\mathbf{r}, t_n) = \sum_{k=1}^{\infty} \lambda^{kN_f} u_d(\mathbf{r}, t_{n+kN_f}), \tag{1.32}$$

and, for all $\varepsilon > 0$,

$$|u_d^{N_f}(\mathbf{r}, t_n) - u_d(\mathbf{r}, t_n)| = O\left(\left(\frac{\lambda_U}{\lambda} - \varepsilon\right)^{-N_f}\right), \quad N_f \to \infty. \tag{1.33}$$

Each of these results carries important consequences for the convergence rate and accuracy guarantees of the CQ method. The estimate (1.32) is an aliasing-like result, and carries the unfortunate implication that accuracy is dependent on the magnitude of the solution *in the future*, that is, on the solution beyond the final time $N_t(t_{n+1} - t_n)$ sought. This is certainly a challenge in the context of multiple scattering, which may slow the rate of decay of the scattered field. Turning to the estimate (1.33), the convergence rate is impacted by the proximity of the maximum radius $\lambda_U$ of analyticity to the contour $\lambda$, which is generally not known and which does depend in a complex manner on the a variety of poles, including scattering poles [114] associated with the scattering geometry under consideration, as well as poles inherent in the incident signal, the time-marching algorithm, and the specific choice used of integral equation formulation or other frequency-domain solution methodologies. Indeed, experiments in [20, Fig. 12] demonstrate the significant role that these poles play in determining accuracy of the overall scheme, by testing the use of a variety of frequency-domain integral equation formulations and showing that the errors specifically from inversion in some cases exceed the error from the underlying time-marching method. What is more, to achieve certain benefits in

the pole distributions, some of the more successful CQ methods utilize first-kind formulations, typically requiring use of frequency-domain algorithms which can be significantly less efficient than their second-kind counterparts.

In light of the uncertainty just described, it may be tempting to choose $\lambda \ll 1$ (moving the integration contour away from the $|z| = \lambda_U$ contour as much as possible) to increase the convergence rate, but, unfortunately, numerical truncation error dictates that $\lambda$ cannot be chosen too small or instability will result [13]. Clearly, the inversion errors described above can be mitigated by the additional computational cost of choosing $N_f$ larger, as suggested earlier. In practice, however, it may be unknown and difficult to quantify and disentangle the precise magnitude of error introduced by the time-stepping error $|u(\mathbf{r}, t_n) - u_d(\mathbf{r}, t_n)|$ versus inversion error $|u_d(\mathbf{r}, t_n) - u_d^{N_f}(\mathbf{r}, t_n)|$, leaving the practitioner in a difficult position when targeting a precise error level. Even still, virtually all results in the literature do operate under the (computationally taxing, yet still inaccurate) $N_f = N_t$ regime.

In addition to $Z$-transform-inversion errors, the numerical dissipation and dispersion introduced by the underlying time-domain finite difference discretizations present an additional important source of error in the CQ approach [13, 40], as discussed previously in the context of other time-marching algorithms. These errors can, as always in time-marching contexts, be managed by utilizing a number of timesteps which varies super-linearly with frequency [13, §4.3] (that is, faster than the number of sampling points required for uniformly accurate interpolation), but the computational cost associated with such procedures can be significant.

The memory requirements of the CQ method can be significantly impacted by its reliance on a certain "infinite time-tail," which is described in [107, Ch. 5]:

> The sequence of problems [ . . . ] presents the serious disadvantage of having an infinite tail. In other words, the passage through the Laplace domain introduces a regularization of the wave equation that eliminates the Huygens' principle that so clearly appears in the time domain retarded operators and potentials.

The infinite tail impacts the computing costs of the CQ method in two different ways, namely: 1) as the CQ time-step tends to zero for a fixed final time $T$; and 2) as the final time $T$ grows for a fixed time-step. While the growth in point 1) can be slowed to a certain extent by appealing to Laplace-domain decay rates of

compactly-supported, smooth incident data [10] (whose $Z$-transform counterpart generally decays much faster than the error arising from the time-stepping scheme utilized, and can thus be broadly neglected up to the prescribed error tolerance), the infinite-tail growth in point 2) has remained untreated, and it does give rise to linear growth in the overall CQ computing and memory cost per time-step as $T \to \infty$.

### 3.3.2 Previous hybrid methods: direct Fourier transform in time [91]

Without reliance on finite difference approximations, the direct Fourier transform method proposed in [91] proceeds by Fourier transformation of the time domain wave equation followed by solution of the resulting Helmholtz equations for a range of frequencies and inverse transformation to the time-domain using the transform pair

$$U^t(\mathbf{r},\omega) = \int_{-\infty}^{\infty} u(\mathbf{r},t)\mathrm{e}^{\mathrm{i}\omega t}\,\mathrm{d}t, \qquad u(\mathbf{r},t) = \frac{1}{2\pi}\int_{-\infty}^{\infty} U^t(\mathbf{r},\omega)\mathrm{e}^{-\mathrm{i}\omega t}\,\mathrm{d}\omega \tag{1.34}$$

(see Remark 2). In detail, for general boundary values $b = b(\mathbf{r},t)$ (Equation (1.6)), reference [91] uses a plane wave representation of the form

$$B^t(\mathbf{r},\omega) = \frac{1}{(2\pi)^d}\int_{S^{d-1}} B^{\mathbf{r},t}(\mathbf{p},\omega)\mathrm{e}^{\mathrm{i}\kappa(\omega)\mathbf{p}\cdot\mathbf{r}}\,\mathrm{d}\mathbf{p}, \tag{1.35}$$

so that full solution $U^t$ can be reconstructed on the basis of the solutions $U^t = U^t_{\mathbf{p}}$ of Helmholtz problems (1.7), where $\kappa = \kappa(\omega) = \omega/c$, and where the sound-soft boundary values are given by the plane wave $\mathrm{e}^{\mathrm{i}\kappa(\omega)\mathbf{p}\cdot\mathbf{r}}$ in the direction of the vector $\mathbf{p}$. The numerical examples in [91] assume overall boundary data of this form for a single incidence vector $\mathbf{p}$—that is, a uni-directional incident wave field.

Importantly, the resulting direct Fourier method does not suffer from dispersion errors in the time variable. In the contribution [91], the needed Helmholtz solutions are obtained by means of a certain "operator-expansion" technique, and assumes the incident field is given by a plane wave modulated by a Gaussian envelope in frequency domain in order that the needed Fourier integrals are approximated using the classical Gauss-Hermite quadrature rule.

Except for simple geometries, the use of the operator-expansion method limits the overall accuracy to the point that in many cases, it is difficult to discern convergence. This difficulty could be addressed by switching to a modern, more effective, frequency-domain technique. Most importantly, however, the use of any generic numerical integration procedure for the evaluation of the necessary inverse Fourier

transforms for large $t$, including the highly accurate Gauss-Hermite rule used in [91], does lead to difficulties—in view of the highly-oscillatory character, with respect to $\omega$, of the exponential factor in the right-hand expression in (1.34) for large values of $t$. Indeed, evaluation of the aforementioned inverse Fourier transform for required time sample values up to the final time $T$ on the basis of such procedures requires use of a number $N$ of frequency discretization points (and hence a number of required frequency-domain solutions) which is proportional to $T$. Calling $P$ the average cost of these frequency-domain solutions, and including the overall $O(T^2)$ computational cost required by the evaluation of the $O(T)$-cost Gauss-Hermite inverse transform for each $t_n \leq T$, the overall cost of the algorithm [91] can be estimated as

$$TP + T^2. \tag{1.36}$$

This estimate must be contrasted with the cost required by classical finite-difference methods—which is proportional to the first power of $T$. More significant, however, is the linear increase in the number of frequency-domain solutions required, since the average cost $P$ of each of these is the dominant cost of the algorithm.

### 3.4 Accuracy and computational costs

Estimates on the accuracy of hybrid methods follow from well-established results on convergence of the associated frequency-domain solution techniques together with corresponding accuracy estimates on the underlying treatment of frequency/time discretizations. The CQ method (Section 3.3.1) has typically used low-order Galerkin spatial discretizations [11], although the recent contribution [80] does incorporate a high-order frequency-domain solver. From an implementation perspective, retaining full accuracy with CQ methods is challenging when using commonly-implemented Nyström methods making use of Martensen-Kussmaul kernel-splitting quadrature rules due to significant cancellation errors arising for complex frequencies with a large imaginary part [117], so mildly more complicated alternative frequency-domain discretization methods are necessitated. Frequency/time discretization errors in the CQ method, on the other hand, arise from the time-stepping scheme used and the numerical discretization selected of a certain complex contour integral. Typically, BDF2 is chosen as the underlying CQ time-stepping scheme, yielding second order accuracy in time—but see also [9] for use of higher-order temporal CQ discretizations and their associated computing costs. Concerning the CQ complex-contour quadrature, on the other hand, the trapezoidal quadrature rule that is used most often in this context can be an important source of numerical error (see [20] and

the previous discussion in Section 3.3.1). The direct Fourier Transform method [91] (Section 3.3.2), in turn, exhibits high-order Gauss-Hermite convergence in time, but generally poor spatial convergence for the frequency-domain problems (but see Section 3.3.2 in these regards). The fast hybrid method proposed in this thesis, finally, relies on well-known Nyström frequency-domain methods, which generally exhibit superalgebraically-fast convergence (that is, convergence faster than any power of the discretization mesh), together with exponentially convergent methods for evaluating frequency/time transforms (except, in the 2D cases with low-frequency content for which arbitrarily high but not exponential convergence is obtained). In sum, the accuracy of the CQ methods is mostly limited by the errors arising in the time-stepping evolution scheme if the necessary complex integrations are performed with sufficient accuracy. The direct Fourier method [91] and the fast hybrid method proposed in this thesis, in turn, enjoy highly favorable convergence properties as discretizations are refined.

The total computational costs required by the various hybrid algorithms under consideration will be quantified in terms of the number $N$ of time-points $t_n$ ($1 \leq n \leq N$) at which the solution is desired, as well as the average computing cost $P$ required by each one of the necessary frequency-domain solutions. Roughly speaking (up to logarithmic factors), the CQ methods entail a computing cost proportional to $NP$—that is, the method requires a number of frequency-domain solutions that grows linearly with time. In more detail, for example, reference [10, Sec. 4] proposes a CQ algorithm for which it reports a computing cost of $O(N \log^2(N)P)$ operations. According to Section 3.3.2, in turn, the Direct Fourier Transform method requires $O(N^2) + O(NP)$ operations.

## 4 Contributions in and outline of this thesis

The purpose of this thesis is to propose a radically-new approach to efficient numerical solution of these time-dependent wave propagation problems. As described in the preceding sections, all previous methods, hybrid or otherwise, incur total simulation costs which grow linearly with final simulation time. These costs arise directly in time stepping methods (including the convolution quadrature class of time stepping methods) from the fact that the cost per time step is constant. One goal of this thesis is to show that these costs are asymptotically suboptimal, and that indeed a constant amount of computational work and memory requirement suffices to solve the problem at arbitrarily large times. The approach is to exploit the linear time-invariance (LTI) properties of these physical problems. Time-invariance is the

property that a system's output (e.g. the scattering wave solution $u(\mathbf{r}, t)$), while truly a time-dependent function, is only indirectly dependent on time through the time-dependence of the input (e.g. the incident wave $u^{inc}(\mathbf{r}, t)$); that is, there is no intrinsic time-variability of the physical system. In the context of ordinary differential equations, this is known as an *autonomous* system, with a popular method for solving such systems being phase-space descriptions. In our context of a physical system described by a PDE, we have that since the PDE is linear, the solution is the result of the convolution of its Green function with with data. Further, since it is time-invariant, the same fixed set of frequency-domain impulse responses might be expected to be sufficient to produce solutions for all time. This idea is mathematically-expressed as a certain "windowing-and-recentering" procedure for the Fourier transform so that determination of the time-domain response for one time-period can be re-used for different time-dependent forcing. This is the intuition that the thesis more rigorously develops, and the hope that it seeks to show is realizable.

Certain difficulties arise in the efficient solution of wave scattering problems by frequency/time hybrid methods related to approximation of quantities in forward and inverse transforms, and strategies for numerical resolution of these difficulties are presented in this thesis. For incident pulses of arbitrary duration, the proposed approach employs a *smoothly time-windowed Fourier transformation technique* (detailed in Chapter 2), which, without resorting to use of refined frequency discretizations, re-centers both the incident field and the scattering solution in time and thus effectively handles the fast oscillations that occur in the scattering solution as a function of the Fourier-transform variable $\omega$. On the other hand, for inverse Fourier transforms, special quadrature techniques are needed to produce accurate solutions at arbitrarily large times without an associated increasing computational burden. Therefore, in contrast to the CQ and the direct-transform methods, the new approach can be applied in the presence of arbitrary incident fields on the basis of a fixed set of frequency-domain solutions. Favorable properties of the method include its time-parallel character, its time-leaping abilities and $O(1)$ cost of evaluation at any given time, however large, and, therefore, its $O(N)$ cost for a total full $N$ time-step history of the solution. The algorithm remains uniformly (spectrally) accurate in time for arbitrarily long times, with complete absence of temporal dispersion errors.

The proposed hybrid method relies on the use of a sequence of smooth windowing functions (the sum of all of which equals unity) to smoothly partition time into a

sequence of windowed time-intervals. The claimed overall $O(N)$ time cost with uniform-accuracy for arbitrarily large times can be achieved for any given incident field through use of time partitions of relatively large but fixed width, leading to fixed computational cost per partition for arbitrarily long times. In order to achieve such large-time uniform accuracy at fixed cost per window, in turn, a new quadrature method for the evaluation of windowed Fourier transform integrals is introduced which does not require use of finer and finer discretizations for large times—despite the increasingly oscillatory character, as time grows, of a certain complex exponential factor in the transform integrands. The time evaluation procedure requires computation of certain "scaled convolutions" (with a sinc function kernel) which can be additionally accelerated on the basis of the Fractional Fourier Transform [7].

The hybrid methodology described in this thesis lends itself naturally, in a number of ways, to high-performance load-balanced parallel computing. While full development of such efficient parallelization strategies will be left for future work, here we present some considerations in these regards. The simplest, and perhaps most important, parallel acceleration strategy in the context of the proposed method concerns the set of frequency domain solutions it requires, which can clearly be produced in an embarrassingly parallel fashion—whereby frequency-domain problems are distributed among the available computing cores. The evaluation of near fields, on the other hand, also presents significant opportunities for parallel acceleration. Indeed, the time-trace calculations on a prescribed region $\mathcal{R}$ in space could be handled by distributing subsets of $\mathcal{R}$ among various core groupings, or by relying on frequency parallelization for evaluation of the necessary frequency-domain near fields, or a combination of the two—depending on 1) the parallelization method used (if any) for the frequency-domain problems themselves [22, 30, 31, 44], 2) the physical extent of the region $\mathcal{R}$, and 3) the number of frequencies that need to be considered for a given problem. Time parallelism, finally, can easily be achieved as a by-product of the smooth time-partitioning approach. The multiple levels of parallelism inherent in the algorithm should provide significant flexibility for parallel implementations that exploit the differing capabilities of various computer architectures.

In terms of computational costs: as shown in Chapter 2, the proposed fast hybrid method requires $rP + O(N)$ operations to evaluate the solution at $N$ time points (where $r$ is the number, independent of $N$, of frequency-domain solutions each of average cost $P$ required by the method to reach a given accuracy for arbitrarily long time). Note that while the previous hybrid methods require the solution of an

increasing number of Helmholtz problems as time grows, the proposed fast hybrid method does not—a fact which lies at the heart of the method's claimed $O(1)$-in-time sampling cost for arbitrarily large times $t$. In terms of memory storage, the fast hybrid method requires $rV$ memory units for sampling at arbitrarily large times, where $V$ denotes the average value of the storage needed for each one of the necessary frequency-domain solutions. Of course, storage of the entire time history on a given set of spatial points, which may or may not be desired, does require a total of $O(N)$ memory units.

This thesis is organized as follows. Chapter 2 introduces the main ingredients of new hybrid frequency/time methods, utilizing continuous-time Fourier transformation. The focus of Chapter 2 is on decoupling the number of frequencies at which Helmholtz problems are required to be solved for accurate solutions from the final solution time, but commits simplifying assumptions about the nature of the incident fields under consideration: that they, for instance, be a plane-wave propagating in a single direction, or some other simple source. Chapter 3 generalizes the methods, leading to methods for incident fields of a fully arbitrary nature which retain the efficiency already developed. Chapter 3 introduces algorithms in two spatial dimensions relying on known time-asymptotics to retain $O(1)$ computational cost despite the slow time-decay exhibited for such problems. Chapter 4 develops a stopping criterion algorithm which allows that certain field contributions can be omitted without sacrificing accuracy, and in order to establish the theoretical validity of such a criterion, an extensive foray into time-dependent scattering theory is made. The theoretically-justified algorithms having been established, the overall $O(1)$ cost to sample the solution at arbitrarily-large times is achieved. In view of its spectral time accuracy, absence of stability constraints, fast algorithmic implementations, easy use in conjunction with any existing frequency-domain solver, and highly competitive computational and memory requirements compared to available alternatives, the proposed method should prove attractive in a number of contexts in science and engineering. Conversely, on the theory side, the new types of time-dependent decay estimates are of both numerical relevance and are intrinsically of theoretical interest.

*Chapter 2*

# A NOVEL FOURIER FREQUENCY–TIME METHOD FOR ACOUSTIC WAVE SCATTERING

**Overview**

This chapter proposes a frequency/time hybrid integral-equation method for the time-dependent wave equation, and is demonstrated in two and three-dimensional spatial domains. Relying on Fourier Transformation in time, the method utilizes a fixed (time-independent) number of frequency-domain integral-equation solutions to evaluate, with errors that are superalgebraically-small, time domain solutions for arbitrarily long times. The approach relies on two main elements, namely 1) a smooth time-windowing methodology that enables accurate band-limited representations for arbitrarily-long time signals, and 2) a novel Fourier transform approach which, in a time-parallel manner and without causing spurious periodicity effects, delivers numerically dispersionless spectrally-accurate solutions.

In practice, the proposed methodology enjoys a number of attractive properties, including high accuracy without numerical dispersion error; an ability to effectively leverage existing frequency-domain scattering solvers for arbitrary, potentially complex spatial domains; an ability to treat dispersive media (i.e., background media with temporally-varying wave-speeds in accordance with the frequency content of incident waves—see also Appendix A) as well as media with spatially-varying wave-speeds; dimensional reduction (if integral equation methods are used as the frequency domain solver component); natural parallel decoupling of the associated frequency-domain components; and, most notably, time-leaping, time parallelism, and $O(1)$ cost for solution sampling at arbitrarily-large times without requirement

---

[1] T. G. Anderson, O. P. Bruno, and M. Lyon. "High-order, Dispersionless "Fast-Hybrid" Wave Equation Solver. Part I: O(1) Sampling Cost via Incident-Field Windowing and Recentering". In: *SIAM Journal on Scientific Computing* 42.2 (Apr. 2020), A1348–A1379. DOI: 10.1137/19m1251953.

[2] T. G. Anderson, O. P. Bruno, and M. Lyon. *High-order, Dispersionless "Fast-Hybrid" Wave Equation Solver. Part II: Window Tracking, Spatio-Temporal Parallelism, General Incident Fields*. 2020, in preparation.

of intermediate time evaluation. A similar hybrid technique can be obtained on the basis of Laplace transforms instead of Fourier transforms. Use of the Laplace-based technique would be advantageous for treatment of certain types of initial/boundary-value problems with non-vanishing initial conditions, but we do not consider a Laplace-based approach in any detail here. The proposed frequency-time hybridization strategy, which generalizes to any linear partial differential equation in the time domain for which frequency-domain solutions can be obtained (including e.g. the time-domain Maxwell equations), and which is applicable in a wide range of scientific and engineering contexts, provides significant advantages over other available alternatives such as volumetric discretization, time-domain integral equations, and convolution-quadrature approaches.

The theoretical discussions in the first sections of the present chapter are restricted to configurations for which the time-dependent excitations propagate along a single incidence direction—which is, in fact, one of the most common incident fields arising in applications—but our numerical results section includes examples that incorporate incident fields of other (generic) types ( Table 2.4 and Figure 2.7). The development of algorithms for treatment of the general-incidence case on the basis of precomputation strategies that utilize plane waves or other bases of incident fields will be left for Section 9 of this chapter.

The layout of this chapter is as follows. Section 5 introduces the smooth time-partitioning technique that underlies the proposed accelerated treatment of signals of arbitrary long duration, while Section 6 puts forth a new quadrature rule for the fast spectral evaluation of Fourier transform integrals, with high-order accuracy and $O(1)$ large-time sampling costs. An overall algorithmic description is presented in Section 7, and a variety of numerical results are presented in Section 8. Then, finally, methods for the efficient solution of problems for arbitrary incident fields are presented in Section 9, and numerical demonstrations are given.

## 5 Smooth time-partitioning Fourier-transformation strategy

An efficient smooth time-partitioning *"windowing-and-recentering"* solution algorithm is proposed in this section which is based on a number of novel methodologies. The algorithm first expresses the solution $u$ of (1.6), for arbitrary large times $T$, in terms of solutions $u_k$ arising from incident fields that are compactly supported in time: $u(\mathbf{r}, t) = \sum_{k=1}^{K} u_k(\mathbf{r}, t)$ ($K = O(T)$). Assuming the incident fields can be represented with a given error tolerance $\varepsilon$ within a time-frequency bandwidth $W$,

the re-centering component of the strategy presented in Section 5.2 produces all of the functions $u_k$ in terms of a certain *fixed finite set* $\mathcal{F} = \{\psi^t_{\mathbf{p}}(\cdot, \omega_j),\ (1 \le j \le J)\}$ of frequency-domain solutions appropriate for the assumed temporal bandwidth $W$ (cf. equations (2.13) and (2.16)). The re-utilization of a fixed set of boundary integral densities $\left\{\psi^t_{\mathbf{p}}\right\}$ (and hence the requirement of a fixed number $J$ of solutions of the integral equation (1.19) for evaluation of $u(\mathbf{r}, t)$ for arbitrarily long times $t$), is a key element leading to the effectiveness of the proposed algorithm for incident signals of arbitrarily-long duration.

## 5.1 Time partitioning, windowing and re-centering, and the Fourier transform

Motivated by Equation (1.34), let $(f, F)$ denote a Fourier Transform pair

$$F(\omega) = \int_0^T f(t)\mathrm{e}^{\mathrm{i}\omega t}\,\mathrm{d}t, \quad f(t) = \frac{1}{2\pi}\int_{-\infty}^{\infty} F(\omega)\mathrm{e}^{-\mathrm{i}\omega t}\,\mathrm{d}\omega, \tag{2.1}$$

for a (finitely or infinitely) *smooth compactly supported* function $f(t)$, assumed zero except for $t \in [0, T]$ $(T > 0)$ (as there arise, e.g., in the smooth time-partitioning strategy described in Section 5.2). In this case, the Fourier transform on the left-hand side of (2.1) is an integral over a finite (but potentially large) time interval.

In the context of our problem, it is useful to consider the dependence of the oscillation rate of the function $F(\omega)$ on the parameter $T$. Figure 2.1 demonstrates the situation for a representative "large-$T$" chirped function $f$ depicted in the left-hand image, in the figure: the Fourier transform $F(\omega)$, depicted on the right-hand image is clearly highly oscillatory. Loosely speaking, the highly-oscillatory character of the function $F(\omega)$ stems from corresponding fast oscillation in the factor $\mathrm{e}^{\mathrm{i}\omega t}$ contained in the left-hand integrand in Equation (2.1) for each fixed large value of $t$. The consequence is that a very fine discretization mesh $\omega_j$, containing $O(T)$ elements, would be required to obtain $f(t)$ from $F(\omega)$ on the basis of the right-hand expression in (2.1). In the context of a hybrid frequency-time solver, this would entail use of a number $O(T)$ of applications of the most expensive part of the overall algorithm: the boundary integral equations solver—which would make the overall time-domain algorithm unacceptably slow for long-time simulations. This section describes a new Fourier transform algorithm that produces $f(t)$ (left image in Figure 2.1) within a prescribed accuracy tolerance, and for any value of $T$, however large, by means of a $T$-independent (small) set of discrete frequency values $\omega_j$ $(-W \le \omega_j \le W$, $j = 0, \ldots, J)$.

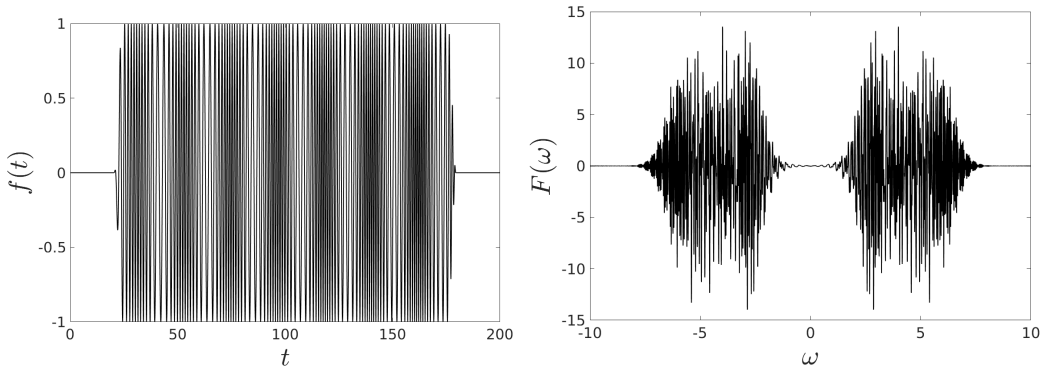


Figure 2.1: Left: Smooth, long duration time signal $f(t)$ as given in (2.34), windowed to have support in the interval $20 \leq t \leq 180$. Right: Real part of the Fourier Transform $F(\omega)$ of $f(t)$. The Fourier transform $F(\omega)$ is highly oscillatory on account of the large $t$ values contained in the left-hand integrand in (2.1).

The proposed strategy for the large-$T$ Fourier transform problem is based on use of a partition-of-unity (POU) set $\mathcal{P} = \{w_k(t) \,|\, k = 1, \ldots, K\}$ of "well-spaced" windowing functions, where $w_k$ is supported in a neighborhood of the point $s = s_k$ for certain "support centers" $s_k \in [0, T]$ $(1 \leq k \leq K)$ satisfying, for some constants $H_1, H_2 > 0$, the minimum-spacing property $s_{k+1} - s_k \geq H_1$, as well as the maximum width condition $w_k(t) = 0$ for $|t - s_k| > H_2$ and the partition-of-unity relation $\sum_{k=1}^{K} w_k = 1$. Setting $H = H_1 = H_2$ in our test cases we use POU sets based on the following parameter selections:

a) $s_{k+1} - s_k = 3H/2$,

b) $w_k(t) = 1$ in a neighborhood $|t - s_k| < H/2$,

c) $w_k(t) = 0$ for $|t - s_k| > H$, and

d) $\sum_{k=1}^{K} w_k(t) = 1 \quad$ for all $\quad t \in [0, T]$.

Note that, since $H$ is (or, more generally $H_1$ and $H_2$ are) $T$-independent, the integer $K$ is necessarily an $O(T)$ quantity. In practice, we use the prescription $w_k(t) = w(t - s_k)$, with partition centers and window function given by $s_k = 3(k-1)H/2$ (the parameter choice $H = 10$ was used in all cases in this thesis unless stated

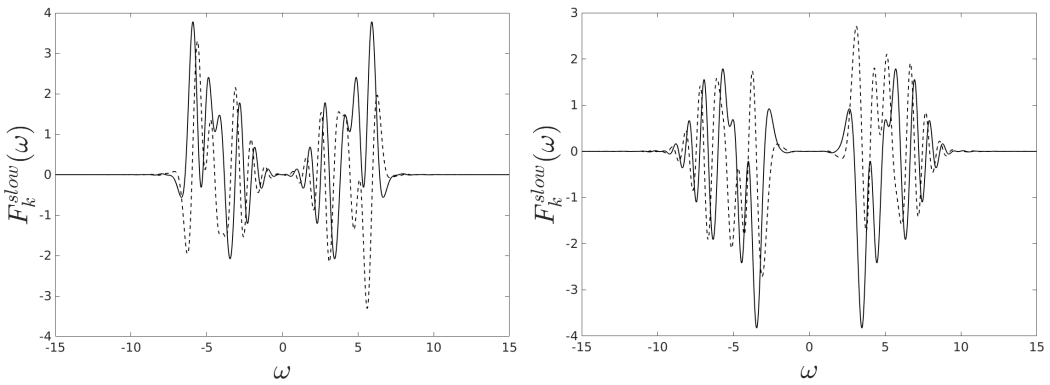


Figure 2.2: Fourier Transform of two windowed partitions of the long duration signal shown in Figure 2.1, each with partition width $H = 10$. With reference to the text, the left and right figures depict the transform corresponding, respectively, to partition centers at $s_k = 35$ ($k = 4$) and $s_k = 155$ ($k = 16$). In each case, the solid and dashed traces depict the real and imaginary parts of the Fourier Transform, respectively. The transforms are both less than $10^{-4}$ outside the plotted region.

otherwise) and

$$w(t) = \begin{cases} 1 - \eta(\frac{t+H}{H/2}), & -H \le t \le -H/2 \\ 1, & -H/2 < t < H/2 \\ \eta(\frac{t-H/2}{H/2}), & H/2 \le t \le H \\ 0, & |t| > H, \end{cases} \tag{2.2}$$

respectively, where we use the smooth windowing function $\eta \in C_c^\infty([-1,1]), \eta(u) = \exp(\frac{2e^{-1/u}}{u-1})$.

Using the partition of unity $\mathcal{P}$ and letting $f_k(t) = w_k(t)f(t)$, for $\omega \in [-W, W]$ we obtain the expression

$$F(\omega) = \sum_{k=1}^{K} F_k(\omega), \quad \text{where} \quad F_k(\omega) = \int_{s_k - H_2}^{s_k + H_2} f_k(t) e^{i\omega t}\, dt, \tag{2.3}$$

which resembles the type of integrals used in connection with the windowed Fourier transform [67]. Now, centering the integration interval around the origin, we obtain

$$F_k(\omega) = \int_{-H_2}^{H_2} f_k(t + s_k) e^{i\omega(t+s_k)}\, dt = e^{i\omega s_k} F_k^{slow}(\omega) \tag{2.4}$$

where

$$F_k^{slow}(\omega) = \int_{-H_2}^{H_2} f_k(t + s_k) e^{i\omega t}\, dt. \tag{2.5}$$

The "slow" superscript refers to the fact that, since $t$ in (2.5) is "small" (it satisfies $-H_2 \le t \le H_2$), it follows that the integrand (2.5) only contains slowly oscillating

exponential functions of $\omega$, and thus $F_k^{slow}(\omega)$ is itself slowly oscillatory. Thus (2.4) expresses $F_k(\omega)$ as product of two terms: the (generically) highly oscillatory exponential term $e^{i\omega s_k}$ (which arises for signals whose support center is away from the origin *in time*), on one hand, and the slowly oscillatory term $F_k^{slow}(\omega)$, on the other. Figure 2.2 displays the real and imaginary parts of $F_k^{slow}$ for two values of $k$, namely $k = 4$ and $k = 16$. Note that despite the differing centers in time, the functions are similarly oscillatory and both are much less oscillatory than the Fourier transform depicted in Figure 2.1.

**Remark 3.** *Since $f$ is smooth and compactly supported, iterated integration by parts in the integral expressions that define $F(\omega)$, $F_k(\omega)$, and $F_k^{slow}(\omega)$ (equations* (2.1)*,* (2.4)*, and* (2.5)*), and associated expressions for the derivatives of these functions of any positive order, shows that these functions and their derivatives decay as $1/\omega^n$ as $\omega \to \pm\infty$ for all $n > 1$ for which $f \in C^n$. In other words, for smooth functions $f$, these three functions, along with each one of their derivatives with respect to $\omega$ (of any order), decay superalgebraically fast as $\omega \to \pm\infty$. Additionally, in the two latter cases, the superalgebraically-fast decay (for each fixed order of differentiation) is uniform in $k$.*

**Remark 4.** *Let $G : \mathbb{R} \to \mathbb{C}$, $G = G(\omega)$, denote a function that decays super-algebraically fast, along with each one of its derivatives, as $\omega \to \infty$. Then, repeated use of integration by parts on the inverse Fourier transform expression $g(t) = \frac{1}{2\pi}\int_{-\infty}^{\infty} G(\omega)e^{-i\omega t}\,d\omega$ shows that the error in the approximation*

$$g(t) \approx \frac{1}{2\pi}\int_{-W}^{W} G(\omega)e^{-i\omega t}\,d\omega$$

*decays super-algebraically fast as $W \to \infty$.*

**Remark 5.** *Let $G = G(\omega)$ denote a superalgebraically-decaying function, as in Remark* 4*. Then, repeated use of integration by parts in the integral expressions for the Fourier coefficients $g_n$ shows that the expansion of $G$ as a $2W$-periodic Fourier series*

$$G(\omega) \approx \sum_{n=-\infty}^{\infty} g_n e^{in\pi\omega/W}, \quad -W \le \omega \le W,$$

*together with all of its derivatives, converge to $G(\omega)$ and its respective derivatives uniformly and super-algebraically fast, as $W \to \infty$, throughout the interval $[-W, W]$.*

## 5.2 Windowed and re-centered wave equation and solutions with slow $\omega$ dependence

In order to evaluate numerically the solution of the problem (1.6), we apply the smooth time partitioning strategy developed in Section 5.1 to the boundary-condition function $b(\mathbf{r}, t)$ in (1.6c) (as a function of $t$ for each fixed value of $\mathbf{r}$). Thus, using the window functions $w_k(t)$ described in the previous section, we define two different types of windowed boundary-condition functions $b_k = b_k(\mathbf{r}, t)$, namely 1) The function

$$b_k(\mathbf{r}, t) = w_k(t) b(\mathbf{r}, t), \tag{2.6}$$

which can be used for general incident fields $b(\mathbf{r}, t)$, as well as, 2) Specifically for incident fields of the form (1.8), the function

$$b_k(\mathbf{r}, t) = \frac{1}{2\pi} \int_{-\infty}^{\infty} B_k^t(\omega) \mathrm{e}^{\mathrm{i}(\kappa(\omega)\mathbf{p}\cdot\mathbf{r} - \omega t)} \, \mathrm{d}\omega \quad \text{with} \quad \kappa(\omega) = \omega/c, \tag{2.7}$$

where, letting

$$a_k(t) = w_k(t) a(t) \tag{2.8}$$

we have set

$$B_k^t(\omega) = \int_{-\infty}^{\infty} a_k(t) \mathrm{e}^{\mathrm{i}\omega t} \, \mathrm{d}t = \int_{-\infty}^{\infty} w_k(t) a(t) \mathrm{e}^{\mathrm{i}\omega t} \, \mathrm{d}t. \tag{2.9}$$

Note that both definitions of $b_k(\mathbf{r}, t)$ imply $\sum_{k=1}^{K} b_k(\mathbf{r}, t) = b(\mathbf{r}, t)$. In view of Remark 1, most of the present chapter (except Section 9) uses the boundary condition function (2.7).

**Remark 6.** *Note that the function $b_k(\mathbf{r}, t)$ as results from Equation* (2.7) *(which is used throughout this thesis with only a few exceptions) is a solution to the wave equation, but that the function $b_k(\mathbf{r}, t)$ from Equation* (2.6) *is not. Section* 9 *is devoted to numerical treatment along the lines of this thesis for wave problems with boundary values that arise from Equation* (2.6)*.*

Letting $u_k(\mathbf{r}, t)$ $(1 \le k \le K)$ denote the solution to (1.6) with boundary-condition function $b(\mathbf{r}, t)$ substituted by $b_k(\mathbf{r}, t)$, we clearly have

$$u(\mathbf{r}, t) = \sum_{k=1}^{K} u_k(\mathbf{r}, t). \tag{2.10}$$

This expression is the basis of the time-domain solver proposed in this thesis.

**Remark 7.** *As discussed extensively in Chapter* 4*, in view of Huygens' principle in three dimensions, and a certain windowing reallocation strategy in two dimensions, a fixed, geometry-dependent, number M (independent of $K = O(T)$) of solutions $u_k$ need to be included for any space-time evaluation region, irrespective of the time duration T for which the solution is evaluated. The geometry-dependence of the parameter M relates closely to the trapping character [93, 96] of the underlying scattering geometry; while M may grow large for slowly-decaying scattered fields, the finite-duration character of the incident field is guaranteed by this theory to yield an overall-bounded number of active partitions. This is the basis of tracking strategies for identifying the "active" time-partition solutions, which will be presented elsewhere. Figure* 2.5*, which displays the computed functions $u_k$ for $k = 1, 2, 3$, and in which the solution for each partition is only plotted if it exceeds a certain tolerance anywhere in the entire domain of interest, illustrates, in a rudimentary fashion, some of the principles inherent in those strategies.*

Accurate numerical approximations of the solutions $u_k$ can be produced as indicated in what follows. Considering the boundary condition function $b_k(\mathbf{r}, t)$ in Equation (2.7), Equations (2.3) and (2.5) yield

$$B^t(\omega) = \sum_{k=1}^{K} B_k^t(\omega), \quad \text{and} \quad B_k^t(\omega) = \mathrm{e}^{\mathrm{i}\omega s_k} B_k^{slow}(\omega). \tag{2.11}$$

Thus, denoting by $U_k^t(\mathbf{r}, \omega)$ and $U_k^{slow}(\mathbf{r}, \omega)$ the frequency domain solutions of the problem (1.7) with $B^t$ replaced by $B_k^t(\omega)\mathrm{e}^{\mathrm{i}\kappa(\omega)\mathbf{p}\cdot\mathbf{r}}$ and $B_k^{slow}(\omega)\mathrm{e}^{\mathrm{i}\kappa(\omega)\mathbf{p}\cdot\mathbf{r}}$, respectively, we obtain the representations

$$u_k(\mathbf{r}, t) = \frac{1}{2\pi}\int_{-\infty}^{\infty} U_k^t(\mathbf{r}, \omega)\mathrm{e}^{-\mathrm{i}\omega t}\,\mathrm{d}\omega = \frac{1}{2\pi}\int_{-\infty}^{\infty} U_k^{slow}(\mathbf{r}, \omega)\mathrm{e}^{-\mathrm{i}\omega(t-s_k)}\,\mathrm{d}\omega. \tag{2.12}$$

Since $U_k^{slow}$ is approximately band-limited (because $B_k^{slow}$ is, see Remark 3), it follows from (2.12) and Remark 4 that $u_k(\mathbf{r}, t)$ can be approximated by the strictly band-limited function $u_k^W$:

$$u_k(\mathbf{r}, t) \approx u_k^W(\mathbf{r}, t) = \frac{1}{2\pi}\int_{-W}^{W} U_k^{slow}(\mathbf{r}, \omega)\mathrm{e}^{-\mathrm{i}\omega(t-s_k)}\,\mathrm{d}\omega \tag{2.13}$$

with superalgebraically small errors (uniform in $t$ and $k$) as the bandwidth $W$ grows.

Section 6 presents a quadrature algorithm that, on the basis of a finite set of frequencies $\mathcal{F} = \{\omega_j : j = 1, \ldots, J\}$, approximates, with errors uniform-in-$t$ and

decaying rapidly as $J$ increases, the highly-oscillatory integral (2.13), and thus produces the numerical approximation $u_k^{W,J} \approx u_k^W$, by means of spectral interpolation of the slowly-varying quantity $U_k^{slow}(\cdot,\omega)$ *with respect to* $\omega$. The quantity $U_k^{slow}$, in turn, is dependent on frequency-domain incident data $B_k^{slow}$ obtained (via use of the numerical transform techniques introduced in Section 6.1 for the function $a_k = w_k a$) from the relation

$$B_k^{slow}(\omega) = \int_{-H}^{H} a_k(t + s_k)\mathrm{e}^{\mathrm{i}\omega t}\,\mathrm{d}t, \tag{2.14}$$

and boundary integral "scattering" densities $\psi_{\mathbf{p}}^t$, where $\psi_{\mathbf{p}}^t$ are solutions of Equation (1.19) with $B^t$ replaced by $\mathrm{e}^{\mathrm{i}\kappa(\omega)\mathbf{p}\cdot\mathbf{r}}$. Specifically, defining

$$\psi_k^{slow}(\mathbf{r}',\omega) = B_k^{slow}(\omega)\psi_{\mathbf{p}}^t(\mathbf{r}',\omega), \tag{2.15}$$

for the time-partition-specific boundary density, we have

$$\begin{aligned} U_k^{slow}(\mathbf{r},\omega) &= \int_\Gamma \psi_k^{slow}(\mathbf{r}',\omega)G_\omega(\mathbf{r},\mathbf{r}')\,\mathrm{d}\sigma(\mathbf{r}') \\ &= B_k^{slow}(\omega)\int_\Gamma \psi_{\mathbf{p}}^t(\mathbf{r}',\omega)G_\omega(\mathbf{r},\mathbf{r}')\,\mathrm{d}\sigma(\mathbf{r}'). \end{aligned} \tag{2.16}$$

Indeed, in view of Remark 6 the windowed incident field $b_k$ is also a solution to the wave equation, and its Fourier transform at a frequency $\omega$ is a plane wave, so that transient scattering can be entirely characterized by Helmholtz solutions with plane-wave incidence. It follows that for a given bandwidth $W$, all the needed function values $U_k^{slow}(\mathbf{r},\omega_j)$ can be produced in terms of the fixed ($k$-independent, $W$-dependent) finite set $\Psi = \{\psi_{\mathbf{p}}^t(\cdot,\omega_j) : j = 1,\ldots,J\}$ of boundary integral densities. The re-utilization of the fixed ($k$-independent) set $\Psi$ of "expensive" integral densities is a crucial element leading to the efficiency of the overall hybrid algorithm.

## 6 FFT-based $O(1)$-cost Fourier transform at large times

This section presents an effective algorithm for the numerical evaluation of truncated Fourier integrals of the form

$$F(\omega) = \int_{-H}^{H} f(t)\mathrm{e}^{\mathrm{i}\omega t}\,\mathrm{d}t \quad \text{and} \quad f(t) = \frac{1}{2\pi}\int_{-W}^{W} F(\omega)\mathrm{e}^{-\mathrm{i}\omega t}\,\mathrm{d}\omega \tag{2.17}$$

(cf. Equations (2.5) and (2.13)), at arbitrarily large evaluation arguments $t$ and $\omega$. Here, it is assumed that $f$ is a smooth function of time $t \in \mathbb{R}$ which vanishes outside the interval $[-H,H]$. Similarly, with the possible exception of an inverse-logarithmic singularity of $F(\omega)$ at $\omega = 0$ for certain two-dimensional applications

(see Section 6.2), $F$ is an infinitely smooth function for all frequencies $\omega$—which is additionally superalgebraically small outside the interval $[-W, W]$. The case in which a singularity exists in Equation (2.17) at $\omega = 0$ is handled in Section 6.2 by utilizing a decomposition of the form

$$f(t) = \left( \int_{-W}^{-w_c} + \int_{-w_c}^{w_c} + \int_{w_c}^{W} \right) F(\omega) \mathrm{e}^{-\mathrm{i}\omega t} \, \mathrm{d}\omega, \tag{2.18}$$

together with a specialized quadrature rule for the middle integral; the function $F$ is smooth (though not necessarily periodic) in the integration intervals $[-W, -\omega_c]$ and $[\omega_c, W]$.

Use of trapezoidal rule integration might appear advantageous in these contexts, since, for such boundary-vanishing integrands, the trapezoidal quadrature rule exhibits superalgebraically-fast convergence (at least in the smooth $F$ case), and, importantly, unlike the Gauss-Hermite rule used in [91], it can be efficiently evaluated by means of FFTs. However, as the evaluation arguments $t$ or $\omega$ grow, the integrands in (2.17) become more and more oscillatory. Both the Gauss-Hermite and the trapezoidal rule (and, indeed, any quadrature rule based on standard interpolation techniques) require use of finer and finer meshes to avoid completely inaccurate approximations as the evaluation argument increases (see Section 5.1). Failure to resolve this difficulty would lead to a fundamental breakdown in the algorithm—as it would be necessary for the scheme to produce an increasing number of (expensive) boundary integral equation solutions, leading to rapidly increasing costs, as evaluation times grow.

**Remark 8.** *For definiteness, the presentation in this section is restricted to the right-hand integral in* (2.17)*; the corresponding algorithm for the left-hand integral is entirely analogous.*

**Remark 9.** *A direct examination of the trapezoidal approximation*

$$f(t) = \frac{1}{2\pi} \int_{-W}^{W} F(\omega) \mathrm{e}^{-\mathrm{i}t\omega} \, \mathrm{d}\omega \approx \frac{W}{2\pi m} \sum_{k=0}^{m-1} F(\omega_k) \mathrm{e}^{-\mathrm{i}t\omega_k} \quad (\omega_k = -W + k\,\Delta\omega) \tag{2.19}$$

*shows that, as is well known, quadrature errors in the trapezoidal quadrature rule for "large" $t$ manifest themselves as "aliasing," that is, spurious periodicity in the $t$ variable [6, 59, 66, 86].*

The method proposed in the present Section 6 resolves the difficulties mentioned in the last paragraph: it eliminates aliasing errors without recourse to frequency

mesh refinement, and it evaluates (on the basis of FFTs) the time-domain solution in constant computing time per temporal evaluation point—so that, as in finite-difference time-marching algorithms, the overall cost per time-step of the time propagation algorithm does not grow as time increases.

## 6.1 Smooth $F(\omega)$: FFT-based reduction to "scaled convolution"

This section considers the problem of evaluation of Fourier integrals similar to those in (2.17) (or, in 2D contexts, the integrals with smooth integrands in Equation (2.18)) under the assumption that the functions $f$ and $F$ are infinitely smooth in the domain of integration. In the context of Equation (2.13) in dimension $d = 3$, the smoothness assumption on $F$ is always satisfied, as it is for dimension $d = 2$ provided that, e.g., $F(\omega) = U_k^{slow}(\mathbf{r}, \omega)\mathrm{e}^{\mathrm{i}\omega s_k}$ vanishes in a neighborhood of $\omega = 0$. The singular $d = 2$ case is tackled in Section 6.2.

The proposed smooth-$F$ approach proceeds by trigonometric-series expansion of the integrand function $F$ followed by use of certain "scaled convolutions" introduced in Section 6.1.1; a fast FFT-based algorithm for evaluation of such convolution-like quantities is then described in Section 6.1.2.

### 6.1.1 Transform approximation via Fourier series expansion

In this section, we develop a quadrature rule for the general transform integral

$$I_a^b\,[F](t) = \int_a^b F(\omega)\mathrm{e}^{-\mathrm{i}\omega t}\,\mathrm{d}\omega, \tag{2.20}$$

or, equivalently,

$$I_a^b\,[F](t) = \mathrm{e}^{-\mathrm{i}\delta t}\int_{-A}^{A} F(\delta+\omega)\mathrm{e}^{-\mathrm{i}\omega t}\,\mathrm{d}\omega, \quad \text{where} \quad A = \frac{b-a}{2} \quad \text{and} \quad \delta = \frac{b+a}{2}. \tag{2.21}$$

Although $F(\delta + \omega)$ may not be a periodic function of $\omega$ in the integration interval $[-A, A]$, for a prescribed positive even integer $M$ we utilize a trigonometric polynomial of the form

$$F(\delta+\omega) \approx \sum_{m=-M/2}^{M/2-1} c_m \mathrm{e}^{\mathrm{i}\frac{2\pi}{P}m\omega} \tag{2.22}$$

of a certain periodicity $P$, that closely approximates $F(\delta + \omega)$ for $\omega \in [-A, A]$.

**Remark 10.** *As indicated below, in the context of this thesis, $F(\delta + \omega)$ is most often a smoothly periodic function in $[-A, A]$ (with $A$ equal to the bandlimit $W$); in*

*such cases, we take* $P = 2A$*, and* (2.22) *is obtained as a regular Discrete Fourier Transform (DFT) in* $[-A, A]$*. Exceptions do arise in certain two-dimensional situations (Section* 6.2*) where* $F(\delta+\omega)$ *is smooth but not periodic in* $[-A, A]$ *(cf. the first and last integrals in* (2.18)*); in such cases an accurate Fourier approximation of a certain period* $P \neq 2A$ *is obtained in our algorithm on the basis of the FC(Gram) Fourier Continuation method [2, 32]. In the periodic case, the errors inherent in the approximation* (2.22) *tend to zero super-algebraically fast (faster than any negative power of* $M$ *[3, Lemma 7.3.3], cf. also Remark* 5*), while the errors arising from the Fourier Continuation method used in the non-periodic case decay as a user-prescribed negative power of* $M$*.*

Substituting (2.22) into (2.21) and integrating term-wise yields the approximation

$$\begin{aligned} I_a^b\,[F](t) &\approx \mathrm{e}^{-\mathrm{i}\delta t} \sum_{m=-M/2}^{M/2-1} c_m \int_{-A}^{A} \mathrm{e}^{-\mathrm{i}\frac{2\pi}{P}(\alpha t-m)\omega}\,\mathrm{d}\omega \\ &= \mathrm{e}^{-\mathrm{i}\delta t} \sum_{m=-M/2}^{M/2-1} c_m \frac{P}{\pi(\alpha t-m)} \sin\left(\pi\frac{2A}{P}(\alpha t-m)\right), \end{aligned} \tag{2.23}$$

where we have set $\alpha = \frac{P}{2\pi}$. In view of (2.23), for a given *user-prescribed (!)* equi-spaced time-evaluation grid $\{t_n = n\Delta t\}_{n=N_1}^{N_2}$, we may write, letting $\beta = \alpha\Delta t$,

$$I_a^b\,[F](t_n) \approx \mathrm{e}^{-\mathrm{i}\delta t_n} \sum_{m=-M/2}^{M/2-1} c_m b_{\beta n-m}, \quad \text{where} \quad b_q \coloneqq 2A\,\mathrm{sinc}\left(\frac{2A}{P}q\right). \tag{2.24}$$

Note that, paralleling the fast Fourier series convergence in the periodic case, equations (2.23) and (2.24) provide super-algebraically close approximations of $I_a^b\,[F](t)$. In the non-periodic case, these equations provide a user-prescribed algebraic order of accuracy. In either case, the errors in (2.23) and (2.24) are uniform in $t$ and $n$, respectively: for a given error tolerance $\varepsilon$, there exists an integer $M_0$ (independent of $t$ and $t_n$) such that, for all $M \geq M_0$, the approximation errors in (2.23) and (2.24) are less than $\varepsilon$ for all $t \in \mathbb{R}$ and all relevant values $t_n$, respectively.

**Remark 11.** *It is useful to note that the aforementioned* $t$*- and* $t_n$*-independent errors in* (2.23) *and* (2.24) *stem solely from corresponding errors in the expansion* (2.22)*—and thus, can be achieved on the basis of values of the function* $F(\delta+\omega)$ *on a fixed (*$t$*-independent) finite set* $\mathcal{F}^{smooth}$ *of frequency mesh points, cf. Section* 7*.*

Since generically $\beta \neq 1$ (indeed, $\beta \notin \mathbb{Z}$ generically), the quantity $\sum_m c_m b_{\beta n-m}$ in (2.24) is not a discrete convolution, but it is, rather, a "discrete scaled convolu-

tion" [100]. Like regular discrete convolutions, scaled convolutions can accurately be produced by means of FFTs [100]—although the algorithm for scaled convolutions is somewhat more complicated than the standard FFT convolution approach. Still, the fast scaled convolution algorithm is a useful tool: it runs in $O(L \log L)$ operations (where $L = \max(N_2 - N_1, M)$), and it produces highly accurate results; details are presented in Section 6.1.2.

### 6.1.2 FFT-accelerated evaluation of scaled discrete convolutions

The quadrature method introduced in Section 6.1.1 reduces the evaluation of the right-hand transform in (2.17) for values $t = t_n$ (for a given range $0 \le n - n_0 \le N - 1$ with $n_0 \in \mathbb{Z}$ and $N \in \mathbb{N}$) to evaluation of scaled convolutions of the form

$$d_n = \sum_{m=-M/2}^{M/2-1} c_m b_{\beta m - \gamma n}, \quad 0 \le n - n_0 \le N - 1, \tag{2.25}$$

where the coefficients $c_m$ are complex numbers that make up a certain "input vector" $\vec{c} = (c_{-M/2}, \ldots, c_{-M/2-1})$, and where the "convolution kernel" $b$ is a function of its real-valued sub-index $q$: $b_q = b(q)$. (Compare (2.24) and (2.25) and note the specific scaled convolution kernel $b_q$ and parameter value $\gamma = 1$ used in the former equation.) This section presents an algorithm which evaluates the sum (2.25) for all required values of $n$ at FFT speeds.

To describe the algorithm, let $L$ denote a certain positive even integer, to be defined below, which is larger than or equal to the maximum of $N$ and $M$. The convolution input vector $\vec{c}$ is symmetrically zero-padded to form a new vector $\vec{c} = (c_{-L/2}, c_{-L/2+1}, \ldots, c_{L/2-1})$ of length $L$. New elements are also added to the list of evaluation indices in (2.25) so that the overall list contains the $L$ elements in the indicial vector $\vec{n} = (n_0 - L/2, n_0 - L/2 + 1, \ldots, n_0 + L/2 - 1)$. Following [100], for technical reasons, the length $L$ is determined by the relation $L \ge L_0$, where $L_0$ denotes the smallest even integer for which the kernel index parameter $q = \beta m - \gamma n$ lies in the range $-L_0/2 \le q \le L_0/2 - 1$ for $-M/2 \le m \le M/2 - 1$, $0 \le n - n_0 \le N - 1$. (As pointed out below, selections satisfying $L > L_0$ are occasionally necessary to achieve a prescribed error tolerance.) In view of these selections, the scaled convolution expression (2.25) is embedded in the analogous but more favorably structured convolution expression

$$d_n = \sum_{m=-L/2}^{L/2-1} c_m b_{\beta m - \gamma n}, \quad -L/2 \le n - n_0 \le L/2 - 1, \tag{2.26}$$

| $M$ | Direct (s) | Fast (s) | $\varepsilon^{\text{Fast}}$ |
|---|---|---|---|
| $10^1$ | $5.6 \cdot 10^{-2}$ | $8.3 \cdot 10^{-3}$ | $6.6 \cdot 10^{-3}$ |
| $10^2$ | $8.3 \cdot 10^{-2}$ | $7.9 \cdot 10^{-3}$ | $1.9 \cdot 10^{-7}$ |
| $10^3$ | $1.8 \cdot 10^{-1}$ | $7.8 \cdot 10^{-3}$ | $1.6 \cdot 10^{-8}$ |
| $10^4$ | $1.4 \cdot 10^{0}$ | $8.2 \cdot 10^{-3}$ | $7.9 \cdot 10^{-7}$ |

| $N$ | Direct (s) | Fast (s) | $\varepsilon^{\text{Fast}}$ |
|---|---|---|---|
| $10^1$ | $1.5 \cdot 10^{-3}$ | $1.1 \cdot 10^{-2}$ | $6.2 \cdot 10^{-6}$ |
| $10^2$ | $1.2 \cdot 10^{-2}$ | $7.5 \cdot 10^{-3}$ | $5.8 \cdot 10^{-6}$ |
| $10^3$ | $8.8 \cdot 10^{-2}$ | $8.1 \cdot 10^{-3}$ | $4.7 \cdot 10^{-6}$ |
| $10^4$ | $7.1 \cdot 10^{-1}$ | $8.0 \cdot 10^{-3}$ | $2.6 \cdot 10^{-7}$ |
| $10^5$ | $7.5 \cdot 10^{0}$ | $9.3 \cdot 10^{-2}$ | $2.1 \cdot 10^{-9}$ |
| $10^6$ | $9.4 \cdot 10^{1}$ | $1.5 \cdot 10^{0}$ | $2.6 \cdot 10^{-10}$ |
| $10^7$ | $2.8 \cdot 10^{3}$ | $2.3 \cdot 10^{1}$ | $5.5 \cdot 10^{-9}$ |

Table 2.1: Computing times required for evaluation of the size-$M$ scaled convolution (2.24) by means of the Direct and Fast algorithms described in the text at a number $N$ of time points $t_n$, and errors $\varepsilon^{\text{Fast}}$ associated with the Fast algorithm. (By definition, the Direct algorithm provides the exact convolution results, up to roundoff.) Left: $N = 10^4$. Right: $M = 5000$.

Using the $\gamma$-fractional discrete Fourier transform $C_p^{(\gamma)}$ (that is to say, the fractional Fourier transform based on roots of unity parameter $\gamma$ as in [7]) together with the discrete Fourier transform $B_p$,

$$C_p^{(\gamma)} = \sum_{m=-L/2}^{L/2-1} c_m \mathrm{e}^{-\mathrm{i}\frac{2\pi\gamma mp}{L}}, \quad B_p = \sum_{m=-L/2}^{L/2-1} b_m \mathrm{e}^{-\mathrm{i}\frac{2\pi mp}{L}},$$

an application of the convolution theorem yields [100]

$$d_n = \sum_{m=-L/2}^{L/2-1} c_m b_{\beta m-\gamma n} \approx \frac{1}{L} \sum_{p=-L/2}^{L/2-1} C_p^{(\gamma)} B_p \mathrm{e}^{\mathrm{i}\frac{2\pi\beta np}{L}}, \quad -L/2 \le n - n_0 \le L/2 - 1, \tag{2.27}$$

reducing, in particular, the (approximate) evaluation of the desired values $d_n$ in (2.25) to evaluation of a discrete Fourier transform and a $\gamma$-fractional discrete Fourier transform, both of size $L$, followed by evaluation of the $L$-term inverse $\beta$-fractional Fourier transform on the right-hand side of (2.27). The necessary discrete Fourier transform can of course be evaluated by means of the FFT algorithm. The fractional Fourier transforms (FRFTs) can also be accelerated on the basis of the FFT-based fractional Fourier transform algorithms, at an $O(L \log L)$ cost of approximately four times that of an $L$-point FFT; see [7]. The error inherent in the approximation (2.27) is a quantity of order $O(L^{-2})$, which, in our applications, generally yields any desired accuracy in very fast computing times by selecting appropriate values of the parameter $L$.

To demonstrate the accelerated scaled-convolution algorithm, we evaluate the transform (2.25) for several values of $N$, with certain coefficients $c_m$ ($-M/2 \le m \le$

$M/2-1$) and with $b_q$ as in (2.24). (The particular selection of the coefficients $c_m$ is immaterial in the context of the present demonstration, but, for reference, we mention that the coefficients used in the example were obtained as the coefficients of the $M$-term FC expansion (2.22) with $F(\omega) = \mathrm{e}^{-\frac{1}{4}(\omega-10)^2}\mathrm{e}^{-\mathrm{i}8\omega}$ in the interval $[8, 15]$. This specific scaled convolution arises as the method in Section 6.1.1 is applied to the evaluation of (2.20) on $[0, T]$, with $T = N\Delta t$ and $\Delta t = 0.2$.) Letting $\widetilde{d}_n$ denote the approximation of $d_n$ produced by the fast algorithm, Table 2.1 displays the $\ell^\infty$ error $\varepsilon^{\mathrm{Fast}} = \max_n |d_n - \widetilde{d}_n|$ as well as the time required by the fast method to produce the $M$-coefficient sum at the required $N$ evaluation points. The computations were performed in MATLAB on an Intel Core i7-8650U CPU.

### 6.2 Non-smooth $F(\omega)$: singular quadrature for 2D low frequency scattering

This section concerns the evaluation of the inverse transform in (2.17) for cases in which $F$ contains an (integrable) singularity at $\omega = 0$. In the context of the proposed wave equation solver, this occurs in the evaluation of (2.13) in the $d = 2$ case (where for each spatial point $\mathbf{r}$ we have $F(\omega) = U_k^{\mathrm{slow}}(\mathbf{r}, \omega)\mathrm{e}^{\mathrm{i}\omega s_k}$) since, as is known [88, 119], in two dimensions the solutions to the Helmholtz equation vary as an integrable function of $\log\omega$ which vanishes at $\omega = 0$. (Special treatments are not necessary in the $d = 3$ case, where, given incident fields with smooth $\omega$-dependence, the Helmholtz solutions vary smoothly with $\omega$ for all real values of $\omega$ [77, 120].)

To design our quadrature rule in the non-smooth case, we recall the decomposition (2.18),

$$f(t_\ell) = \left(\int_{-W}^{-w_c} + \int_{-w_c}^{w_c} + \int_{w_c}^{W}\right) F(\omega)\mathrm{e}^{-\mathrm{i}\omega t_\ell}\,\mathrm{d}\omega =: I_-(t_\ell) + I_0(t_\ell) + I_+(t_\ell), \quad (2.28)$$

where using the notation introduced in (2.20), $I_-(t_\ell) = I_{-W}^{-w_c}[F](t_\ell)$ and $I_+(t_\ell) = I_{w_c}^{W}[F](t_\ell)$ can be treated effectively by means of the Fourier-based quadrature method developed in Section 6.1. Unfortunately, an application of that approach to $I_0(t_\ell) = I_{-w_c}^{w_c}[F](t_\ell)$ would not give rise to high-order accuracy, in view of the slow convergence of the Fourier expansion of $F$ in the interval $[-w_c, w_c]$—that arises from the singularity of $F$ at $\omega = 0$. We therefore develop a special quadrature rule for evaluation of the half-interval integral

$$I_0^{\omega_c}[F](t) = \int_0^{\omega_c} F(\omega)\mathrm{e}^{-\mathrm{i}t\omega}\,\mathrm{d}\omega \quad (2.29)$$

that retains the main attractive features of the integration methods developed in the previous section: high-order quadrature at fixed cost for evaluation at arbitrarily large times $t$.

**Remark 12.** *As in Section* 6.1*, the aforementioned t-independent errors can be achieved on the basis of fixed (t-independent) finite set, which will be denoted by* $\mathcal{F}^{sing}$ *in the present context, of frequency mesh points. The procedure used here, however, does not rely on Fourier approximation of F, cf. Remark* 11.

In order to evaluate the Fourier integral $I_0(t_\ell)$ at fixed cost for arbitrarily large times $t_\ell$, despite the presence of increasingly oscillatory behavior of the transform kernel, we rely on a certain *modified* "Filon-Clenshaw-Curtis" high-order quadrature approach [52] for non-smooth $F(\omega)$. The *classical* Filon-Clenshaw-Curtis method [108], which assumes a smooth function $F$, involves replacement of $F$ by its polynomial interpolant $Q_{\mathcal{N}}F$ at the Clenshaw-Curtis points followed by exact computation of certain associated "modified moments" (which are given by integrals of the Chebyshev polynomials multiplied by the oscillatory Fourier kernel). Importantly, this classical procedure eliminates the need to interpolate the target transform function at large numbers of frequency points as time increases. Additionally, on account of the selection of Clenshaw-Curtis interpolation points, the polynomial interpolants coincide with rapidly convergent Chebyshev approximations, and, therefore, the integration procedure converges with high-order accuracy. The accuracy resulting from use of a Chebyshev-based approach, which is very high for any value of $t$, actually improves as time increases: as shown in [52], the error in the method [108] asymptotically decreases to zero as $t \to \infty$.

The modified Filon-Clenshaw-Curtis method [52] we use in the present non-smooth-$F$ case (where $F$ is singular at $\omega = 0$ only) proceeds on the basis of a graded set

$$\Pi_{\mathcal{M},q} \coloneqq \left\{ \mu_j \coloneqq \omega_c \left( \frac{j}{\mathcal{M}} \right)^q : j = 1, \ldots, \mathcal{M} \right\}, \tag{2.30}$$

of points in $(0, \omega_c]$ which are used to form subintervals $(\mu_j, \mu_{j+1})$ $(1 \le j \le \mathcal{M} - 1)$. For a given meshsize $\mathcal{N}$, each one of these subintervals is then discretized by means of a Clenshaw-Curtis mesh containing $\mathcal{N}$ points, and all of these meshes are combined in a single mesh set $\mathcal{F}^{\text{sing}}$ (which contains a total of $|\mathcal{F}^{\text{sing}}| = 2(\mathcal{M}-1)\mathcal{N}$ points) that is to be used for evaluation of the integral $I_0$. Using this mesh, the Clenshaw-Curtis quadrature rule is applied to the evaluation of $I_{\mu_j}^{\mu_{j+1}}[F](t)$ (see Equation (2.20)). The integral $I_0^{\omega_c}[F](t)$ is finally approximated by a composite quadrature rule that mirrors the exact relation

$$I_0^{\omega_c}[F](t) = \sum_{j=2}^{\mathcal{M}} I_{\mu_{j-1}}^{\mu_j}[F](t). \tag{2.31}$$

The error introduced by this quadrature rule is discussed extensively in [52], and is of course dependent on the strength of the singularity. Briefly, in our context, and assuming $q > \mathcal{N} + 1$, the convergence order as $\mathcal{N} \to \infty$ is determined by the number $\mathcal{M}$ of integration subintervals used: letting $I_{\mathcal{N}} \approx I$ denote the approximate value produced by the composite quadrature rule using $\mathcal{N}$ Clenshaw-Curtis points per subinterval, we find the error in $I_{\mathcal{N}}$ satisfies [52, Thm. 3.6]

$$|I[F] - I_{\mathcal{N}}[F]| = O(\mathcal{M}^{-(1+\mathcal{N})}) \quad \text{as} \quad \mathcal{N} \to \infty.$$

Whenever necessary (i.e. for two-dimensional problems containing nonzero content at zero-frequency), the numerical results presented in Section 8 were produced using the values $\mathcal{M} = 4$, $\mathcal{N} = 8$, and $q = 9.1 > \mathcal{N} + 1$. Of course, two-dimensional problems whose frequency spectrum is bounded away from the origin, and three-dimensional problems (which always enjoy a smooth frequency dependence even around $\omega = 0$), do not require the use of the quadrature rule described above. The computational cost of this algorithm does not grow with increasing evaluation time $t$, consistent with the $O(1)$ large time sampling cost for the overall hybrid method.

## 7 Fast-hybrid wave equation solver: overall algorithm description

Utilizing a number of concepts presented in the previous sections and additional notations, including:

- An incident field $b$ of the form (1.8) for a given direction $\mathbf{p}$;
- A set $\mathcal{F} = \{\omega_1, \ldots, \omega_J\}$ of frequencies (n.b. $\mathcal{F} = \mathcal{F}^{\text{smooth}} \cup \mathcal{F}^{\text{sing}}$ in the 2D case, and $\mathcal{F} = \mathcal{F}^{\text{smooth}}$ in the 3D case, cf. Remark 11 and Remark 12)) used to discretize both the slow $H$-windowed Fourier transform $B_k^{slow}$ (cf. (2.14)) and the corresponding slow frequency scattered fields $U_k^{slow}$ (cf. (2.16));
- A set $C$ (of cardinality $N_\Gamma$) of scattering-boundary discretization points;
- Sets $\mathcal{R}$ (of cardinality $N_{\mathbf{r}}$) and $\mathcal{T} = \{t_\ell : 1 \le \ell \le N_t\}$) (of cardinality $N_t$) of discrete spatial and temporal observation points at which the scattered field is to be produced;

the single-incidence (see Remark 1)) time-domain algorithm introduced in this chapter is summarized in the following prescriptions.

F1 Evaluate numerically the windowed incident-field signal functions $w_k(t)a(t)$, in (2.8) ($k = 1, \ldots, K$), over a temporal mesh adequate for evaluation of the Fourier transforms mentioned in Step [F2].

F2 Obtain the boundary condition functions $B_k^{slow}(\omega)$ at frequency mesh values $\omega = \omega_j \in \mathcal{F}$ ($1 \leq j \leq J$) by Fourier transformation of the windowed signals in [F1], in accordance to (2.14).

F3 Solve a total of $J$ integral equations (1.19) under plane-wave incidence with incidence vector $\mathbf{p}$ (see Remark 1) at the frequencies $\omega_j \in \mathcal{F}$, to produce, for each $j$, boundary integral densities $\psi^t = \psi^t_{\mathbf{p}}(\mathbf{r}', \omega_j)$, $\mathbf{r}' \in C$.

F4 For each partition index $k = 1, \ldots, K$, produce the frequency-domain scattering boundary integral density $\psi_k^{slow}$ with support in $[-W, W]$ on the basis of the densities $\psi^t_{\mathbf{p}}$ via an application of Equation (2.15).

F5 Complete the frequency domain portion of the algorithm by evaluating, at each point $\mathbf{r} \in \mathcal{R}$, the frequency-domain solution $U_k^{slow}(\mathbf{r}, \omega_j)$ in Equation (2.16) by numerical evaluation of the layer potential integral in that equation, using the density values $\psi_k^{slow}(\mathbf{r}', \omega_j)$ at boundary points $\mathbf{r}' \in C$.

In order to evaluate the solution $u$ for all points in the set $\mathcal{R}$, and for all times in the set $\mathcal{T}$, the algorithm proceeds by transforming each windowed solution back to the time domain using the quadrature methods presented in Section 6. The following prescriptions thus complete the overall hybrid solver.

T0 For $k = 1$ to $K$ and for each $\mathbf{r} \in \mathcal{R}$ do:

T1 a) (3D case) Obtain the coefficients $c_m = c_m(\mathbf{r})$ of the Fourier series expansions of the form (2.22) for the functions $F(\omega) = U_k^{slow}(\mathbf{r}, \omega)$ in the interval $\omega \in [-W, W]$.

b) (2D case) Obtain the coefficients $c_m^{(1)} = c_m^{(1)}(\mathbf{r})$ and $c_m^{(2)} = c_m^{(2)}(\mathbf{r})$ of the Fourier series expansions of the form (2.22) for the functions $F(\omega) = U_k^{slow}(\mathbf{r}, \omega)$ in the domains $[-W, -\omega_c]$ and $[\omega_c, W]$, respectively. (n.b. $\mathcal{F}^{\text{smooth}}$ is a discretization of the set $[-W, -\omega_c] \cup [\omega_c, W]$.)

T2 a) (3D case) Evaluate the discrete scaled convolution using the fast algorithms described in Section 6.1.2 with coefficients $c_m = c_m(\mathbf{r})$ obtained in (T1a) which, on account of Equations (2.13) and (2.20), yields $u_k(\mathbf{r}, t)$ for $t \in \mathcal{T}$.

b) (2D case) Evaluate two discrete scaled convolutions using the fast algorithms described in Section 6.1.2 with coefficients $c_m = c_m^{(1)}(\mathbf{r})$ and $c_m = c_m^{(2)}(\mathbf{r})$ to produce, for all $t \in \mathcal{T}$, $I_- = I_-(t)$ and $I_+ = I_+(t)$ for $F = U_k^{slow}$ as in Section 6.2.

c) (2D case continued) Evaluate the singular integral approximation $I_0$ using the methods in Section 6.2 with the frequency points in $\mathcal{F}^{\text{sing}}$.

d) (2D case continued) Evaluate $u_k(\mathbf{r}, t) = I_-(t) + I_0(t) + I_+(t)$ for $t \in \mathcal{T}$ (cf. (2.28)).

T4 End do

T5 Evaluate $u = \sum_{k=1}^{K} u_k(\mathbf{r}, t)$ (cf. Equation (2.10), (2.32)).

T6 End

**Remark 13.** *Calling $u_k^{W,J}$ the numerical approximations to the functions $u_k$ produced under the finite bandwidth $W$ and on the basis of the $J$ quadrature points in $\mathcal{F}$, the equation in algorithm step [T5] can more precisely be expressed in the form*

$$u(\mathbf{r}, t) \approx \sum_{k=1}^{K} u_k^{W,J}(\mathbf{r}, t). \tag{2.32}$$

*The errors $e = e(W, J)$ inherent in this approximation decay superalgebraically fast* uniformly in $\mathbf{r}$ and *$t$ as $W$ grows (see Remark* 4*). The frequency-quadrature errors resulting from the methodology described in Section* 6 *for the integral in* (2.13)*, further, decay superalgebraically fast (or, in the two-dimensional case, with prescribed high-order) as $J$ increases,* uniformly in *$t$ (see Section* 6.1.1 *and Section* 6.2 *for a full discussion of frequency-quadrature errors). Solutions with quadrature errors uniform in $\mathbf{r}$ can be obtained either on the basis of the time-domain single layer potential for* (1.6) *(Kirchhoff formula) for the time-dependent density $\psi_k$, or by means of an adequate treatment of the high-frequency oscillations in frequency-domain space that, in accordance with Equation* (2.16)*, arise for large values of $|\mathbf{r}|$.*

## 8 Numerical results

After a brief demonstration of the proposed quadrature rule in a simple context (Section 8.1), this section demonstrates the convergence of the overall algorithm (Section 8.2) and it presents solutions produced by the solver in the two- and three-dimensional contexts (Sections 8.3 to 8.4). In particular, Section 8.3 presents a

few spatial screenshots of long-time propagation experiments (enabled by the time-partitioning methodology described in Section 5, see Figure 2.5), as well as, in Figure 2.6, results for a configuration which gives rise to significant numbers of multiple-scattering events. Section 8.4, finally, presents a variety of three-dimensional examples, including accuracy as well as computational- and memory-cost comparisons with results produced by means of recently introduced convolution-quadrature and time-domain integral-equation algorithms. Section 8.4 also illustrates the applicability of the methods introduced in this thesis to a scattering surface provided in the form of a CAD description (Computer Aided Design).

## 8.1 Fourier transform quadrature demonstration

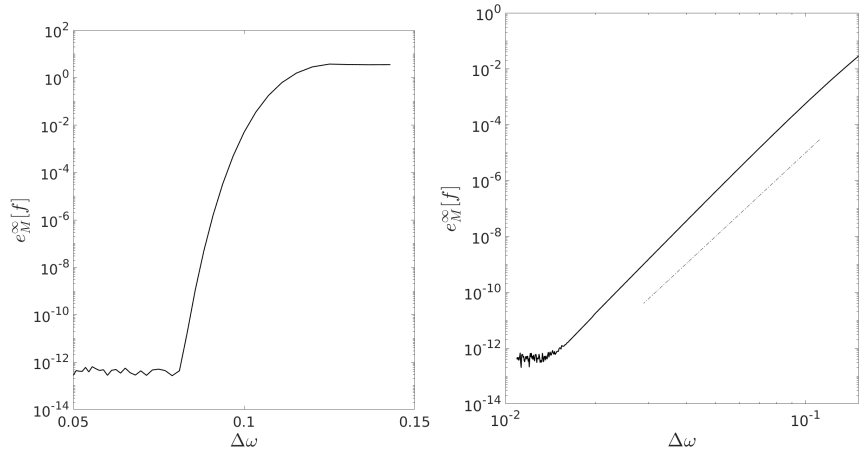


Figure 2.3: Error $e_M^{\infty}$ resulting from the DFT-based (left) and 10th-order FC(Gram)-based (right) FRFT-accelerated Fourier Transform methods (cf. Remark 10) as a function of $\Delta\omega$. The right figure also includes a 10th-order slope, for reference.

Figure 2.3 presents results of an application (to the function $F(\omega) = \mathrm{e}^{-\frac{1}{4}\omega^2}\mathrm{e}^{\mathrm{i}10\omega}$) of two main components of the Fourier-transform algorithms described in Section 6.1, namely the algorithms that evaluate trigonometric expansions (2.22) by means of DFT on one hand, and on the basis of the FC(Gram) algorithm of accuracy order 10, on the other (cf. Remark 10). (FC expansions of order other than 10 can of course be used, but order-10 expansions were found perfectly satisfactory in our contexts.) Noting that $|F(-12)| = |F(12)| \approx \varepsilon_{\text{mach}}$ (where $\varepsilon_{\text{mach}}$ denotes machine precision), the left (resp. right) portion of Figure 2.3 displays the accuracy of the Fourier-series based (resp. the FC(Gram)-based) algorithm presented in Section 6.1 for evaluation of Fourier integrals of the form (2.20) in interval $[-12, 12]$ (resp. in the interval $[0, 12]$). The fast (high-order) convergence of the quadrature method as

$\Delta\omega \to 0$ that is demonstrated in the present simple example has a significant impact on the efficiency of the algorithm—which requires solution of an expensive integral equation (1.19) for each frequency discretization point $\omega_j \in \mathcal{F}^{\text{smooth}}$, $\omega_{j+1} - \omega_j = \Delta\omega$, for $j = 2, \ldots, |\mathcal{F}^{\text{smooth}}| = M$ (cf. Remark 11).

## 8.2 Solution convergence

This section presents solution of a problem of scattering under incident radiation $u^{inc}(\mathbf{r}, t)$ given by the Fourier transform of the function

$$U^{inc}(\mathbf{r}, \omega) = \mathrm{e}^{-\frac{(\omega-\omega_0)^2}{\sigma^2}} \mathrm{e}^{\mathrm{i}\omega\widehat{\mathbf{k}}_{inc}\cdot\mathbf{r}} \tag{2.33}$$

with respect to $\omega$, with $\omega_0 = 12$, $\sigma = 2$ and, letting $\mathbf{k} = \mathbf{e}_x + \frac{1}{2}\mathbf{e}_y$, $\widehat{\mathbf{k}}_{inc} = \frac{\mathbf{k}}{\|\mathbf{k}\|}$. The scatterer is a two-dimensional kite-shaped structure $(r_1(t), r_2(t)) = (\cos(t) + 0.65\cos(2t) - 0.65, 1.5\sin(t))$, $(0 \le t \le 2\pi)$ which is also used in the subsequent example (cf. Figure 2.5). Figure 2.4 presents the time trace of the scattered field displayed in the left image at the observation point $(2, 2)$, which lies at a distance of approximately 1.9 spatial units from the scattering boundary. The right image in Figure 2.4 displays the error $e$ in the center image as a function of $\Delta\omega$. (For simplicity, the fixed numerical bandwidth value $W = 24$ together with a sufficiently fine fixed spatial discretization were used in all cases to ensure frequency domain solution errors of the order of machine precision.) The right image clearly demonstrates the superalgebraically-fast convergence of the algorithm (relative to a converged reference solution computed with $\Delta\omega = 0.12$) as the frequency-domain discretization is refined.

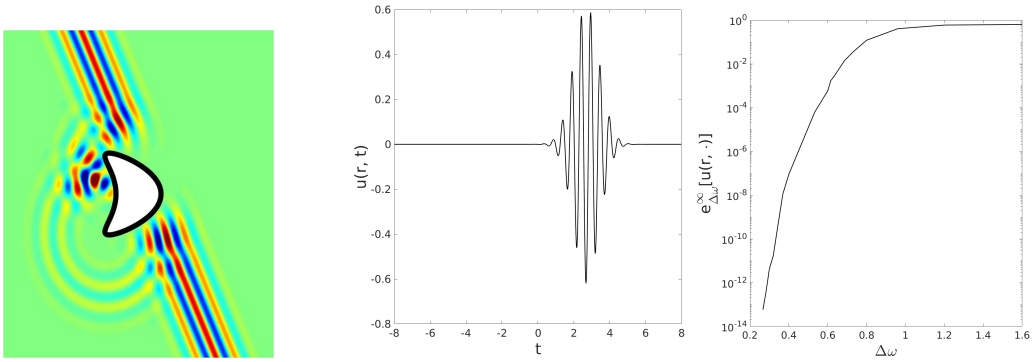


Figure 2.4: Scattered field (left), time trace at point $\mathbf{r} = (2, 2)$ exterior to the scatterer (center) and maximum all-time error $e^{\infty}_{\Delta\omega}$ at $\mathbf{r} = (2, 2)$ as a function of the frequency-domain discretization $\Delta\omega$ (right) resulting from an application of the overall fast hybrid method to the problem considered in Section 8.2.

### 8.3 Full solver demonstration: 2D examples

This section presents results produced by the proposed methodology for two 2D problems of sound-soft scattering—each of which demonstrates a significant aspect of the proposed approach.

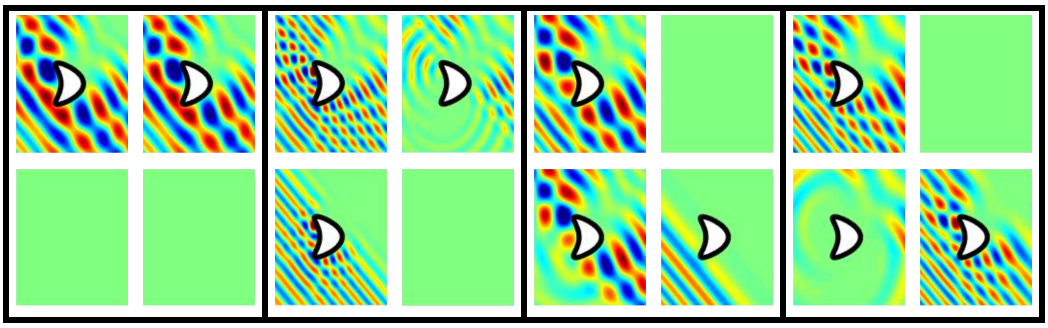

Figure 2.5: 2D active-partition tracking demonstration. Each of the four large panels show the solution at increasing times, left to right.

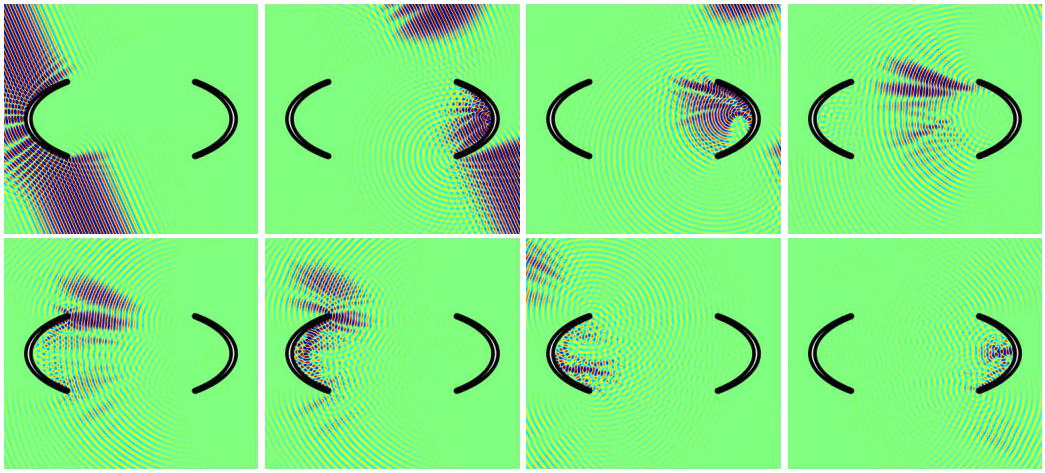

Figure 2.6: Total fields in the "Whispering Gallery" experiment mentioned in the text. Note the multiple reflections that take place at the elliptical surfaces which, over long propagation times, give rise to a significant number of scattering events. The time sequence starts left-to-right on the first row, and then continues left-to-right on the second row.

Results for incident wave-trains of longer duration, which include a time-domain chirp of the form

$$\begin{aligned} u^{inc}(\mathbf{r},t) &= -a(t-\mathbf{r}\cdot\widehat{\mathbf{k}}_{inc}), \quad \text{with} \\ a(t) &= \sin(g(t)+\frac{1}{4000}g^2(t)), \\ g(t) &= 4t+6\cos(\frac{t}{\sqrt{12}}), \end{aligned} \tag{2.34}$$

and $\widehat{\mathbf{k}}_{inc}$ as in Section 8.2, are presented in Figure 2.5, which demonstrates the time partitioning strategy (2.7) in conjunction with the active partition-tracking method mentioned in Remark 7. The four large panels in this figure display results corresponding to four subsequent time snapshots. In each one of the panels, the top-left subfigure presents the total field $u^{tot}(\mathbf{r}, t)$ at the time represented by the panel. The remaining subfigures in each panel show the contribution to $u^{tot}(\mathbf{r}, t)$ from each one of the three corresponding time-windowed partitions used in this example. As indicated in Remark 7, blank subfigures in Figure 2.5 indicate that the corresponding partition does not contribute to $u^{tot}$ at the time snapshot represented by the panel. Using an adequate number of time windows (of window width $H = 10$) as well as a total of 200 frequency domain solutions (with bandlimit $W = 15$), time domain solutions at any required time can be obtained.

Figure 2.6 demonstrates the ability of the proposed method to account for complex multiple-scattering effects over long periods of time. The upper left image in this figure displays an incident wave impinging on a "whispering gallery" geometry; subsequent images to the right and in the lower sections of the figure present solution snapshots at a variety of representative times.

### 8.4 Full solver demonstration: 3D examples and comparisons

This section demonstrates the character of the proposed algorithm for 3D problems of sound-soft scattering, and it provides performance comparisons with two solvers introduced recently. All numerical experiments in this section were obtained by means of a Modern Fortran implementation of the proposed approach, using the Intel Fortran compiler version 17.0, on a 24-core system containing two 12-core Xeon E5-2670 CPUs [1]. The first example concerns a problem of scattering by a sphere of physical radius 1.6 (whose choice facilitates certain comparisons) illuminated under plane-wave incidence given by $u^{inc}(\mathbf{r}, t) = -a(t - \widehat{\mathbf{k}} \cdot \mathbf{r})$, where the signal function $a$ is given by $a(t) = 5\mathrm{e}^{-(t-6)^2/2}$. The frequency domain was truncated to the interval $[-W, W]$ with numerical bandwidth $W = 6.5$, and the problem was then discretized with respect to frequency on the basis of 41 ($J = 80$) equi-spaced frequencies $\omega$ in the interval $[0, W]$. Approximate solutions to the integral equation (1.19) for each one of these frequencies were obtained by means of the linear system solver GMRES with a relative residual tolerance of $10^{-8}$. Table 2.2 (left) lists the frequency domain spatial discretization parameters used. The row labeled "This work" in Table 2.3

[1] Thanks are due to Emmanuel Garza for facilitating the use of the existing 3D frequency-domain codes [30].

Parameter selection, comparison with [14].

| $\omega$ | $N$ | $N_\beta$ | $N_{\text{split}}$ | $\varepsilon$ |
|---|---|---|---|---|
| $[5.5, 6.5]$ | 20 | 150 | 3 | $9.0 \cdot 10^{-8}$ |
| $[4.5, 5.5]$ | 22 | 150 | 2 | $6.7 \cdot 10^{-9}$ |
| $[3.5, 4.5]$ | 21 | 150 | 2 | $1.3 \cdot 10^{-8}$ |
| $[2.5, 3.5]$ | 21 | 130 | 2 | $3.1 \cdot 10^{-8}$ |
| $[1.5, 2.5]$ | 21 | 120 | 2 | $2.7 \cdot 10^{-8}$ |
| $[0.0, 1.5]$ | 20 | 100 | 2 | $5.1 \cdot 10^{-8}$ |

Parameter selection, comparison with [9].

| $\omega$ | $N$ | $N_\beta$ | $N_{\text{split}}$ | $\varepsilon$ |
|---|---|---|---|---|
| $[25, 45]$ | 20 | 90 | 3 | $1.2 \cdot 10^{-4}$ |
| $[20, 25]$ | 18 | 90 | 3 | $1.4 \cdot 10^{-4}$ |
| $[10, 20]$ | 15 | 90 | 3 | $2.8 \cdot 10^{-4}$ |
| $[5.0, 10]$ | 12 | 90 | 2 | $1.8 \cdot 10^{-4}$ |
| $[0.0, 5.0]$ | 10 | 90 | 2 | $1.9 \cdot 10^{-5}$ |

Table 2.2: Spatial discretizations used for the frequency-domain solver [30] in connection with comparisons with references [14] and [9] and associated numerical errors, for the $\omega$-ranges as listed in the first column of each table. In particular, the tables demonstrate that, as expected, finer discretizations need to be used, for a given desired accuracy, as the acoustical-size of the problems treated grows. In these tables, $N^2$ and $N_{\text{split}}^2$ denote the number of points per patch and the number of patch subdivisions of the original 6-patch geometry used, respectively, so that the total number of degrees of freedom is $6N^2N_{\text{split}}^2$. (For the definition and significance of the parameter $N_\beta$, see [30].) The quantity $\varepsilon$, finally, equals the numerical error at the spatial point $\mathbf{r} = \mathbf{r}_0$ with $\mathbf{r}_0$ as indicated in the text in each comparison case, for the solution at frequency equal to the upper limit of the frequency interval. Mie series solutions were used in all cases as references for determination of the solution errors $\varepsilon$.

presents the maximum solution error resulting from an application of the proposed solver together with the corresponding walltime and memory usage. We see that a computing time of approximately four minutes and a memory allocation of 1.2 GB suffice to produce the solution with an absolute maximum error (measured relative to an exact solution obtained via a Mie series representation) of the order of $10^{-7}$ at the observation point $\mathbf{r} = (-1.8, 0, 0)$, or 0.2 units away from the scatterer.

This example can be related to a test case considered in [14], which introduces a temporally and spatially high-order time-domain integral equation solver, implemented in Matlab, which relies on the built-in sparse matrix-vector multiplication function for time-stepping and a precompiled Fortran function for assembly of the system matrix. A scattering configuration including a physically realizable incident field is considered in [14, Sec. 4.3] which presents computing times but reports errors in the median. For comparison purposes, however, it seems more appropriate to quantify errors in some adequate norm—and, thus, we chose to provide a comparison with results presented in Sec. 4.2 of that paper—where a "cruller" scattering surface of diameter 3.2 is used, which is illuminated by an artificial (not physically realizable but commonly used as a test case) point source emanating from a point interior to

the surface. In lieu of solving for the specialized cruller geometry, we compare those results to the sphere results provided above. Noting that, with the same diameter, the sphere has a larger surface area (32.2 square units) than the cruller geometry (23.5 square units), the sphere problem may be considered to be a somewhat more challenging test case in regard to memory usage and computing cost. Errors for the test case in [14, Sec. 4.2] can be read from the second contour plot provided for the cruller geometry in [14, Fig. 8], which displays an error of approximately $10^{-7}$ for $h = \Delta t \approx 0.0367$. The memory usage and computing time required by that test can be deduced from [14, Sec. 4.3], and they amount to 290 GB of memory and 101.75 minutes of computing time. (The $101.75 = 23 + \frac{30}{8} \times 21$ minute computing time estimate was obtained as the sum of precomputation and time-stepping times, as reported in [14, Sec. 4.3], but accounting for a simulation over 30 time units, instead of the 8 time units reported in that section.) In view of Table 2.3, we suggest that, even for short propagation times, the proposed method compares very favorably with the approach [14] in terms of both computational time and memory requirements.

| — | $\|\|e\|\|_\infty$ | Time | Mem. |
|---|---|---|---|
| This work | $1.6 \cdot 10^{-7}$ | 4.1 | 1.2 |
| Ref. [14] | $\approx 10^{-7}$ | 101.75 | 290 |

Table 2.3: Comparison with results in [14]. "This work" data corresponds to runs on a 24-core computer with Sandy Bridge microarchitecture, while reference [14] reports use of a 28-core computer with the more recent Broadwell microarchitecture. The columns "Time" and "Mem." list the required wall times (in minutes) and the memory usage (in GB).

| — | $\|\|e\|\|_\infty$ | Time | Mem. |
|---|---|---|---|
| This work | $2.2 \cdot 10^{-4}$ | 4.3 | 1.6 |
| Ref. [9] | $2.1 \cdot 10^{-3}$ | 40.1 | 56.8 |

Table 2.4: Comparison with results in [9]. As in that reference, the computational times are reported in CPU core-hours. The columns "Time" and "Mem." list the required CPU core-hours and the memory usage (in GB). The results in [9] (accelerated) correspond to runs on Santa Rosa Opteron CPUs, while the results in "This work" (unaccelerated) were obtained on the more recent Intel Sandy Bridge CPUs.

The next example in this section concerns the scattering of a wide-band signal of the form $u^{inc}(\mathbf{r}, t) = -0.33 \sum_{i=1}^{3} \exp\left[\frac{(t-\mathbf{e}_i \cdot \mathbf{r} - 6\,\sigma - 1)^2}{\sigma^2}\right]$ from the unit sphere, where we have set $\mathbf{e}_1 = (1, 0, 0)$, $\mathbf{e}_2 = (0, 1, 0)$, $\mathbf{e}_3 = (0, 0, 1)$, and $\sigma = 0.1$. We solve this problem to an absolute error level of $2.2 \cdot 10^{-4}$ (evaluated by comparison with the exact solution obtained via a multi-incidence Mie series representation) at the observation point $\mathbf{r} = \mathbf{r}_0 = (2.5, 0, 0)$. The frequency domain was truncated to the interval $[-W, W]$ with numerical bandwidth $W = 45$, and the problem was then

discretized with respect to frequency on the basis of 91 ($J = 180$) equi-spaced frequencies $\omega$ in the interval $[0, W]$. Approximate solutions to the integral equation (1.19) for each one of these frequencies were obtained by means of the linear system solver GMRES with a relative residual tolerance of $10^{-4}$. Table 2.2 (right) lists the frequency domain spatial discretization parameters used. Figure 2.7 displays a time-trace of our solution, and Table 2.4 presents relevant performance indicators; the core time listed for our solver was calculated as 24 times the wall time required by the parallelized frequency-domain solver to solve all 91 frequency-domain problems in the 24-core system used, followed by a single core run that evaluates the time trace. Each frequency domain problem was run, in parallel, on all 24 cores.

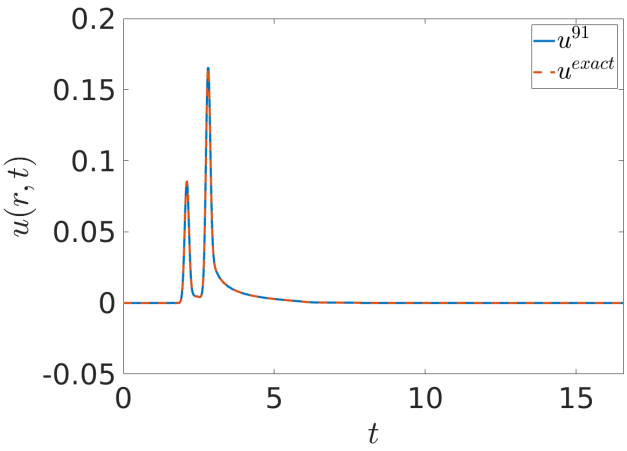


Figure 2.7: Scattering of a wide-band signal from the unit sphere. This figure presents the time traces of the exact and numerical scattered field computed (on the basis of 91 frequency-domain solutions) by the proposed hybrid method. Corresponding results produced by a novel convolution-quadrature implementation can be found in [9, Figure 5].

This wide-band sphere-scattering example was previously considered in the most recent high-performance implementation [9], including fast multipole and $\mathcal{H}$-matrix acceleration, of the convolution quadrature method. The accuracies produced and the computational costs required by both the present solver (for which frequency-domain solutions were computed without use of acceleration methods) and the one introduced in [9] are presented in Table 2.4, including CPU core-hours and memory storage. We see that, even without the significant benefits that would arise from frequency-domain operator acceleration in the present context, the proposed solver requires significantly shorter computing times and lower memory allocations, by factors of approximately ten and thirty-five, respectively, when compared with those

required by the solver [9]. (Note: the contribution [9] does not directly report the solution error, but it does provide graphical evidence by comparing the time-traces of the solutions obtained, at the observation point $\mathbf{r} = \mathbf{r}_0 = (2.5, 0, 0)$, by means of two different spatio-temporal discretizations, for which it was reported that "on this scale [the scale of the graph] the solutions are practically indistinguishable." A direct comparison of the dataset values (which was kindly provided to us by the authors [76]) to the exact Mie solution allowed us to determine a maximum error of $2.1 \cdot 10^{-3}$ in the wide-band sphere test in [9]. Our solution is also graphically indistinguishable from the time-domain response calculated by means of a Mie series, and we report a numerical-solution error of $2.2 \cdot 10^{-4}$.)

Finally, Figure 2.8 presents results of an application of the proposed algorithm to a 3D scatterer (represented by the multi-patch CAD description displayed in the figure), for the Gaussian-modulated incident field

$$U^{inc}(\mathbf{r}, \omega) = \mathrm{e}^{-\frac{(\omega-\omega_0)^2}{\sigma^2}} \mathrm{e}^{\mathrm{i}\omega\widehat{\mathbf{k}}_{inc}\cdot\mathbf{r}}$$

with $\omega_0 = 15$, $\sigma = 2$ and $\widehat{\mathbf{k}}_{inc} = \mathbf{e}_z$. (This figure was prepared using the VisIt visualization tool [42].) A total of 250 frequency domain integral-equation solutions of Equation (1.19) for frequencies below the numerical bandlimit $W = 25$, which were produced by the methodology and software described in [30], suffice to produce the solution for all times.

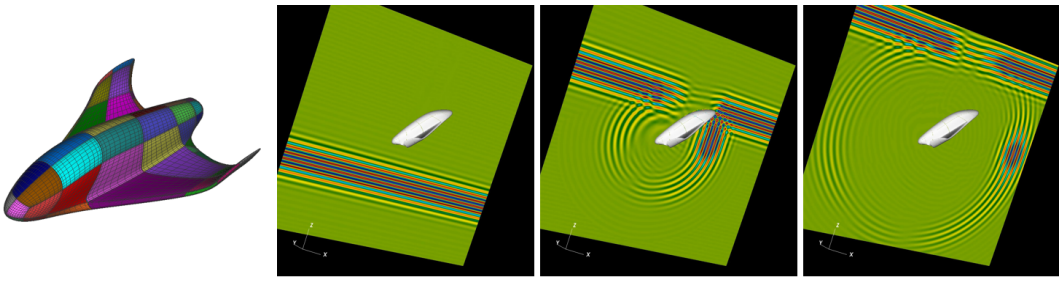

Figure 2.8: Field scattered by a 3D glider structure.

### 8.5 Long-time 3D numerical demonstration

This section demonstrates the capability of the proposed methodology for the simulation of long-time scattering. We use the identical glider geometry to that introduced

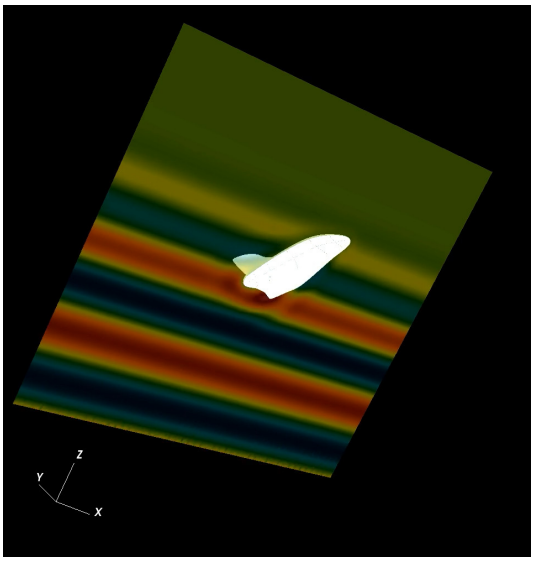


Figure 2.9: A snapshot of the total field (from all $K = 12$ time windows), near the beginning of the 3D scattering of the long-duration impinging wave.

in the previous subsection. The incident field used was generated by the chirp signal

$$\begin{aligned} u^{inc}(\mathbf{r}, t) &= f(t - \mathbf{r} \cdot \widehat{\mathbf{k}}_{\text{inc}}), \quad \text{with} \\ f(t) &= \sin(g(t) + \frac{1}{4000} g^2(t)), \\ g(t) &= 4t + 6\cos(\frac{t}{\sqrt{12}}), \end{aligned} \tag{2.35}$$

in the direction $\widehat{\mathbf{k}}_{\text{inc}} = (0, 0, 1)$.

The simulation was run on a machine with 2x 12-core Intel Xeon CPUs running at 2.30 GHz, with 128 GB of memory. Using a numerical bandwidth of $W = 15$ for this problem, a total of 81 ($J = 160$) integral equations were solved. The solution was computed on a 250x250 grid with 1600 time samples covering $t \in [0, 200]$; see Figure 2.9 and Figure 2.10. Some timings required to produce the final solution are given in Table 2.5.

## 9 General incident fields and boundary values

This section provides an extension of the hybrid scattering-solver methodology proposed elsewhere in the present Chapter 2 that enables treatment of arbitrary Dirichlet boundary values—not necessarily given (as they are in the setting of scattering problems) by the boundary values of an "incident-field" solution of the wave equation. In particular, this section concerns the use of the hybrid method to treat the scattering of generic incident fields (i.e., arbitrary solutions to the wave

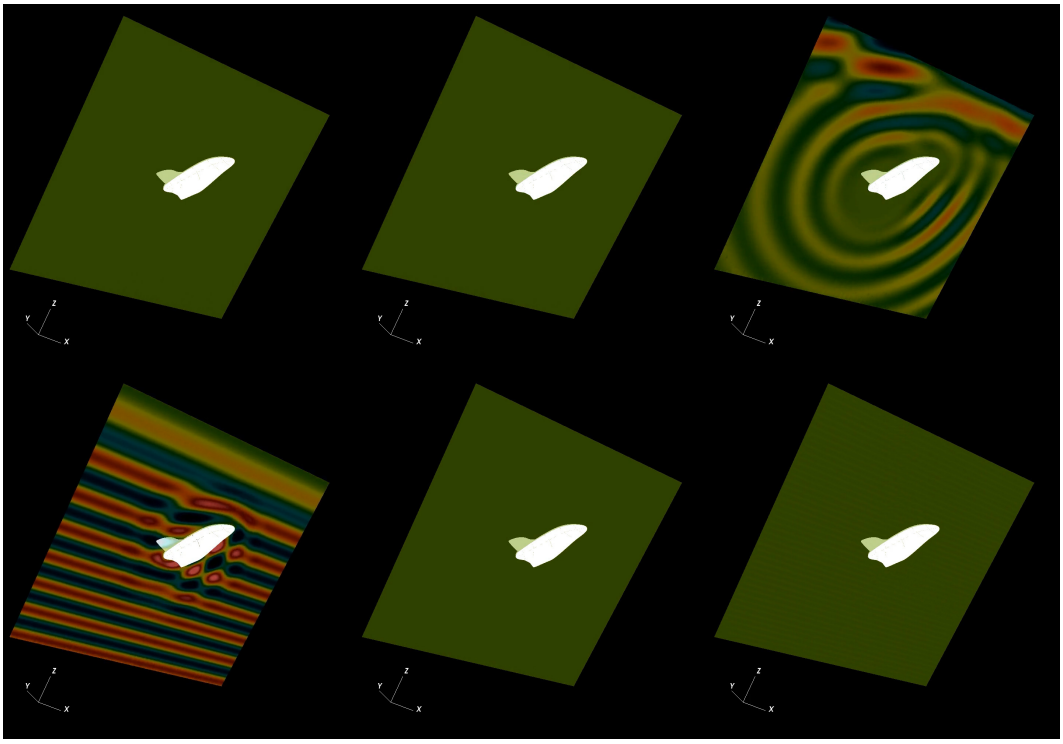

Figure 2.10: Array figure showing solutions from the first 6 (of $K = 12$) time windows, which demonstrates the many wavelengths of (dispersion-error free) 3D wave scattering simulated in the proposed methodology.

| Solution step | Time |
|---|---|
| Freq. Int. Eq. Setup | 38 [min.] |
| Freq. Int. Eq. Solve | 28 [min.] |
| Freq. Field Eval. | 11 [min.] |
| Transient Field Eval. | 140 [sec.] |
| **Total CPU time** | **81 [min.]** |

Table 2.5: Required computing times to produce the total field for the scattering of the chirp incident field from a glider geometry. In particular, 1.4 billion evaluations of $u_k$ were required for the transient field evaluation step; while the cost of all other solution steps are independent of both desired solution time and $T^{\text{inc}}$, the transient field evaluation costs do grow with time in the absence of the methods introduced in Chapter 4.

equation Equation (1.6) in free space rather than the sum of a few sources or plane waves). It is easy to see that this is a more challenging problem than the problems treated earlier in this chapter, by considering e.g. an incident plane wave (or source) whose direction of propagation (resp. location) varies over time, as demonstrated in Figure 2.12. This chapter proposes a hybrid frequency-time method that still delivers an $O(1)$ cost for arbitrarily-large-time solution evaluation.

In the case of arbitrary boundary data, windowing of the form (2.7) used so far throughout this chapter is not applicable, and indeed the windowed boundary data for the wave equation introduced in Chapter 2 for this context was (see (2.6))

$$b_k(\mathbf{r}, t) = w_k(t) b(\mathbf{r}, t), \quad 1 \leq k \leq K, \tag{2.36}$$

where $b$ is the incident field and $w_k$ is the compactly-supported temporal window function, centered at $t = s_k$. Inspection of Equation (2.36) shows that $b_k(\mathbf{r}, t)$ no longer satisfies the wave equation (cf. the boundary condition windowing Equation (2.7) which remains a solution).

The approach, outlined in what follows, is to solve, for each required discrete frequency $\omega$, a number of frequency-domain problems (of identical frequency $\omega$) with varying boundary incidence, where the set of boundary values forms an approximating basis for the windowed boundary data. Indeed, in order to facilitate the re-use of integral equation solutions across time windows where the spatial variation of incidence could be significantly different, we note that it is essential to represent an arbitrary incident field in some compatible basis, so that such basis elements can be re-used across time partitions. Discussion of the growth of the number of these problems and their associated cost as the acoustical size of the problem increases is presented in Section 9.2. We note that the use of an iterative solver such as GMRES to solve the linear algebra problem arising from discretization of the integral equation (e.g. (1.21)) may be prohibitively expensive because no use can be made of the fact that the same linear operator (i.e., a discretization of the Helmholtz equation at a given frequency $\omega$) is used in each problem. We thus propose to utilize a direct solver (e.g. any of the fast direct solvers mentioned in Section 9.2) to rapidly solve, for each frequency, these multiple right-hand side problems. Then, the desired boundary density function is synthesized as a combination of these auxiliary boundary integral equation solutions. Crucially, none of the frequency-domain problems need to be re-solved for each new time partition $k$, as the problems, e.g. the integral equations, to be solved are independent of time-domain information—thereby preserving the $O(1)$ claimed required Helmholtz solves.

### 9.1 Boundary value approximation via spectral boundary basis

At the highest-level, the proposed approach to the treatment of long-duration incident fields of a fully general nature relies on accurate approximations of arbitrary Dirichlet data by a certain limited basis. The method proposed in this subsection is applicable in three dimensions, and is included for completeness, while the method demonstrated in all experiments in two dimensions is given in the following subsection.

The procedure begins by first Fourier transforming the windowed time-domain boundary data for each $\mathbf{r} \in \Gamma$,

$$B_k^{slow}(\mathbf{r}, \omega) = \int_{-H}^{H} b_k(\mathbf{r}, t + s_k) \mathrm{e}^{\mathrm{i}\omega t} \, \mathrm{d}t,$$

which produces for each $\mathbf{r} \in \Gamma$ the frequency-domain boundary data $B_k^t(\mathbf{r}, \omega)$ through the relation $B_k^t(\mathbf{r}, \omega) = \mathrm{e}^{\mathrm{i}\omega s_k} B_k^{slow}(\mathbf{r}, \omega)$ (see (2.11)).

The problem then becomes one of approximation of, for each $\omega \in \mathcal{F}$, the on-surface functions $B_k^{slow}(\mathbf{r}, \omega)$. An elementary strategy proceeds by considering a decomposition of the surface $\Gamma$ into a union of $N_\gamma$ non-overlapping "logically-quadrilateral" parametrized patches as introduced in [30] (the presentation here closely follows the presentation there). More specifically, given $N_\gamma$ parametrization functions $\chi_\ell$

$$\chi_\ell : [-1, 1]^2 \to \mathbb{R}^3, \quad \ell = 1, \ldots, N_\gamma,$$

that cover the surface $\Gamma$,

$$\Gamma = \bigcup_{\ell=1}^{N_\gamma} \left\{ \chi_\ell(x, y) | (x, y) \in [-1, 1]^2 \right\}.$$

Letting $\Gamma_\ell$ be the subset of $\Gamma$ covered by $\chi_\ell$, the mapping $\chi_\ell$ thus maps coordinates $(x, y)$ on the logical unit square onto the points $\mathbf{r} \in \Gamma_\ell \subset \Gamma$. It is known that Chebyshev functions possess excellent approximation properties on the unit square. Thus, an effective basis in which to express arbitrary incident data is the set of $N_{\mathcal{B}}^2$ product-Chebyshev functions

$$B_k^{slow}(\chi_\ell(x, y), \omega) = \sum_{m=0}^{N_{\mathcal{B}}} \sum_{n=0}^{N_{\mathcal{B}}} a_{\ell mn} T_m(x) T_n(y).$$

Thus, define the basis set

$$\mathcal{B} = \{\beta_{\ell mn}(\mathbf{r}) : \beta_{\ell mn} \equiv 0 \text{ for } \mathbf{r} \notin \Gamma_\ell;\ \beta_{\ell mn}(\chi_\ell(x, y)) = T_m(x) T_n(y) \text{ for } \mathbf{r} \in \Gamma_\ell\}.$$

Define the solution set $\mathcal{Z}(\omega) = \{\zeta_{\ell mn}(\mathbf{r},\omega) : \ell = 1,\ldots,N_\gamma;\ m,n = 1,\ldots,N_\mathcal{B}\}$ as the solution of the Helmholtz boundary integral equation at frequency $\omega$ with boundary data $\beta_{\ell mn}$. (Note that, despite the discontinuous nature of the basis elements in $\mathcal{B}$ at the boundary of the patches $\Gamma_\ell$, smooth solutions $\psi_k$ can in fact still be represented in this basis.) An effective approximation then becomes

$$\psi_k^{slow}(\mathbf{r},\omega) = \sum_{\ell=1}^{N_\gamma}\sum_{m=0}^{N_\mathcal{B}}\sum_{n=0}^{N_\mathcal{B}} a_{\ell mn}\zeta_{\ell mn}(\mathbf{r},\omega), \quad \mathbf{r}\in\Gamma. \tag{2.37}$$

Use of fast direct solvers can be effective for the efficient solution, for each $\omega \in \mathcal{F}$, of each of the integral equations with right-hand sides taken from the set $\mathcal{B}$ (with $N_\gamma N_\mathcal{B}^2$ elements). The general boundary data problem in three dimensions requires use of adequately efficient direct solvers for surface scattering problems (see also Section 9.2 for more details, including cost estimates and asymptotics) which we have not as yet implemented, and which have been left for future work. Instead, we shift focus to the two-dimensional problem which is more computationally tractable at the present time.

### 9.1.1 Boundary value Fourier series expansion method

In two dimensions, the number of required degrees of freedom is often small enough to use direct solvers. We restrict our presentation now to two-dimensional problems, and consider the boundary of the obstacle to be parametrized by the smoothly periodic function $\mathbf{r} = \mathbf{r}(\tau)$, with $\tau \in [0, 2\pi]$, implying it can be expanded in a trigonometric series:

$$\mathbf{r}(\tau) \approx \sum_{n=-N/2}^{N/2-1} c_n \mathrm{e}^{-\mathrm{i}n\tau},$$

with error decaying rapidly as $N \to \infty$. (Note that in the case of a multiply-connected scatterer, the strategy described requires modification since the parametrization is no longer smoothly periodic, a case discussed later in this section.) First, as in the previous section, we Fourier transform the windowed boundary functions $b_k(\mathbf{r},t)$, $(1 \le k \le K)$, producing frequency-domain boundary incidence functions $B_k^{slow}(\mathbf{r},\omega)$. Next, expanding these functions into Fourier series, we have

$$B_k^{slow}(\mathbf{r}(\tau),\omega) = \sum_{n=-N/2}^{N/2-1} \mathcal{I}_n \mathrm{e}^{-\mathrm{i}n\tau}, \tag{2.38}$$

with a cost of $O(N\log(N))$ to find the coefficients $\{\mathcal{I}_n\}$. We solve boundary integral equations for each basis element in $\mathcal{B} = \{\mathrm{e}^{-\mathrm{i}n\tau},\ (-N/2 \le n \le N/2-1)\}$ of boundary

conditions; using the indirect formulation (1.21), we solve

$$\frac{1}{2}\zeta_n(\mathbf{r},\omega) + (K_\omega\zeta_n)(\mathbf{r},\omega) - \mathrm{i}\eta(S_\omega\zeta_n)(\mathbf{r},\omega) = \mathrm{e}^{-\mathrm{i}n\tau(\mathbf{r})}, \quad \mathbf{r}\in\Gamma. \tag{2.39}$$

which yields the solution set $\mathcal{Z} = \{\zeta_n(\mathbf{r}(\tau),\omega),\ (-N/2 \le n \le N/2-1)\}$. It is important to observe that solution of Equation (2.39) for each element of $\mathcal{B}$ involves the same system matrix, and therefore the strategy we propose makes use of this fact, utilizing direct solvers in order to re-use a factorization across each of the solves for the elements of $\mathcal{B}$. Thus, while the factorization stage needed for an initial solve may cost, for each $\omega$, $O(N_{\mathrm{dof}}^3)$ [62] (as would be required for solution even with a simple source or incident field), the cost a solve for each of the elements of $\mathcal{B}$ is only $O(N_{\mathrm{dof}})$, making the cost of solving a generic scattering problem with a direct solver a minor additional expense as compared to many of the problems discussed in Section 9.2. The boundary density is reconstructed via linearity as

$$\varphi_k^{slow}(\mathbf{r}(\tau),\omega) = \sum_{n=-N/2}^{N/2-1} \mathcal{I}_n\zeta_n(\mathbf{r}(\tau),\omega).$$

With the boundary density corresponding to the appropriate right-hand side having been found, solution can proceed via evaluation of Equation (1.20), and application of the hybrid methodology for obtaining the desired time-domain scattering solution can proceed.

**Remark 14.** *While it is true that the cardinality $N$ of $\mathcal{B}$ corresponding to twice the maximum Fourier harmonic used is not explicitly dependent on the numerical bandlimit $W$, the required $N$ for accuracy considerations is indeed implicitly related, since a minimum number of points per wavelength is required to resolve arbitrary functions with bandlimit $W$.*

So far in this section, it has been assumed that the parametrization function $\mathbf{r} = \mathbf{r}(\tau)$ is smoothly-periodic, so that the density can be represented as a Fourier series expansion in the parametrization variable $\tau$. If the domain is multiply-connected, however, the parametrization will be discontinuous, as the parametrization jumps to another element of the domain, and the lack of smoothness would cripple convergence of the approximating harmonic series. In what follows, it is explained how the method can be fully generalized.

Let $\Gamma = \cup_{i=1}^{N_\Gamma} \Gamma_i$ with each $\Gamma_i$ a closed curve bounding the region $\Omega_i$. Letting $\mathbf{r}_i = \mathbf{r}_i(\tau)$ be a smooth parametrization of $\Gamma_i$ with inverse $\tau_i$, define the function

$$\beta_{i,n}(\mathbf{r}) = \begin{cases} \mathrm{e}^{-\mathrm{i}n\tau_i(\mathbf{r})}, & \mathbf{r} \in \Gamma_i, \\ 0, & \mathbf{r} \notin \Gamma_i. \end{cases}$$

The boundary data corresponds to solving the Dirichlet Helmholtz problem

$$\begin{cases} \Delta U^t + \kappa^2(\omega) U^t = 0, \quad \mathbf{r} \in \Omega, \\ U^t = \mathrm{e}^{-\mathrm{i}n\tau_i(\mathbf{r})}, \quad \mathbf{r} \in \Gamma_i, \\ U^t = 0, \quad \mathbf{r} \in \Gamma \setminus \Gamma_i. \end{cases} \tag{2.40}$$

The basis set equals $\mathcal{B} = \{\beta_{i,n} : i = 1, \ldots, N_\Gamma; n = -N/2, \ldots, N/2 - 1\}$, and following solution of (1.21) for each $B^t = \beta_{i,n}$, we have the density reconstructed via

$$\varphi_k^{slow}(\mathbf{r}, \omega) = \sum_{i=1}^{N_\Gamma} \sum_{n=-N/2}^{N/2-1} \mathcal{I}_{i,n} \zeta_{i,n}(\mathbf{r}, \omega)$$

### 9.2 General boundary data: cost estimates and comparisons

As indicated in Remark 1, this section briefly discusses extensions of the proposed hybrid method that enable solution of problem (1.6) for arbitrary incidence-field functions $b(\mathbf{r}, t)$ on the basis of a fixed finite set of precomputed frequency-domain solutions that can be obtained in a reasonable computing time. As suggested by that remark, the approach could proceed via expansion of a given incident field in source- or scatterer-centered spherical-harmonic expansions; or scattering-boundary-based synthesis relying on principal-component analysis, etc. (For reference, note that, letting the maximum frequency and scatterer's physical size be denoted by $W$ and $a$, respectively, so that $W \cdot a$ equals the acoustical size of the scatterer at the maximum frequency, $\mathcal{D} = O((Wa)^{d-1})$ ($d = 2, 3$) denotes the number of frequency domain solutions required [54] by the general-incidence hybrid method at the highest frequency—which is also a bound on the number of frequency domain solutions required, per frequency, for each relevant frequency.) The resulting general-incidence method should prove advantageous. Discretization methods based on time-stepping may be more efficient than the hybrid method for small propagation times, since they do not require precomputations. However, the asymptotic cost estimates presented in what follows and the benefits arising from frequency-domain integral-equation acceleration, as opposed to the more complex time-domain integral-equation acceleration, indicate that significant advantages may result, even in the general incidence

case, for scattering problems for which waves traverse the computational domain at least once. Of course, the advantages of the hybrid method are much more significant in the most commonly considered single-incidence case—which requires a much more limited set of precomputed frequency-domain solutions. An efficient implementation of the proposed hybrid method for general right-hand sides requires use of frequency-domain solvers which can rapidly produce multiple-incidence solutions, for each given frequency, on the basis of some precomputed direct matrix inverse or LU factorization, etc. For sufficiently small problems, a direct LU factorization can be used for this purpose, while, for large problems, fast direct solvers [23, 26, 33, 61, 63, 101] could be utilized: after a generally-significant setup cost, the latter methods can produce, for each relevant frequency, all solutions required by the proposed hybrid method at minimal additional cost. To estimate the costs inherent in the use of fast direct methods in the context of the hybrid solver under general incidence, restricting attention to surface scattering problems considered in this thesis, and letting $\widetilde{O}(X) = O(X \log(X))$, the $\mathcal{H}$-matrix setup cost for each one of the $O(Wa)$ required frequencies is a quantity of the order of $\widetilde{O}((Wa)^{d-1})$. Consideration of numerical experiments presented in [24, Tables 7 & 8] and [26, Table 6] suggests that, if computed by means of a $\mathcal{H}$-matrix approach, the cost to obtain all $\mathcal{D}$ frequency-domain solutions required by the hybrid method, for a given frequency, is itself a quantity of order $\widetilde{O}((Wa)^{d-1})$. Thus, the cost required for the evaluation of all necessary frequency domain solutions for all $O(Wa)$ frequencies may be estimated as a quantity of the order of $\widetilde{O}((Wa)^{d})$. Volumetric time stepping methods (based, say, on finite-differences or finite-elements) over a domain of acoustical size $Wa$, on the other hand, require at least a spatio-temporal discretization, and thus a computing cost, of order $O((Wa)^{d+1})$ (for simulations long enough that a single crest can traverse the complete computational domain) if a fixed number of points per wavelength are used. Even larger discretizations would be required, in addition, if dispersion is compensated for by decreasing the time-step $\Delta t$ faster than the frequency grows. In any case, a clearly higher operation count results for volumetric solvers than the one presented above for the hybrid method with $\mathcal{H}$-matrix frequency-domain precomputation. If appropriately-accelerated time-domain integral equations are used instead [8, 14, 55], finally, a cost of $\widetilde{O}((Wa)^{d})$ would result that is asymptotically comparable to the fast-hybrid/direct-solver approach described above—and the relative advantages would depend on other specific characteristics of the methods used, including, in particular, accuracy order and dispersion in time, as well as the quality of the respective acceleration methods used. A comparison of the

unaccelerated hybrid method to a recent unaccelerated time-domain integral equation solver is presented in Section 8.4. For most problems arising in applications, however, the incident fields can be represented by a small number of sources, and, in such cases, an accelerated version of the hybrid method proposed in this thesis already provides clear significant advantages, including improved cost asymptotics, over other methodologies considered in this section.

### 9.3 Numerical demonstrations

This section demonstrates techniques allowing the solution of wave scattering problems with arbitrary incident fields. We consider the scattering of fields due to a point source off a kite-shaped obstacle in two dimensions, with the incident field given by

$$B^t(\mathbf{r},\omega) = \mathrm{e}^{-\frac{(\omega-\omega_0)^2}{\sigma^2}}\frac{\mathrm{i}}{4}H_0^{(1)}(\omega|\mathbf{r}-\mathbf{r}_0|), \tag{2.41}$$

where $\sigma = 2, \omega_0 = 12$, and $\mathbf{r}_0 = (-3,-3)$. While this is a simple enough incident field that we could use the incident field itself as the integral equation right-hand-side, to demonstrate the efficacy of harmonic boundary expansion, we follow the methodology in Section 9. We expand the incident field with $N = 80$ Fourier harmonics and solve the integral equation Equation (1.21), for each $\omega \in \mathcal{F}$, with $B^t(\mathbf{r}(\tau),\omega) = \mathrm{e}^{\mathrm{i}n\tau}, \quad (-N/2 \le n \le N/2-1)$. The LU factorization of the integral equation system for (1.21) at a particular $\omega$ was re-used for all of the required boundary incidences; the solution of the $N = 80$ integral equations per frequency thus only resulted in a 2.5% increase in total solve time. The solution is shown in Figure 2.11.

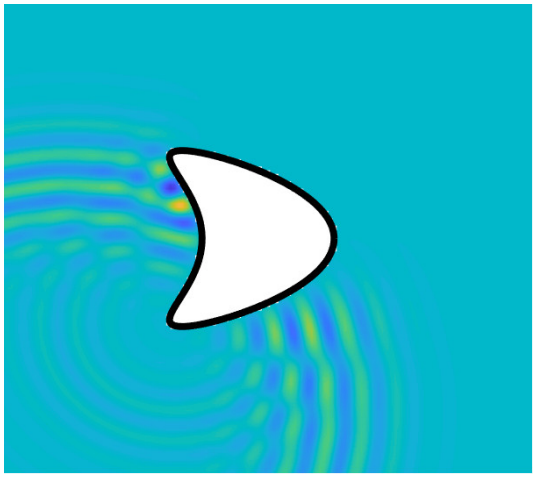

Figure 2.11: Total field resulting due to a point incident source using the generic boundary incidence strategy proposed.

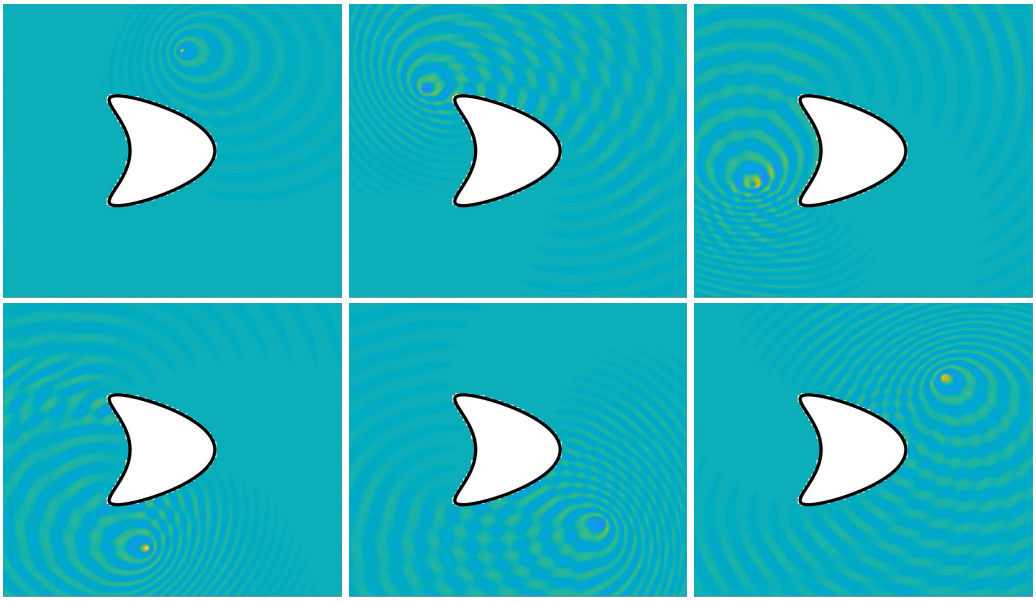

Figure 2.12: Generic incident field demonstration: the total field resulting due to an incident field arising from a moving point source that travels in a circular trajectory around a kite-shaped obstacle. Time increases left to right and from top to bottom.

Figure 2.12 demonstrates the solver for the scattering of a moving and oscillating point source, a fully arbitrary incident field, while Figure 2.13 provides, in turn, a demonstration of the proposed algorithm for a multiply-connected obstacle, also illuminated by a moving point source.

**Conclusion**

This chapter presented the first efficient algorithm for evaluation of time-domain solutions, in two- and three-dimensional space, on the basis of Fourier transformation of frequency domain solutions. The algorithm enjoys superalgebraically-fast spectral convergence in both space and time, it runs in $\mathcal{O}(N_t)$ operations for evaluation of the solution at $N_t$ points in time, and it can produce arbitrarily-large time evaluation of scattered fields at $\mathcal{O}(1)$ cost. The method is additionally embarrassingly parallelizable in time and space, and it is amenable to implementations involving a variety of acceleration techniques based on high performance computing.

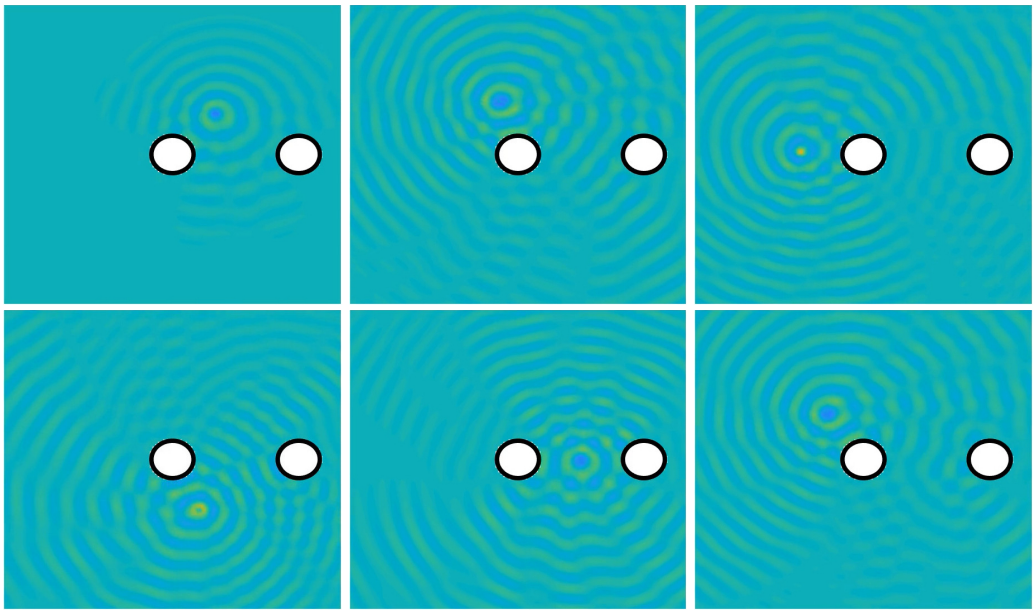

Figure 2.13: Total field resulting from the scattering of an incident field that is induced by a moving point source which travels in a circular trajectory around the left-most circular obstacle, demonstrating proposed wave equation solver in a setting with an arbitrary incident fields and with multiply-connected scattering geometries. Time increases left to right and from top to bottom.

*Chapter 3*

# TWO-DIMENSIONAL LONG-TIME ASYMPTOTICS

"Good thing we live in three dimensions, or else you'd be hearing this class forever."
—Paul Garabedian (paraphr.)

**Overview**

This chapter further develops the methodology proposed in Chapter 2, in a direction specific to two-dimensional scattering, wherein the incident wave even resulting from an instantaneous impulse is of infinite duration (decaying slowly in amplitude), and the number of windows $K$ in the previously-proposed methodology is therefore typically significant. We propose a method in Section 10 that manages the costs incurred by our method by the known slow decay of scattered fields in two dimensions and yields a highly efficient algorithm even for solution over vast stretches of simulation time. Demonstration of this method on problems of scattering, including for trapping geometries, is then presented in Section 11.

## 10 Long-time asymptotics in two spatial dimensions: theory and numerics

This section is concerned with addressing some intrinsic differences between two- and three-dimensional wave propagation, differences that bear important implications for numerical methods. As is well-known (see also (1.9) in Section 2.1), the Green's function

$$G(\mathbf{r},t;\mathbf{r}',t') = \begin{cases} \frac{H(c(t-t')-|\mathbf{r}-\mathbf{r}'|)}{2\pi\sqrt{c^2(t-t')^2-|\mathbf{r}-\mathbf{r}'|^2}} & \text{for} \quad d=2 \quad \text{and} \\ \frac{\delta(c(t-t')-|\mathbf{r}-\mathbf{r}'|)}{4\pi|\mathbf{r}-\mathbf{r}'|} & \text{for} \quad d=3, \end{cases} \tag{3.1}$$

for the acoustic wave equation gives the fundamental (free-space) impulse response at location $\mathbf{r}$ and time $t$ to a disturbance located at $\mathbf{r}'$ that occurred at time $t'$. It is important to note that, while both Green's functions vanish for times $t$ such that $t-t' < |\mathbf{r}-\mathbf{r}'|/c$ (exhibiting the principle of causality), the $d=2$ and $d=3$ functions

[1] T. G. Anderson, O. P. Bruno, and M. Lyon. *High-order, Dispersionless "Fast-Hybrid" Wave Equation Solver. Part II: Window Tracking, Spatio-Temporal Parallelism, General Incident Fields*. 2020, in preparation.

differ in that for times $t$ such that $t - t' > |\mathbf{r} - \mathbf{r}'|/c$ the three-dimensional Green's function vanishes and the two-dimensional Green's function does not. Indeed, the two-dimensional Green's function in that region is a slowly-decreasing function of time $t$, a fact that follows from Hadamard's classical method of descent [68, §29] for the wave equation, whereby the wave equation in two dimensions is viewed as a solution to the three-dimensional wave equation that is constant with respect to one spatial variable. As remarked in the above epigraph, voices from the past are heard infinitely far into the future.

As might be expected, differences of this nature persist in wave scattering problems. Indeed, while for many three-dimensional scattering problems the scattering solutions decay rapidly (for much more discussion of known decay rates in three dimensions, see Section 13.2 of Chapter 4), the solution of the two-dimensional Dirichlet problem, for example, can decay as slowly as $1/(t\log^2(t))$ [98]. (The asymptotics for the Neumann problem were first established in reference [4] and are included along with asymptotics for the Robin and impedance problems in [98, Thm. 6].) Furthermore, the difference in scattering character between the two- and three-dimensional problems is clearly evidenced by a certain result on the solution asymptotics presented in reference [98, Thm. 8], establishing that if a two-dimensional wave equation solution decays superalgebraically fast, it is identically zero (cf. the discussion in regards to three-dimensional decay rates in Section 13.2 showing superalgebraic or exponential decay rates for many classes of obstacle geometries). In our context, the relevant long-time asymptotics to a solution $u$ of (1.6) in $d = 2$ dimensions are given by [98, Thm. 6]

$$u(\mathbf{r}, t) \sim \frac{1}{t}\sum_{j=2}^{\infty}\frac{c_{0,j}(\mathbf{r})}{\log^j(t)} + \sum_{q=1}^{\infty}\frac{1}{t^{2q+1}}\sum_{\substack{j=1-q\\ j\neq 1}}^{\infty}\frac{c_{q,j}(\mathbf{r})}{\log^j(t)}, \quad t\to\infty. \tag{3.2}$$

This asymptotic expression carries important implications for the computational methodology proposed in this thesis. Indeed, in the proposed methodology, the solution $u$ is expressed (see (2.10)) as the sum

$$u(\mathbf{r}, t) = \sum_{k=1}^{K} u_k(\mathbf{r}, t), \tag{3.3}$$

where the functions $u_k$ are solutions to the wave equation (1.6) with Dirichlet data $b$ substituted by a windowed section $b_k$ (supported in $[s_k - H, s_k + H]$) of the overall given incident field. The slow asymptotic decay of solutions $u_k$ implies

that many of the $K = O(T^{inc})$ windows are important for solution accuracy at large times $t$. Indeed, due to the slow time-decay of solutions $u_k$ resulting from incident fields separated by $H$ in time, truncation of the sum in (3.3) to a number of terms independent of $K$ would result in unacceptably large error for large $t$ as $K \to \infty$—since the series of general term $\sum_k 1/((t - s_k)\log^2(t - s_k))$, while convergent, converges extremely slowly. Therefore, in order to avoid large errors as $T^{inc}$ and $t$ grow, a number of terms proportional to $T^{inc}$ must be kept in the sum, in stark contrast with the $d = 3$ case for which often a finite and bounded number of terms accurately represent the solution for arbitrarily large values of $t$ and $T^{inc}$. An interesting conclusion follows, that the "time-leaping" capability of the hybrid method to produce the full solution $u$ is only applicable in three-dimensional contexts, since, in two dimensions, solutions $u_k$ from incident fields in the distant past contribute in a significant manner to the overall solution $u$ over vast stretches of time.

If the final solution time $T$ is proportional to the duration of the incident field, $T \propto T^{inc}$, then since the number of windows $K = O(T^{inc})$, the evaluation of $u$ at time sample points of fixed spacing throughout $[0, T]$ will require $O(TK)$ evaluations of solution components $u_k$, precisely $T$ for each $1 \le k \le K$. Indeed, while the methods of Chapter 2 may ensure that the cost to evaluate the field contribution $u_k$ from any single window with arbitrary $k$ $(1 \le k \le K)$ at a single point in time is only $O(1)$ with respect to $T$, the fact that field contributions may be relevant for a long time is as yet unaddressed. This section proposes an algorithm to efficiently and accurately evaluate the total field $u$ over vast stretches of time while needing only to complete a total of $O(T)$ evaluations of any of the $u_k$ solutions across all of $1 \le k \le K$.

First, let $t_k > s_k$ be a time at which the solution $u_k$ has been identified to enter the asymptotic regime of (3.2) (recall from Chapter 2 that $s_k$ is the time-center of partition $k$). The algorithm then fits a polynomial to $u_k$ on $[t_k, \infty)$ (see also Remark 15), and, in service of this, we make certain manipulations to the asymptotic expansion to render it more amenable for fitting on an infinite interval. Thus, considering the change of variables $z_k(t) = 1/\log(t - s_k)$, the asymptotic expansion of $u_k$ (Equation (3.2) with $u = u_k$) becomes

$$u_k(\mathbf{r}, \mathrm{e}^{1/z_k} + s_k) \sim \sum_{j=2}^{\infty} c_{0,j}(\mathbf{r}) z_k^j \mathrm{e}^{-1/z_k} + \sum_{q=1}^{\infty} \sum_{\substack{j=1-q \\ j\neq 1}}^{\infty} c_{q,j}(\mathbf{r}) z_k^j \mathrm{e}^{-(2q+1)/z_k}. \tag{3.4}$$

It is easy to see from the asymptotics that this is a smooth function of $z_k$ that can be easily fit with polynomials on the bounded interval $[0, z_k(t_k)]$. Before doing this,

for all $k$, $u_k$ is multiplied by $e^{1/z_k}$ (a procedure that further smooths the function, as can be seen by consideration of (3.4)). Then, for $k = 1$, at each spatial point $\mathbf{r}$, a polynomial $P_k^{\mathbf{r}}(z) = P_1^{\mathbf{r}}(z)$ with zero constant term ($P_1^{\mathbf{r}}(0) = 0$) is obtained such that $P_1^{\mathbf{r}}(z_k(t))$ fits $e^{1/z_1}u_1(\mathbf{r}, e^{1/z_1} + s_1)$, in the least-squares sense, over an $n_s$-point equidistant mesh in the interval $[0, z_1(v_1)]$. The zero-vanishing assumption on the least-squares polynomial $P_1^{\mathbf{r}}(z)$ embodies the $u_1 \to 0$ behavior as $t \to +\infty$, which itself corresponds to $z_1(t) \to 0^+$.

The algorithm then proceeds iteratively through the window indices $k$, so that for each $k > 1$ and for a given spatial point $\mathbf{r}$, $P_k^{\mathbf{r}}(z)$ approximates $\sum_{\ell=1}^{k} u_\ell$. More precisely, for $k > 1$ and for each point $\mathbf{r}$ in a selected spatial evaluation set $\mathcal{R}$ (cf. Section 7 in Chapter 2), the polynomial $P_k^{\mathbf{r}}(z)$ with zero constant term ($P_k^{\mathbf{r}}(0) = 0$) is obtained that fits $e^{1/z_k}u_k(\mathbf{r}, s_k + e^{1/z_k(t)}) + P_{k-1}^{\mathbf{r}}(z)$ in a least squares sense over the $n_s$-point equidistant mesh in the interval $[0, z_k(t_k)]$. Therefore, for $t > t_k$, the approximation

$$\sum_{\ell=1}^{k} u_\ell \approx P_k^{\mathbf{r}}(z_k(t))$$

holds, for $t > t_k$, up to the accuracy of the least squares fit and the discretization error underlying the numerical evaluation of the solutions $u_k$. The overall solution can thus be efficiently obtained for all time by completing this procedure for $k = 1, \ldots, K$. Clearly, the entire methodology is enabled by the capability to evaluate $u_k$ on arbitrary time grids without reliance on preceding time values.

**Remark 15.** *For simplicity, the description of the proposed asymptotic polynomial representation assumes use of a single asymptotic-matching polynomial. But use of multiple matching polynomials in the interval* $[0, z_k(t_k)]$*, one corresponding to an unbounded time interval the rest corresponding to bounded time intervals, may be advantageous in practice. For example, for the numerical experiments in Section* 11 *two polynomials of degree five were used for asymptotic approximation within the interval* $[0, z_k(t_k)]$.

## 11 Numerical illustrations

This section demonstrates the effectiveness of the algorithm introduced in this chapter and also presents a variety of examples demonstrating two-dimensional scattering in trapping domains. The first example in this section treats the scattering of a unidirectional plane-wave from a kite-shaped geometry. The kite-shaped region is in fact star-shaped, and thus, due to the lack of multiple scattering, the asymptotic

regime is quickly reached. More specifically, the incident field in this experiment is given by the function $u^{inc}(\mathbf{r}, t) = a(t - \mathbf{k}_{inc} \cdot \mathbf{r})$ in the direction $\mathbf{k}_{inc} = (1, 1)$ using with signal function

$$a(t) = \sin\left(\frac{\pi}{5}\left(2(t+32) - \frac{40}{\pi}\sin\left(\frac{\pi}{40}(t+32)\right)\right)\right). \tag{3.5}$$

The duration of the incident field was taken to be $T^{inc} = 3232$, so that with a window-width $H = 32$, there resulted a number of windows $K = 100$. The frequency-domain was discretized with 491 frequencies in the $\omega$-range $[0, 8]$, with 191 of those in the range from $[0, 0.25]$, so that discretization error was not significant relative to the approximations performed in this section.

The methodology proposed in this section was followed to produce an approximation $\widetilde{u} \approx \sum_{k=1}^{K} u_k$. The function $u_k(\mathbf{r}, t)$ was evaluated at $n_s = 31$ sample points $z_k(t_n)$, $1 \leq n \leq n_s$, equispaced from $z_k = 0.25$ to $z_k = 0.07$. Two degree-5 polynomial fits were made, the first for the 16 sample points in $[0.16, 0.25]$ and the second for the 16 sample points in $[0.07, 0.16]$ (the latter polynomial with the requirement that it is additionally 0 when $z_k = 0$). The asymptotic behavior for this experiment onset at $t_k = s_k + 55$, and the polynomial fit was performed on the interval $[t_k, t_k + H]$. It should be noted that there were no sample points for $z_k < 0.07$, since, under the $z_k$ change of variables, the value of sample points in the $t$ variable becomes infinitely large with the result that the size of $u$ may be smaller than the numerical discretization error from the hybrid methodology presented in Chapter 2—a fact that could otherwise lead to poor interpolation results. In Figure 3.1 the solution $u$ obtained from the full summation Equation (3.3) is compared with the approximation $\tilde{u}$ using the proposed asymptotic fitting methodology. The method produces high-quality approximations that are uniformly-accurate for long times ($K = 100$ windows).

The numerical test was implemented in MATLAB in a single core on workstation with an Intel Xeon E31230 v5 3.4 GHz CPU. The full evaluation of this long-time simulation required $1/10$ seconds per spatial observation point (a figure arrived at by averaging the required time for many spatial observation points). This computation involves evaluate a significant number of Hankel function evaluations, evaluations which can be reused for each window. In order to evaluate the Hankel functions efficiently, certain addition theorems of the Hankel function were utilized, which split the Hankel function into a smooth function and a product of a smooth and of a explicitly-known singular function. In our experiments, this splitting reduced the time to evaluate the required Hankel functions by a factor of seven.

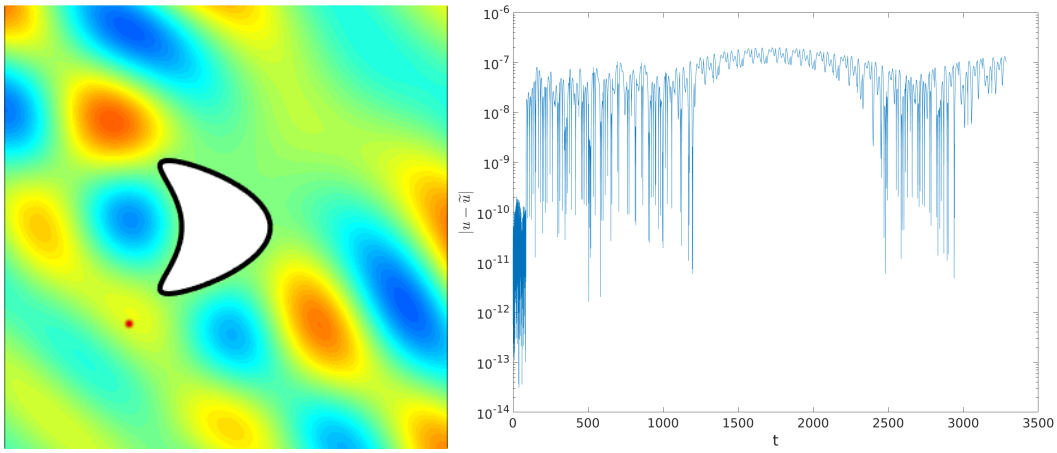


Figure 3.1: Long-time two-dimensional numerical experiment demonstrating the proposed asymptotic-fitting method. Left: Snapshot of representative near-field solution. Right: Error $|u - \widetilde{u}|$ between the true solution $u$ and the result of the asymptotic-fitting strategy $\widetilde{u}$. The error is measured at the marked observation point on the left plot, $(-2\sqrt{2}, -2\sqrt{2})$.

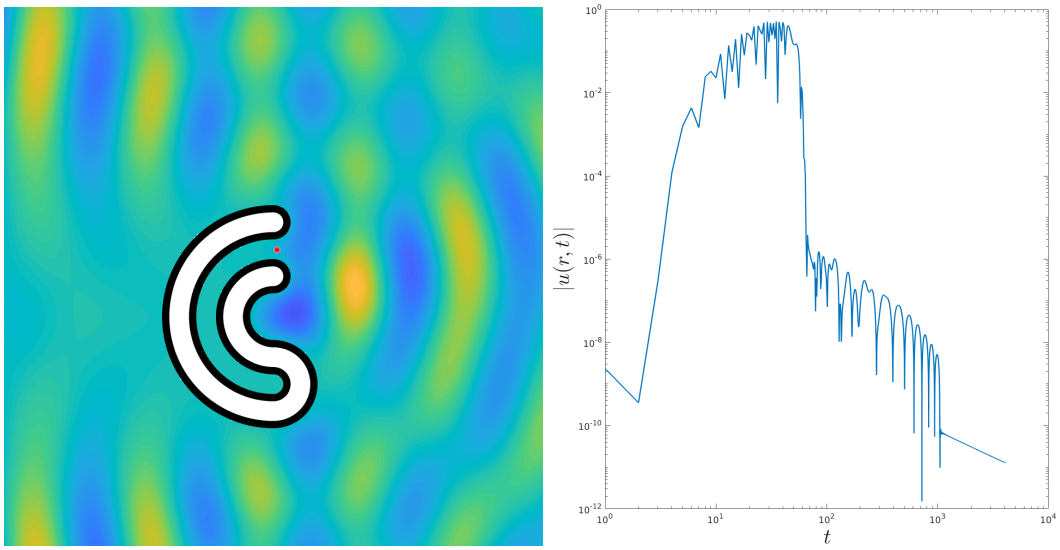


Figure 3.2: Long-time two-dimensional numerical experiment in a trapping region. Left: Snapshot of representative near-field solution. Right: One of the solution components $u_k$ at the spatial location marked on the left plot, computed over more than 1000 time units.

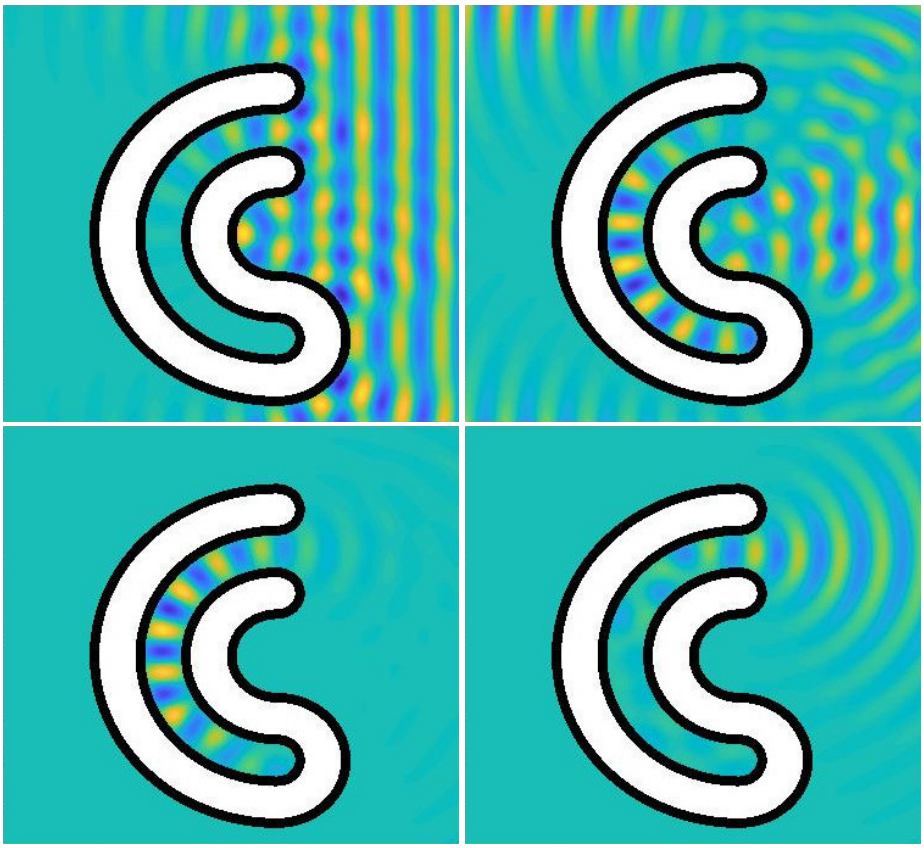

Figure 3.3: Scattering in a two-dimensional trapping geometry, with the intensities being that of the total field. The time sequence starts left-to-right on the first row, and then continues left-to-right on the second row.

A second demonstration focuses on a more strongly-trapping geometry, where an incident plane wave field propagating in the direction $(-1, 0)$ with signal function

$$a(t) = \sin\left(\frac{\pi}{2.5}\left(2(t+32) - \frac{40}{\pi}\sin\left(\frac{\pi}{40}(t+32)\right)\right)\right),$$

impinges on the obstacle pictured in the left-side of Figure 3.2. The observation point is located at $(0, 0.5)$, a point in the opening of the cavity. The slow time-decay of the solution is clearly observable, but so also is the eventual slow asymptotic rate of decay.

To conclude this section, we include some further simulations of this trapping geometry in higher-frequency contexts, with Figure 3.3 and Figure 3.4 showing more clearly the trapping nature of this geometry.

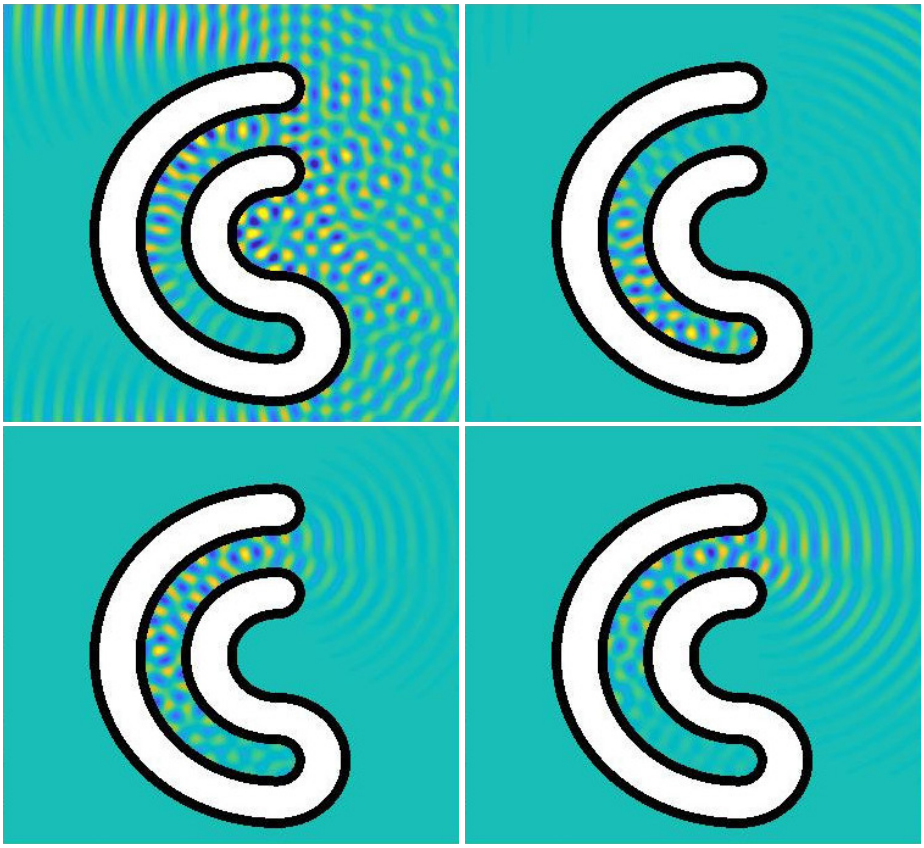

Figure 3.4: Higher-frequency scattering in a two-dimensional trapping geometry, with the intensities being that of the total field. The time sequence starts left-to-right on the first row, and then continues left-to-right on the second row.

*Chapter 4*

# TRACKING ACTIVE TIME WINDOWS VIA NOVEL BOUNDARY-DECAY THEORY

"Men make their own history, but they do not make it as they please; [they make it] under circumstances existing already, given and transmitted from the past"

—Karl Marx (1852)

**Overview**

This chapter proposes techniques to accelerate further the algorithms for computation of solutions to wave scattering problems outlined in Chapter 2 in a three-dimensional (note that $d = 3$ is assumed throughout this chapter) context, through truncation of the sum $u = \sum_{k=1}^{K} u_k$ that produces the solution $u$. While the overall solution $u$ is nominally the sum of of many contributions $u_k$, since the number of terms $K = O(T^{inc})$, the focus of this chapter is on identifying a stopping criterion which readily identifies the elements of this sum that can be safely ignored on a given space-time evaluation region. With such a stopping criterion in hand, the overall solution $u$ can be evaluated on such a space-time region by a sum of appropriate $u_k$ terms, with the number of terms independent of $K$. Thus, owing to the lack of a need to compute terms omitted from the sum, the overall computation can be greatly reduced. In order to perform this truncation with rigorous accuracy guarantees, a theory is developed to bound the size of future values of boundary integral densities for the wave equation based on the size of the historical values of the density. Additionally, estimates are required and given for the rate of temporal decay that can be assured. In both cases, only a finite measurement history (roughly equal to the time it takes a transmitted wave to traverse a distance equal to the obstacle diameter) is

---


[1] T. G. Anderson and O. P. Bruno. *On the decay of time-dependent solutions to the wave equation and finite-time analysis of their boundary integral densities*. 2020, in preparation.

[2] T. G. Anderson, O. P. Bruno, and M. Lyon. *High-order, Dispersionless "Fast-Hybrid" Wave Equation Solver. Part II: Window Tracking, Spatio-Temporal Parallelism, General Incident Fields*. 2020, in preparation.

required to make rigorous estimates on the future size of the density. Therefore, an algorithm can make a decision to drop contributions from a solution component $u_k$ by monitoring the size of the associated boundary integral density $\psi_k$ on an interval of precisely this length. A brief description of ideas and formulas already developed is recalled as needed to motivate the discussion in and provide a concrete setting for this chapter, but the reader is referred to Chapter 2 for further elaboration.

First, recall that a partition of unity of time is set down for the time interval of incidence $[0, T^{inc}]$, which we define using a set of $K = O(T^{inc})$ time-centers $s_k$ ($k = 1, \ldots, K$) and window functions $w_k(t) \in C_c^\infty([s_k - H, s_k + H])$, with window functions defined so that $\sum_{k=1}^K w_k(t) = 1$ for $t \in [0, T^{inc}]$. The restricted class of boundary data (1.6c) treated in Chapter 2 was assumed to be the boundary values of an incident field propagating in only a few directions or owing to one or perhaps only a few sources, with incident fields thus taking the unidirectional exemplary form

$$b(\mathbf{r}, t) = \frac{1}{2\pi} \int_{-\infty}^{\infty} B^t(\omega) \mathrm{e}^{\mathrm{i}(\kappa(\omega)\mathbf{p}\cdot\mathbf{r} - \omega t)} \, \mathrm{d}\omega, \quad \text{with} \quad \kappa(\omega) = \omega/c, \tag{4.1}$$

where the function $B^t$ is defined for a given compactly supported function $a(t)$ as

$$B^t(\omega) = \int_{-\infty}^{\infty} a(t) \mathrm{e}^{\mathrm{i}\omega t} \, \mathrm{d}t. \tag{4.2}$$

Windowed boundary data for this class of incident field were defined as

$$b_k(\mathbf{r}, t) = \frac{1}{2\pi} \int_{-\infty}^{\infty} B_k^t(\omega) \mathrm{e}^{\mathrm{i}(\kappa(\omega)\mathbf{p}\cdot\mathbf{r} - \omega t)} \, \mathrm{d}\omega \quad \text{with} \quad \kappa(\omega) = \omega/c, \tag{4.3}$$

with

$$B_k^t(\omega) = \int_{-\infty}^{\infty} a_k(t) \mathrm{e}^{\mathrm{i}\omega t} \, \mathrm{d}t \quad \text{where} \quad a_k(t) = w_k(t) a(t). \tag{4.4}$$

**Remark 16.** *This chapter assumes, per the discussion in Remark* 6*, that the windowed incident field $b_k(\mathbf{r}, t)$ is also a solution to the wave equation. In our context, temporal windowing of this kind leads to efficient numerical methods when the incident field propagates in only a few directions (or is induced by a limited number of sources), and can otherwise be windowed through a signal function $a_k(t)$ as in Equation* (4.4)*. The assumption that the wave equation boundary values are those of a solution to the wave equation allows the use of a "direct" integral equation formulation for the physical density $\psi_k = \frac{\partial u_k^{tot}}{\partial \mathbf{n}}$, which in frequency domain satisfies Equation* (1.19)*. The main theorems of this chapter, Theorem* 4 *and Theorem* 5*, can be adapted without difficulty to the general incidence case where*

*the frequency-domain (non-physical) boundary integral density $\varphi_k$ satisfies the integral equation* (1.21) *of Brakhage and Werner [25], though see also Remark* 17 *immediately below.*

**Remark 17.** *A major reason that a direct integral equation formulation is preferred throughout this thesis is that the resulting physical density $\psi_k = \frac{\partial u_k^{tot}}{\partial \mathbf{n}}$ is guaranteed to decay at the same rate as the fields $u_k^{tot}$, while in contrast such a property does not hold if an indirect formulation for the density $\varphi_k$ is used. Indeed, note that, as recognized in the literature, the rate of decay with an indirect formulation may be lower than the true decay of the solution to the wave equation, which may thus lead to catastrophic error cancellation in the production of the field u from the density $\varphi$ (cf. the indirect representation formula Equation* (1.20) *which features a difference of two layer operators) at a certain error level [11, 20, 57]. In addition to avoiding such cancellation errors, a direct formulation ensures the success of the window tracking algorithm through an equivalence between the smallness of the density and the field at appropriate (time-lagged) points in time and space, see e.g. Theorem* 1. *In certain cases, however, the use of physical densities is not possible—since physical equations can only be derived in presence of a "scattering problem", that is, a problem for the wave equation for which the boundary conditions are expressed in terms of boundary data corresponding to an incident field which is itself a solution of the wave equation in a neighborhood of the obstacle.*

We note first the method proposed in Chapter 2 and utilized previously in this thesis to obtain the solution $u_k$, which first proceeds by near-field evaluation in the frequency-domain,

$$U_k^{slow}(\mathbf{r}, \omega) = \int_\Gamma \psi_k^{slow}(\mathbf{r}', \omega) G_\omega(\mathbf{r}, \mathbf{r}') \, \mathrm{d}\sigma(\mathbf{r}'), \tag{4.5}$$

followed by inverse Fourier transformation:

$$u_k(\mathbf{r}, t) = \frac{1}{2\pi} \int_{-\infty}^{\infty} U_k^{slow}(\mathbf{r}, \omega) \mathrm{e}^{-\mathrm{i}\omega(t - s_k)} \, \mathrm{d}\omega. \tag{4.6}$$

This chapter proposes use of an alternative approach, using inverse Fourier transformation of the density $\psi_k$,

$$\psi_k(\mathbf{r}', t) = \frac{1}{2\pi} \int_{-\infty}^{\infty} \psi_k^{slow}(\mathbf{r}', \omega) \mathrm{e}^{-\mathrm{i}\omega(t - s_k)} \, \mathrm{d}\omega, \tag{4.7}$$

followed by the use of the Kirchhoff formula (1.15),

$$u_k(\mathbf{r}, t) = \int_\Gamma \frac{\psi_k(\mathbf{r}', t - |\mathbf{r} - \mathbf{r}'|/c)}{4\pi |\mathbf{r} - \mathbf{r}'|} \, \mathrm{d}\sigma(\mathbf{r}'), \quad \mathbf{r} \in \Omega, \tag{4.8}$$

where as in (1.15) the time-dependent density $\psi = \psi_k$ is a physical quantity:

$$\psi_k(\mathbf{r}, t) = \partial_{\mathbf{n}} u_k^{tot}(\mathbf{r}, t). \tag{4.9}$$

Use of the Kirchhoff representation formula is attractive since the stopping criterion for computing the scattered field solutions on arbitrary volumetric regions is thereby dependent on norms of the boundary density, which, being defined on the $(d-1)$-dimensional (and thus two-dimensional in the $d = 3$ setting of this chapter) surface, is computationally efficient to measure.

In any case, the time-domain scattered field response is evaluated as the sum of solutions $u_k$ to (1.6) with boundary data $b_k$,

$$u(\mathbf{r}, t) = \sum_{k=1}^{K} u_k(\mathbf{r}, t), \tag{4.10}$$

although, as discussed in Remark 7, for a rather general class of scattering obstacles, only a bounded number of terms in this sum must actually be included for a given accuracy, even as $K = O(T^{inc}) \to \infty$.

The focus of this chapter is on developing an analytical framework to identify the subset of elements of this sum that are required for an accurate solution $u$ on a given region $\mathcal{R} \times \mathcal{T}$ of spacetime. Thus, Section 12 provides straightforward theorems linking the size of the scattered fields to the size of the densities through standard representation formulas, while Section 13 proves novel estimates on the norms of future temporal evolution of the boundary integral density. In that section, Section 13.1 shows that the density at future times can be bounded by its norm on a finite, identifiable time interval, and Section 13.2 goes further to show that indeed the density decays (superalgebraically fast) relative to the norm's value taken over this time interval. Finally, while Section 8.5 in Chapter 2 included numerical demonstrations of long-time three-dimensional scattering, showing the need for the theory and methodology proposed in this chapter, in Section 14 some tests are presented showing (at unit wave speed) the decay of boundary densities and the relevance of solution contributions when the associated density is small on lengths of time equal to the diameter of the obstacle.

## 12 Decay rates of scattering problems and connections to boundary integral densities

As suggested in Remark 7 of Chapter 2 (cf. also the review above), the algorithm exploits the rapid decay enjoyed by exterior scattering solutions for a vast class

of nontrapping (or, more precisely, non-strongly-trapping) domains $\Omega^c$, to evaluate the field $u$, within a prescribed tolerance $\varepsilon^{\text{tol}}$, on the basis of a truncation of the sum (4.10) using no more than $M$ terms (namely, the terms $u_k$ that have not decayed below the error tolerance at the given time $t$), at all given (possibly distant) space positions, and as time (and thus $K$) grow without bound. This section presents an algorithm that determines the required range of $M$ indices that need to be kept in the sum (4.10) in order to meet the tolerance $\varepsilon^{\text{tol}}$ at a given point $\mathbf{r} \in \Omega$ and for a given time $t$. For computational efficiency, we utilize a somewhat more general strategy, in which we seek an $M$ term truncation of (4.10) which is valid, within the error tolerance $\varepsilon^{\text{tol}}$ for all spatio-temporal points in a given Cartesian subset $\mathcal{R} \times \mathcal{T}$ within the required overall spatio-temporal evaluation domain.

In order to present our algorithm, we consider the representation formula (4.8), that yields the scattered field $u_k$ in terms of the density $\psi_k = \partial^+_{\mathbf{n}} u_k^{tot}$ (Equation (4.9)), and we define $r_{\min} = \min_{\mathbf{r}\in\mathcal{R},\mathbf{r}'\in\Gamma} |\mathbf{r} - \mathbf{r}'|$, and $r_{\max} = \max_{\mathbf{r}\in\mathcal{R},\mathbf{r}'\in\Gamma} |\mathbf{r} - \mathbf{r}'|$. In view of Equation (4.8), we see that if $\psi_k(\mathbf{r}', t) = 0$ for $t > T_k^f$ and for all $\mathbf{r}' \in \Gamma$, then $u_k(\mathbf{r}, t)$ must vanish for all $(\mathbf{r}, t) \in \mathcal{R} \times (T_k^f + r_{\max}/c, \infty)$. Importantly, further, we note that, as it follows, in particular, from Theorem 4 Equation (4.29), if the density $\psi_k$ vanishes for a sufficiently long time interval $I$ after $b_k$ permanently vanishes everywhere on $\Gamma$, then $\psi_k$ will vanish throughout $\Gamma$ for all times subsequent to $I$—a fact that can be visualized physically by considering the portions of the time history of sources and fields that could potentially lead to non-vanishing illumination at a time subsequent to the interval $I$.

This suggests that, provided $\psi_k$ is "small" on the time interval $I$, then $u_k$ ought to be "permanently small" throughout $\mathcal{R}$ for all times after an appropriate ($\mathcal{R}$-dependent) time delay subsequent to the end of the time interval $I$. This fact can be established rigorously under various norms (for obstacles that are in some sense "weakly-nontrapping") on the basis of Equations (4.13)–(4.14) and (4.17)–(4.18), and in view of the density estimates provided by the main Theorem 4 and Theorem 5. (Non-trapping obstacles $\Omega^c$ are those for which a billiard-ball trajectory in $\Omega$, which bounces off the wall $\Gamma$ in accordance with the law of specular reflection, always escapes a region of finite radius encircling the obstacle after traveling a finite total distance [92]; more details concerning the weaker versions of nontrapping concepts mentioned above are provided in Remark 21.)

We present next the first result in this section, which links (in the most immediate manner) the smallness of the density $\psi_k$ to that of the solution $u_k$, and which

also indicates explicitly (Equation (4.11)) the error variation that may occur in the evaluation of the near field from the boundary density—which, like the single-layer potential factor on the right-hand side of the inequality, is uniformly bounded as $\mathbf{r} \to \Gamma$. The simple result is illustrative of the type of guarantees on the smallness of $u_k$ that are desired, yet also motivates certain additional estimates through its primary weakness—that it requires knowledge of the size of the density $\psi_k$ for all future time.

**Proposition 1.** *Let $\varepsilon^{\text{tol}} > 0$ and a bounded set $\mathcal{R} \subset \Omega$ be given, let*

$$S_{\max} = \max_{\mathbf{r}\in\Gamma} \left(S_0 1\right)(\mathbf{r})$$

*where $S_0$ denotes the single-layer operator* (1.12) *with frequency $\omega = 0$, and assume $\|\psi_k(\cdot,t)\|_{L^\infty(\Gamma)} < \varepsilon^{\text{tol}}/S_{\max}$ for all $t > T_k^f$. Then $|u_k(\mathbf{r},t)| \leq \varepsilon^{\text{tol}}$ for all $t > T_k^f + r_{\max}/c$ and for all $\mathbf{r} \in \mathcal{R}$.*

*Proof.* In view of (4.8), we obtain

$$|u_k(\mathbf{r},t)| \leq \frac{1}{4\pi}\left(\sup_{\tau>T_k^f} \|\psi_k(\cdot,\tau)\|_{L^\infty(\Gamma)}\right)\int_\Gamma \frac{d\sigma(\mathbf{r}')}{|\mathbf{r}-\mathbf{r}'|}, \tag{4.11}$$

from which the result follows directly from the maximum principle for the Laplace equation. □

Note that (4.11) shows that $u_k(\mathbf{r},t)$ is small for large $t$ if $\psi_k(\cdot,\tau)$ is small along $\Gamma$ *for all* $\tau > T_k^f$, and functions as a truncation-error estimate as it provides a guarantee on the error committed when the field $u_k$ is ignored—when it is truncated from the sum in Equation (4.10). The main results of this chapter, Theorem 4 and Theorem 5, show that $\psi_k$ need only be small on a *bounded* time interval $I$ of length approximately equal to $\text{diam}(\Gamma)/c$ in order that the density $\psi_k$ be small for all subsequent times—where the smallness of densities and fields is predicated in the sense of various norms used. In particular, for an obstacle that satisfies a certain "$q$-growth condition" related to the trapping strength of an obstacle, Theorem 4 provides $L^2$ temporal bounds on the density over all times after the end of the interval $I$ in terms of the $H^{q+1}$ temporal norm of the density over the interval $I$, and, further, gives uniform bounds in time in terms of $H^{q+2}$ temporal norms of the density, once again over the interval $I$; in all cases, $L^2(\Gamma)$ spatial norms are used. From these results for the density $\psi_k$, $L^2$ and uniform temporal estimates are provided in Theorems 1 to 2 for the fields $u_k$ at all times after an $r_{\max}$-associated time lag beyond the end of time interval $I$.

**Remark 18.** *The truncation-error estimates mentioned above provide a methodology for identification of the times beyond which the scattered field $u_k$ (arising from the* single *incident wave packet $b_k$) is smaller than a desired tolerance $\varepsilon^{tol}$. It follows that the contribution of the scattered field $u_k$ to the overall scattered field $u$ decays with time in a manner that can easily be detected by inspection of the integral density $\psi_k$. More precisely, together with the rapid decay of densities and scattered fields for incident fields of compact support (for nontrapping obstacles by reference [96], and for certain weakly-trapping obstacles by Theorem* 5 *in Section* 13.2 *of this thesis), the results discussed above suggest that the decomposition* (4.10) *may be truncated to*

$$u(\mathbf{r},t) \approx \sum_{k=M_i}^{M_f-1} u_k(\mathbf{r},t), \tag{4.12}$$

*for certain integers $M_i$ and $M_f$, which, while only accounting for a total $M = M_f - M_i$ of "active windows" $b_k$, yields the total scattered field $u(\mathbf{r},t)$ with an error of the order of $\varepsilon^{tol}$, in various norms, and throughout the prescribed region of spacetime $\mathcal{R}\times\mathcal{T}$. (This argument is made fully rigorous in Theorem* 3.*) Thus, without significant accuracy loss, the truncated-approximation approach embodied in Equation* (4.12) *provides significant gains in terms of computing cost, and it gives rise to the overall $O(1)$ method announced in Chapter* 2 *(see also Remark* 7*).*

**Theorem 1.** *Consider a given region of interest $\mathcal{R}\subset\Omega$ at a positive distance from the boundary $\Gamma$. Then for every $\mathbf{r}\in\mathcal{R}$,*

$$\|u_k(\mathbf{r},\cdot)\|_{L^2([r_{\max}/c,\infty))} \le \beta(\mathcal{R})\,\|\psi_k\|_{L^2(\mathbb{R}^+;L^2(\Gamma))}\,, \tag{4.13}$$

*and*

$$\sup_{t>r_{\max}/c} |u_k(\mathbf{r},t)| \le \beta(\mathcal{R}) \sup_{t>0} \|\psi_k(\cdot,t)\|_{L^2(\Gamma)}\,, \tag{4.14}$$

*where $\beta^2(\mathcal{R}) = \max_{\mathbf{r}\in\mathcal{R},\mathbf{r}'\in\Gamma}\int_\Gamma \frac{1}{|\mathbf{r}-\mathbf{r}'|^2}\,\mathrm{d}\sigma(\mathbf{r}')$.*

*Proof.* Applying the Cauchy-Schwarz inequality to the representation formula (1.15) we have

$$\begin{aligned}|u_k(\mathbf{r},t)| &= \left|\int_\Gamma \frac{\psi_k(\mathbf{r}',t-|\mathbf{r}-\mathbf{r}'|/c)}{|\mathbf{r}-\mathbf{r}'|}\,\mathrm{d}\sigma(\mathbf{r}')\right| \\ &\le \left(\int_\Gamma \frac{1}{|\mathbf{r}-\mathbf{r}'|^2}\,\mathrm{d}\sigma(\mathbf{r}')\right)^{1/2}\left(\int_\Gamma |\psi_k(\mathbf{r}',t-|\mathbf{r}-\mathbf{r}'|/c)|^2\,\mathrm{d}\sigma(\mathbf{r}')\right)^{1/2}.\end{aligned}$$

Integrating this equation in time we find,

$$\begin{aligned}\|u_k(\mathbf{r},\cdot)\|^2_{L^2([r_{\max}/c,\infty))} &= \int_{r_{\max}/c}^{\infty} |u_k(\mathbf{r},t)|^2 \,\mathrm{d}t \\ &\leq \beta^2(\mathcal{R}) \int_0^{\infty} \int_\Gamma |\psi_k(\mathbf{r}',t')|^2 \,\mathrm{d}\sigma(\mathbf{r}')\,\mathrm{d}t' \leq \beta^2(\mathcal{R})\,\|\psi_k\|^2_{L^2(\mathbb{R}^+;\,L^2(\Gamma))}\,,\end{aligned} \tag{4.15}$$

or instead maximizing,

$$|u_k(\mathbf{r},t)| \leq \beta(\mathcal{R}) \sup_{t'>0} \|\psi_k(\cdot,t')\|_{L^2(\Gamma)}\,. \tag{4.16}$$

□

It should be noted that as the region of interest $\mathcal{R}$ approaches the boundary $\Gamma$, the estimate in Theorem 1 deteriorates since $\beta \to \infty$ as $r_{\min} \to 0^+$ (cf. the result of Proposition 1 which does not suffer this property). This result can be immediately strengthened for $\mathbf{r}$ arbitrarily close to $\Gamma$ (recovering Proposition 1) if $C^{0,\alpha}$ frequency-explicit operator norm bounds can be established; such estimates would be used in the proof of Theorem 4 rather than the $L^2$-estimates that were utilized. At present, a similar result, Theorem 2, can be shown which demonstrates that the norm of the field in $L^2$ in a spatial evaluation region $\mathcal{R}$ is independent of the proximity of the region $\mathcal{R}$ to the boundary $\Gamma$ (and, as before, is bounded above by the boundary density norm).

**Theorem 2.** *Let $\mathcal{R} \subset \Omega \cap \{|\mathbf{r}| < R\}$, where the Lipschitz obstacle $\Omega^c$ is centered at the origin. Then there exists a $C(R,\Gamma) > 0$ such that,*

$$\|u_k\|_{L^2([r_{\max}/c,\infty));L^2(\mathcal{R}))} \leq C(R,\Gamma)\,\|\psi_k\|_{L^2(\mathbb{R}^+;\,L^2(\Gamma))}\,, \tag{4.17}$$

*and*

$$\sup_{t>r_{\max}/c} \|u_k(\cdot,t)\|_{L^2(\mathcal{R})} \leq C(R,\Gamma) \sup_{t>0} \|\psi_k(\cdot,t)\|_{L^2(\Gamma)}\,. \tag{4.18}$$

*Proof.* Assume (without loss of generality since the obstacle is Lipschitz) that the boundary $\Gamma$ is locally planar; that is, we assume it to be a truncated planar surface in $\mathbb{R}^3$. We have,

$$u_k(\mathbf{r},t) = \int_\Gamma \frac{\psi_k(\mathbf{r}',t-|\mathbf{r}-\mathbf{r}'|/c)}{4\pi|\mathbf{r}-\mathbf{r}'|}\,\mathrm{d}\sigma(\mathbf{r}').$$

Now, integrating the solution over the volume $\mathcal{R}$ and applying Cauchy-Schwarz,

$$\begin{aligned}\|u_k(\cdot,t)\|^2_{L^2(\mathcal{R})} &= \int_{\mathcal{R}} |u_k(\mathbf{r},t)|^2 \,\mathrm{d}V(\mathbf{r}) \\ &\leq \frac{1}{16\pi^2} \int_{\mathcal{R}} \left( \int_\Gamma \psi_k^2(\mathbf{r}',t-|\mathbf{r}-\mathbf{r}'|/c)\,\mathrm{d}\sigma(\mathbf{r}') \right) \left( \int_\Gamma \frac{\mathrm{d}\sigma(\mathbf{r}')}{|\mathbf{r}-\mathbf{r}'|^2} \right) \mathrm{d}V(\mathbf{r})\end{aligned} \tag{4.19}$$

For a given integration point $\mathbf{r} \in \mathcal{R}$, we define the point $\mathbf{r}_0$ as the orthogonal projection of $\mathbf{r}$ on $\Gamma$, and let $z = |\mathbf{r} - \mathbf{r}_0|$. We first integrate on $\Gamma$ in two pieces: one set $\Gamma^{\text{far}}$ defined as the $\mathbf{r}' \in \Gamma$ for which $|\mathbf{r} - \mathbf{r}'| > 1$, and the other $\Gamma^{\text{near}}$ defined as the $\mathbf{r}' \in \Gamma$ for which $|\mathbf{r} - \mathbf{r}'| < 1$. In the former case, the integral in the integrand of (4.19) is always bounded, while the latter case is more delicate but still results in a finite $\|\cdot\|_{L^2(\mathcal{R})}$ norm. Indeed,

$$\begin{aligned}\int_{\Gamma^{\text{near}}} \frac{\mathrm{d}\sigma(\mathbf{r}')}{|\mathbf{r} - \mathbf{r}'|^2} &= \int_{\Gamma^{\text{near}}} \frac{dx'dy'}{z^2 + x'^2 + y'^2} = \int_0^1 \mathrm{d}\rho \int_0^{2\pi} \mathrm{d}\theta \frac{\rho}{z^2 + \rho^2} \\ &= \pi \int_0^1 \frac{\mathrm{d}v}{z^2 + v} = \pi \log\left(\frac{z^2 + 1}{z^2}\right),\end{aligned}$$

and per Equation (4.19) by integrating this quantity over $\mathcal{R}$ along rays $\mathbf{r} - \mathbf{r}_0$, we find

$$\frac{1}{16\pi^2} \int_{z_{\min}}^{z_{\max}} \int_{\Gamma^{\text{near}}} \frac{\mathrm{d}\sigma(\mathbf{r}')}{|\mathbf{r} - \mathbf{r}'|^2} \mathrm{d}z = \frac{1}{16\pi} \int_{z_{\min}}^{z_{\max}} \log\left(\frac{z^2 + 1}{z^2}\right) \mathrm{d}z.$$

It is clear that as $z_{\min} \to 0$, this integral remains finite, so, for arbitrary compact sets, we have shown

$$\frac{1}{16\pi^2} \int_{\mathcal{R}} \left( \int_{\Gamma} \frac{\mathrm{d}\sigma(\mathbf{r}')}{|\mathbf{r} - \mathbf{r}'|^2} \right) \mathrm{d}V(\mathbf{r}) \leq C(R, \Gamma).$$

where $C(R, \Gamma)$ is independent of $r_{\min}$.

Returning focus to (4.19) and considering $t > r_{\max}/c$, we find that by integrating in time,

$$\|u_k\|^2_{L^2([r_{\max}/c, \infty); L^2(\mathcal{R}))} \leq C(R, \Gamma) \, \|\psi_k\|^2_{L^2(\mathbb{R}^+; L^2(\Gamma))},$$

or instead maximizing,

$$\sup_{t > r_{\max}/c} \|u_k(\cdot, t)\|^2_{L^2(\mathcal{R})} \leq C(R, \Gamma) \sup_{t' > 0} \|\psi_k(\cdot, t')\|^2_{L^2(\Gamma)}.$$

□

The final theorem ties Theorem 1, bounds on the scattered field values $u_k$ in terms of the density $\psi_k$, to the theory, developed in the following sections and culminating in Theorem 5, that provides bounds and decay rates on the density $\psi_k$. In this manner, a stopping criterion is thus determined for each window, identifying a time at which to truncate its inclusion in the sum (4.12). The density bounds and decay results are proven only for non-strongly-trapping obstacles, those obstacles said to satisfy a certain $q$-growth condition given in Definition 2 of the next section.

**Theorem 3.** *Assume that the Lipschitz obstacle $\Omega^c$ satisfies a q-growth condition. Assume the incident wave with boundary values $\gamma^+ b \in C^\infty(\mathbb{R}; H^1(\Gamma))$ and $\gamma^+ \partial_{\mathbf{n}} b \in C^\infty(\mathbb{R}; L^2(\Gamma))$ is normalized so that $\|\gamma^+ \partial_{\mathbf{n}} b\|_{H^p(\mathbb{R};L^2(\Gamma))} \leq 1$ and $\|\gamma^+ b\|_{H^{p+1}(\mathbb{R};L^2(\Gamma))} \leq 1$ for a certain $p > 0$. For given real numbers $D_{\mathbf{r}} > 0$ and $D_t > 0$, and a given error tolerance $\varepsilon^{tol}$, there exists an integer $M$ such that for any set $\mathcal{R} \subset \Omega$ of diameter no larger than $D_{\mathbf{r}}$ and for any time interval $\mathcal{T}$ of length no larger than $D_t$, there exist integers $M_i$ and $M_f$ satisfying $M_f - M_i = M$, and such that truncation of the sum* (4.10) *to the range $M_i \leq k \leq M_f - 1$ in the sum* (4.12) *produces the value $u(\mathbf{r}, t)$ within an error tolerance of the order of $\varepsilon^{\text{tol}}$ throughout $\mathcal{R} \times \mathcal{T}$.*

*Proof.* Let $\mathcal{T}_1 = \min\{t \in \mathcal{T}\}$ and $\mathcal{T}_2 = \max\{t \in \mathcal{T}\}$ be the starting and ending times of the time evaluation region $\mathcal{T}$ that satisfies $\mathcal{T}_2 - \mathcal{T}_1 < D_t$ , and recall the definitions $r_{\min} = \min_{\mathbf{r}\in\mathcal{R},\mathbf{r}'\in\Gamma} |\mathbf{r} - \mathbf{r}'|$, $r_{\max} = \max_{\mathbf{r}\in\mathcal{R},\mathbf{r}'\in\Gamma} |\mathbf{r} - \mathbf{r}'|$.

First, by causality there will be no contributions from scattering solutions that are the result of incident fields that have not yet impinged on the obstacle. Choosing $M_f$ as the smallest positive integer such that $s_{M_f} - H + r_{\min}/c > \mathcal{T}_2$ ensures that for $t \in \mathcal{T}$ solutions $u_k$ for all $k \geq M_f$ can be excluded from the sum in Equation (4.10) with zero error. Indeed, this follows since the incident field $\gamma^+ b_k$ is zero on the obstacle for $t < s_{M_f} - H$ for all $k \geq M_f$,

Next, we estimate the remaining solution contributions through their boundary integral densities. Letting $n$ be a positive integer $n > 2$, letting $1 \leq k \leq M_f - 1$, and using $T_*$ and $\tau$ as in the setting of Section 13, consider the time interval $I_k = [T_k^f - T_* - 2\tau - r_{\max}/c, T_k^f - r_{\max}/c)$ for some $T_k^f > s_k + H + T_* + 2\tau$ as an interval $I_k$ (see point 1 in Remark 20) on which the bound

$$\left\|\psi_k^*\right\|_{H^{n(q+1)+1}(I_k;\, L^2(\Gamma))} \leq \varepsilon^{\text{tol}} \tag{4.20}$$

holds, where $\psi_k^*$ is defined as

$$\psi_k^*(\mathbf{r}, t) = w_+(t - T_k^f + T_* + 2\tau + r_{\max}/c) w_-(t - T_k^f + r_{\max}/c) \psi_k(\mathbf{r}, t).$$

Indeed, we can establish that $\psi_k^* \in H^{n(q+1)+1}(\mathbb{R}; L^2(\Gamma))$ by Lemma 1 since the incident data is smooth. Furthermore, it follows that there exists an interval $I_k$ on which the bound (4.20) holds by using Theorem 5 applied to the density $\psi_k$ on the interval $\mathcal{I}_k$ laying temporally immediately after the incident field vanishes on $\Omega^c$. In more detail, on this interval $\mathcal{I}_k$ the density $\psi_k$ can be bounded above by the

initial data $b_k$ through the Lemma 1 estimate Equation (4.31). Then, taking $T$ large in the estimate from Theorem 5 guarantees the existence of the interval $I_k$. Now, it is assumed that $\|\gamma^+\partial_{\mathbf{n}}b\|_{H^{n(q+1)+2}(\mathbb{R};\,L^2(\Gamma))} \leq 1$ and $\|\gamma^+ b\|_{H^{n(q+1)+1}(\mathbb{R};\,L^2(\Gamma))} \leq 1$, it follows from Theorem 5 (and Lemma 2) that $T_k^f = s_k + T^f$ for some $T^f > 0$, and so an $M_i$ exists independent of the incident field. Define $M_i$ as the smallest integer such that Equation (4.20) holds for $T_k^f > \mathcal{T}_1$, with $T^f$ chosen as small as possible while maintaining the validity of (4.20).

Then, by use of Theorem 5 again, we have

$$\sup_{t>T_k^f - r_{\max}/c+T} \|\psi_k(\cdot,t)\|_{L^2(\Gamma)} \leq CT^{1-n}\left\|\psi_k^*\right\|_{H^{n(q+1)+1}(I_k;\,L^2(\Gamma))} \leq C\varepsilon^{\mathrm{tol}}T^{1-n}. \quad (4.21)$$

Next, using Theorem 1 and the bound (4.21) we have for all $\mathbf{r} \in \mathcal{R}$ the bound

$$\sup_{t>T_k^f+T} |u_k(\mathbf{r},t)| \leq C\beta(\mathcal{R})T^{1-n}\varepsilon^{\mathrm{tol}}.$$

The temporal partitions satisfy a certain well-spaced property $s_{k+1} - s_k \geq H$ (see Section 5.1), a property which, together with the fact noted earlier that $T_k^f = s_k + T^f$, implies that for $t > T_{M_i}^f + T$, the bound

$$\sup_{t>T_{M_i}^f+T} |u_k(\mathbf{r},t)| \leq C\beta(\mathcal{R})(T + (M_i - k)H)^{1-n}\varepsilon^{tol}$$

holds for all $k < M_i$ and all $\mathbf{r} \in \mathcal{R}$. Therefore it is possible to estimate the error committed by the truncation of the sum (4.10) as

$$\begin{aligned}
\sup_{\substack{t\in\mathcal{T}\\ \mathbf{r}\in\mathcal{R}}}\left|u(\mathbf{r},t) - \sum_{k=M_i}^{M_f-1} u_k(\mathbf{r},t)\right| &\leq \sup_{\substack{t\in\mathcal{T}\\ \mathbf{r}\in\mathcal{R}}}\left(\sum_{k=1}^{M_i-1}|u_k(\mathbf{r},t)| + \sum_{k=M_f}^{K}|u_k(\mathbf{r},t)|\right)\\
&= \sup_{\substack{t\in\mathcal{T}\\ \mathbf{r}\in\mathcal{R}}}\sum_{k=1}^{M_i-1}|u_k(\mathbf{r},t)|\\
&\leq C_1\beta(\mathcal{R})\varepsilon^{tol}\sum_{k=1}^{M_i-1}((M_i-k)H)^{1-n}\\
&\leq C_1\beta(\mathcal{R})\varepsilon^{tol}\sum_{k=1}^{\infty}((M_i-k)H)^{1-n} = C\beta(\mathcal{R})\varepsilon^{tol},
\end{aligned}$$

where the constant $C$ is independent of the incident field $b$ and its duration $T^{\mathrm{inc}}$ (and thus of $K$). Thus only $M = M_f - M_i$ solution components $u_k$ are required to approximate the solution $u$ by the truncation in (4.12) with errors that are uniformly-bounded for all time. □

The proof of Theorem 3 was constructive, immediately leading to an algorithm for the identification of $M_i$ and $M_f$ (cf. Remark 19). The essential estimates on the boundary densities used above in the proof are the subject of the following section.

**Remark 19.** *Theorem* 3 *guarantees that a K-independent subset of the solution components $u_k$ (scattering solutions due to incident field $b_k$, $1 \leq k \leq K$) are required to produce the solution on any bounded space-time region of interest. In conjunction with the methods of Chapter* 2 *that require only $O(1)$ Helmholtz solves to accurately sample the solution at any time, this theorem justifies the claim of an overall $O(1)$ cost to the method, since the number of solution components $u_k$ that must be computed on any given region of space-time is independent of $T^{inc}$.*

*Another proof approach would be to argue that each individual time window stopping time $T_k^f$ can be determined from direct observation of $\psi_k^*$ on finite time intervals. Indeed, in practice it may be more efficient to determine the required solution components by direct inspection of the norm of the boundary densities $\psi_k$ on finite intervals of time in conjunction with Theorem* 5*; see also the numerical results in Section* 14 *of this chapter.*

## 13 Finite-time-history estimates on boundary densities for scattering problems

### 13.1 Finite-time-history boundary density estimates uniform over $\mathbb{R}^+$

As mentioned above, this section develops estimates for the future size of the density. To the author's knowledge no estimates of a similar or related character are reported in the literature. Certain definitions and assumptions are required to provide a setting for the statement of Theorem 4.

**Definition 1.** *For a given $\omega_0 > 0$ and a given $\Gamma = \partial\Omega$, the boundary of a Lipschitz domain, define the operator*

$$A_\omega = \frac{1}{2} I + K_\omega^* - \mathrm{i}\eta S_\omega, \quad \textit{with} \quad \eta = \begin{cases} 1, & \textit{if } 0 < \omega < \omega_0 \\ \omega, & \textit{if } \omega \geq \omega_0. \end{cases} \tag{4.22}$$

**Assumptions and definitions for lemmas and theorems.** *It is assumed that*

1. *A choice is made of window width $\tau$ and window functions $w_+, w_- \in C^\infty$ satisfying $w_- + w_+ = 1$, with*

$$w_-(t) = \begin{cases} 1 \textit{ for } t < -\tau \\ 0 \textit{ for } t \geq 0 \end{cases}, \quad w_+(t) = \begin{cases} 0 \textit{ for } t < -\tau \\ 1 \textit{ for } t \geq 0, \end{cases} \tag{4.23}$$

2. *For all time, the compactly-supported incident field $b_k(\mathbf{r}, t)$ is a solution to the wave equation in the interior region $\Omega^c \cup \Gamma$ and in a subset-of-$\Omega$ strip surrounding $\Gamma$,*

3. *The temporal support of $b_k$ (in $\Omega^c \cup \Gamma$) lies before the time interval*

$$I = [-T_* - 2\tau, 0), \tag{4.24}$$

*where $T_* := \mathrm{diam}(\Gamma)/c$, and*

4. *The density $\psi_k$ solves (in $L^2(\Gamma)$) Equation (1.16) for an incident field $b_k$, and in terms of this density $\psi_k$ define the auxiliary densities $\psi_-(\mathbf{r}, t) = w_-(t)\psi_k(\mathbf{r}, t)$, $\psi_+(\mathbf{r}, t) = w_+(t)\psi_k(\mathbf{r}, t)$, and*

$$\psi_*(\mathbf{r}, t) = w_+(t + T_* + \tau)w_-(t)\psi_k(\mathbf{r}, t), \tag{4.25}$$

*the latter clearly having temporal support in the time interval $I$.*

**Remark 20.** *1. The arguments that follow, in this section and the next, present estimates, in the form of upper bounds, on the density for $t > 0$ in terms of norms of the density over an interval $I$ that immediately precedes $t = 0$. The choice of $t = 0$ for the temporal location to make this argument is entirely without loss of generality and, in fact, all results hold for the density $\psi_k$ following any time period of the length of $I$ (in terms of norms over that interval) occurring after $b_k$ vanishes.*

2. *In a slight abuse of notation, we have dropped the subscript $k$ in the definitions of the density functions $\psi_-$, $\psi_+$, and $\psi_*$, even though such quantities are clearly dependent on the time partition index $k$. All analysis in this section as well as the following one considers a fixed time partition, and the convention of dropping the subscript index is done for notational simplicity. We also emphasize here the purpose of the functions $w_-$ and $w_+$ is so that the partition of unity of the density*

$$\psi_k(\cdot, t) = \psi_-(\cdot, t) + \psi_+(\cdot, t),$$

*holds for all time $t$.*

3. *We observe that the temporal supports "*supp*" of the functions $\psi_-$ and $\psi_+$ satisfy* $\mathrm{supp}\,\psi_- \subset (-\infty, 0)$ *and* $\mathrm{supp}\,\psi_+ \subset [-\tau, \infty)$ *on $\Gamma$. We wish to bound $\psi_k$ in the $L^2(\mathbb{R}^+; L^2(\Gamma))$ norm, and as an upper bound on that we bound $\psi_+$ in*

*$L^2$ in the slightly larger time interval $[-\tau, \infty)$. In order to do so, we identify the density $\psi_+$ as satisfying a scattering problem posed with small data—a certain relevant portion of the density history $\psi_-$. (More precisely, the density $\psi_*$ is measured in the* finite *time interval $I$ defined in* (4.24)*.)*

The frequency-domain boundary integral equation density $\psi_k^t$ is a physical quantity (see Equation (4.9)), independent of the choice of coupling parameter $\eta$ (cf. Definition 1), a fact which allows flexibility in the choice of coupling parameter as $\omega$ varies. This is important since bounds on $\left\|A_\omega^{-1}\right\|_{L^2(\Gamma)\to L^2(\Gamma)}$ are generally established for high-enough frequencies (indeed, at the present time, investigation of such estimates forms a highly-active research area with intended application in the numerical analysis of frequency-domain boundary element methods). In the low-frequency limit, a different coupling parameter (see the right-hand side of (4.22)) is required for the operator $A_\omega^{-1}$ in order to have uniformly-in-$\omega$ bounded norms (which are additionally independent of the trapping character of the obstacle) as $\omega \to 0^+$. Such high-frequency trapping estimates are coupled with low-frequency estimates in the following definition.

**Definition 2.** *For nonnegative integer $q$, we say that a Lipschitz obstacle satisfies a $q$-*growth *condition if, for the integral equation operator $A_\omega$ (c.f. Definition* 1*), the bound*

$$\|A_\omega^{-1}\|_{L^2(\Gamma)\to L^2(\Gamma)} \le C(1+\omega^2)^{q/2}, \quad C = C(\Gamma) > 0 \tag{4.26}$$

*holds, or, equivalently, that for $C_1 = C_1(\Gamma) > 0$ and $C_2 = C_2(\Gamma) > 0$, the bound*

$$\left\|A_\omega^{-1}\right\|_{L^2(\Gamma)\to L^2(\Gamma)} \le \begin{cases} C_1, & \text{if } \omega \le \omega_0 \\ C_2\omega^q, & \text{if } \omega > \omega_0, \end{cases} \tag{4.27}$$

*holds for all real $\omega \ge 0$.*

**Remark 21.** *It is known that Definition* 2 *is satisfied with $q = 0$, $q = 1$, $q = 2$ and $q = 3$ for various classes of obstacles. For example, reference [15, Thm. 1.13] shows that a smooth* nontrapping *obstacle (in which, according to [15, Def. 1.1], each billiard ball trajectory escapes from a ball of finite radius after finitely many bounces) satisfies* (4.26) *with $q = 0$. A related $q = 0$ result is presented in [39] for merely Lipschitz domains, but under the stronger assumption that the obstacle is star-shaped. Reference [37] shows that for "hyperbolic" trapping regions (in which all periodic billiard ball trajectories are unstable), a merely logarithmic growth in $\omega$ results, while for certain "parabolic" trapping regions, stronger ($q = 2$ or*

*$q = 3$) growth takes place. It is also known that much more strongly-trapping obstacles exist, including obstacles for which exponentially-large inverse operator norms $\left\|A_\omega^{-1}\right\|_{L^2(\Gamma)\to L^2(\Gamma)}$ occur [19, 35, 81] (and which, therefore, do not satisfy the $q$-growth condition for any $q$).*

*Additionally, it is known [19, Thm. 2.10] that for all Lipschitz obstacles, the integral equation operator $A_\omega$ satisfies the low-frequency estimate in Equation* (4.27) *(and inherent in Equation* (4.26)*)—rendering the $q$-growth condition truly one about high-frequency asymptotic behavior.*

**Remark 22.** *An interesting fact to note is that the result of reference [74], showing, for the first time, temporal rates of decay (indeed, an exponential rate) for wave scattering from a trapping obstacle (in that case, the trapping structure was a union of two disjoint convex obstacles), answered in the negative a conjecture by Lax and Phillips [83, p. 158] that all trapping obstacles have a sequence of resonances $\lambda_j$ such that $\operatorname{Im}\lambda_j \to 0^-$ and $\left|\operatorname{Re}\lambda_j\right| \to \infty$ as $j \to \infty$. (For more details see also [110]. See also [104] for results that show the challenge of establishing localized energy decay rates for trapping obstacles.) The results were later [73] generalized to arbitrary unions of strictly-convex obstacles that together satisfy both (1) a certain separation criterion and (2) that each connected piece is not contained in the convex hull of any two other pieces; such obstacles correspond to the $q = 1$ "hyperbolic" trapping region case mentioned above, and a numerical example of wave scattering from a closely-related obstacle is given in Section* 14.

**Remark 23.** *It can be seen that there exist connected trapping obstacles, including some which possess cavities, that satisfy the $q$-growth condition of Definition* 2 *for some value of $q$. Let*

$$\Omega_1 = \{\mathbf{r} = (r_1, r_2, r_3) : -1/2 \le r_1 \le 1/2, -1/2 \le r_2 \le 1/2, 0 \le r_3 \le 1\}.$$

*Then $\Omega^c = \{\mathbf{r} : |r_j| \le 1\} \setminus \Omega_1$ is an $(R_0, R_1, a)$ parallel trapping obstacle in the sense of [37, Def. 1.9], for $R_1 > \mathrm{e}^{1/4} R_0$, $R_0 \ge \sqrt{3/2}$, and $a = 1$. Note that $\Omega^c$ is a cube with a smaller cuboid removed from one of its faces and can be visualized in Figure* 4.1.

*Since $\Omega^c$ is Lipschitz, by [37, Cor. 1.14 and Rem. 1.16] it follows that $\Omega^c$ satisfies a $q$-growth condition with $q = 3$. Smoothing of the corners of this obstacle results in a connected trapping obstacle that satisfies a $q$-growth condition with $q = 2$.*

**Definition 3.** *We denote by $\gamma^+$ and $\gamma^-$ the well-known trace operators for functions in $\Omega$ and $\Omega^c$, respectively, onto $\Gamma$, which, for a Lipschitz obstacle, each have a unique extension to a bounded linear operator*

$$\gamma^+ : H^s(\Omega) \to H^{s-1/2}(\Gamma),$$

*and*

$$\gamma^- : H^s(\Omega^c) \to H^{s-1/2}(\Gamma),$$

*for $1/2 < s \leq 1$ [90].*

**Theorem 4.** *Let $q$ denote a nonnegative integer, and assume $\Omega^c$ satisfies the $q$-growth condition (Definition 2). For a given nonnegative integer $p$, if the incident field $b_k$ satisfies $\gamma^+ b_k \in H^{p+q+2}(\mathbb{R}; H^1(\Gamma))$ and $\gamma^+ \partial_{\mathbf{n}} b_k \in H^{p+q+1}(\mathbb{R}; L^2(\Gamma))$, the density at future times (relative to the time interval $I$) can be bounded in the $H^p(\mathbb{R}^+; L^2(\Gamma))$ norm as*

$$\|\psi_k\|_{H^p(\mathbb{R}^+; L^2(\Gamma))} \leq C(\Gamma, \tau, p) \, \|\psi_*\|_{H^{p+q+1}(I; L^2(\Gamma))} \, . \tag{4.28}$$

*The choice of $p = 1$, additionally, allows the uniform estimate in time of*

$$\sup_{t>0} \|\psi_k(\cdot, t)\|_{L^2(\Gamma)} \leq C(\Gamma, \tau) \, \|\psi_*\|_{H^{q+2}(I; L^2(\Gamma))} \, . \tag{4.29}$$

A proof outline of the results leading to Theorem 4 is sketched briefly in what follows. After the incident field has completely passed the obstacle (considered without loss of generality to be $t > 0$ for simplicity), scattering from the surface itself is the sole source of radiation for other points on the obstacle, and so the boundary density encodes all information about future scattering events. The relationship expressed in a certain time-dependent single-layer integral equation, of the density at future times to its state at past times can be understood itself as a scattering problem, though only of the energy that will be relevant to future scattering events and not that share of the energy radiating to infinity. Bounds on the scattering operator's inverse leads to a conclusion that the future density is small, in $L^2(\Gamma)$ and in various temporal norms. More specifically, a Fourier transform is taken and recent [15, 36, 37, 39, 70, 109] wavenumber-explicit bounds for the integral operators are used to bound the $L^2(\Gamma)$-norm of the density as a function of time, that is, in $\|\cdot\|_{L^2(\mathbb{R}^+; L^2(\Gamma))}$. A similar approach is followed for the time-derivative of the incident field data, leading to a bound on the future density in the $\|\cdot\|_{H^1(\mathbb{R}^+; L^2(\Gamma))}$ norm, and finally, via the Sobolev lemma, to uniform bounds in time. The proof approach intertwines frequency and time domain to leverage both frequency-domain and time-domain estimates;

thus, the proof of Theorem 4 proceeds by an excursion into time domain to exploit Huygens' principle (see the computations leading to (4.60) and the estimate leading to (4.67)) as well as sharp frequency-domain boundary integral operator estimates discussed in Definition 2.

The proof of Theorem 4 relies on the results presented in Lemmas 1 through 6 and is delayed in the presentation until these lemmas have been stated and proved. The first two of these lemmas establish the regularity of the temporal density $\psi_k$ for all time $t$ (Lemma 1) and on finite time intervals (Lemma 2); see also Remark 26.

**Remark 24.** *Without loss of generality, the incident field $b(\mathbf{r}, t)$ is assumed to be real-valued. It follows that the density $\psi(\mathbf{r}, t)$ which solves Equation* (1.16) *is real-valued, which implies that its Fourier transform $\psi^t(\mathbf{r}, \omega)$ obeys the Hermitian symmetry relation*

$$\psi^t(\mathbf{r}, -\omega) = \overline{\psi^t(\mathbf{r}, \omega)}. \tag{4.30}$$

*Therefore, our studies of frequency-domain operator norms are therefore restricted to the $\omega > 0$ case, as is often done in mathematical frequency-domain scattering theory [15, 19, 37]. The same symmetry relations apply for quantities such as $\psi_k$, $h(\mathbf{r}, t)$, $\psi_\pm(\mathbf{r}, t)$, $\psi_*(\mathbf{r}, t)$, etc. that are defined in terms of the real-valued $\psi$.*

**Lemma 1.** *For an obstacle satisfying a $q$-growth condition, assume that the incident field $b_k$ satisfies $\gamma^+ b_k \in H^{p+q+1}(\mathbb{R};\, L^2(\Gamma))$ and $\gamma^+ \partial_{\mathbf{n}} b_k \in H^{p+q}(\mathbb{R}; L^2(\Gamma))$. Then the scattering density $\psi_k$ satisfies $\psi_k \in H^p(\mathbb{R}; L^2(\Gamma))$. In particular, the density satisfies*

$$\|\psi_k\|_{H^p(\mathbb{R};\, L^2(\Gamma))} \leq C_1(\Gamma) \left\|\gamma^+ \partial_{\mathbf{n}} b_k\right\|_{H^{p+q}(\mathbb{R};\, L^2(\Gamma))} + C_2(\Gamma) \left\|\gamma^+ b_k\right\|_{H^{p+q+1}(\mathbb{R};\, L^2(\Gamma))}. \tag{4.31}$$

*Additionally, if both $\gamma^+ b_k \in H^{p+q+2}(\mathbb{R}; L^2(\Gamma))$ and $\gamma^+ \partial_{\mathbf{n}} b_k \in H^{p+q+1}(\mathbb{R}; L^2(\Gamma))$ are satisfied, then the density $\psi_k \in C^p(\mathbb{R}; L^2(\Gamma))$.*

*Proof.* The frequency domain integral equation (1.19) is satisfied with $\psi^t = \psi_k^t$ and $B^t = B_k^t$, and is written again below as

$$A_\omega \psi_k^t = \gamma^+ \partial_{\mathbf{n}} B_k^t - \mathrm{i}\eta \gamma^+ B_k^t.$$

Clearly,

$$(1+\omega^2)^{p/2} \psi_k^t = (1+\omega^2)^{p/2} A_\omega^{-1} \left(\gamma^+ \partial_{\mathbf{n}} B_k^t - \mathrm{i}\eta \gamma^+ B_k^t\right).$$

In view of Definition 2 for a bound on the norm of $A_\omega^{-1}$, and since by Definition 1 the coupling parameter $\eta$ satisfies $|\eta| \le (1+\omega^2)^{1/2}$ we find,

$$\begin{aligned}(1+\omega^2)^p \left\|\psi_k^t(\cdot,\omega)\right\|^2_{L^2(\Gamma)} \le & C(1+\omega^2)^{p+q}\left(\left\|\gamma^+\partial_{\mathbf{n}}B_k^t(\cdot,\omega)\right\|^2_{L^2(\Gamma)}\right.\\ &\left.+|\eta|^2\left\|\gamma^+B_k^t(\cdot,\omega)\right\|^2_{L^2(\Gamma)}\right)\\ \le\ & C(1+\omega^2)^{p+q}\left\|\gamma^+\partial_{\mathbf{n}}B_k^t(\cdot,\omega)\right\|^2_{L^2(\Gamma)} + C(1+\omega^2)^{p+q+1}\left\|\gamma^+B_k^t(\cdot,\omega)\right\|^2_{L^2(\Gamma)},\end{aligned}$$

and then integrating,

$$\begin{aligned}\|\psi_k\|^2_{H^p(\mathbb{R};\,L^2(\Gamma))} \le\ & C_1\int_{-\infty}^{\infty}(1+\omega^2)^{p+q}\left\|\gamma^+\partial_{\mathbf{n}}B_k^t(\cdot,\omega)\right\|^2_{L^2(\Gamma)}\,\mathrm{d}\omega\\ &+C_2\int_{-\infty}^{\infty}(1+\omega^2)^{p+q+1}\left\|\gamma^+B_k^t(\cdot,\omega)\right\|^2_{L^2(\Gamma)}\,\mathrm{d}\omega\\ =\ & C_1\left\|\gamma^+\partial_{\mathbf{n}}b_k\right\|^2_{H^{p+q}(\mathbb{R};\,L^2(\Gamma))}+C_2\left\|\gamma^+b_k\right\|^2_{H^{p+q+1}(\mathbb{R};\,L^2(\Gamma))}<\infty.\end{aligned}$$

Therefore, $\psi_k \in H^p(\mathbb{R};\,L^2(\Gamma))$. The claim $\psi_k \in C^p(\mathbb{R};\,L^2(\Gamma))$ follows from application of the first claim with $p$ substituted with $p+1$ and the use of the Sobolev lemma [58, Lemma 6.5]. □

**Definition 4** (Laplace transform and Laplace-domain operators)**.** *Let $s=\sigma+\mathrm{i}\omega$, with $\sigma,\omega\in\mathbb{R}$. We recall the familiar definition of the Laplace transform of a function $f(t)$, $t\ge 0$,*

$$F(s)=\mathcal{L}\{f\}(s)=\int_0^\infty f(t)\mathrm{e}^{-st}\,\mathrm{d}t. \tag{4.32}$$

*As is known, the inverse Laplace transform of a function $F(s)$, with all singularities of $F$ having real part less than $\sigma_0>0$, is defined via the Bromwich contour integral on the line* $\mathrm{Re}(s)=\sigma\ge\sigma_0$,

$$f(t)=\mathcal{L}^{-1}\{F\}(t)=\lim_{\omega\to\infty}\frac{1}{2\pi\mathrm{i}}\int_{\sigma-\mathrm{i}\omega}^{\sigma+\mathrm{i}\omega}F(s)\mathrm{e}^{st}\,ds. \tag{4.33}$$

*It will be useful to recall also the Laplace-domain boundary integral operators*

$$\left(S_s\mu\right)(\mathbf{r})=\int_\Gamma G_s(\mathbf{r},\mathbf{r}')\mu(\mathbf{r}')\,\mathrm{d}\sigma(\mathbf{r}'),\quad \mathbf{r}\in\Gamma, \tag{4.34}$$

$$\left(K_s^*\mu\right)(\mathbf{r})=\int_\Gamma\frac{\partial G_s(\mathbf{r},\mathbf{r}')}{\partial\mathbf{n}(\mathbf{r})}\mu(\mathbf{r}')\,\mathrm{d}\sigma(\mathbf{r}'),\quad \mathbf{r}\in\Gamma, \tag{4.35}$$

*and*

$$A_s=\frac{1}{2}I+K_s^*+sS_s, \tag{4.36}$$

*where $G_s(\mathbf{r},\mathbf{r}')=\mathrm{e}^{-s|\mathbf{r}-\mathbf{r}'|}/(4\pi|\mathbf{r}-\mathbf{r}'|)$ is the Green's function of the modified Helmholtz equation (i.e. the wave equation in Laplace domain).*

**Lemma 2.** *Assume that the incident field $b_k$ satisfies $\gamma^+ b_k \in H^{p+1}(\mathbb{R}; L^2(\Gamma))$ and $\gamma^+ \partial_{\mathbf{n}} b_k \in H^p(\mathbb{R}; L^2(\Gamma))$, and further assume that the incident field $b_k$ and its derivatives $\partial_t^i b_k$, $1 \le i \le p$, are supported in the time interval $[T_i, T_i + T]$ on $\Gamma$, for some finite $T > 0$. Then the restriction of the boundary density $\psi_k$ to $[T_i, T_i + T]$ for satisfies $\psi_k \in H^p([T_i, T_i + T]; L^2(\Gamma))$.*

*Proof.* First, define the time-shifted density $\widetilde{\psi}(\mathbf{r}, t) = \psi_k(\mathbf{r}, t - T_i)$ and incident field $\widetilde{b}(\mathbf{r}, t) = b_k(\mathbf{r}, t - T_i)$, in order to align with the domain of definition of the Laplace transform (4.32). We therefore need to prove that the restriction of $\widetilde{\psi}$ to $[0, T]$ satisfies $\widetilde{\psi} \in H^p([0, T]; L^2(\Gamma))$. As a compactly supported function, the incident field data $\widetilde{b}$ has a well-defined Laplace transform that has no poles in the complex plane to the right of some real line $\mathrm{Re}(s) = \sigma_0 > 0$, and we denote the Laplace transform as $\mathcal{B}(\mathbf{r}, s) = \mathcal{L}\{\widetilde{b}(\mathbf{r}, \cdot)\}(s)$, and therefore $\partial_{\mathbf{n}}\mathcal{B}(\mathbf{r}, s) = \mathcal{L}\{\partial_{\mathbf{n}}\widetilde{b}(\mathbf{r}, \cdot)\}(s)$. We show that the density $\widetilde{\psi} \in H^p([0, T]; L^2(\Gamma))$ by first establishing bounds for the Laplace-domain density $\widetilde{\Psi}(\mathbf{r}, s) = \mathcal{L}\{\widetilde{\psi}(\mathbf{r}, \cdot)\}(s)$.

As is well-established, $\widetilde{\Psi}$ satisfies the Laplace-domain combined-field integral equation (cf. Equation (1.19))

$$\left(A_s \widetilde{\Psi}\right)(\mathbf{r}, s) = \gamma^+ \partial_{\mathbf{n}} \mathcal{B}(\mathbf{r}, s) + s\gamma^+ \mathcal{B}(\mathbf{r}, s), \tag{4.37}$$

where $A_s$ is as defined in (4.36). The inverse of the operator $A_s$ is uniformly bounded [41, Thm. 4.2] in the Laplace variable $s$, i.e. for all $\mathrm{Re}(s) > \sigma_0$

$$\left\|A_s^{-1}\right\|_{L^2(\Gamma) \to L^2(\Gamma)} \le C, \quad C > 0 \text{ and independent of } s, \tag{4.38}$$

which, used in conjunction with (4.37), yields the estimate

$$\begin{aligned}\left\|\widetilde{\Psi}(\cdot, s)\right\|_{L^2(\Gamma)} &\le \left\|A_s^{-1}\right\|_{L^2(\Gamma \to L^2(\Gamma)} \left(\left\|\gamma^+ \partial_{\mathbf{n}} \mathcal{B}(\cdot, s)\right\|_{L^2(\Gamma)} + |s| \left\|\gamma^+ \mathcal{B}(\cdot, s)\right\|_{L^2(\Gamma)}\right) \\ &\le C \left\|\gamma^+ \partial_{\mathbf{n}} \mathcal{B}(\cdot, s)\right\|_{L^2(\Gamma)} + C|s| \left\|\gamma^+ \mathcal{B}(\cdot, s)\right\|_{L^2(\Gamma)}, \quad \mathrm{Re}(s) \ge \sigma_0 > 0.\end{aligned}$$

Applying Parseval's formula yields the desired conclusion $\widetilde{\psi} \in H^p([0, T]; L^2(\Gamma))$, by a well-established argument due to Lubich [87, Lemma 2.1] based on Laplace-domain boundary integral density estimates of precisely this form. □

Recalling the definitions and assumptions made at the beginning of this section (in particular, the definitions of $\psi_-$, $\psi_+$, and $\psi_*$, as well as the trace operators $\gamma^\pm$ on $\Gamma$ from Definition 3), Lemmas 3 to 6 below provide estimates related to the density $\psi_+$ as well as operator bounds in the frequency domain that are used in the proof of Theorem 4.

**Lemma 3** (Direct second-kind integral equations for the Fourier transform of $\psi_+$.)**.** *Assume $\gamma^+ b_k \in H^{q+1}(\mathbb{R}; H^1(\Gamma))$ and $\gamma^+ \partial_{\mathbf{n}} b_k \in H^q(\mathbb{R}; L^2(\Gamma))$. For each fixed $\omega \geq 0$ the Fourier-transformed density $\psi_+^t$ satisfies the second-kind integral equation*

$$\left(A_\omega \psi_+^t\right)(\mathbf{r}, \omega) = \gamma^- \partial_{\mathbf{n}} H^t(\mathbf{r}, \omega) - \mathrm{i}\eta \gamma^+ H^t(\mathbf{r}, \omega), \quad \mathbf{r} \in \Gamma, \tag{4.39}$$

*where $A_\omega = \frac{1}{2} I + K_\omega^* - \mathrm{i}\eta S_\omega$, and*

$$H^t(\mathbf{r}, \omega) = B_k^t(\mathbf{r}, \omega) - \left(S_\omega \psi_-^t\right)(\mathbf{r}, \omega). \tag{4.40}$$

*Proof.* Consider the single layer time domain integral equation (1.16) satisfied by $\psi_k$:

$$\int_{-\infty}^{t} \int_\Gamma \frac{\delta\left(t - t' - |\mathbf{r} - \mathbf{r}'|/c\right) \psi_k(\mathbf{r}', t')}{4\pi |\mathbf{r} - \mathbf{r}'|} \, \mathrm{d}\sigma(\mathbf{r}') \, \mathrm{d}t' = \gamma^+ b_k(\mathbf{r}, t), \quad -\infty < t < \infty, \tag{4.41}$$

where by Lemma 1 (applied with $p = 0$) the density satisfies $\psi_k \in L^2(\mathbb{R}; L^2(\Gamma))$. Rewriting this equation as

$$\int_\Gamma \frac{\psi_k(\mathbf{r}', t - |\mathbf{r} - \mathbf{r}'|/c)}{4\pi |\mathbf{r} - \mathbf{r}'|} \, \mathrm{d}\sigma(\mathbf{r}') = \gamma^+ b_k(\mathbf{r}, t),$$

and Fourier transforming gives the equation

$$(S_\omega \psi_k^t)(\mathbf{r}, \omega) = \gamma^+ B_k^t(\mathbf{r}, \omega), \mathbf{r} \in \Gamma.$$

Since by assumption $\gamma^+ B_k^t(\cdot, \omega) \in H^1(\Gamma)$, in view of reference [38, Thm. 2.25] we know this equation admits a unique solution $\psi_k^t(\cdot, \omega) \in L^2(\Gamma)$ for almost every $\omega$. Using the partition of unity decomposition

$$\psi_k = (w_- + w_+)\psi_k = \psi_- + \psi_+, \tag{4.42}$$

which follows from Equation (4.23), Equation (4.41) may be re-expressed in the form

$$\int_{-\infty}^{t} \int_\Gamma \frac{\delta\left(t - t' - |\mathbf{r} - \mathbf{r}'|/c\right) \psi_+(\mathbf{r}', t')}{4\pi |\mathbf{r} - \mathbf{r}'|} \, \mathrm{d}\sigma(\mathbf{r}') \, \mathrm{d}t' = \gamma^+ h(\mathbf{r}, t), \tag{4.43}$$

where

$$h(\mathbf{r}, t) = b_k(\mathbf{r}, t) - u_-(\mathbf{r}, t), \tag{4.44}$$

and

$$u_-(\mathbf{r}, t) := \int_{-\infty}^{t} \int_\Gamma \frac{\delta\left(t - t' - |\mathbf{r} - \mathbf{r}'|/c\right) \psi_-(\mathbf{r}', t')}{4\pi |\mathbf{r} - \mathbf{r}'|} \, \mathrm{d}\sigma(\mathbf{r}') \, \mathrm{d}t'.$$

Note in particular that $\psi_+$ (resp. $\psi_-$), and thus its Fourier transform $\psi_+^t$ (resp. $\psi_-^t$), is an element of $L^2(\Gamma)$.

Fourier transforming (4.43) yields the frequency-domain single-layer integral equation

$$(S_\omega \psi_+^t)(\mathbf{r}, \omega) = \gamma^+ H^t(\mathbf{r}, \omega), \mathbf{r} \in \Gamma. \tag{4.45}$$

for $\psi_+^t$, the Fourier transform of $\psi_+$, where $H^t$ is the Fourier transform of $h$ given in (4.44),

$$H^t(\mathbf{r}, t) = B_k^t(\mathbf{r}, \omega) - \left(S_\omega \psi_-^t\right)(\mathbf{r}, \omega).$$

Next, we consider the Dirichlet problems $\Delta v^\pm + \kappa^2(\omega) v^\pm = 0$, $\kappa(\omega) = \omega/c$, for the homogeneous Helmholtz equation in the domains $\Omega$ and $\Omega^c$, with $v^+$ and $v^-$ defined in $\Omega$ in $\Omega^c$, respectively, and with Dirichlet data $\gamma^+ v^+ = \gamma^- v^- = -\gamma^+ H^t$. Of course, since $H^t$ is a solution of the Helmholtz equation in $\Omega^c$, it follows that $v^- = -H^t$. Reference [46, Lemma 3.4] provides the representation formulas

$$v^+(\mathbf{r}, \omega) = -\langle \gamma^+ \partial_{\mathbf{n}} v^+ - \gamma^- \partial_{\mathbf{n}} v^-, G_\omega(\mathbf{r}, \cdot)\rangle, \quad \mathbf{r} \in \Omega, \tag{4.46}$$

and

$$v^-(\mathbf{r}, \omega) = -\langle \gamma^+ \partial_{\mathbf{n}} v^+ - \gamma^- \partial_{\mathbf{n}} v^-, G_\omega(\mathbf{r}, \cdot)\rangle, \quad \mathbf{r} \in \Omega^c, \tag{4.47}$$

where $\langle \cdot, \cdot \rangle$ denotes the duality pairing of the Sobolev spaces $H^s(\Gamma)$ and $H^{-s}(\Gamma)$. But, in view of [38, Cor. 2.28] we have $\gamma^+ \partial_{\mathbf{n}} v^+ \in L^2(\Gamma)$ and $\gamma^- \partial_{\mathbf{n}} v^- \in L^2(\Gamma)$, so Equation (4.46) and Equation (4.47) may be re-expressed in the form

$$v^+(\mathbf{r}, \omega) = -\int_\Gamma \left(\gamma^+ \partial_{\mathbf{n}} v^+ - \gamma^- \partial_{\mathbf{n}} v^-\right) G_\omega(\mathbf{r}, \mathbf{r}') \, \mathrm{d}\sigma(\mathbf{r}'), \quad \mathbf{r} \in \Omega, \tag{4.48}$$

and

$$v^-(\mathbf{r}, \omega) = -\int_\Gamma \left(\gamma^+ \partial_{\mathbf{n}} v^+ - \gamma^- \partial_{\mathbf{n}} v^-\right) G_\omega(\mathbf{r}, \mathbf{r}') \, \mathrm{d}\sigma(\mathbf{r}'), \quad \mathbf{r} \in \Omega^c. \tag{4.49}$$

Since the single-layer operator $S_\omega$ (cf. (1.12)) applied to an $L^2(\Gamma)$ density is continuous throughout $\mathbb{R}^3$ [90, Thm. 6.11], taking the interior trace $\gamma^-$ of Equation (4.49) yields the integral equation $(S_\omega \lambda) = \gamma^+ H^t$. But (4.45) tells us that $\lambda = \psi_+^t$ is also a solution of this equation and therefore, by uniqueness of $L^2(\Gamma)$ solutions [38, Thm. 2.25], we have

$$\psi_+^t = \gamma^+ \partial_{\mathbf{n}} v^+ + \gamma^- \partial_{\mathbf{n}} H^t. \tag{4.50}$$

In view of this equation, we may re-express (4.48) in the form

$$v^+(\mathbf{r}, \omega) = -\int_\Gamma \psi_+^t(\mathbf{r}', \omega) G_\omega(\mathbf{r}, \mathbf{r}') \, \mathrm{d}\sigma(\mathbf{r}'), \quad \mathbf{r} \in \Omega. \tag{4.51}$$

In order to obtain an integral equation which, unlike Equation (4.45), is uniquely solvable at all frequencies, we follow [34] and combine Equation (4.45) with the equation

$$\gamma^+\partial_{\mathbf{n}}v^+(\mathbf{r},\omega) = -\int_\Gamma \psi_+^t(\mathbf{r}',\omega)\partial_{\mathbf{n}(\mathbf{r})}G_\omega(\mathbf{r},\mathbf{r}')\,\mathrm{d}\sigma(\mathbf{r}') + \frac{1}{2}\psi_+^t, \quad \text{for} \quad \mathbf{r}\in\Gamma. \tag{4.52}$$

that results as the outer normal derivative operator on $\Gamma$ is applied to the representation formula (4.51). In detail, Equation (4.52) follows from the well-known jump relations [90, p. 219] that

$$\lim_{\varepsilon\to 0^+}\mathbf{n}(\mathbf{r})\cdot\nabla\int_\Gamma \mu(\mathbf{r}')G_\omega(\mathbf{r}+\varepsilon\mathbf{n}(\mathbf{r}),\mathbf{r}')\,\mathrm{d}\sigma(\mathbf{r}') = \left(-\frac{1}{2}I + K_\omega^*\right)\mu(\mathbf{r}),\ \mathbf{r}\in\Gamma, \tag{4.53}$$

for the operator equal to the normal derivative on $\Gamma$ of the single-layer potential with density $\mu$ in the space $L^2(\Gamma)$ (cf. [46, Thm. 1]). Using (4.50) to rewrite the left-hand-side of (4.52) gives the second-kind integral equation for $\psi_+^t$,

$$\frac{1}{2}\psi_+^t(\mathbf{r},\omega) + \left(K_\omega^*\psi_+^t\right)(\mathbf{r},\omega) = \gamma^-\partial_{\mathbf{n}}H^t(\mathbf{r},\omega). \tag{4.54}$$

posed for $\psi_+^t \in L^2(\Gamma)$ [46, Thm. 1(iv)]. Finally, a linear combination of (4.45) and (4.54) yields the combined field integral equation

$$\left(A_\omega\psi_+^t\right)(\mathbf{r},\omega) = \gamma^-\partial_{\mathbf{n}}H^t(\mathbf{r},\omega) - \mathrm{i}\eta\gamma^+H^t(\mathbf{r},\omega), \quad \mathbf{r}\in\Gamma, \tag{4.55}$$

where $A_\omega = \frac{1}{2}I + K_\omega^* - \mathrm{i}\eta S_\omega$. This equation is uniquely solvable [38, Thm. 2.27], and its solution is the previously-defined Fourier transform $\psi_+^t(\cdot,\omega)\in L^2(\Gamma)$ of the time-domain solution $\psi_+$.

□

**Remark 25.** *The direct second-kind integral equation* (4.39) *we have derived is atypical in that the density and the right-hand-side involve interior data, the quantity* $\gamma^-\partial_{\mathbf{n}}H^t$*. This nontrivial choice is essential to the proof's success, since we need to jointly satisfy two requirements, namely (1) that the density satisfies* (4.45)*, and (2) that the resulting combined field integral operator (the one in* (4.39)*) has available frequency-explicit norm bounds. Its appropriateness for use in numerical methods is not at issue since the specific choice of integral equation for the physical density* $\psi_k$*, while relevant to the proof of the theorem statement, is not in any way used in the numerical solution methods.*

**Lemma 4** (Frequency-explicit stability bounds for the solution of the frequency-domain equation (4.39))**.** *For an obstacle satisfying a $q$-growth condition, the density $\psi_+$ satisfies*

$$\begin{aligned}\left\|\psi_+^t\right\|^2_{L^2(\mathbb{R};\, L^2(\Gamma))} \leq C_1 \int_{|\omega|>\omega_0} \omega^{2q} \left\|\gamma^- \partial_{\mathbf{n}} H^t(\cdot,\omega) - \mathrm{i}\omega\gamma^+ H^t(\cdot.\omega)\right\|^2_{L^2(\Gamma)} \,\mathrm{d}\omega \\ + C_2 \int_{-\omega_0}^{0} \left\|\gamma^- \partial_{\mathbf{n}} H^t(\cdot,\omega) + \mathrm{i}\gamma^+ H^t(\cdot,\omega)\right\|^2_{L^2(\Gamma)} \,\mathrm{d}\omega \\ + C_2 \int_{0}^{\omega_0} \left\|\gamma^- \partial_{\mathbf{n}} H^t(\cdot,\omega) - \mathrm{i}\gamma^+ H^t(\cdot,\omega)\right\|^2_{L^2(\Gamma)} \,\mathrm{d}\omega.\end{aligned} \tag{4.56}$$

*Proof.* It is known that $A_\omega$ is invertible for every $\omega \in \mathbb{R}$ for $\mathrm{Re}(\eta) \neq 0$, so that the solution of (4.39) is $\psi_+^t = A_\omega^{-1}\left(\partial_{\mathbf{n}}^- H^t - \mathrm{i}\eta H^t\right)$. We therefore have the frequency-wise bound in terms of its operator norm,

$$\|\psi_+^t(\cdot,\omega)\|_{L^2(\Gamma)} \leq \|A_\omega^{-1}\|_{L^2(\Gamma)\to L^2(\Gamma)} \left\|\gamma^- \partial_{\mathbf{n}} H^t(\cdot,\omega) - \mathrm{i}\eta\gamma^+ H^t(\cdot,\omega)\right\|_{L^2(\Gamma)},$$

for all $\omega \geq 0$.

Since, by assumption, the obstacle satisfies a $q$-growth condition, in view of Equation (4.27) we find that for $\omega > \omega_0$,

$$\|\psi_+^t(\cdot,\omega)\|_{L^2(\Gamma)} \leq C_1\omega^{2q} \left\|\gamma^- \partial_{\mathbf{n}} H^t(\cdot,\omega) - \mathrm{i}\omega\gamma^+ H^t(\cdot,\omega)\right\|_{L^2(\Gamma)}, \tag{4.57}$$

and we find that for $0 \leq \omega < \omega_0$,

$$\|\psi_+^t(\cdot,\omega)\|_{L^2(\Gamma)} \leq C_2 \left\|\gamma^- \partial_{\mathbf{n}} H^t(\cdot,\omega) - \mathrm{i}\gamma^+ H^t(\cdot,\omega)\right\|_{L^2(\Gamma)}. \tag{4.58}$$

For $\omega < 0$ (see Equation (4.30)), it is noted that $\left\|\psi_+^t(\cdot,\omega)\right\|_{L^2(\Gamma)} = \left\|\psi_+^t(\cdot,|\omega|)\right\|_{L^2(\Gamma)}$, and so by Hermitian symmetry for $\omega < -\omega_0$,

$$\begin{aligned}\|\psi_+^t(\cdot,\omega)\|_{L^2(\Gamma)} &\leq C_1\omega^{2q} \left\|\gamma^- \partial_{\mathbf{n}} H^t(\cdot,|\omega|) - \mathrm{i}|\omega|\gamma^+ H^t(\cdot,|\omega|)\right\|_{L^2(\Gamma)} \\ &= C_1\omega^{2q} \left\|\gamma^- \partial_{\mathbf{n}} H^t(\cdot,\omega) - \mathrm{i}\omega\gamma^+ H^t(\cdot,\omega)\right\|_{L^2(\Gamma)}.\end{aligned}$$

Similarly, for $-\omega_0 < \omega < 0$,

$$\begin{aligned}\|\psi_+^t(\cdot,\omega)\|_{L^2(\Gamma)} &\leq C_2 \left\|\gamma^- \partial_{\mathbf{n}} H^t(\cdot,|\omega|) - \mathrm{i}\gamma^+ H^t(\cdot,|\omega|)\right\|_{L^2(\Gamma)} \\ &= C_2 \left\|\gamma^- \partial_{\mathbf{n}} H^t(\cdot,\omega) + \mathrm{i}\gamma^+ H^t(\cdot,\omega)\right\|_{L^2(\Gamma)}.\end{aligned}$$

We can then bound in $L^2$ of frequency using the estimate

$$\begin{aligned}\left\|\psi_+^t\right\|^2_{L^2(\mathbb{R};\, L^2(\Gamma))} &= \int_\Gamma \int_{-\infty}^{\infty} |\psi_+^t(\mathbf{r},\omega)|^2 \,\mathrm{d}\omega \,\mathrm{d}\sigma(\mathbf{r}) = \int_{-\infty}^{\infty} \left\|\psi_+^t(\cdot,\omega)\right\|^2_{L^2(\Gamma)} \,\mathrm{d}\omega \\ &\leq C_1 \int_{|\omega|>\omega_0} \omega^{2q} \left\|\gamma^- \partial_{\mathbf{n}} H^t(\cdot,\omega) - \mathrm{i}\omega\gamma^+ H^t(\cdot,\omega)\right\|^2_{L^2(\Gamma)} \,\mathrm{d}\omega \\ &\quad + C_2 \int_{-\omega_0}^{0} \left\|\gamma^- \partial_{\mathbf{n}} H^t(\cdot,\omega) + \mathrm{i}\gamma^+ H^t(\cdot,\omega)\right\|^2_{L^2(\Gamma)} \,\mathrm{d}\omega \\ &\quad + C_2 \int_{0}^{\omega_0} \left\|\gamma^- \partial_{\mathbf{n}} H^t(\cdot,\omega) - \mathrm{i}\gamma^+ H^t(\cdot,\omega)\right\|^2_{L^2(\Gamma)} \,\mathrm{d}\omega,\end{aligned} \tag{4.59}$$

as was to be shown. □

**Lemma 5** (Relating the incident field $h$ to a limited time history density.)**.** *With $u_*$ denoting the time-domain single-layer potential with density $\psi_*$, the function $h$ satisfies*

$$h(\mathbf{r},t) = \begin{cases} -u_*(\mathbf{r},t), & t \geq -\tau \\ 0, & t < -\tau \end{cases} \quad \textit{for} \quad \mathbf{r} \in \Omega^c \cup \Gamma, \tag{4.60}$$

*and has bounded temporal support for $\mathbf{r} \in \Omega^c \cup \Gamma$,*

$$\operatorname{supp} h(\mathbf{r},\cdot) \subset [-\tau, T_*]. \tag{4.61}$$

*Proof.* By assumption, the incident field $b_k(\mathbf{r},t)$ vanishes for $(\mathbf{r},t) \in (\Omega^c \cup \Gamma) \times [-T_* - 2\tau, \infty)$. Considering specifically the time region $t > -\tau$, we see then that $h(\mathbf{r},t) = -u_-(\mathbf{r},t)$ for all $\mathbf{r} \in \Omega^c \cup \Gamma$. Recalling the definition of $T_*$ from Section 13.1, $T_* = \max_{\mathbf{r},\mathbf{r}'\in\Gamma} |\mathbf{r}-\mathbf{r}'|/c$, we find that, for $t > -\tau$ and $t' < -T_* - \tau$ we have $t - t' - |\mathbf{r}-\mathbf{r}'|/c > 0$. Because this is the quantity in the delta function in the Green's function the density at these time values does not contribute, so, for all $\mathbf{r} \in \Omega^c \cup \Gamma$ and for all $t > -\tau$, we have a restriction in the integration region to the finite space-time region $\Gamma \times [-T_* - \tau, t]$,

$$\begin{aligned} h(\mathbf{r},t) = -u_-(\mathbf{r},t) &= -\int_{-T_*-\tau}^{t} \int_\Gamma \frac{\delta\left(t - t' - |\mathbf{r}-\mathbf{r}'|/c\right) w_-(t')\psi(\mathbf{r}',t')}{4\pi|\mathbf{r}-\mathbf{r}'|} \,\mathrm{d}\sigma(\mathbf{r}') \,\mathrm{d}t' \\ &= -\int_{-T_*-\tau}^{t} \int_\Gamma \frac{\delta\left(t - t' - |\mathbf{r}-\mathbf{r}'|/c\right) w_+(t'+T_*+\tau) w_-(t')\psi(\mathbf{r}',t')}{4\pi|\mathbf{r}-\mathbf{r}'|} \,\mathrm{d}\sigma(\mathbf{r}') \,\mathrm{d}t' \\ &= -\int_{-T_*-\tau}^{t} \int_\Gamma \frac{\delta\left(t - t' - |\mathbf{r}-\mathbf{r}'|/c\right) \psi_*(\mathbf{r}',t')}{4\pi|\mathbf{r}-\mathbf{r}'|} \,\mathrm{d}\sigma(\mathbf{r}') \,\mathrm{d}t', \end{aligned}$$

where the last equality is the definition of $\psi$, Equation (4.25). It is useful to define the time-domain single layer potential

$$u_*(\mathbf{r},t) = \int_{-\infty}^{t} \int_\Gamma \frac{\delta\left(t - t' - |\mathbf{r}-\mathbf{r}'|/c\right) \psi_*(\mathbf{r}',t')}{4\pi|\mathbf{r}-\mathbf{r}'|} \,\mathrm{d}\sigma(\mathbf{r}') \,\mathrm{d}t', \tag{4.62}$$

so that $h(\mathbf{r},t) = -u_*(\mathbf{r},t)$ for $(\mathbf{r},t) \in (\Omega^c \cup \Gamma)\times[-\tau,\infty)$. Now, because $\psi_+(\mathbf{r},t) \equiv 0$ for all $t < -\tau$, it follows from (4.43) that $h(\mathbf{r},t) = 0$ for $(\mathbf{r},t) \in (\Omega^c \cup \Gamma)\times(-\infty,-\tau)$, and so

$$h(\mathbf{r},t) = \begin{cases} -u_*(\mathbf{r},t), & t \geq -\tau \\ 0, & t < -\tau \end{cases} \quad \text{for} \quad \mathbf{r} \in \Omega^c \cup \Gamma, \tag{4.63}$$

showing (4.60).

It remains to show the bounded support of $h$. Recall from the definition of $\psi_*$ that $\operatorname{supp}\psi_*(\mathbf{r},\cdot) \subset I = [-T_* - 2\tau, 0)$, for all $\mathbf{r} \in \Gamma$. Therefore, rewriting (4.62)

$$u_*(\mathbf{r},t) = \int_\Gamma \frac{\psi_*(\mathbf{r}', t - |\mathbf{r}-\mathbf{r}'|/c)}{4\pi|\mathbf{r}-\mathbf{r}'|}\,\mathrm{d}\sigma(\mathbf{r}'),$$

and noting that $|\mathbf{r}-\mathbf{r}'|/c < T_*$ for all $\mathbf{r},\mathbf{r}' \in \Omega^c \cup \Gamma$, it follows that $h(\mathbf{r},t) = 0$ for $(\mathbf{r},t) \in (\Omega^c \cup \Gamma) \times [T_*,\infty)$. Notice that the function $h(\mathbf{r},t) = b_k - u_-$ (whose trace is the boundary data for the integral equation (4.43) with solution $\psi_+$) thus has bounded temporal support on $\Omega^c \cup \Gamma$, even at certain times for which scattering due to the incident field $b$ is occurring. □

**Lemma 6.** *For all $\omega \geq 0$, the operator norm bounds*

$$\|(\gamma^- \partial_{\mathbf{n}} - \mathrm{i}\omega)\, S_\omega\|_{L^2(\Gamma)\to L^2(\Gamma)} \leq C_1(1+\omega^2)^{1/2}, \tag{4.64}$$

*and*

$$\|(\gamma^- \partial_{\mathbf{n}} \pm \mathrm{i})\, S_\omega\|_{L^2(\Gamma)\to L^2(\Gamma)} \leq C_2(1+\omega^2)^{1/2}, \tag{4.65}$$

*hold with $C_1 = C_1(\Gamma) > 0$ and $C_2 = C_2(\Gamma) > 0$.*

*Proof.* Let $\mu \in L^2(\Gamma)$ and define the potential $U(\mathbf{r}) = (S_\omega\mu)(\mathbf{r})$. Jump properties of the derivative of the single layer give that for $\mathbf{r} \in \Gamma$, $\gamma^-\partial_{\mathbf{n}}U(\mathbf{r}) = \frac{1}{2}\mu(\mathbf{r}) + \left(K_\omega^*\mu\right)(\mathbf{r})$. The references [36, Thms. 3.3 and 3.5] and [70, Thm. A.1 by J. Galkowski] establish that there exist constants $D_1, D_2, D_3 > 0$ such that for all $\omega$,

$$\|S_\omega\|_{L^2(\Gamma)\to L^2(\Gamma)} \leq D_1, \quad \text{and} \quad \left\|K_\omega^*\right\|_{L^2(\Gamma)\to L^2(\Gamma)} \leq D_2\omega^{1/6}\log\omega + D_3,$$

and, moreover, these estimates are sharp (modulo the logarithmic factors in the latter). Therefore,

$$\begin{aligned} \|(\gamma^-\partial_{\mathbf{n}} - \mathrm{i}\omega)\, U\|_{L^2(\Gamma)} &\leq \left\|\frac{1}{2}I + K_\omega^* - \mathrm{i}\omega S_\omega\right\|_{L^2(\Gamma)\to L^2(\Gamma)} \|\mu\|_{L^2(\Gamma)} \\ &\leq (\widetilde{D}_1 + \widetilde{D}_2\omega)\,\|\mu\|_{L^2(\Gamma)} \\ &\leq C_1(1+\omega^2)^{1/2}\,\|\mu\|_{L^2(\Gamma)}\,. \end{aligned}$$

Similarly,

$$\|(\gamma^- \partial_{\mathbf{n}} \pm \mathrm{i})\, U\|_{L^2(\Gamma)} \leq C_2 (1+\omega^2)^{1/2} \|\mu\|_{L^2(\Gamma)}\,.$$

□

The necessary lemmas having been established, the proof of Theorem 4 can now be presented.

*Proof of Theorem* 4. ***Step I: $L^2$-in-time bounds on $\psi_+$ in terms of a small-data limited time history density.***

We want to show that the space-time norms of $\psi_+$ can be bounded in terms of $\|\psi_*\|_{H^s(I;L^2(\Gamma))}$ for some $s$. Since the incident field data satisfies $\gamma^+ b_k \in H^{p+q+1}(\mathbb{R};H^1(\Gamma))$ and $\gamma^+\partial_{\mathbf{n}} b_k \in H^{p+q}(\mathbb{R};L^2(\Gamma))$, the conditions of Lemma 3 are met. Then, applying Lemma 3 and Lemma 4, we find ourselves with the bound (4.56) for the density $\psi_+$ which we restate below,

$$\begin{aligned}\left\|\psi_+^t\right\|^2_{L^2(\mathbb{R};L^2(\Gamma))} \leq C_1 &\int_{|\omega|>\omega_0} \omega^{2q} \left\|\gamma^-\partial_{\mathbf{n}} H^t(\cdot,\omega) - \mathrm{i}\omega\gamma^+ H^t(\cdot.\omega)\right\|^2_{L^2(\Gamma)}\,\mathrm{d}\omega \\ &+ C_2 \int_{-\omega_0}^{0} \left\|\gamma^-\partial_{\mathbf{n}} H^t(\cdot,\omega) + \mathrm{i}\gamma^+ H^t(\cdot,\omega)\right\|^2_{L^2(\Gamma)}\,\mathrm{d}\omega \\ &+ C_2 \int_{0}^{\omega_0} \left\|\gamma^-\partial_{\mathbf{n}} H^t(\cdot,\omega) - \mathrm{i}\gamma^+ H^t(\cdot,\omega)\right\|^2_{L^2(\Gamma)}\,\mathrm{d}\omega.\end{aligned} \tag{4.66}$$

Based on the expressions in the above integrands, define the differential operators $\mathcal{S}$ and $\mathcal{T}_\pm$ by

$$\mathcal{S}(\cdot)(\mathbf{r},t) = \left(\mathrm{i}\frac{\partial}{\partial t}\right)^q \left(\gamma^-\partial_{\mathbf{n}} + \frac{\partial}{\partial t}\gamma^+\right), \quad \text{and} \quad \mathcal{T}_\pm(\cdot)(\mathbf{r},t) = \left(\gamma^-\partial_{\mathbf{n}} \pm \mathrm{i}\gamma^+\right),$$

which have the Fourier symbols,

$$\hat{\mathcal{S}}(\cdot)(\mathbf{r},\omega) \coloneqq \omega^q \left(\gamma^-\partial_{\mathbf{n}} - \mathrm{i}\omega\gamma^+\right), \quad \text{and} \quad \hat{\mathcal{T}}_\pm(\cdot)(\mathbf{r},\omega) \coloneqq \left(\gamma^-\partial_{\mathbf{n}} \pm \mathrm{i}\gamma^+\right).$$

Continuing on the estimate (4.56) and using the compact temporal support of $h$

proved in Lemma 5,

$$\begin{aligned}
\left\|\psi_+^t\right\|^2_{L^2(\mathbb{R};\, L^2(\Gamma))} \leq & \int_{|\omega|>\omega_0} C_1 \left\|\hat{\mathcal{S}} H^t(\cdot,\omega)\right\|^2_{L^2(\Gamma)} \,\mathrm{d}\omega + \int_{-\omega_0}^{0} C_2 \left\|\hat{\mathcal{T}}_+ H^t(\cdot,\omega)\right\|^2_{L^2(\Gamma)} \,\mathrm{d}\omega \\
& + \int_0^{\omega_0} C_2 \left\|\hat{\mathcal{T}}_- H^t(\cdot,\omega)\right\|^2_{L^2(\Gamma)} \,\mathrm{d}\omega \\
\leq C_1 \int_\Gamma \int_{-\infty}^{\infty} \left|\hat{\mathcal{S}} H^t(\mathbf{r},\omega)\right|^2 \,\mathrm{d}\omega\,\mathrm{d}\sigma(\mathbf{r}) & + C_2 \int_\Gamma \int_{-\infty}^{\infty} \left|\hat{\mathcal{T}}_+ H^t(\mathbf{r},\omega)\right|^2 \,\mathrm{d}\omega\,\mathrm{d}\sigma(\mathbf{r}) \\
& + C_2 \int_\Gamma \int_{-\infty}^{\infty} \left|\hat{\mathcal{T}}_- H^t(\mathbf{r},\omega)\right|^2 \,\mathrm{d}\omega\,\mathrm{d}\sigma(\mathbf{r}) \\
= C_1 \int_\Gamma \int_{-\infty}^{\infty} |\mathcal{S} h(\mathbf{r},t)|^2 \,\mathrm{d}t\,\mathrm{d}\sigma(\mathbf{r}) & + C_2 \int_\Gamma \int_{-\infty}^{\infty} |\mathcal{T}_+ h(\mathbf{r},t)|^2 \,\mathrm{d}t\,\mathrm{d}\sigma(\mathbf{r}) \\
& + C_2 \int_\Gamma \int_{-\infty}^{\infty} |\mathcal{T}_- h(\mathbf{r},t)|^2 \,\mathrm{d}t\,\mathrm{d}\sigma(\mathbf{r}) \\
= C_1 \int_\Gamma \int_{-\tau}^{\infty} |\mathcal{S} u_*(\mathbf{r},t)|^2 \,\mathrm{d}t\,\mathrm{d}\sigma(\mathbf{r}) & + C_2 \int_\Gamma \int_{-\tau}^{\infty} |\mathcal{T}_- u_*(\mathbf{r},t)|^2 \,\mathrm{d}t\,\mathrm{d}\sigma(\mathbf{r}) \\
& + C_2 \int_\Gamma \int_{-\tau}^{\infty} |\mathcal{T}_+ u_*(\mathbf{r},t)|^2 \,\mathrm{d}t\,\mathrm{d}\sigma(\mathbf{r})
\end{aligned}$$

where we used (4.60) to recast the bounds in terms of $u_*$ in time-domain. Finally, we thus have

$$\begin{aligned}
\left\|\psi_+^t\right\|^2_{L^2(\mathbb{R};\, L^2(\Gamma))} \leq & C_1 \int_\Gamma \int_{-\infty}^{\infty} |\mathcal{S} u_*(\mathbf{r},t)|^2 \,\mathrm{d}t\,\mathrm{d}\sigma(\mathbf{r}) \\
& + C_2 \int_\Gamma \int_{-\infty}^{\infty} |\mathcal{T}_+ u_*(\mathbf{r},t)|^2 \,\mathrm{d}t\,\mathrm{d}\sigma(\mathbf{r}) + C_2 \int_\Gamma \int_{-\infty}^{\infty} |\mathcal{T}_- u_*(\mathbf{r},t)|^2 \,\mathrm{d}t\,\mathrm{d}\sigma(\mathbf{r}),
\end{aligned} \tag{4.67}$$

Note that it is critical that $\mathcal{S}$ and $\mathcal{T}$ are temporally-local differential operators so that for $t < -\tau$ the fact that $h = 0$ implies also $\mathcal{S}h = 0$ and $\mathcal{T}h = 0$. Using Plancherel's theorem again,

$$\begin{aligned}
\left\|\psi_+^t\right\|^2_{L^2(\mathbb{R};\, L^2(\Gamma))} \leq & C_1 \int_{-\infty}^{\infty} \left\|\hat{\mathcal{S}} U_*^t(\cdot,\omega)\right\|^2_{L^2(\Gamma)} \,\mathrm{d}\omega + C_2 \int_{-\infty}^{\infty} \left\|\hat{\mathcal{T}}_+ U_*^t(\cdot,\omega)\right\|^2_{L^2(\Gamma)} \,\mathrm{d}\omega \\
& + C_2 \int_{-\infty}^{\infty} \left\|\hat{\mathcal{T}}_- U_*^t(\cdot,\omega)\right\|^2_{L^2(\Gamma)} \,\mathrm{d}\omega.
\end{aligned} \tag{4.68}$$

Since $u_*$ is a time-domain single-layer potential with density $\psi_*$, the quantities $\left\|\hat{\mathcal{S}} U_*^t(\cdot,\omega)\right\|_{L^2(\Gamma)}$ and $\left\|\hat{\mathcal{T}}_\pm U_*^t(\cdot,\omega)\right\|_{L^2(\Gamma)}$ in (4.68) can be bounded frequency-wise using Lemma 6. Using (4.64) and (4.65) as well as the fact that $\omega^{2q} \leq (1+\omega^2)^q$

and merging all previous constants into the constant $C$,

$$\begin{aligned}\|\psi_+\|^2_{L^2(\mathbb{R}^+;\,L^2(\Gamma))} &\leq \|\psi_+\|^2_{L^2(\mathbb{R};\,L^2(\Gamma))} = \left\|\psi_+^t\right\|^2_{L^2(\Gamma)\times L^2(\mathbb{R};\,L^2(\Gamma))} \\ &\leq C_1 \int_{-\infty}^{\infty} \omega^{2q}\left(1+\omega^2\right)\left\|\psi_*^t(\cdot,\omega)\right\|^2_{L^2(\Gamma)}\,\mathrm{d}\omega \\ &\qquad + C_2\int_{-\infty}^{\infty}\left(1+\omega^2\right)\left\|\psi_*^t(\cdot,\omega)\right\|^2_{L^2(\Gamma)}\,\mathrm{d}\omega \\ &\leq C\int_{-\infty}^{\infty}\left(1+\omega^2\right)^{q+1}\left\|\psi_*^t(\cdot,\omega)\right\|^2_{L^2(\Gamma)}\,\mathrm{d}\omega < \infty.\end{aligned}$$

Indeed, since the incident field boundary values satisfy $\gamma^+ b_k \in H^{q+2}(\mathbb{R};L^2(\Gamma))$ and $\gamma^+\partial_{\mathbf{n}} b_k \in H^{q+1}(\mathbb{R};L^2(\Gamma))$, by Lemma 2 it follows that $\psi_* \in H^{q+1}(I;L^2(\Gamma))$, and we have therefore shown

$$\|\psi_+\|_{L^2(\mathbb{R}^+;\,L^2(\Gamma))} \leq C\,\|\psi_*\|_{H^{q+1}(I;\,L^2(\Gamma))}\,, \quad C = C(\Gamma,\tau,p), \tag{4.69}$$

which is Equation (4.28) in the $p=0$ case.

***Step II: $H^p$- and uniform-in-time bounds.*** In order to develop uniform-in-time bounds, we will utilize Sobolev embedding theorems by proving bounds in time in $H^p(\mathbb{R}^+;L^2(\Gamma))$. When the incident field is a sufficiently smooth function of time, we define $\partial^p\psi_k = \frac{\partial^p}{\partial t^p}\psi_k(\mathbf{r},t)$ for $p>0$, which is the quantity we seek to bound. Indeed, by Lemma 1 given $\gamma^+ b_k \in H^{p+q+2}(\mathbb{R};L^2(\Gamma))$ and $\gamma^+\partial_{\mathbf{n}} b_k \in H^{p+q+1}(\mathbb{R};\,L^2(\Gamma))$ the density $\psi_k$ solving (4.43) is in $C^p(\mathbb{R};\,L^2(\Gamma))$ and thus by mapping properties of the single-layer [46, Thm. 1] the function $h \in C^p(\mathbb{R};H^1(\Gamma))$. Considering Equation (4.43), we have

$$\int_\Gamma \frac{\psi_+(\mathbf{r}',t-|\mathbf{r}-\mathbf{r}'|/c)}{4\pi|\mathbf{r}-\mathbf{r}'|}\,\mathrm{d}\sigma(\mathbf{r}') = -\gamma^+ h(\mathbf{r},t),$$

Differentiating this equation as a function of time and rewriting as a convolution with the time-domain Green's function we have

$$\int_{-\infty}^{t}\int_\Gamma \frac{\delta\left(t-t'-|\mathbf{r}-\mathbf{r}'|/c\right)\partial^p\psi_+(\mathbf{r}',t')}{4\pi|\mathbf{r}-\mathbf{r}'|}\,\mathrm{d}\sigma(\mathbf{r}')\,\mathrm{d}t' = -\partial^p\gamma^+ h(\mathbf{r},t),$$

This equation for the evolution of $\partial^p\psi_+$ is precisely Equation (4.43), with $p$-times temporally-differentiated data. Repeating Lemmas 3 to 5 and Step I of this proof again, then, with $\partial^p h(\mathbf{r},t)$ on the right-hand side of (4.43) instead will yield bounds on $\partial^p\psi_+$.

Thus, with routine applications of the Leibniz formula and triangle inequalities, we find that we have the analogue of (4.69) for $p$-differentiated data

$$\|\partial^p\psi_+\|_{L^2(\mathbb{R}^+;\,L^2(\Gamma))} \leq C\,\|\psi_*\|_{H^{p+1}(I;\,L^2(\Gamma))} < \infty, \quad C = C(\Gamma,\tau,p), \tag{4.70}$$

and, in conjunction with (4.69), we have thus shown (4.28),

$$\|\psi_+\|_{H^p(\mathbb{R}^+;\, L^2(\Gamma))} \leq C(\Gamma, \tau, p)\, \|\psi_*\|_{H^{p+q+1}(I;\, L^2(\Gamma))} < \infty.$$

Indeed, $\psi_* \in H^{p+q+1}(I; L^2(\Gamma))$ by virtue of Lemma 2 since the incident field data $b_k \in H^{p+q+2}(\mathbb{R}; L^2(\Gamma))$ and $\partial_{\mathbf{n}} b_k \in H^{p+q+1}(\mathbb{R}; L^2(\Gamma))$.

Applying this result with $p = 1$ together with the one-dimensional Sobolev lemma [58, Lemma 6.5] yields

$$\begin{aligned} \sup_{t>0} \|\psi(\cdot, t)\|_{L^2(\Gamma)} &\leq \widetilde{C}\, \|\psi\|_{H^{q+1}(\mathbb{R}^+;\, L^2(\Gamma))} = \widetilde{C}\, \|\psi_+\|_{H^{q+1}(\mathbb{R}^+;\, L^2(\Gamma))} \\ &\leq C(\Gamma, \tau)\, \|\psi_*\|_{H^{q+2}(I;\, L^2(\Gamma))}, \end{aligned} \tag{4.71}$$

which is (4.29), that which was to be shown. □

**Remark 26.** *The bound* (4.70) *(or* (4.69) *in the* $p = 0$ *case) estimates the norm of* $\psi_+ \in H^p(\mathbb{R}^+; L^2(\Gamma))$ *in terms of the norm of* $\psi_* \in H^{p+q+1}(I; L^2(\Gamma))$. *To actually establish that* $\psi_*$ *is in* $H^{p+q+1}(I; L^2(\Gamma))$*—that is, is sufficiently smooth* on a bounded time interval*—we used the Laplace-domain result Lemma* 2*, which required only that* $\gamma^+ b_k \in H^{p+q+2}(\mathbb{R}; L^2(\Gamma))$ *and* $\gamma^+ \partial_{\mathbf{n}} b_k \in H^{p+q+1}(\mathbb{R}; L^2(\Gamma))$. *Note that the Laplace-domain estimate Lemma* 2 *is independent of the trapping character, as it only provides bounds on finite time intervals and thus is not informative of (nor, fortunately for the purposes of Theorem* 4*, hampered by the need to account for) the decay properties of the solution affected by multiple scattering. It is interesting to note that the argument of Theorem* 4 *still goes through without reliance on Lemma* 2 *through use of Lemma* 1 *with the additional regularity assumption* $\gamma^+ b_k \in H^{p+2q+2}(\mathbb{R}; L^2(\Gamma))$ *and* $\gamma^+ \partial_{\mathbf{n}} b_k \in H^{p+2q+1}(\mathbb{R}; L^2(\Gamma))$*, ensuring* $\psi_k$ *and therefore also* $\psi_*(\cdot, t) = w_+(t + T_* + \tau) w_-(t) \psi_k(\cdot, t)$ *are in* $H^{p+q+1}(\mathbb{R}; L^2(\Gamma)) \subset H^{p+q+1}(I; L^2(\Gamma))$. *The finite time-interval Laplace-domain estimate can thus be seen to bootstrap the estimate on* $\mathbb{R}^+$*, so that the overall result requires less data regularity than required by a purely Fourier-domain argument.*

### 13.2 Superalgebraic decay estimates of finite-time-history boundary densities

This section extends the theoretical results of the previous section, establishing not only that the density $\psi_k$ is bounded in various Sobolev norms in $\mathbb{R}^+$ by the size of the density on some preceding finite subinterval of the time history as was shown in Theorem 4, but also through Theorem 5, that the Sobolev norms of the density on time intervals of the form $[T, \infty)$, $T > 0$, decay rapidly as $T \to \infty$. More precisely, given sufficient smoothness of the incident field, we show that the density

decays faster than any inverse power of $T$. This result is crucial in view of the time-windowing methodology proposed in Chapter 2, since, in that context, there are many windows that contribute to the overall solution and whose computation is not desired over the entire space-time region of interest. In this context, the guarantees of Theorem 4 only provide for a uniform bound over $\mathbb{R}^+$, and the possible accumulation of errors from many such windows is problematic for rigorous guarantees of overall solution accuracy. In contrast, the Theorem 5 estimates on the interval $[T, \infty), T > 0$, that decay rapidly as $T \to \infty$ are of course greatly advantageous in connection with the algorithm presented in Section 12 (specifically, for Theorem 3), as they provide a termination criterion for computation of each one of the temporal densities $\psi_k$ arising from the temporal windowing procedure proposed in Chapter 2. Indeed, neglecting the contribution of many windows adds provably-small additional error, as can be seen by summing the geometric series present in the proof of Theorem 3.

Roughly speaking, Theorem 5 establishes that if the surface density is measured to be small for a certain period of time (approximately equal to the time it takes for a signal to traverse a distance equal to the diameter of the obstacle), then it not only remains small for all time thereafter, but, further, it decays superalgebraically fast starting from the small observed value. In contrast, previous works [57, 94–96] claim exponential decay of the solution $u$ only relative to the total energy of the incident wave $b$.

In a less algorithmic and a more theoretical direction, this analysis can be viewed in the context of the study of boundary integral density and local energy decay rates for the wave equation. The study of temporal decay rates of wave scattering of compactly-supported (finite energy) incident fields by bounded obstacles began in the $d = 3$ case with reference [122] predicting exponential decay rates on compact subsets of the domain $\Omega$ in the case of a spherical scatterer (though see also [65, Rem. 1]). These results were later extended to general "star-shaped" obstacles [95], with further generalization achieved in reference [96] to a wide class of "nontrapping" obstacles (see also Remark 21). Most of the remaining results in this area can be found in references [16, 73, 74, 82, 83, 93, 94]—see also Remark 22 that discusses the results of references [73, 74], which together with reference [16] represent the only known local energy decay estimates for trapping structures.

There has been much less work concerning the decay of the densities themselves, although, in view of Theorems 1 through 3 in Section 12 of the present chapter and the preceding discussion concerning decay rates of the wave equation itself, such

results can be very useful with regards to both theory and numerical implementation. In this connection, the author is only aware of reference [57], which uses techniques from classical scattering theory to show (only for nontrapping obstacles) that the integral equation operator $A_\omega$ can be analytically continued to an invertible operator $A_{\omega,\sigma}$ on the uniform strip $-\sigma < \mathrm{Im}(\omega) \leq 0$ along the entire real $\omega$ axis, and it conjectures that the inverse operator $A^{-1}_{\omega,\sigma}$ satisfies in that strip the bound $\left\|A^{-1}_{\omega,\sigma}\right\|_{L^2(\Gamma)\to L^2(\Gamma)} \leq C(\sigma)(1+|\omega|^2)^{q/2}$ for some $q$. The claimed result on exponential decay in that reference rests entirely on the validity of this conjecture via a straightforward application of Cauchy's theorem.

We proceed instead by using known results that establish $q$-growth bounds of the form

$$\left\|A^{-1}_{\omega}\right\|_{L^2(\Gamma)\to L^2(\Gamma)} \leq C(1+\omega^2)^{q/2}, \quad \omega \geq 0,$$

for *real values* of $\omega$, under a variety of geometric contexts (cf. Remark 21), including "parabolic" and "hyperbolic" trapping domains, nontrapping domains, etc. Utilizing these $q$-growth bounds we establish, in Theorem 5, that, for smooth incident fields of compact temporal support, the scattering density (and, thus, the fields) decay superalgebraically fast (i.e. faster than any negative power of $t$) as $t$ grows. In fact, Theorem 5 provides a new avenue to the study of decay rates for wave scattering problems for new classes of obstacles which can be shown to satisfy the $q$-growth condition given in Definition 2. In particular, we conclude that superalgebraically-fast decay takes place for all such obstacle types listed in Remark 21. As an example, in view of the result [37], which shows that parabolic trapping regions satisfy the $q$-growth condition with $q = 2$ (or $q = 3$—see also Remark 23), Theorem 5 shows that superalgebraically-fast decay takes place for parabolic trapping regions—for which no decay results were previously known. Examples are provided in Figure 4.1 of such trapping obstacles, for which no decay rates were hitherto established. Indeed, this is the first result showing decay rates for any kind of connected trapping obstacle (see Remark 23, and cf. the results of references [16, 73, 74] showing decay for classes of obstacle formed by certain finite unions of several obstacles, the only previously-established decay rates for a trapping obstacle of any kind). In contrast, our superalgebraic decay results are weaker than the *exponential* decay results presented for certain other obstacle types previously studied [73, 96], and they could be strengthened by extending the present results into the complex frequency domain, perhaps along the lines of [28, 29]. Indeed, it has been suggested [37, p. 855] that generalization from existing methods [47] could be utilized to pursue wave equation

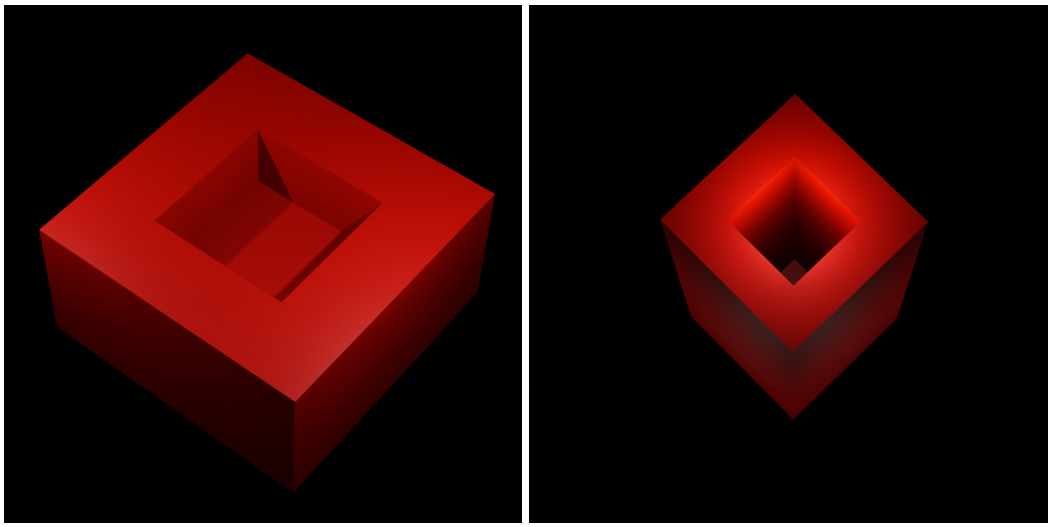

Figure 4.1: Examples of connected trapping obstacles that satisfy a $q$-growth condition ($q = 3$) and for which superalgebraically-fast wave equation time decay rates are established in this thesis. Left: Visualization of the obstacle given in Remark 23, and which serves to demonstrate the existence of connected trapping obstacles satisfying the $q$-growth condition of Definition 2. Right: An elongated cavity trapping obstacle, with a vertical dimension of 12 units and rectangular dimensions of 4 units, that also satisfies a $q$-growth condition ($q = 3$).

decay (and, indeed, possibly exponential decay).

We first state the main result, Theorem 5, and then outline the proof approach. It may be helpful to recall the definitions and assumptions made at the beginning of Section 13.1, which are assumed throughout this section; in particular note that per Equation (4.25) is $k$-dependent (though for notational ease this $k$-dependence is suppressed—see point 2 in Remark 20) and is supported in time in the bounded interval $I$ defined in Equation (4.24).

**Theorem 5.** *Let $\Gamma$ be the boundary of an obstacle satisfying a $q$-growth condition, and let $n$ and $p$ be given positive and nonnegative integers, respectively. Assume that the incident field $b_k$ satisfies $\gamma^+ b_k \in H^{p+(n+1)(q+1)}(\mathbb{R}; H^1(\Gamma))$ and $\gamma^+ \partial_{\mathbf{n}} b_k \in H^{p+n(q+1)+q}(\mathbb{R}; L^2(\Gamma))$. For arbitrary $T > 1$, the density $\psi_k$ can be bounded in the $H^p([T,\infty); L^2(\Gamma))$ norm as*

$$\|\psi_k\|_{H^p([T,\infty);L^2(\Gamma))} \leq C(\Gamma,\tau,p,n)T^{1-n}\,\|\psi_*\|_{H^{p+n(q+1)}(I;L^2(\Gamma))}\,. \tag{4.72}$$

*The choice of $p = 1$, additionally, allows the uniform estimate in time of*

$$\sup_{t>T}\|\psi_k(\cdot,t)\|_{L^2(\Gamma)} \leq C(\Gamma,\tau,n)T^{1-n}\,\|\psi_*\|_{H^{n(q+1)+1}(I;L^2(\Gamma))}\,. \tag{4.73}$$

The proof of Theorem 5 proceeds by certain Fourier-shifting and convolution techniques and an overall approach based on integration-by-parts, and will require differentiation of the boundary integral density as a function of frequency $\omega$. Estimating the resultant frequency-derivative terms in this approach necessitates establishing certain continuity results on the boundary integral density in frequency-domain, as well as new analysis on certain frequency-differentiated boundary integral operators. Thus, Definition 5 introduces certain frequency-differentiated boundary integral operators, and, in Lemma 7, certain frequency-explicit norms for these operators are given. Lemma 9, in turn, guarantees that for smooth data, the frequency-domain integral equation solution is continuously differentiable as a function of frequency, and Lemma 10 provides pointwise bounds on such derivatives (for obstacles satisfying a $q$-growth condition). Finally, Lemma 11 is a technical lemma (of a similar character to some elements of the proof of Theorem 4), establishing bounds on the integrals of certain quantities that arise from the estimates in Lemma 10. The proof of Theorem 5 concludes the section.

A certain "time-history" technique used for the proof of Theorem 5 relies critically on use of certain finite-time boundary integral relations, according to which, the solution at any time future to a certain time point, can be obtained exactly, in absence of additional illumination, from the solution values in a finite time interval prior the given time point. Upon Fourier transformation, this approach allows us to leverage existing $q$-growth bounds on the inverse frequency-domain integral operators. The proof of decay then results by integration by parts in the frequency domain. Importantly, the technical Lemma 11 makes essential use of the bounded temporal support of the right-hand-side function $h(\mathbf{r}, t)$, established in Lemma 5, in order to obtain an upper bound on certain powers of the temporal variable $t$ that arise from frequency-differentiation. This is one of the main enabling steps in the overall decay proof, in that it allows for a study based purely on operator-norm estimates for real frequencies $\omega$ to establish decay rates for scattering problems. As indicated in [37] alternative complex-variable approaches would require use of resolvent bounds for complex values of $\omega$, which are not available at this time.

Before proceeding it is necessary to first define and establish properties of frequency-differentiated boundary integral operators.

**Definition 5.** *For $m \in \mathbb{N}$, with reference to Definition* 1*, define the operators*

$$\partial_\omega^m A_\omega = \begin{cases} \partial_\omega^m K_\omega^* - \mathrm{i}\partial_\omega^m S_\omega, & \text{for} \quad 0 \le \omega < \omega_0 \\ \partial_\omega^m K_\omega^* - \mathrm{i}m\partial_\omega^{m-1} S_\omega - \mathrm{i}\omega\partial_\omega^m S_\omega, & \text{for} \quad \omega > \omega_0, \end{cases} \tag{4.74}$$

*where*

$$\left(\left(\partial_\omega^m K_\omega^*\right)\mu\right)(\mathbf{r}) \coloneqq \int_\Gamma \left(\partial_\omega^m \frac{\partial G_\omega(\mathbf{r},\mathbf{r}')}{\partial \mathbf{n}(\mathbf{r})}\right)\mu(\mathbf{r}')\,\mathrm{d}\sigma(\mathbf{r}'), \quad \mathbf{r} \in \Gamma, \tag{4.75}$$

*and*

$$\left(\left(\partial_\omega^m S_\omega\right)\mu\right)(\mathbf{r}) \coloneqq \int_\Gamma \left(\partial_\omega^m G_\omega(\mathbf{r},\mathbf{r}')\right)\mu(\mathbf{r}')\,\mathrm{d}\sigma(\mathbf{r}'), \quad \mathbf{r} \in \Gamma. \tag{4.76}$$

**Lemma 7.** *The boundary integral operator $A_\omega$ defined in Definition* 1 *can be continuously differentiated with respect to the parameter $\omega \ge 0$ at every $\omega \ne \omega_0$. That is, for $m \in \mathbb{N}$ and letting $\omega = \omega_* + \Delta\omega$, $\Delta\omega \in \mathbb{R}$,*

$$\lim_{\Delta\omega\to 0} \frac{\partial_\omega^{m-1} A_\omega - \partial_\omega^{m-1} A_{\omega_*}}{\Delta\omega} = \partial_\omega^m A_{\omega_*}, \tag{4.77}$$

*where $\partial_\omega^i A_\omega$ is as defined in Equation* (4.74) *(and $\partial_\omega^0 = I$) and all operators are understood in the sense of $L^2(\Gamma)$. The operator $\partial_\omega^m A_\omega$, $m \in \mathbb{N}$, satisfies the operator norm bound*

$$\|\partial_\omega^m A_\omega\|_{L^2(\Gamma)\to L^2(\Gamma)} \le C_1 + C_2\omega \tag{4.78}$$

*for all nonnegative $\omega \ne \omega_0$, where the finite constants $C_j = C_j(\Gamma, m) > 0$ are $\omega$-independent.*

*Proof of Lemma* 7. We must show for an arbitrary fixed $\omega_* \ge 0$, that for any $f \in L^2(\Gamma)$ and $m \in \mathbb{N}$, the limit

$$\lim_{\Delta\omega\to 0} \left\| \left( \frac{\partial_\omega^{m-1} A_\omega - \partial_\omega^{m-1} A_{\omega_*}}{\Delta\omega} - \partial_\omega^m A_{\omega_*} \right) f \right\|_{L^2(\Gamma)} = 0.$$

Assuming that the result holds for $m-1$ and $m-2$, we use induction on $m$ (the base case $m = 1$ proceeds identically to below, except that terms with a $(m-1)$ factor are taken to be zero). Considering $\omega_* > \omega_0$,

$$\begin{aligned} &\lim_{\Delta\omega\to 0} \left\| \left( \frac{\partial_\omega^{m-1} A_\omega - \partial_\omega^{m-1} A_{\omega_*}}{\Delta\omega} - \partial_\omega^m A_{\omega_*} \right) f \right\|_{L^2(\Gamma)} \\ &\quad = \lim_{\Delta\omega\to 0} \int_\Gamma \left| \left( \frac{(\partial_\omega^{m-1} A_\omega f)(\mathbf{r}) - (\partial_\omega^{m-1} A_{\omega_*} f)(\mathbf{r})}{\Delta\omega} \right) - (\partial_\omega A_{\omega_*} f)(\mathbf{r}) \right|^2 \mathrm{d}\sigma(\mathbf{r}) \end{aligned}$$

Expanding the first integrand (the quotient) in this quantity reveals

$$\begin{aligned}
&\lim_{\Delta\omega\to 0}\frac{1}{\Delta\omega}\left((\partial_\omega^{m-1}A_\omega f)(\mathbf{r})-(\partial_\omega^{m-1}A_{\omega_*}f)(\mathbf{r})\right)=\\
&\quad\lim_{\Delta\omega\to 0}\Bigg[\int_\Gamma\frac{1}{\Delta\omega}\left(\partial_\omega^{m-1}\frac{\partial G_\omega(\mathbf{r},\mathbf{r}')}{\partial\mathbf{n}(\mathbf{r})}-\partial_\omega^{m-1}\frac{\partial G_{\omega_*}(\mathbf{r},\mathbf{r}')}{\partial\mathbf{n}(\mathbf{r})}\right)f(\mathbf{r}')\,\mathrm{d}\sigma(\mathbf{r}')\\
&\qquad-\mathrm{i}(m-1)\int_\Gamma\frac{1}{\Delta\omega}\left(\partial_\omega^{m-2}G_\omega(\mathbf{r},\mathbf{r}')-\partial_\omega^{m-2}G_{\omega_*}(\mathbf{r},\mathbf{r}')\right)f(\mathbf{r}')\,\mathrm{d}\sigma(\mathbf{r}')\\
&\qquad-\mathrm{i}\left(\frac{\omega}{\Delta\omega}\int_\Gamma\partial_\omega^{m-1}G_\omega(\mathbf{r},\mathbf{r}')f(\mathbf{r})\,\mathrm{d}\sigma(\mathbf{r}')\right.\\
&\qquad\left.-\frac{\omega_*}{\Delta\omega}\int_\Gamma\partial_\omega^{m-1}G_{\omega_*}(\mathbf{r},\mathbf{r}')f(\mathbf{r})\,\mathrm{d}\sigma(\mathbf{r}')\right)\Bigg],
\end{aligned}$$

while the last two terms can be expressed as

$$\begin{aligned}
&\lim_{\Delta\omega\to 0}\int_\Gamma\partial_\omega^{m-1}G_\omega(\mathbf{r},\mathbf{r}')f(\mathbf{r}')\,\mathrm{d}\sigma(\mathbf{r}')\\
&\qquad+\lim_{\Delta\omega\to 0}\omega_*\int_\Gamma\frac{1}{\Delta\omega}\left(\partial_\omega^{m-1}G_\omega(\mathbf{r},\mathbf{r}')-\partial_\omega^{m-1}G_{\omega_*}(\mathbf{r},\mathbf{r}')\right)f(\mathbf{r}')\,\mathrm{d}\sigma(\mathbf{r}').
\end{aligned}$$

Using dominated convergence (the functions $G_\omega$ are smooth with respect to $\omega$, and thus every term in the preceding expressions can be bounded independently of $\Delta\omega$), we obtain

$$\begin{aligned}
&\lim_{\Delta\omega\to 0}\frac{1}{\Delta\omega}\left((\partial_\omega^{m-1}A_\omega f)(\mathbf{r})-(\partial_\omega^{m-1}A_{\omega_*}f)(\mathbf{r})\right)\\
&\quad=\int_\Gamma\left(\partial_\omega^m\frac{\partial G_{\omega_*}(\mathbf{r},\mathbf{r}')}{\partial\mathbf{n}(\mathbf{r})}-\mathrm{i}(m-1)\partial_\omega^{m-1}G_{\omega_*}(\mathbf{r},\mathbf{r}')\right)f(\mathbf{r})\,\mathrm{d}\sigma(\mathbf{r}')\\
&\qquad-\mathrm{i}\int_\Gamma\partial_\omega^{m-1}G_{\omega_*}(\mathbf{r},\mathbf{r}')f(\mathbf{r}\,\mathrm{d}\sigma(\mathbf{r}')-\mathrm{i}\omega_*\int_\Gamma\partial_\omega^m G_\omega(\mathbf{r},\mathbf{r}')f(\mathbf{r})\,\mathrm{d}\sigma(\mathbf{r}')\\
&\quad=(\partial_\omega^m K_{\omega_*}^* f)(\mathbf{r})-\mathrm{i}m(\partial_\omega^{m-1}S_{\omega_*}f)(\mathbf{r})-\mathrm{i}\omega_*(\partial_\omega^m S_{\omega_*}f)(\mathbf{r})\\
&\quad=(\partial_\omega^m A_{\omega_*}f)(\mathbf{r}).
\end{aligned}$$

Thus as desired,

$$\lim_{\Delta\omega\to 0}\left\|\left(\frac{\partial_\omega^{m-1}A_\omega-\partial_\omega^{m-1}A_{\omega_*}}{\Delta\omega}-\partial_\omega^m A_{\omega_*}\right)f\right\|_{L^2(\Gamma)}=0.$$

The case $0\le\omega_*<\omega_0$ proceeds similarly, but is simpler due to the simpler form of definition of $A_\omega$ in that regime and is omitted for brevity.

We next show the frequency-explicit operator norm bound in (4.78). For $0\le\omega<\omega_0$, we have (first case in Equation (4.74))

$$\partial_\omega^m A_\omega=\partial_\omega^m K_\omega^*-\mathrm{i}\partial_\omega^m S_\omega,$$

and therefore,

$$\|\partial_\omega^m A_\omega\|_{L^2(\Gamma)\to L^2(\Gamma)} \leq \|\partial_\omega^m K_\omega^*\|_{L^2(\Gamma)\to L^2(\Gamma)} + \|\partial_\omega^m S_\omega\|_{L^2(\Gamma)\to L^2(\Gamma)}. \tag{4.79}$$

For $\omega > \omega_0$, we have (second case in Equation (4.74))

$$\partial_\omega^m A_\omega = \partial_\omega^m K_\omega^* - \mathrm{i}m\partial_\omega^{m-1} S_\omega - \mathrm{i}\omega\partial_\omega^m S_\omega,$$

and therefore,

$$\begin{aligned}\|\partial_\omega^m A_\omega\|_{L^2(\Gamma)\to L^2(\Gamma)} \leq\ & \|\partial_\omega^m K_\omega^*\|_{L^2(\Gamma)\to L^2(\Gamma)} \\ & + m\|\partial_\omega^{m-1} S_\omega\|_{L^2(\Gamma)\to L^2(\Gamma)} + \omega\|\partial_\omega^m S_\omega\|_{L^2(\Gamma)\to L^2(\Gamma)}.\end{aligned} \tag{4.80}$$

Clearly, the desired bound (4.78) follows immediately from bounds on the norms of the operators in (4.79) and (4.80) and specifically, that the boundary integral operator $\partial_\omega^m K_\omega^*$ defined by (4.75) satisfies

$$\|\partial_\omega^m K_\omega^*\|_{L^2(\Gamma)\to L^2(\Gamma)} \leq \begin{cases} C_1\omega, & \text{if m = 1,} \\ C_1\omega + C_2, & \text{otherwise,} \end{cases} \tag{4.81}$$

while the boundary integral operator $\partial_\omega^m S_\omega$ defined by (4.76) satisfies

$$\|\partial_\omega^m S_\omega\|_{L^2(\Gamma)\to L^2(\Gamma)} \leq C_2. \tag{4.82}$$

To prove that (4.81) and (4.82) hold, we extend (using the same proof techniques—namely upper-bounds on the integral operator kernel in conjunction with the Riesz-Thorin interpolation theorem) the results of [36] beyond the $m = 0$ case proved there, and consequently we assume $m \geq 1$ below. More specifically, for an integral operator

$$T\mu(\mathbf{r}) = \int_\Gamma \kappa(\mathbf{r}, \mathbf{r}')\mu(\mathbf{r}')\mathrm{d}\sigma(\mathbf{r}'),$$

the Riesz-Thorin interpolation theorem [64, Thm. 1.3.4] guarantees that

$$\|T\|_{L^2(\Gamma)\to L^2(\Gamma)} \leq \|T\|^{1/2}_{L^1(\Gamma)\to L^1(\Gamma)} \|T\|^{1/2}_{L^\infty(\Gamma)\to L^\infty(\Gamma)},$$

where

$$\|T\|_{L^1(\Gamma)\to L^1(\Gamma)} = \text{ess sup}_{\mathbf{r}'\in\Gamma} \int_\Gamma |\kappa(\mathbf{r}, \mathbf{r}')|\ \mathrm{d}\sigma(\mathbf{r}),$$

and

$$\|T\|_{L^\infty(\Gamma)\to L^\infty(\Gamma)} = \text{ess sup}_{\mathbf{r}\in\Gamma} \int_\Gamma |\kappa(\mathbf{r}, \mathbf{r}')|\ \mathrm{d}\sigma(\mathbf{r}').$$

Further, if $|\kappa(\mathbf{r},\mathbf{r}')| \le \tilde{\kappa}(\mathbf{r},\mathbf{r}')$ for all $\mathbf{r},\mathbf{r}' \in \Gamma$ and $\tilde{\kappa}(\mathbf{r},\mathbf{r}') = \tilde{\kappa}(\mathbf{r}',\mathbf{r})$, then clearly

$$\|T\|_{L^2(\Gamma)\to L^2(\Gamma)} \le \operatorname{ess\,sup}_{\mathbf{r}\in\Gamma} \int_\Gamma \tilde{\kappa}(\mathbf{r},\mathbf{r}')\,\mathrm{d}\sigma(\mathbf{r}').$$

We first show the result for $T = \partial_\omega^m K_\omega^*$. A computation shows

$$\kappa(\mathbf{r},\mathbf{r}') = \partial_\omega^m \frac{\partial G_\omega(\mathbf{r},\mathbf{r}')}{\partial \mathbf{n}(\mathbf{r})} = \frac{(\mathbf{r}-\mathbf{r}')\cdot\nu(\mathbf{r})}{4\pi|\mathbf{r}-\mathbf{r}'|^3} \mathrm{e}^{\mathrm{i}\omega|\mathbf{r}-\mathbf{r}'|} \left(\mathrm{i}|\mathbf{r}-\mathbf{r}'|\right)^m \left(\mathrm{i}\omega|\mathbf{r}-\mathbf{r}'| + m - 1\right).$$

Defining $\tilde{\kappa}_m(\mathbf{r},\mathbf{r}') = \frac{1}{4\pi|\mathbf{r}-\mathbf{r}'|^{2-m}} \left(\omega \operatorname{diam}(\Gamma) + m - 1\right)$, we see that $|\kappa(\mathbf{r},\mathbf{r}')| \le \tilde{\kappa}_m(\mathbf{r},\mathbf{r}')$, and therefore

$$\begin{aligned}\|\partial_\omega^m K_\omega^*\|_{L^2(\Gamma)\to L^2(\Gamma)} &\le \operatorname{ess\,sup}_{\mathbf{r}\in\Gamma} \int_\Gamma \tilde{\kappa}_m(\mathbf{r},\mathbf{r}')\,\mathrm{d}\sigma(\mathbf{r}') \\ &\le \begin{cases} C_1\omega, & \text{if m = 1,} \\ C_1\omega + C_2, & \text{otherwise,} \end{cases}\end{aligned}$$

provided $\Gamma$ is a Lipschitz boundary. This shows Equation (4.81).

Next, we consider $T = \partial_\omega^m S_\omega$. Clearly,

$$\kappa(\mathbf{r},\mathbf{r}') = \partial_\omega^m G_\omega(\mathbf{r},\mathbf{r}') = \left(\mathrm{i}|\mathbf{r}-\mathbf{r}'|\right)^m \frac{\mathrm{e}^{\mathrm{i}\omega|\mathbf{r}-\mathbf{r}'|}}{|\mathbf{r}-\mathbf{r}'|}.$$

Defining $\tilde{\kappa}_m(\mathbf{r},\mathbf{r}') = \operatorname{diam}(\Gamma)^{m-1}$, we see that $|\kappa(\mathbf{r},\mathbf{r}')| \le \tilde{\kappa}_m(\mathbf{r},\mathbf{r}')$, and therefore

$$\|\partial_\omega^m K_\omega^*\|_{L^2(\Gamma)\to L^2(\Gamma)} \le \operatorname{ess\,sup}_{\mathbf{r}\in\Gamma} \int_\Gamma \tilde{\kappa}_m(\mathbf{r},\mathbf{r}')\,\mathrm{d}\sigma(\mathbf{r}') \le C_3.$$

This shows Equation (4.82). □

**Lemma 8** (Ramm [105])**.** *Consider the parametrized linear bounded operator $A_\omega : L^2(\Gamma) \to L^2(\Gamma)$ and parametrized function $f(\omega) \in L^2(\Gamma)$, as well as the equation for $\mu(\omega) \in L^2(\Gamma)$,*

$$A_\omega \mu(\omega) = f(\omega), \tag{4.83}$$

*for each $\omega \in \Delta$, where $\Delta \subset \mathbb{R}$ is an open bounded set. Assume that*

1. *Equation* (4.83) *is uniquely solvable for every $\omega \in \Delta_0 = \{\omega : |\omega - \omega_0| \le r\}$, for some $r > 0$ and $\omega_0 \in \Delta$, $\Delta_0 \subset \Delta$,*
2. *$f(\omega)$ is continuous with respect to $\omega \in \Delta_0$, $\sup_{\omega\in\Delta_0} \|f(\omega)\|_{L^2(\Gamma)} \le c_0$,*
3. *$\lim_{h\to 0} \sup_{\omega\in\Delta_0, v\in M} \|(A_{\omega+h} - A_\omega)v\|_{L^2(\Gamma)} = 0$, where $M$ is an arbitrary bounded subset of $L^2(\Gamma)$,*

4. *and that* $\sup_{\omega\in\Delta_0, f\in N} \left\|A_\omega^{-1} f\right\|_{L^2(\Gamma)} \leq c_1$*, where* $N$ *is an arbitrary bounded subset of* $L^2(\Gamma)$ *and where* $c_1$ *may depend on* $N$*.*

*Then,*

$$\lim_{h\to 0} \|\mu(\omega + h) - \mu(\omega)\|_{L^2(\Gamma)} = 0.$$

**Lemma 9.** *Let* $R \in C^m(\mathbb{R}^+ \setminus \omega_0; L^2(\Gamma))$*, and let* $\mu$ *be the solution of the integral equation*

$$(A_\omega \mu)(\mathbf{r}, \omega) = R(\mathbf{r}, \omega),$$

*and defined for negative* $\omega$ *by Hermitian symmetry. Then*

$$\mu \in C^m(\mathbb{R}; L^2(\Gamma)),$$

*and there exist constants* $\{c_i^m,\ i = 1, \ldots, m\}$ *such that for all* $\omega \in \mathbb{R}^+ \setminus \omega_0$*,*

$$\left(A_\omega \left(\partial_\omega^m \mu\right)\right)(\mathbf{r}, \omega) = \partial_\omega^m R(\mathbf{r}, \omega) - \sum_{i=1}^{m} c_i^m \left(\partial_\omega^i A_\omega\right)\left(\partial_\omega^{m-i}\mu\right)(\mathbf{r}, \omega), \tag{4.84}$$

*where equality is in the sense of* $L^2(\Gamma)$*.*

*Proof.* Because $A_\omega$ is an invertible linear operator that is continuous and bounded as a function of the parameter $\omega$, and $R$ is a continuous map into $L^2(\Gamma)$ for all nonnegative $\omega \neq \omega_0$, the conditions of Lemma 8 are met (for the operator $A_\omega$ and right-hand side $R$), and by that lemma, it follows that $\mu$ is also a continuous function of $\omega$. Thus, Equation (4.84) is trivially true for $m = 0$. The argument then proceeds by induction in $p$, where it is assumed that for each $p \leq s$ (and $s < m$, since the induction must terminate at $s + 1 = m$ depending on the regularity of $R$), $\mu \in C^p$ and that (4.84) holds. We must show that the function $\mu = \mu(\mathbf{r}, \omega)$ is $s + 1$ times differentiable in $\omega$, or, more precisely, that $\mu \in C^{s+1}(\mathbb{R}; L^2(\Gamma))$. We must further show that there exists $\{c_i^{s+1},\ i = 1, \ldots, s + 1\}$ so that (4.84) holds for $s + 1$. (The spatial $\mathbf{r}$-dependence of $\mu$ is suppressed below for clarity, but all equality is in the sense of $L^2(\Gamma)$.)

For an arbitrary nonnegative $\omega_* \neq \omega_0$, let $\omega = \omega_* + \Delta\omega$, $\Delta\omega \in \mathbb{R}$. We wish to show that $\partial_\omega^s \mu$ is differentiable at $\omega_*$, and do this by showing a certain quotient of increments has a finite limit. By assumption, $\mu$ satisfies

$$A_\omega \partial_\omega^s \mu(\omega) = \partial_\omega^s R(\omega) - \sum_{p=1}^{s} c_p^s (\partial_\omega^p A_\omega) \partial_\omega^{s-p} \mu(\omega),$$

and

$$A_{\omega_*}\partial_\omega^s\mu(\omega_*) = \partial_\omega^s R(\omega_*) - \sum_{p=1}^{s} c_p^s(\partial_\omega^p A_{\omega_*})\partial_\omega^{s-p}\mu(\omega_*).$$

Subtracting the second equation from the first, adding and subtracting $A_{\omega_*}\partial_\omega^s\mu(\omega)$ on the left, and moving some terms to the right-hand side yields

$$\begin{aligned}A_{\omega_*}\partial_\omega^s\mu(\omega) - A_{\omega_*}\partial_\omega^s\mu(\omega_*) &= \partial_\omega^s R(\omega) - \partial_\omega^s R(\omega_*)\\ &\quad - \sum_{p=1}^{s} c_p^s\left[(\partial_\omega^p A_\omega)\partial_\omega^{s-p}\mu(\omega) - (\partial_\omega^p A_{\omega_*})\partial_\omega^{s-p}\mu(\omega_*)\right] - (A_\omega - A_{\omega_*})\partial_\omega^s\mu(\omega).\end{aligned}$$

Considering the expression in brackets in the preceding equation, adding zero results in the identity

$$\begin{aligned}(\partial_\omega^p A_\omega)\partial_\omega^{s-p}\mu(\omega) - (\partial_\omega^p A_{\omega_*})\partial_\omega^{s-p}\mu(\omega_*) &=\\ &\left(\partial_\omega^p A_\omega - \partial_\omega^p A_{\omega_*}\right)\left(\partial_\omega^{s-p}\mu(\omega) - \partial_\omega^{s-p}\mu(\omega_*)\right)\\ &- \left(\partial_\omega^p A_\omega - \partial_\omega^p A_{\omega_*}^p\right)\partial_\omega^{s-p}\mu(\omega_*) + (\partial_\omega^p A_{\omega_*})\left(\partial_\omega^{s-p}\mu(\omega) - \partial_\omega^{s-p}(\omega_*)\right),\end{aligned}$$

which we use to rewrite that same equation as

$$\begin{aligned}A_{\omega_*}\partial_\omega^s\mu(\omega) - A_{\omega_*}\partial_\omega^s\mu(\omega_*) &= \partial_\omega^s R(\omega) - \partial_\omega^s R(\omega_*)\\ &\quad - \sum_{p=1}^{s} c_p^s\left[\left(\partial_\omega^p A_\omega - \partial_\omega^p A_{\omega_*}\right)\left(\partial_\omega^{s-p}\mu(\omega) - \partial_\omega^{s-p}\mu(\omega_*)\right)\right.\\ &\qquad \left. - \left(\partial_\omega^p A_\omega - \partial_\omega^p A_{\omega_*}^p\right)\partial_\omega^{s-p}\mu(\omega_*) + (\partial_\omega^p A_{\omega_*})\left(\partial_\omega^{s-p}\mu(\omega) - \partial_\omega^{s-p}\mu(\omega_*)\right)\right]\\ &\quad - (A_\omega - A_{\omega_*})\partial_\omega^s\mu(\omega).\end{aligned}$$

Multiplying this equation by $A_{\omega_*}^{-1}$, we next show that the quotient of differences $\frac{1}{\Delta\omega}\left(\partial_\omega^s\mu(\omega) - \partial_\omega^s\mu(\omega_*)\right)$ inherent in this equation has a finite limit for each $\omega_*$. Using the triangle inequality, we have

$$\begin{aligned}\lim_{\Delta\omega\to 0}\Bigg\|&\frac{1}{\Delta\omega}\left(\partial_\omega^s\mu(\omega) - \partial_\omega^s\mu(\omega_*)\right) - A_{\omega_*}^{-1}\partial_\omega^{s+1}R(\omega_*)\\ &-A_{\omega_*}^{-1}\sum_{p=1}^{s+1} c_p^{s+1}(\partial_\omega^p A_\omega)\partial_\omega^{s+1-p}\mu(\omega_*)\Bigg\|_{L^2(\Gamma)}\\ &\le \lim_{\Delta\omega\to 0}\left\|A_{\omega_*}^{-1}\right\|_{L^2(\Gamma)\to L^2(\Gamma)}\left\|\frac{1}{\Delta\omega}\left(\partial_\omega^s R(\omega) - \partial_\omega^s R(\omega_*)\right) - \partial_\omega^{s+1}R(\omega_*)\right\|_{L^2(\Gamma)}\end{aligned}$$

$$+\lim_{\Delta\omega\to 0}\left\|A_{\omega_*}^{-1}\right\|_{L^2(\Gamma)\to L^2(\Gamma)}\left\|\sum_{p=1}^{s}c_p^s\left[\frac{\partial_\omega^p A_\omega-\partial_\omega^p A_{\omega_*}}{\Delta\omega}\left(\partial_\omega^{s-p}\mu(\omega)-\partial_\omega^{s-p}\mu(\omega_*)\right)\right.\right.$$
$$\left.-\frac{\partial_\omega^p A_\omega-\partial_\omega^p A_{\omega_*}}{\Delta\omega}\partial_\omega^{s-p}\mu(\omega_*)+\left(\partial_\omega^p A_{\omega_*}\right)\frac{\partial_\omega^{s-p}\mu(\omega)-\partial_\omega^{s-p}\mu(\omega_*)}{\Delta\omega}\right]$$
$$\left.+\frac{A_\omega-A_{\omega_*}}{\Delta\omega}\partial_\omega^s\mu(\omega)+\sum_{p=1}^{s+1}c_p^{s+1}(\partial_\omega^p A_{\omega_*})\partial_\omega^{s+1-p}\mu\right\|_{L^2(\Gamma)}$$

Since by hypothesis $R\in C^m$ and $s+1\leq m$, the first limit on the right-hand side of this inequality vanishes. In the second limit expression, the first term in the sum also vanishes since firstly by Lemma 7, $\frac{\partial_\omega^p A_\omega-\partial_\omega^p A_{\omega_*}}{\Delta\omega}\to\partial_\omega^{p+1}A_{\omega_*}$, while at the same time $\partial_\omega^{s-p}\mu$ is continuous by the inductive hypothesis in order that the quantity $\|\partial_\omega^{s-p}\mu(\omega)-\partial_\omega^{s-p}\mu(\omega_*)\|_{L^2(\Gamma)}\to 0$ as $\Delta\omega\to 0$. We thus have

$$\lim_{\Delta\omega\to 0}\left\|\frac{1}{\Delta\omega}\left(A_{\omega_*}\partial_\omega^s\mu(\omega)-A_{\omega_*}\partial_\omega^s\mu(\omega_*)\right)-\partial_\omega^{s+1}R(\omega_*)\right.$$
$$\left.-\sum_{p=1}^{s+1}c_p^{s+1}(\partial_\omega^p A_\omega)\partial_\omega^{s+1-p}\mu(\omega_*)\right\|_{L^2(\Gamma)}$$
$$\leq\lim_{\Delta\omega\to 0}C\left\|\sum_{p=1}^{s}c_p^s\left[(\partial_\omega^p A_{\omega_*})\partial_\omega^{s+1-p}\mu(\omega_*)-(\partial_\omega^{p+1}A_{\omega_*})\partial_\omega^{s-p}\mu(\omega_*)\right]\right.$$
$$\left.+\frac{A_\omega-A_{\omega_*}}{\Delta\omega}\partial_\omega^s\mu(\omega)+\sum_{p=1}^{s+1}c_p^{s+1}(\partial_\omega^p A_{\omega_*})\partial_\omega^{s+1-p}\mu(\omega_*)\right\|_{L^2(\Gamma)}.$$

Using the identity

$$\frac{A_\omega-A_{\omega_*}}{\Delta\omega}\partial_\omega^s\mu(\omega)=\frac{A_\omega-A_{\omega_*}}{\Delta\omega}\left(\partial_\omega^s\mu(\omega)-\partial_\omega^s\mu(\omega_*)\right)+\frac{A_\omega-A_{\omega_*}}{\Delta\omega}\partial_\omega^s\mu(\omega_*)$$

and the triangle inequality we further have

$$\lim_{\Delta\omega\to 0}\left\|\frac{1}{\Delta\omega}\left(A_{\omega_*}\partial_\omega^s\mu(\omega)-A_{\omega_*}\partial_\omega^s\mu(\omega_*)\right)-\partial_\omega^{s+1}R(\omega_*)\right.$$
$$\left.-\sum_{p=1}^{s+1}c_p^{s+1}(\partial_\omega^p A_\omega)\partial_\omega^{s+1-p}\mu(\omega_*)\right\|_{L^2(\Gamma)}$$

$$\leq \lim_{\Delta\omega\to 0} C \left\| \sum_{p=1}^{s} c_p^s \left[ (\partial_\omega^p A_{\omega_*}) \partial_\omega^{s+1-p} \mu(\omega_*) - (\partial_\omega^{p+1} A_{\omega_*}) \partial_\omega^{s-p} \mu(\omega_*) \right] \right.$$
$$\left. + \frac{A_\omega - A_{\omega_*}}{\Delta\omega} \partial_\omega^s \mu(\omega_*) + \sum_{p=1}^{s+1} c_p^{s+1} (\partial_\omega^p A_{\omega_*}) \partial_\omega^{s+1-p} \mu(\omega_*) \right\|_{L^2(\Gamma)}$$
$$+ \lim_{\Delta\omega\to 0} C \left\| \frac{A_\omega - A_{\omega_*}}{\Delta\omega} \left( \partial_\omega^s \mu(\omega) - \partial_\omega^s \mu(\omega_*) \right) \right\|_{L^2(\Gamma)}.$$

The second limit on the right-hand side clearly vanishes since $\mu$ is $s$-times continuously differentiable at $\omega_*$, while, conversely, the limit of the expression $\frac{A_\omega - A_{\omega_*}}{\Delta\omega} \to \partial_\omega A_{\omega_*}$. Finally, therefore, the limit obeys the inequality

$$\lim_{\Delta\omega\to 0} \left\| \frac{1}{\Delta\omega} \left( A_{\omega_*} \partial_\omega^s \mu(\omega) - A_{\omega_*} \partial_\omega^s \mu(\omega_*) \right) - \partial_\omega^{s+1} R(\omega_*) \right.$$
$$\left. - \sum_{p=1}^{s+1} c_p^{s+1} (\partial_\omega^p A_\omega) \partial_\omega^{s+1-p} \mu(\omega_*) \right\|_{L^2(\Gamma)}$$
$$\leq C \left\| \sum_{p=1}^{s} c_p^s \left[ (\partial_\omega^p A_{\omega_*}) \partial_\omega^{s+1-p} \mu(\omega_*) - (\partial_\omega^{p+1} A_{\omega_*}) \partial_\omega^{s-p} \mu(\omega_*) \right] \right.$$
$$\left. + (\partial_\omega A_{\omega_*}) \partial_\omega^s \mu(\omega_*) + \sum_{p=1}^{s+1} c_p^{s+1} (\partial_\omega^p A_{\omega_*}) \partial_\omega^{s+1-p} \mu(\omega_*) \right\|_{L^2(\Gamma)}.$$

Making the selections $c_1^{s+1} = -1 + c_1^s$, $c_p^{s+1} = -c_p^s + c_{p-1}^s$ $(p = 2, \ldots, s)$, $c_{s+1}^{s+1} = c_s^s$ ensures that the right-hand side, a fixed quantity independent of $\Delta\omega$, vanishes. This shows that $\partial_\omega^s \mu$ is differentiable and establishes that Equation (4.84) holds for arbitrary $\omega = \omega_*$. Continuity of $\partial_\omega^{s+1} \mu$ follows, as in the case for $\mu$, by application of the result of Lemma 8 since the right-hand-side of (4.84) is continuous by the inductive hypothesis, and, as previously mentioned, the operator $A_\omega$ satisfies the required conditions for that lemma. □

**Lemma 10.** *Assume the obstacle satisfies a q-growth condition. Let* $R \in C^m(\mathbb{R}^+ \setminus \omega_0; L^2(\Gamma))$*, and let* $\mu$ *be the solution of the integral equation*

$$(A_\omega \mu)(\mathbf{r}, \omega) = R(\mathbf{r}, \omega),$$

*for each* $\omega \geq 0$ *and defined for negative* $\omega$ *by Hermitian symmetry. Then there exist*

*coefficients* $b_{ij}^m > 0$ *and* $c_i^m > 0$ *such that for* $\omega \neq \pm\omega_0$*, we have*

$$\begin{aligned}\left\|\partial_\omega^m \mu(\cdot,\omega)\right\|_{L^2(\Gamma)} \leq \sum_{i=0}^{m-1}\left(\sum_{j=0}^{(i+1)(q+1)-1} b_{ij}^m|\omega|^j \left\|\partial_\omega^{m-i} R(\cdot,|\omega|)\right\|_{L^2(\Gamma)}\right) \\ + \sum_{i=0}^{m(q+1)} c_i^m|\omega|^i \left\|\mu(\cdot,\omega)\right\|_{L^2(\Gamma)},\end{aligned} \tag{4.85}$$

*and coefficients* $d_{ij}^m > 0$ *and* $e_i^m > 0$ *so that for* $\omega \neq \pm\omega_0$*, we have*

$$\begin{aligned}\left\|\partial_\omega^m \mu(\cdot,\omega)\right\|_{L^2(\Gamma)}^2 \leq \sum_{i=0}^{m-1}\left(\sum_{j=0}^{(i+1)(q+1)-1} d_{ij}^m\omega^{2j} \left\|\partial_\omega^{m-i} R(\cdot,|\omega|)\right\|_{L^2(\Gamma)}^2\right) \\ + \sum_{i=0}^{m(q+1)} e_i^m\omega^{2i} \left\|\mu(\cdot,\omega)\right\|_{L^2(\Gamma)}^2.\end{aligned} \tag{4.86}$$

*Proof.* By Lemma 9, $\mu \in C^m(\mathbb{R}; L^2(\Gamma))$ so for $\omega \neq \pm\omega_0$ all quantities in the inequalities are well-defined, and there exist $a_k^{s+1}$ such that for $\omega \in \mathbb{R}^+ \setminus \omega_0$ the equation

$$\left(\partial_\omega^{s+1}\mu\right)(\mathbf{r},\omega) = A_\omega^{-1}\left(\partial_\omega^{s+1}R(\mathbf{r},\omega) - \sum_{k=1}^{s+1} a_k^{s+1}(\partial_\omega^k A_\omega)(\partial_\omega^{s+1-k}\mu)(\mathbf{r},\omega)\right)$$

holds in $L^2(\Gamma)$. To prove the bound (4.85), assume the result holds for $m \leq s$, and consider $m = s+1$ (the base case $m = 0$ is trivially satisfied as the first sum in the inequality is dropped). Using Definition 2 of the $q$-growth condition as well as operator norms from Lemma 7 (Equation (4.78)), there exist positive $C_1, C_2, \alpha_{k0}$, and $\alpha_{k1}$ such that for all $\omega \in \mathbb{R}^+ \setminus \omega_0$, the inequalities $\left\|A_\omega^{-1}\right\|_{L^2(\Gamma)\to L^2(\Gamma)} \leq C_1 + C_2\omega^q$ and $\left\|\partial_\omega^k A_\omega\right\|_{L^2(\Gamma)\to L^2(\Gamma)} \leq \alpha_{k0} + \alpha_{k1}\omega$ hold, and therefore we obtain for $\omega \neq \pm\omega_0$,

$$\begin{aligned}\left\|\partial_\omega^{s+1}\mu(\cdot,\omega)\right\|_{L^2(\Gamma)} \leq (C_1 + C_2|\omega|^q)\left(\left\|\partial_\omega^{s+1}R(\cdot,\omega)\right\|_{L^2(\Gamma)}\right. \\ \left. + \sum_{k=1}^{s+1}|a_k^{s+1}|(\alpha_{k0} + \alpha_{k1}|\omega|)\left\|\partial_\omega^{s+1-k}\mu(\cdot,\omega)\right\|_{L^2(\Gamma)}\right).\end{aligned} \tag{4.87}$$

Substituting in the result of the inductive hypothesis (that is, that Equation (4.85)

holds for $m \leq s$),

$$\begin{aligned}\left\|\partial_\omega^{s+1}\mu(\cdot,\omega)\right\|_{L^2(\Gamma)} \leq{}& \left(C_1 + C_2|\omega|^q\right)\left\|\partial_\omega^{s+1}R(\cdot,\omega)\right\|_{L^2(\Gamma)} \\ &+ \sum_{k=1}^{s+1}|a_k^{s+1}|\left(C_1\alpha_{k0} + C_2\alpha_{k0}|\omega|^q + C_1\alpha_{k1}|\omega| + C_2\alpha_{k1}|\omega|^{q+1}\right)\cdot \\ &\quad\cdot\left[\sum_{i=0}^{s-k}\sum_{j=0}^{(i+1)(q+1)-1} b_{ij}^{s+1-k}|\omega|^j\left\|\partial_\omega^{s+1-k-i}R(\cdot,\omega)\right\|_{L^2(\Gamma)}\right. \\ &\qquad\left. + \sum_{i=0}^{(s+1-k)(q+1)} c_i^{s+1-k}|\omega|^i\left\|\mu(\cdot,\omega)\right\|_{L^2(\Gamma)}\right],\end{aligned}$$

and then, expanding the products results in the inequality

$$\begin{aligned}\left\|\partial_\omega^{s+1}\mu(\cdot,\omega)\right\|_{L^2(\Gamma)} \leq{}& \left(C_1 + C_2|\omega|^q\right)\left\|\partial_\omega^{s+1}R(\cdot,\omega)\right\|_{L^2(\Gamma)} \\ &+ \sum_{k=1}^{s+1}\sum_{i=0}^{s-k}\sum_{j=0}^{(i+1)(q+1)-1}|a_k^{s+1}|b_{ij}^{s+1-k}\left(C_1\alpha_{k0}|\omega|^j + C_2\alpha_{k0}|\omega|^{q+j}\right. \\ &\qquad\left. + C_1\alpha_{k1}|\omega|^{j+1} + C_2\alpha_{k1}|\omega|^{q+j+1}\right)\left\|\partial_\omega^{s+1-k-i}R(\cdot,\omega)\right\|_{L^2(\Gamma)} \\ &+ \sum_{k=1}^{s+1}\sum_{i=0}^{(s+1-k)(q+1)}|a_k^{s+1}|c_i^{s+1-k}\left(C_1\alpha_{k0}|\omega|^i + C_2\alpha_{k0}|\omega|^{q+i}\right. \\ &\qquad\left. + C_1\alpha_{k1}|\omega|^{i+1} + C_2\alpha_{k1}|\omega|^{q+i+1}\right)\left\|\mu(\cdot,\omega)\right\|_{L^2(\Gamma)}.\end{aligned}$$

Considering this final inequality, it can be seen that the maximal power of $|\omega|$ in the first sum-term expression is at the indices $k = 1$, $i = s - 1$ and $j = s(q + 1) - 1$, for which the term present in the above inequality is $|\omega|^{q+(s(q+1)-1)+1}\left\|\partial_\omega R(\cdot,\omega)\right\|_{L^2(\Gamma)} = |\omega|^{(s+1)(q+1)-1}\left\|\partial_\omega R(\cdot,\omega)\right\|_{L^2(\Gamma)}$, and which is found in (4.85) for $m = s + 1$. Similarly, the maximal power of $|\omega|$ in the second sum-term expression is at the indices $k = 1$ and $i = s(q + 1)$, for which the term in the above inequality above equals $|\omega|^{(s+1)(q+1)}\left\|\mu(\cdot,\omega)\right\|_{L^2(\Gamma)}$, which is also present in (4.85) for $m = s + 1$. Since inspection of this final inequality shows that there is no term of the form $|\omega|^j\left\|\partial_\omega^{s+1-k-i}R(\cdot,\omega)\right\|_{L^2(\Gamma)}$ or $|\omega|^i\left\|\mu(\cdot,\omega)\right\|_{L^2(\Gamma)}$ that is not also present in Equation (4.85) for $m = s + 1$, inequality (4.85) is established.

The inequality (4.86) follows immediately from (4.85) using the formula $\left\|\sum_{i=1}^m f_i\right\|^2 \leq m\sum_{i=1}^m\left\|f_i\right\|^2$. □

**Lemma 11.** *For $\omega \geq 0$ let*

$$R(\mathbf{r},\omega) = \left(\gamma^-\partial_{\mathbf{n}} - \mathrm{i}\eta\gamma^+\right)H^t(\mathbf{r},\omega), \quad \mathbf{r}\in\Gamma,$$

*where $H^t$ is defined by Equation* (4.40) *and $\eta$ is as defined in Definition* 1*, and assume $R \in C^m(\mathbb{R}^+ \setminus \omega_0;\, L^2(\Gamma))$ and $\psi_* \in H^{n+1}(I; L^2(\Gamma))$ for some $n > 0$. Then for $0 \le i \le m$ and $0 \le j \le n$*

$$\int_0^\infty \omega^{2j} \left\| \partial_\omega^{m-i} R(\cdot, \omega) \right\|_{L^2(\Gamma)}^2 \, \mathrm{d}\omega \le C \left\| \psi_* \right\|_{H^{j+1}(I;\, L^2(\Gamma))}^2 ,$$

*where $C$ is independent of $\psi$.*

*Proof.* We have

$$\int_0^\infty \omega^{2j} \left\| \partial_\omega^{m-i} R(\cdot, \omega) \right\|_{L^2(\Gamma)}^2 \, \mathrm{d}\omega = \int_\Gamma \int_0^\infty \left| \widehat{S}_{ijm} H^t(\mathbf{r}, \omega) \right|^2 \, \mathrm{d}\omega \, \mathrm{d}\sigma(\mathbf{r}), \tag{4.88}$$

where the operator $\hat{S}_{ijm}$ is defined as

$$\widehat{S}_{ijm} = \omega^j \partial_\omega^{m-i} \left( \gamma^- \partial_{\mathbf{n}} - \mathrm{i}\eta\gamma^+ \right).$$

Now, $\eta$ is defined piecewise as $\eta = \omega$ for $\omega > \omega_0$ and $\eta = 1$ for $0 \le \omega < \omega_0$. The argument requires certain estimates to be made in time-domain, and, for that reason, it becomes useful to consider the splitting of (4.88)

$$\begin{aligned} &\int_0^\infty \omega^{2j} \left\| \partial_\omega^{m-i} R(\cdot, \omega) \right\|_{L^2(\Gamma)}^2 \, \mathrm{d}\omega \\ &\qquad = \int_\Gamma \left( \int_0^{\omega_0} + \int_{\omega_0}^\infty \right) \left| \widehat{S}_{ijm} H^t(\mathbf{r}, \omega) \right|^2 \, \mathrm{d}\omega \, \mathrm{d}\sigma(\mathbf{r}). \end{aligned}$$

Then, with a view to matching $\widehat{S}_{ijm}$ on each integration region, define the operators with Fourier symbols

$$\widehat{S}^1_{ijm} = \omega^j \partial_\omega^{m-i} (\gamma^- \partial_{\mathbf{n}} - \mathrm{i}\omega\gamma^+), \quad \text{and} \quad \widehat{S}^2_{ijm} = \omega^j \partial_\omega^{m-i} (\gamma^- \partial_{\mathbf{n}} - \mathrm{i}\gamma^+)$$

and which are in time-domain

$$S^1_{ijm} = (\mathrm{i}\frac{\partial}{\partial t})^j (it)^{m-i} (\gamma^- \partial_{\mathbf{n}} + \frac{\partial}{\partial t}\gamma^+), \quad \text{and} \quad S^2_{ijm} = (\mathrm{i}\frac{\partial}{\partial t})^j (it)^{m-i} (\gamma^- \partial_{\mathbf{n}} - \mathrm{i}\gamma^+).$$

These definitions are used in conjunction with Plancherel's theorem to observe that

$$\begin{aligned} &\int_0^\infty \omega^{2j} \left\| \partial_\omega^{m-i} R(\cdot, \omega) \right\|_{L^2(\Gamma)}^2 \, \mathrm{d}\omega \\ &\qquad \le \int_\Gamma \int_{-\infty}^\infty \left| \widehat{S}^1_{ijm} H^t(\mathbf{r}, \omega) \right|^2 \, \mathrm{d}\omega \, \mathrm{d}\sigma(\mathbf{r}) + \int_\Gamma \int_{-\infty}^\infty \left| \widehat{S}^2_{ijm} H^t(\mathbf{r}, \omega) \right|^2 \, \mathrm{d}\omega \, \mathrm{d}\sigma(\mathbf{r}) \\ &\qquad = \int_\Gamma \int_{-\infty}^\infty \left| S^1_{ijm} h(\mathbf{r}, t) \right|^2 \, \mathrm{d}t \, \mathrm{d}\sigma(\mathbf{r}) + \int_\Gamma \int_{-\infty}^\infty \left| S^2_{ijm} h(\mathbf{r}, t) \right|^2 \, \mathrm{d}t \, \mathrm{d}\sigma(\mathbf{r}) \\ &\qquad = \int_\Gamma \int_{-\tau}^{T_*} \left| S^1_{ijm} u_*(\mathbf{r}, t) \right|^2 \, \mathrm{d}t \, \mathrm{d}\sigma(\mathbf{r}) + \int_\Gamma \int_{-\tau}^{T_*} \left| S^2_{ijm} u_*(\mathbf{r}, t) \right|^2 \, \mathrm{d}t \, \mathrm{d}\sigma(\mathbf{r}), \end{aligned}$$

where the last equality follows by using the result of Lemma 5, that on $\Gamma$ the function $h$ is temporally supported in $[-\tau, T_*]$ and is equal to $u_*$ on $\Gamma \times [-\tau, T_*]$. Defining for clarity the functions $\tilde{u}_1 = (\gamma^- \partial_{\mathbf{n}} + \frac{\partial}{\partial t}\gamma^+)u_*$ and $\tilde{u}_2 = (\gamma^- \partial_{\mathbf{n}} - \mathrm{i}\gamma^+)u_*$, we have by the Leibniz product rule

$$\begin{aligned}
&\int_0^\infty \omega^{2j} \left\| \partial_\omega^{m-i} R(\cdot, \omega) \right\|_{L^2(\Gamma)}^2 \, \mathrm{d}\omega \\
&\qquad \leq \int_\Gamma \int_{-\tau}^{T_*} \left| (\mathrm{i}\frac{\partial}{\partial t})^j (it)^{m-i} \tilde{u}_1(\mathbf{r}, t) \right|^2 \, \mathrm{d}t \, \mathrm{d}\sigma(\mathbf{r}) \\
&\qquad\qquad + \int_\Gamma \int_{-\tau}^{T_*} \left| (\mathrm{i}\frac{\partial}{\partial t})^j (it)^{m-i} \tilde{u}_2(\mathbf{r}, t) \right|^2 \, \mathrm{d}t \, \mathrm{d}\sigma(\mathbf{r}) \\
&\qquad = \int_\Gamma \int_{-\tau}^{T_*} \left| \sum_{\ell=0}^{j} a_\ell \left( \frac{\partial^\ell}{\partial t^\ell} (it)^{m-i} \right) \left( \frac{\partial^{j-\ell}}{\partial t^{j-\ell}} \tilde{u}_1(\mathbf{r}, t) \right) \right|^2 \, \mathrm{d}t \, \mathrm{d}\sigma(\mathbf{r}) \\
&\qquad\qquad + \int_\Gamma \int_{-\tau}^{T_*} \left| \sum_{\ell=0}^{j} a_\ell \left( \frac{\partial^\ell}{\partial t^\ell} (\mathrm{i}t)^{m-i} \right) \left( \frac{\partial^{j-\ell}}{\partial t^{j-\ell}} \tilde{u}_2(\mathbf{r}, t) \right) \right|^2 \, \mathrm{d}t \, \mathrm{d}\sigma(\mathbf{r}).
\end{aligned}$$

Considering the derivative $\frac{\partial^\ell}{\partial t^\ell}(\mathrm{i}t)^{m-i}$ in these expressions, we further have

$$\begin{aligned}
&\int_0^\infty \omega^{2j} \left\| \partial_\omega^{m-i} R(\cdot, \omega) \right\|_{L^2(\Gamma)}^2 \, \mathrm{d}\omega \\
&\qquad = \int_\Gamma \int_{-\tau}^{T_*} \left| \sum_{\ell=0}^{j} \tilde{a}_\ell \left( i^{m-i} t^{m-i-\ell} \right) \left( \frac{\partial^{j-\ell}}{\partial t^{j-\ell}} \tilde{u}_1(\mathbf{r}, t) \right) \right|^2 \, \mathrm{d}t \, \mathrm{d}\sigma(\mathbf{r}) \\
&\qquad\qquad + \int_\Gamma \int_{-\tau}^{T_*} \left| \sum_{\ell=0}^{j} \tilde{a}_\ell \left( i^{m-i} t^{m-i-\ell} \right) \left( \frac{\partial^{j-\ell}}{\partial t^{j-\ell}} \tilde{u}_2(\mathbf{r}, t) \right) \right|^2 \, \mathrm{d}t \, \mathrm{d}\sigma(\mathbf{r}),
\end{aligned}$$

where $\tilde{a}_\ell = \frac{(m-i)!}{(m-i-\ell)!} a_\ell$ for $m - i - \ell \geq 0$ and $\tilde{a}_\ell = 0$ for $m - i - \ell < 0$. Since the $t$-integration region is limited to the bounded region $[-\tau, T_*]$ the factors $t^{m-i-\ell}$ can be bounded above by a constant, and thus

$$\begin{aligned}
&\int_0^\infty \omega^{2j} \left\| \partial_\omega^{m-i} R(\cdot, \omega) \right\|_{L^2(\Gamma)}^2 \, \mathrm{d}\omega \\
&\qquad \leq C_1 \sum_{\ell=0}^{j} \int_\Gamma \int_{-\tau}^{T_*} \left( \left| \frac{\partial^\ell}{\partial t^\ell} \tilde{u}_1(\mathbf{r}, t) \right|^2 + \left| \frac{\partial^\ell}{\partial t^\ell} \tilde{u}_2(\mathbf{r}, t) \right|^2 \right) \mathrm{d}t \, \mathrm{d}\sigma(\mathbf{r}) \\
&\qquad \leq C_1 \sum_{\ell=0}^{j} \int_\Gamma \int_{-\infty}^{\infty} \left( \left| \frac{\partial^\ell}{\partial t^\ell} \tilde{u}_1(\mathbf{r}, t) \right|^2 + \left| \frac{\partial^\ell}{\partial t^\ell} \tilde{u}_2(\mathbf{r}, t) \right|^2 \right) \mathrm{d}t \, \mathrm{d}\sigma(\mathbf{r}),
\end{aligned}$$

where the last inequality estimates above the $L^2$ norm on the finite region $[-\tau, T_*]$ by the full $L^2(\mathbb{R})$ norm. Recalling the definitions of $\tilde{u}_1$ and $\tilde{u}_2$ as $\tilde{u}_1 = (\gamma^- \partial_{\mathbf{n}} + \frac{\partial}{\partial t}\gamma^+)u_*$

and $\tilde{u}_2 = (\gamma^- \partial_{\mathbf{n}} - \mathrm{i}\gamma^+) u_*$, we thus continue in the frequency domain and estimate,

$$\begin{aligned}
&\int_0^\infty \omega^{2j} \left\| \partial_\omega^{m-i} R(\cdot,\omega) \right\|_{L^2(\Gamma)}^2 \, \mathrm{d}\omega \\
&\qquad \leq C_1 \sum_{\ell=0}^{j} \left( \int_\Gamma \int_{-\infty}^{\infty} \left| \omega^\ell (\gamma^- \partial_{\mathbf{n}} - \mathrm{i}\omega\gamma^+) U_*^t(\mathbf{r},\omega) \right|^2 \, \mathrm{d}\omega \, \mathrm{d}\sigma(\mathbf{r}) \right. \\
&\qquad\qquad \left. + \int_\Gamma \int_{-\infty}^{\infty} \left| \omega^\ell (\gamma^- \partial_{\mathbf{n}} - \mathrm{i}\gamma^+) U_*^t(\mathbf{r},\omega) \right|^2 \, \mathrm{d}\omega \, \mathrm{d}\sigma(\mathbf{r}) \right) \\
&\qquad \leq C_1 \int_\Gamma \int_{-\infty}^{\infty} \left| (1+\omega^2)^{j/2} (\gamma^- \partial_{\mathbf{n}} - \mathrm{i}\omega\gamma^+) U_*^t(\mathbf{r},\omega) \right|^2 \, \mathrm{d}\omega \, \mathrm{d}\sigma(\mathbf{r}) \\
&\qquad\quad + C_1 \int_\Gamma \int_{-\infty}^{\infty} \left| (1+\omega^2)^{j/2} (\gamma^- \partial_{\mathbf{n}} - \mathrm{i}\gamma^+) U_*^t(\mathbf{r},\omega) \right|^2 \, \mathrm{d}\omega \, \mathrm{d}\sigma(\mathbf{r}).
\end{aligned}$$

We thus have shown the estimate

$$\begin{aligned}
\int_0^\infty \omega^{2j} \left\| \partial_\omega^{m-i} R(\cdot,\omega) \right\|_{L^2(\Gamma)}^2 \, \mathrm{d}\omega &\leq C_1 \int_{-\infty}^{\infty} (1+\omega^2)^j \left\| (\partial_{\mathbf{n}}^- - \mathrm{i}\omega) U_*^t(\cdot,\omega) \right\|_{L^2(\Gamma)}^2 \, \mathrm{d}\omega \\
&\quad + C_1 \int_{-\infty}^{\infty} (1+\omega^2)^j \left\| (\gamma^- \partial_{\mathbf{n}} - \mathrm{i}\gamma^+) U_*^t(\cdot,\omega) \right\|_{L^2(\Gamma)}^2 \, \mathrm{d}\omega.
\end{aligned} \tag{4.89}$$

By Lemma 6, the frequency-wise operator bounds

$$\left\| (\gamma^- \partial_{\mathbf{n}} - \mathrm{i}\omega\gamma^+) U_*^t(\cdot,\omega) \right\|_{L^2(\Gamma)} \leq D (1+\omega^2)^{1/2} \left\| \psi_*^t(\cdot,\omega) \right\|_{L^2(\Gamma)} \tag{4.90}$$

and

$$\left\| (\gamma^- \partial_{\mathbf{n}} - \mathrm{i}\gamma^+) U_*^t(\cdot,\omega) \right\|_{L^2(\Gamma)} \leq E (1+\omega^2)^{1/2} \left\| \psi_*^t(\cdot,\omega) \right\|_{L^2(\Gamma)}, \tag{4.91}$$

hold for some $D, E > 0$ independent of $\omega$ and $\psi$. Using Equations (4.90) and (4.91) in Equation (4.89), we conclude

$$\begin{aligned}
&\int_0^\infty \omega^{2j} \left\| \partial_\omega^{q-i} R(\cdot,\omega) \right\|_{L^2(\Gamma)}^2 \, \mathrm{d}\omega \\
&\qquad \leq \int_{-\infty}^{\infty} C_2 (1+\omega^2)^{j+1} \left\| \psi_*^t(\cdot,\omega) \right\|_{L^2(\Gamma)}^2 \, \mathrm{d}\omega \\
&\qquad\qquad + \int_{-\infty}^{\infty} C_3 (1+\omega^2)^{j+1} \left\| \psi_*^t(\cdot,\omega) \right\|_{L^2(\Gamma)}^2 \, \mathrm{d}\omega. \\
&\qquad \leq C \left\| \psi_*^t \right\|_{H^{j+1}(\mathbb{R};\, L^2(\Gamma))} = C \left\| \psi_* \right\|_{H^{j+1}(I;\, L^2(\Gamma))}.
\end{aligned}$$

□

With Lemmas 7 through 11 having been established, it is now possible to conclude with the proof of Theorem 5.

*Proof of Theorem* 5. Define $w(t)$, a nonnegative bounded $C_c^\infty(\mathbb{R})$ function, $w(t) \leq 1$, satisfying (for given window width parameters $\tau$ and $T_w$),

$$w(t) = \begin{cases} 0 & \text{if } t < -\tau \\ 1 & \text{if } 0 \leq t \leq T_w \\ 0 & \text{if } t > T_w + \tau. \end{cases} \tag{4.92}$$

Define also $w_T(t) = w(t - T)$.

In order to study the decay of $\|\psi_+(\cdot, t)\|_{L^2(\Gamma)}$ on $t > T$, we consider first the bound

$$\begin{aligned} \|\psi_k\|^2_{L^2([T,T+T_w);\, L^2(\Gamma))} &= \int_T^{T+T_w} \|\psi_+(\mathbf{r}, t)\|^2_{L^2(\Gamma)}\, \mathrm{d}t \\ &\leq \int_{-\infty}^{\infty} \|w_T(t)\psi_+(\cdot, t)\|^2_{L^2(\Gamma)}\, \mathrm{d}t = \|w_T\psi_+\|^2_{L^2(\mathbb{R};\, L^2(\Gamma))}, \end{aligned} \tag{4.93}$$

and show that $\psi_k$ in this norm decays as $T \to \infty$. The result on $[T, \infty)$ then follows by summing an infinite number of the norms of the desired quantity over such bounded-intervals.

The function $(w_T\psi_+)(\mathbf{r}, t)$ can be written using the convolution theorem as

$$\left(w_T\psi_+\right)(\mathbf{r}, t) = \int_{-\infty}^{\infty} \left(\hat{w}_T * \psi_+^t\right)(\mathbf{r}, \omega) \mathrm{e}^{-i\omega t}\, \mathrm{d}\omega. \tag{4.94}$$

But, in view of the definition of $w$ in Equation (4.92) and the subsequent definition of $w_T$, we have $\hat{w}_T = \mathrm{e}^{\mathrm{i}\omega T}\hat{w}(\omega)$, and, thus, integration by parts yields

$$\begin{aligned} \left(\hat{w}_T * \psi_+^t\right)(\mathbf{r}, \omega) &= \int_{-\infty}^{\infty} \mathrm{e}^{i\tau T}\hat{w}(\tau)\psi_+^t(\mathbf{r}, \omega - \tau) d\tau \\ &= -\int_{-\infty}^{\infty} \frac{1}{iT}\mathrm{e}^{i\tau T}\left(\hat{w}'(\tau)\psi_+^t(\mathbf{r}, \omega - \tau) - \hat{w}(\tau)\partial_\omega\psi_+^t(\mathbf{r}, \omega - \tau)\right) d\tau, \end{aligned} \tag{4.95}$$

where the boundary terms at $\pm\infty$ in the integration by parts calculation vanish because $|\psi_+^t| \to 0$ as $|\omega| \to \infty$. This can be repeated given sufficient smoothness of $\psi_+^t(\mathbf{r}, \cdot)$. Indeed, since $\psi_+^t \in C^n$ by Lemma 9,

$$\left(\hat{w}_T * \psi_+^t\right)(\mathbf{r}, \omega) = \left(-\frac{1}{iT}\right)^n \int_{-\infty}^{\infty} \mathrm{e}^{i\tau T}\left(\sum_{m=0}^{n} a_i \left(\partial^{n-m}\hat{w}(\tau)\right)\left(\partial_\omega^m\psi_+^t(\mathbf{r}, \omega - \tau)\right)\right) d\tau, \tag{4.96}$$

where all boundary terms vanish since $|\partial_\omega^m \psi_+^t| \to 0$ as $|\omega| \to \infty$ for all $m < n$. The vanishing of such boundary terms results from Lemma 10, which ensures that for $m < n$, the limit of $\left\|\partial_\omega^m \psi_+^t(\cdot,\omega)\right\|_{L^2(\Gamma)} \to 0$ as $|\omega| \to \infty$ if the limit $|\omega|^{m(q+1)} \left\|\psi_+^t(\cdot,\omega)\right\|_{L^2(\Gamma))} \to 0$—a fact satisfied for $\psi_+ \in H^{m(q+1)}(\mathbb{R}; L^2(\Gamma))$ which is itself ensured by Lemma 1 together with the hypothesis of the present theorem that $\gamma^+ b_k \in H^{(n+1)(q+1)}(\mathbb{R}; L^2(\Gamma))$ and $\gamma^+ \partial_{\mathbf{n}} b_k \in H^{n(q+1)+q}(\mathbb{R}; L^2(\Gamma))$.

Therefore, using Plancherel's theorem,

$$\begin{aligned}
\|w_T \psi_+\|^2_{L^2(\mathbb{R};\, L^2(\Gamma))} &= \left\|\widehat{(w_T \psi_+)}\right\|^2_{L^2(\mathbb{R};\, L^2(\Gamma))} = \left\|\hat{w}_T * \psi_+^t\right\|^2_{L^2(\mathbb{R};\, L^2(\Gamma))} \\
&= \int_{-\infty}^{\infty} \int_\Gamma \left|\left(\hat{w}_T * \psi_+^t\right)(\mathbf{r},\omega)\right|^2 \, \mathrm{d}\sigma(\mathbf{r})\, \mathrm{d}\omega \\
&= \int_\Gamma \left\|\left(\hat{w}_T * \psi_+^t(\mathbf{r},\cdot)\right)\right\|^2_{L^2} \, \mathrm{d}\sigma(\mathbf{r}). \\
&\leq \int_\Gamma (n+1) T^{-2n} \sum_{m=0}^{n} \left\| a_m \left( (\mathrm{e}^{\mathrm{i}T\cdot} \partial^{n-m} \hat{w}) * (\partial_\omega^m \psi_+^t) \right)(\mathbf{r},\cdot) \right\|^2_{L^2} \, \mathrm{d}\sigma(\mathbf{r}),
\end{aligned}$$

where we used the fact that $\| \sum_{i=1}^n f_i \|^2 \leq n \sum_{i=1}^n \|f_i\|^2$. Note the presence of $\mathrm{e}^{\mathrm{i}T\cdot}$ in the final convolution expression above, arising from the $\mathrm{e}^{\mathrm{i}\tau T}$ in Equation (4.96); this term has unit absolute value and so is irrelevant to the $L^1$ estimates that follow. Indeed, because of the fact that $\mathrm{e}^{\mathrm{i}\tau T} \partial_\omega^{n-m} \hat{w}(\tau)$ is an element of $L^1(\mathbb{R})$ (and with a norm value independent of $T$), application of Young's inequality yields a bound on the temporal $L^2$ norm of the convolution in terms of $\mathrm{e}^{\mathrm{i}T\cdot} \partial^{n-m} \hat{w} \in L^1(\mathbb{R})$ and $\partial^m \psi_+^t(\mathbf{r},\cdot) \in L^2(\mathbb{R})$,

$$\begin{aligned}
\|w_T \psi_+\|^2_{L^2(\mathbb{R};\, L^2(\Gamma))} &\leq \int_\Gamma (n+1) T^{-2n} \sum_{m=0}^{n} |a_i|^2 \, \|\partial^{n-m} \hat{w}\|^2_{L^1} \left\|\partial_\omega^m \psi_+^t(\mathbf{r},\cdot)\right\|^2_{L^2} \, \mathrm{d}\sigma(\mathbf{r}) \\
&\leq C(n,\tau,T_w) T^{-2n} \sum_{m=0}^{n} \int_\Gamma \left\|\partial_\omega^m \psi_+^t(\mathbf{r},\cdot)\right\|^2_{L^2} \, \mathrm{d}\sigma(\mathbf{r}) \\
&= C(n,\tau,T_w) T^{-2n} \sum_{m=0}^{n} \left\|\partial_\omega^m \psi_+^t\right\|^2_{L^2(\mathbb{R};\, L^2(\Gamma))}.
\end{aligned} \tag{4.97}$$

Indeed $w \in C_c^\infty$, so it is assured that $\hat{w}$ and its derivatives are in $L^1$, since the Fourier transform is a continuous operator mapping the Schwartz class of test functions into itself. The constant $C(n,\tau,T_w)$ depends on $T_w$ only through the $L^1$ norm of $\hat{w}$ and its derivatives, and is independent of $T$. Note that (in a slight abuse of notation) the $\left\|\partial_\omega^m \psi_+^t\right\|_{L^2(\mathbb{R};L^2(\Gamma))}$ terms on the right-hand-sides of Equation (4.97) are

written as norm values for clarity, but their finiteness has not yet been established—a requirement that is satisfied next.

Indeed, in order to bound terms in the last expression on the right-hand-side of Equation (4.97), we note that from Lemma 3 we have that $\psi_+^t$ satisfies, for nonnegative $\omega$, the integral equation

$$\left(A_\omega \psi_+^t\right)(\mathbf{r},\omega) = R(\mathbf{r},\omega),$$

where $R(\mathbf{r},\omega) = \gamma^- \partial_n H^t(r,\omega) - i\eta\gamma^+ H^t(r,\omega)$. Now, we utilize the estimate (4.86) from Lemma 10 which shows that for $m \leq n$, there exist constants $d_{ij}^m > 0$ and $e_i^m > 0$ such that for all $\omega \neq \pm\omega_0$,

$$\begin{aligned}\left\|\partial_\omega^m \psi_+^t(\cdot,\omega)\right\|_{L^2(\Gamma)}^2 \leq \sum_{i=0}^{m-1} \sum_{j=0}^{(i+1)(q+1)-1} d_{ij}^m \omega^{2j} \left\|\partial_\omega^{m-i} R(\cdot,|\omega|)\right\|_{L^2(\Gamma)}^2 \\ + \sum_{i=0}^{m(q+1)} e_i^m \omega^{2i} \left\|\psi_+^t(\cdot,\omega)\right\|_{L^2(\Gamma)}^2 .\end{aligned} \tag{4.98}$$

Integrating this estimate, we have,

$$\begin{aligned}\int_{-\infty}^{\infty} \left\|\partial_\omega^m \psi_+^t(\cdot,\omega)\right\|_{L^2(\Gamma)}^2 \mathrm{d}\omega \leq \sum_{i=0}^{m-1} \sum_{j=0}^{(i+1)(q+1)-1} 2d_{ij}^m \int_0^{\infty} \omega^{2j} \left\|\partial_\omega^{m-i} R(\cdot,\omega)\right\|_{L^2(\Gamma)}^2 \mathrm{d}\omega \\ + \sum_{i=0}^{m(q+1)} e_i^m \int_{-\infty}^{\infty} \omega^{2i} \left\|\psi_+^t(\cdot,\omega)\right\|_{L^2(\Gamma)}^2 \mathrm{d}\omega.\end{aligned}$$

Using the estimates of Lemma 11 for each term in the first sum in the right-hand-side expression and Theorem 4 for each of the terms in the second sum, we thus have, for $m \leq n$,

$$\begin{aligned}\int_{-\infty}^{\infty} \left\|\partial_\omega^m \ \psi_+^t(\cdot,\omega)\right\|_{L^2(\Gamma)}^2 \mathrm{d}\omega \leq C_1 \left\|\psi_+\right\|_{H^{m(q+1)-1}(I;L^2(\Gamma))} + C_2 \left\|\psi_+\right\|_{H^{m(q+1)}(\mathbb{R};L^2(\Gamma))} \\ \leq C_3 \left\|\psi_*\right\|_{H^{m(q+1)}(I;L^2(\Gamma))} \leq C_3 \left\|\psi_*\right\|_{H^{n(q+1)}(I;L^2(\Gamma))} < \infty,\end{aligned}$$

with $C_1, C_2, C_3 > 0$ independent of $\psi$. Indeed, $\psi_* \in H^{n(q+1)}(I;L^2(\Gamma))$ by Lemma 2 since $\gamma^+ b_k \in H^{n(q+1)+1}(\mathbb{R};L^2(\Gamma))$ and $\gamma^+ \partial_{\mathbf{n}} b_k \in H^{n(q+1)}(\mathbb{R};L^2(\Gamma))$, and therefore it follows that $\partial_\omega^m \psi_+^t \in L^2(\mathbb{R};L^2(\Gamma))$ for $m \leq n$ (in particular, justifying the use of the norm in (4.97)). In view of Equation (4.93), the estimate $\left\|\partial_\omega^m \psi_+\right\|_{L^2(\mathbb{R};L^2(\Gamma))} \leq C \left\|\psi_*\right\|_{H^{n(q+1)}(I;L^2(\Gamma))}$, $m \leq n$, that was just shown can be used in Equation (4.97) to

yield the bound

$$\|\psi_k\|^2_{L^2([T,T+T_w);\,L^2(\Gamma))} \le \|w_T\psi_+\|^2_{L^2(\mathbb{R};\,L^2(\Gamma)} \le C(n,\tau,T_w)T^{-2n}\sum_{i=0}^{n}\left\|\partial_\omega^i\psi_+^t\right\|^2_{L^2(\mathbb{R};\,L(\Gamma))}$$
$$\le C(\Gamma,\tau,n,T_w)T^{-2n}\sum_{i=0}^{n}C_i\,\|\psi_*\|^2_{H^{i(q+1)}(I;\,L^2(\Gamma))}\,.$$

By norm equivalence, then,

$$\|\psi_k\|^2_{L^2([T,T+T_w);\,L^2(\Gamma))} \le C(\Gamma,\tau,n,T_w)T^{-2n}\,\|\psi_*\|^2_{H^{n(q+1)}(I;\,L^2(\Gamma))}\,, \tag{4.99}$$

with $C = C(\Gamma,\tau,n,T_w)$ independent of $T$ and $\psi$.

Since $\gamma^+ b_k \in H^{p+2}(\mathbb{R};L^2(\Gamma))$ and $\gamma^+\partial_{\mathbf{n}} \in H^{p+1}(\mathbb{R};L^2(\Gamma))$, by Lemma 2 the density satisfies $\psi_k \in C^p(\mathbb{R};L^2(\Gamma))$. Bounds on $\left\|\partial_t^p\psi_k\right\|_{L^2([T,T+T_w);\,L^2(\Gamma))}$ follow analogously to that in the proof of Theorem 4, resulting in the estimate

$$\left\|\partial_t^p\psi_k\right\|^2_{L^2([T,T+T_w);\,L^2(\Gamma))} \le C(n,\tau,T_w)T^{-2n}\,\|\psi_*\|^2_{H^{p+n(q+1)}(I;\,L^2(\Gamma))}\,, \tag{4.100}$$

and therefore yielding the bound

$$\|\psi_k\|_{H^p([T,T+T_w);\,L^2(\Gamma))} \le C(\Gamma,\tau,p,n,T_w)T^{-n}\,\|\psi_*\|_{H^{p+n(q+1)}(I;\,L^2(\Gamma))}\,, \tag{4.101}$$

where, as before, $\psi_* \in H^{p+n(q+1)}(I;L^2(\Gamma))$ by Lemma 2 using the assumed incident field regularity $\gamma^+ b_k \in H^{p+n(q+1)+1}(\mathbb{R};L^2(\Gamma))$ and $\gamma^+\partial_{\mathbf{n}} b_k \in H^{p+n(q+1)}(\mathbb{R};L^2(\Gamma))$.

Bounds on $\psi_k$ in $[T,\infty)$ follow by adding the contributions from the bounded subintervals,

$$\|\psi_k\|_{H^p([T,\infty);\,L^2(\Gamma))} = \lim_{L\to\infty}\sum_{\ell=0}^{L}\|\psi_k\|_{H^p([T+\ell T_w,T+(\ell+1)T_w);\,L^2(\Gamma))}$$
$$\le C(\Gamma,\tau,p,n,T_w)\,\|\psi_*\|_{H^{p+n(q+1)}(I;\,L^2(\Gamma))}\lim_{L\to\infty}\sum_{\ell=0}^{L}(T+\ell T_w)^{-n}.$$

Since for $T > 1$ the summand $(T+\ell T_w)^{-n}$ is an eventually strictly decreasing and positive function, it is easy to see that for $\ell > \ell_*$, $(T+\ell T_w)^{-n} \le \int_{\ell-1}^{\ell}(T+xT_w)^{-n}\mathrm{d}x$. and therefore

$$\sum_{\ell=0}^{\infty}(T+\ell T_w)^{-n} \le CT^{-n+1},$$

thus proving

$$\|\psi_k\|_{H^p([T,\infty);\,L^2(\Gamma))} \le C(\Gamma,\tau,p,n,T_w)T^{1-n}\,\|\psi_*\|_{H^{p+n(q+1)}(I;\,L^2(\Gamma))}\,,$$

which is the claimed estimate (4.72). The result (4.73) follows from use of (4.72) with $p = 1$ and the use of the Sobolev lemma [58, Lemma 6.5].

□

## 14 Window tracking for long-time 3D simulations

This section demonstrates the proposed method, implicit in Theorem 3, on a variety of scattering problems with long-duration incident fields, in both nontrapping and trapping contexts.

We next investigate long-time numerical simulations with a trapping geometry consisting of a union of several ($N = 8$) well-separated spheres $S_i$, with the union having the property that the convex hull of any two spheres $S_i$ and $S_j$ does not intersect with any other sphere $S_\ell$, $1 \leq i, j, \ell \leq N$; see Figure 4.3 for a geometry view. This geometry is closely related to certain geometries introduced in reference [73], which have been shown to be weakly-trapping (they satisfy a $q$-growth condition with $q = 1$ due to the weak logarithmic-in-$\omega$ growth of their operator norms [37], cf. Remark 21). In fact, the geometry considered here is slightly more trapping (and thus more computationally challenging) than considered in that body of literature, due to the spheres being more closely-positioned, and thus exhibiting more evident and interesting multiple-scattering behavior. It is not known if the geometry tested satisfies a $q$-growth condition.

The incident field is given by Equation (2.35), in the direction $\widehat{\mathbf{k}}_{\text{inc}} = (1, 1, 1)$. Using a numerical bandwidth $W = 20$, the frequency-domain interval $[-W, W]$ was discretized with 250 frequencies and a maximum spatial discretization of $97,200$ degrees of freedom. Each frequency-domain problem was solved with GMRES to a relative residual of $10^{-5}$. Figure 4.2 displays the total field $u_k^{tot}$ for the single $k = 4$ window, while Figure 4.3 is an intensity plot of the corresponding boundary integral density. In particular, on the right-hand side of Figure 4.3, the interior-facing regions of the multiply-connected obstacle are illuminated from scattering off other regions of the obstacle, demonstrating the multiple-scattering that occurs in trapping geometries.

Figure 4.4 is a demonstration of a window-tracking methodology for this geometry. It plots a barchart which shows the time intervals when the density $\psi_k$ is measured to be above a certain $\varepsilon^{tol}$ tolerance. These numerical experiments that demonstrate the potential of stopping-time-based analysis of wave equation solution components $u_k$ through representation formulas based on the density $\psi_k$ were performed prior to and indeed spurred the theoretical developments introduced in this section. One experiment selected a stopping time based on the ending time value of a certain time interval $I_k$ with length exceeding $\text{diam}(\Omega^c)/c$ on which $\sup_{t \in I_k} \|\psi_k(\cdot, t)\|_{L^\infty(\Gamma)} < \varepsilon^{tol}$. Indeed, exclusion of terms $u_k$ from the sum $\sum_{k=1}^K u_k$ based on the stopping

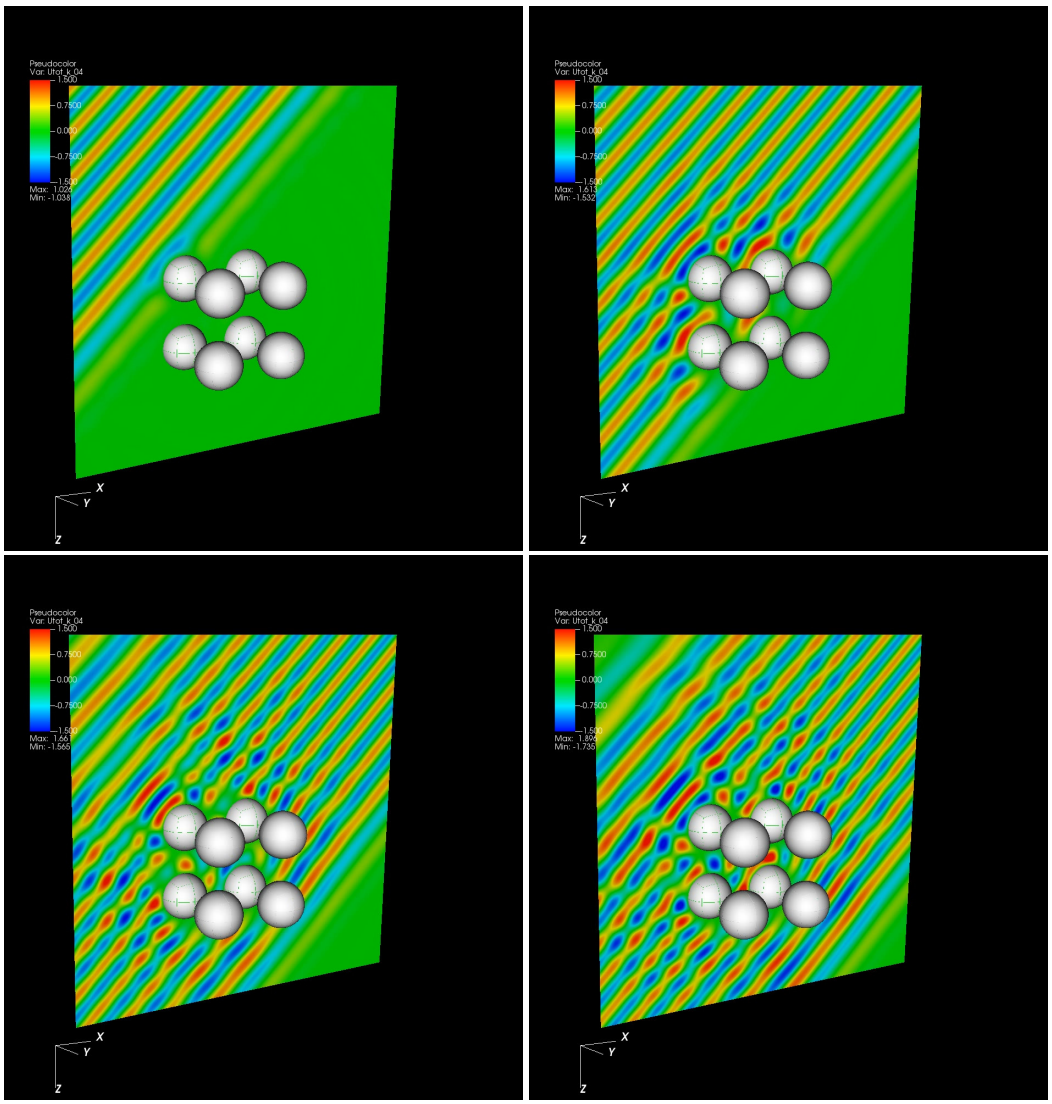

Figure 4.2: Snapshots of the total field $u_k^{tot}$ ($k = 4$) resulting from the scattering of a plane wave from an array of spheres trapping obstacle. Time proceeds left to right and from top to bottom.

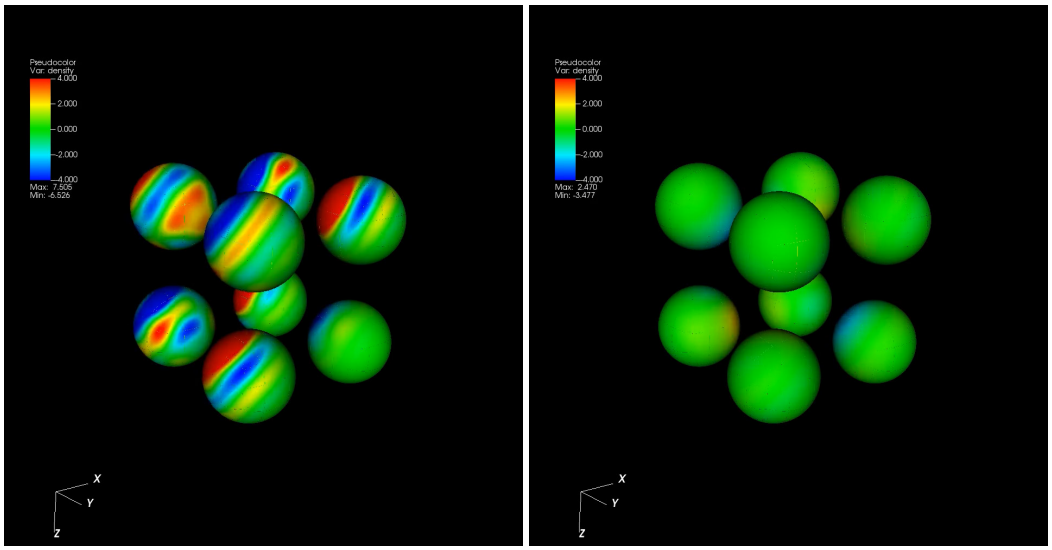


Figure 4.3: Snapshots of the boundary integral density $\psi_k$ ($k = 4$) resulting from the scattering of a plane wave from an array of spheres trapping obstacle. Time proceeds left to right, showing first on the left the initial impinging of the plane wave as well as later on the right the multiple-scattering of the wave by the (weakly) trapping obstacle.

time for $\psi_k$ (cf. Theorem 3) with the tolerance $\varepsilon^{tol} = 10^{-3}$ resulted, for the planar region depicted in Figure 4.2, in solution errors of no more than $7.2 \cdot 10^{-4}$.

**Conclusion**

This chapter has proposed a framework for investigating the temporal decay of the boundary densities and field quantities associated with wave scattering. Elementary relationships were derived between the field quantities and these boundary integral equation solutions (densities), which motivated the in-depth study presented in Section 13. It was established not only that it is possible to estimate the future size of the density based on norms of the density on a finite interval of time related to the physical size of the obstacle, but also that the densities decay (superalgebraically fast) relative to such estimates and in a quantifiable manner related to their degree of trapping. As referenced in the abstract, this chapter includes the first decay rate for wave scattering from a connected trapping obstacle. Finally, some numerical examples were presented showing the capability of this theory in practice, including for trapping geometries.

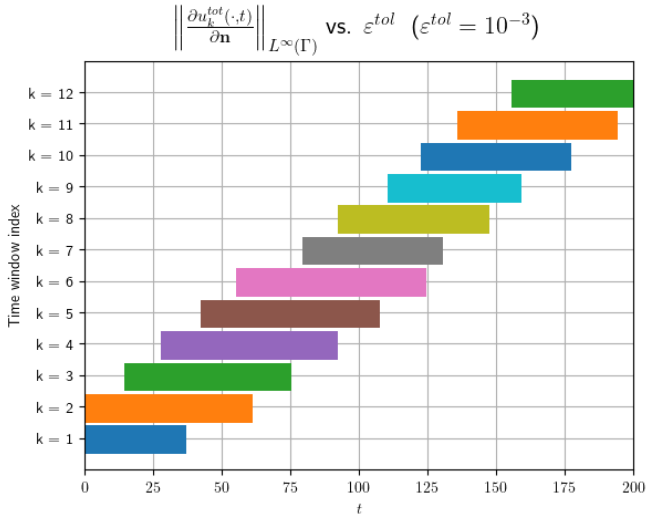


Figure 4.4: Timeline plot of the significance of the boundary density on $\Gamma$ relative to a tolerance $\varepsilon^{tol}$. The horizontal axis indicates simulation time (of the chirp signal), while the vertical axis lists the time window in consideration. For a given window, the bar is only plotted on regions of time where the norm of the density has exceeded $\varepsilon^{tol}$. The colors are for contrast only and are otherwise not meaningful.

*Chapter 5*

# CONCLUSION AND OUTLOOK

"If you have come this far you probably know already and have strong feelings [ . . . ], and if you don't it will not make your life any better to find out [ . . . ] and develop strong feelings."
—Matt Levine (2019)

This thesis has proposed and demonstrated a new approach to the numerical computation of wave scattering. Unlike all previous numerical solution methods, the cost to evaluate the solution at an advanced time $T$ is a nonincreasing function of $T$—a claimed $O(1)$ overall cost with respect to the evaluation time. A number of elements presented establish this overall claim, the most significant being the result of Chapter 2, that Helmholtz equations at only $O(1)$ distinct frequencies need be solved to accurately produce solutions at arbitrarily-large solution times. As argued in that chapter, this promise is fulfilled as the result of a combination of two techniques, which overall serve to decouple the required number of frequencies at which the solution is required from the solution time: (1) a certain windowing-and-recentering procedure for the incident field to analytically factor out high-frequency phases in the forward Fourier transform (of the incident field) as well as (2) a specialized quadrature technique to enable numerically-accurate inverse Fourier transforms of band-limited functions (the scattered fields) at arbitrarily-large times. Chapter 2 also demonstrated certain generalizations of the first-proposed method in the context of fully generic incident fields, such as e.g. moving point sources.

Chapter 3 addressed certain problems that arise from the slow time-decay of solutions in two-dimensional scattering, by the introduction of a method which relies on known asymptotic results for the long-time behavior of two-dimensional wave equation solutions and which interpolates distantly far-future times to fit the coefficients of this asymptotic approximation. Of course, this exploited the feature, unique to hybrid frequency/time methods, that the solution at (highly-)advanced times can be evaluated before the solution at earlier times.

In Chapter 4, the focus shifted to three-dimensional scattering, and, in that chapter, techniques for further acceleration were proposed in conjunction with some novel estimates on time-dependent boundary densities. These estimates bounded the

norms of future evolution of the density in terms of the norm of the boundary density on a finite time-history of length related precisely to the non-dimensional physical size of the obstacle. Furthermore, the theory assures superalgebraic temporal decay of the densities relative to these estimates, and indeed led to new results in scattering theory. As mentioned in that chapter, work in this area is ongoing, to demonstrate the success of this new theory in algorithms.

Of course, as described in the introduction, the ideas inherent to this thesis are of a far more generic nature than implied by their demonstration only on the acoustic wave equation. The advantages outlined transfer without difficulty to closely-related problems in elasticity and electromagnetism, and will certainly be the focus of future research. Even for acoustics, investigations of hybrid frequency/time methods applied in the context of frequency-dependent dispersive media are ongoing (see also Appendix A) and have already shown significant promise and success. A possible future direction concerns a specialized treatment of highly-trapping obstacles, for which, owing to the many reflections and thus the more oscillatory character of the scattered field in frequency-domain, hybrid frequency-time methods currently require an increasing number of Helmholtz solutions (as the degree of trapping increases), even for incident fields of a short duration. New applications in nonlinear waves and inverse problems are also possible and will be the topic of future inquiries.

It is submitted that the frequency-time hybrid solvers proposed in this thesis form the basis of a highly-advantageous methodology and perspective for the efficient simulation of time-dependent wave propagation and scattering. This thesis has perhaps additionally opened new directions for the development of numerical algorithms as well as solution of theoretical questions in the field of wave scattering.

*Appendix A*

# HYBRID FREQUENCY-TIME METHODS FOR COMPLEX MEDIA

This appendix is concerned with wave propagation in complex media, in contrast to the scattering in homogeneous "linear" media (characterized by a linear dispersion ratio $\kappa(\omega)$, cf. Equation (1.7)) considered in the rest of this thesis. Complex media may be associated with propagation that is frequency-dependent, with attenuation and wavespeed variation per frequency, or (possibly additionally) associated with propagation with a spatially-varying wavespeed. This appendix focuses on the former problem, though it is noted that with an adequate variable-coefficient Helmholtz solver similar methodologies apply to the latter problem. As reviewed in Chapter 1 a wide variety of methods (broadly, Finite Difference Time Domain (FDTD), Finite Element Time Domain (FETD), and Time-Domain Boundary Integral Equation methods) in the literature have been developed for solving surface scattering problems and some have been adapted to situations involving strongly dispersive media, see e.g. [21]. A key feature of the methodology introduced in this thesis is its reliance on solution of frequency-domain problems, for which frequency-dependent media properties can often be very simply described, as a "black-box" element of the solution procedure. This feature leads straightforwardly to a method for solving wave scattering problems in dispersive media. We present the relevant equations and relations in a simplified, one-dimensional context, though everything presented transfers directly to the multi-dimensional case where true scattering occurs.

We briefly review prior work in numerical methods for simulation of waves propagating in dispersive media. Foundational work in reference [99] derived from first principles a model of attenuation losses, due to a number $N$ of various relaxation mechanisms, in the form of a first-principles-derived wave equation of temporal order $N + 2$, with a resulting reduced wave equation of a frequency-dependent wavenumber. Instead of solving a time-domain PDE of possibly high order, others focused on developing a theory for simulating lossy media via modeling time-fractional derivative operators as convolutions, see e.g. references [111, 112]. The review [103] points out the substantial (and increasing, with desired final simulation time) memory burden this approach implies. Reference [85] sought to ameliorate this issue by using a recursive algorithm for the time-fractional derivative with lim-

ited history, though [103] also notes that in addition to being ad-hoc this requires *a priori* fitting of coefficients for each power law to physical or simulated data, e.g. with FDTD. We find also that the contribution [115] uses space-fractional derivative operators, avoiding these issues. These methods require evaluation of convolutions over the time history at every time-step, which can be costly in terms of required memory and computational effort. In the context of time-domain boundary integral equation solvers, reference [21] extends methods developed for linear homogeneous wave propagation to strongly dispersive media, relying on contour integration to produce an auxiliary time-domain Green's function and leading to more efficient time-domain solvers.

In reference [85], the case of attenuating media is discussed, for which a monochromatic wave $w$ having initial amplitude $w_0$ and frequency $\omega$ shows exponential attenuation over propagation distance $\Delta x$, with amplitude following the frequency power-law attenuation relation

$$\hat{w}(x + \Delta x) = \hat{w}_0(x) e^{-\alpha(\omega)\Delta x}, \quad \text{with} \tag{A.1}$$

$$\alpha(\omega) = \frac{\alpha_0}{(2\pi)^y} |\omega|^y, \quad \text{where} \quad 1 \leq y \leq 2. \tag{A.2}$$

Now, the partial differential equation describing one-dimensional wave propagation in an idealized homogeneous lossless medium with wave speed $c_0$ is

$$\frac{\partial w}{\partial t} + c_0 \frac{\partial w}{\partial x} = 0, \tag{A.3a}$$

$$w(0, t) = p(t), \quad t > 0 \tag{A.3b}$$

which by Fourier transformation is equivalent to the frequency domain equation

$$\frac{\partial W(x, \omega)}{\partial x} - ik(\omega) W(x, \omega) = 0, \quad \text{where} \quad k(\omega) = \beta_0 = \omega / c_0. \tag{A.4}$$

As is well-known, plane wave solutions to this equation are of the form $e^{i(k(\omega)x - \omega t)}$. We turn now to modification of the dispersion relation $k(\omega)$ to model attenuation. In order to satisfy the Kramers-Kronig relations (ensuring analyticity and hence causality of the waves) when adding attenuation, the dispersion relation must be modified [111] to become

$$k(\omega) = \beta_0 + \beta'(\omega) + i\alpha(\omega) = \beta_0 + iL_\gamma(\omega), \tag{A.5}$$

where the relative dispersion $\beta'(\omega)$ is

$$\beta'(\omega) = -\frac{\alpha_0}{(2\pi)^y} \cot((y + 1)\pi/2) \omega |\omega|^{y-1}, \tag{A.6}$$

and we have defined the function $L_\gamma$ to be the change in the dispersion relation due to the dispersive media. Reference [112] develops a causal time-domain wave equation

$$\frac{\partial w(x,t)}{\partial x} + \frac{1}{c_0}\frac{\partial w(x,t)}{\partial t} L_\gamma(t) * w(x,t) = 0, \tag{A.7a}$$

$$w(0,t) = p(t), \quad t \geq 0, \tag{A.7b}$$

to describe wave motion with this attenuative behavior. Reference [85], in turn, describes a modified FDTD-type numerical method to numerically handle the resulting convolution integrals using certain recursive algorithms. In that work, the numerical validation against simulation data is performed by simulation of a chirp signal propagating in a lossy medium (castor oil), between two reference points P1 and P2 that are separated by 1 cm (cf. [85, Fig. 2]). The chirp signal used is

$$p(t) = \cos\left(2\pi\left(\left(\frac{f_e - f_s}{2t_p}\right)t^2 + f_s t + 1/4\right)\right), \tag{A.8}$$

with "start" frequency $f_s = 100\,\text{kHz}$ and "end" frequency $f_e = 3\,\text{MHz}$ over a pulse width of $t_p = 10\,\mu s$. Note that the chirp signal attains the start and end frequencies at the beginning and end of a 10-$\mu s$ observation window. The physical characteristics of the medium correspond to castor oil and are $y = 1.4$, $c_0 = 1525\text{m/s}$, $\alpha_0 = 2.0\,\text{dB} / (\text{cm MHz}^\text{y})$. Note that the wavespeed in the attenuating medium for a given frequency $\omega$ is

$$c(\omega) = \frac{\omega}{k(\omega)} = \frac{\omega}{\beta_0 + \beta'(\omega)} = c_0\frac{1}{1 + \beta'(\omega)/\beta_0}, \tag{A.9}$$

while in a neutral medium of identical wavespeed it is trivially $c_0(\omega) = \omega/\beta_0 = c_0$.

As a proof of concept for the applicability of hybrid-type methods to dispersive media, we show that a simple application of the hybrid method for this problem yields identical results as the numerical-experimental validation in that contribution. The frequency domain problems to be solved are

$$\frac{\partial W(x,\omega)}{\partial x} - ik(\omega)W(x,\omega) = 0, \quad 0 < x < \infty \tag{A.10a}$$

$$W(0,\omega) = \widehat{p}(\omega), \tag{A.10b}$$

which have, for each $\omega$, solutions $W(x,\omega) = \widehat{p}(\omega)e^{ik(\omega)x}$ and which produce the time domain solution via the inverse Fourier transform

$$w(x,t) = \frac{1}{2\pi}\int_{-\infty}^{\infty} W(x,\omega)e^{-i\omega t}\,d\omega. \tag{A.11}$$

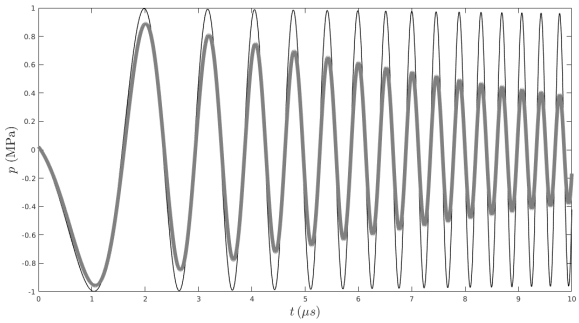


Figure A.1: Time-shifted solutions at reference points described in the text, computed using the hybrid method.

We use the hybrid frequency/time methodology developed in Chapter 2 to numerically solving the problem ((A.7)); that is, we transform the incoming wave $p(t)$ into discrete Fourier space, on a fixed set of frequency mesh points $\omega_j$ $(1 \leq j \leq J)$, and then inverse transform using this fixed set to produce solutions for arbitrarily large time. We show in Figure A.1 the time-shifted solutions $w(x,t)$ at the previously mentioned reference points P1 and P2. One detail warrants mentioning when interpreting Figure A.1: the solutions are measured at two spatial points, separated by $\Delta x = 1$ cm, so for easy comparison they must be time-shifted by an appropriate time offset $t_o$. For a neutral medium a natural choice would be $t_o = \Delta x/c_0$; however, because a generic incident signal propagates through the medium with a variety of wavespeeds over the active frequency range $100\,\text{kHz} \leq f \leq 3\,\text{MHz}$ due to the variable dispersion relation in Equation (A.5), no single shift is adequate. To ensure that the highest-frequency components are in phase when comparing the solutions at P1 and P2, we shift the solution at point P2 by

$$t_o = \frac{\Delta x}{c(\omega_e)} = \frac{\Delta x}{c_0}\left(1 + \beta'(\omega_e)/\beta_0\right), \quad \text{where} \quad \omega_e = 2\pi f_e. \tag{A.12}$$

Any differences with the solution in the contribution [85, Fig. 3] produced by the modified (and much more algorithmically involved) FDTD method are imperceptible. The computational time for the entire solution amounted to $1.5s$ on a machine with an Intel Core i7-8650U.

The beauty of using hybrid frequency/time techniques for simulating transient propagation and scattering in complex media is the straightforward reliance on existing frequency-domain solvers at the complex frequencies that correspond directly to the frequency-dependence of the material. Extending the complex media work in this appendix to the setting of scattering problems in multiple dimensions is ongoing.

*Appendix B*

# HYBRID FREQUENCY-TIME METHODS FOR INITIAL-VALUE PROBLEMS

A related problem to the problem (1.6) considered in this thesis is the initial value problem

$$\frac{\partial^2 u(\mathbf{r},t)}{\partial t^2} - c^2\Delta u(\mathbf{r},t) = 0. \quad \mathbf{r}\in\Omega, \quad t>0, \tag{B.1a}$$

$$u(\mathbf{r},0) = f(\mathbf{r}), \quad \frac{\partial u(\mathbf{r},0)}{\partial t} = g(\mathbf{r}), \quad \mathbf{r}\in\Omega, \tag{B.1b}$$

$$u(\mathbf{r},t) = b(\mathbf{r},t), \quad \mathbf{r}\in\Gamma, \quad t>0, \tag{B.1c}$$

where the functions $f(\mathbf{r})$ and $g(\mathbf{r})$ are suitably smooth functions defined on $\Omega$, and $b(\mathbf{r},t)$ is a suitably smooth and compatible function defined on the boundary $\Gamma = \partial\Omega$ for $t > 0$. Unlike the pure scattering problem (1.6) studied in the majority of this thesis for which Fourier transformation is a natural tool for analysis and numerical solution, initial boundary value problems such as Equation (B.1) are often studied using the Laplace transform. The initial value problem can be seen as somewhat more challenging in that the data is known possibly only for $t \geq 0$, but indeed the Laplace transform is ideally suited for this problem.

For the wave equation, Laplace transformation in time results in the modified Helmholtz equation (sometimes called the Yukawa equation) with, in general, a non-homogeneity that is dependent upon the initial data in Equation (B.1b). It is useful to first recall the familiar definition of the Laplace transform of a function $f(t)$,

$$F(s) = \mathcal{L}\{f\}(s) = \int_0^\infty f(t)e^{-st}\,\mathrm{d}t. \tag{B.2}$$

Applying the Laplace transform in time to the wave equation for each fixed $\mathbf{r}\in\Omega$, we find:

$$\begin{aligned}\mathcal{L}\{u_{tt}(\mathbf{r},\cdot) - c^2\Delta u(\mathbf{r},\cdot)\} &= [e^{-st}u_t(\mathbf{r},t)]_{t=0}^{t=\infty} \\ &\quad + s[e^{-st}u(\mathbf{r},t)]_{t=0}^{t=\infty} + s^2U(\mathbf{r},s) - c^2\Delta U(\mathbf{r},s).\end{aligned}$$

Using the prescribed initial conditions (B.1b), this leads to the modified Helmholtz equation

$$\Delta U(\mathbf{r},s) - (s/c)^2 U(\mathbf{r},s) = -g(\mathbf{r}) - sf(\mathbf{r}), \tag{B.3}$$

with boundary condition

$$U(\mathbf{r}, s) = B(\mathbf{r}, s), \quad \mathbf{r} \in \Gamma. \tag{B.4}$$

As is well-known, the Green's function for this equation is

$$G_s(\mathbf{r}, \mathbf{r}') = \begin{cases} \frac{\mathrm{i}}{4} H_0^{(1)}(\mathrm{i}\frac{s}{c}|\mathbf{r} - \mathbf{r}'|) & \text{for} \quad d = 2, \quad \text{and} \\ \frac{\mathrm{e}^{-\frac{s}{c}|\mathbf{r}-\mathbf{r}'|}}{4\pi|\mathbf{r}-\mathbf{r}'|} & \text{for} \quad d = 3. \end{cases} \tag{B.5}$$

The inhomogeneous modified Helmholtz equation (B.3) can be recast into a homogeneous one by first identifying a solution to the PDE (B.3) without a care for matching the boundary conditions. More specifically, using properties of the Green's function (B.5) we select

$$U_p(\mathbf{r}, s) = \int_\Omega G_s(\mathbf{r}, \mathbf{r}') \, [g(\mathbf{r}) - sf(\mathbf{r})] \, \mathrm{d}\sigma(\mathbf{r}'), \tag{B.6}$$

which satisfies (B.3). Then, the homogeneous modified Helmholtz equation can be solved with modified boundary data to obtain an overall solution $U(\mathbf{r}, s) + U_p(\mathbf{r}, s)$ satisfying the inhomogeneous equation (B.3).

Once required frequency-domain PDEs are solved, a time domain simulation can be obtained by inverting the Laplace transform in accordance with the well-knwon inverse Laplace transform formula

$$f(t) = \mathcal{L}^{-1}\{F\}(t) = \frac{1}{2\pi\mathrm{i}} \int_{\sigma-\mathrm{i}\infty}^{\sigma+\mathrm{i}\infty} \mathrm{e}^{st} F(s) \, \mathrm{d}s, \quad \sigma > \sigma_0, \tag{B.7}$$

where the function $F$ is analytic as a function of $s$ in the half-plane $Re(s) > \sigma_0$ (the $\sigma_0$ is known as the abscissa of convergence of the function $F$).

In contrast to the Fourier case, where the literature for accurate rapid evaluation of Fourier transform at arbitrarily-large times is much more limited, there has been considerable investigation of the Laplace transform inversion problem. Reference [118] has details on existing methods for numerical inversion, as does reference [78] for cases in which, like the present one, production of the solution in frequency-domain requires solution of a (generally expensive) PDE boundary-value problem and not merely the considerably less-expensive point evaluations of a given function. (For an entirely general review of numerical methods for Laplace inversion, see Cohen [43].) The reference [118] points out that there are two main types of inversion formulas, those based only on strictly real samples of the transformed function (the so-called "Post-Widder inversion formulas" [43, Ch. 7]) and those based on deformation of

and quadrature for complex Bromwich contour integrals (B.7). Kuhlman notes that many methods do not place a priority on minimizing the number of samples needed for many inversions at different times. This is important in our context because each "sample" requires the solution of a Helmholtz-type equation which is expensive, and so such inversion methods are disadvantageous. Perhaps the leading candidate in our context is the Weeks method discussed at length in [118].

Other issues arise when using a Hybrid Laplace/time approach, if a Bromwich contour Laplace inversion method is chosen, which implies a need for solutions at complex $s$-values. Clearly, an integral equation method is required that is capable of producing accurate solutions at these wavenumbers. For problems in two-dimensional spatial domains the classical Martensen-Kussmaul rule used in Colton & Kress [45, Ch. 3.5] is no longer sufficient (see [117] for details on why this is unstable for complex frequencies with large imaginary component). Nevertheless, some options do exist, among them a high-order Alpert [1] rule (as recently used in [79] in a CQ context), or other kernel-splitting quadrature rules that retain exponential convergence for complex wavenumbers. One favorable option is the smoothly-windowed piece-wise defined kernel-splitting techniques as in [27, Eq. 30].

One open question is whether the method of Weeks is the best quadrature rule for the purposes of this method, or if instead it would be advantageous to develop new numerical methods for inversion, so as to minimize the number of evaluations (i.e. PDE solves) of the transform function that are required for production of solution values on the desired temporal range. Methods based on Green's formula to reduce the cost of evaluation of (B.6) for values of the particular solution may also be pursued. Clearly, significant questions and challenges do exist for this problem, which are left for future work.

# BIBLIOGRAPHY


[1] B. K. Alpert. "Hybrid Gauss-Trapezoidal Quadrature Rules". In: *SIAM Journal on Scientific Computing* 20.5 (Jan. 1999), pp. 1551–1584. DOI: 10.1137/s1064827597325141.

[2] F. Amlani and O. P. Bruno. "An FC-based spectral solver for elastodynamic problems in general three-dimensional domains". In: *Journal of Computational Physics* 307 (Feb. 2016), pp. 333–354. DOI: 10.1016/j.jcp.2015.11.060.

[3] K. E. Atkinson. *The Numerical Solution of Integral Equations of the Second Kind (Cambridge Monographs on Applied and Computational Mathematics)*. Cambridge University Press, 2009. ISBN: 0521102839.

[4] V. M. Babich. "On the asymptotics of Green's functions for certain wave problems. II. Nonstationary case". In: *Matematicheskii Sbornik* 129.1 (1972), pp. 44–57.

[5] I. M. Babuška and S. A. Sauter. "Is the Pollution Effect of the FEM Avoidable for the Helmholtz Equation Considering High Wave Numbers?" In: *SIAM Journal on Numerical Analysis* 34.6 (Dec. 1997), pp. 2392–2423. DOI: 10.1137/s0036142994269186.

[6] D. H. Bailey and P. N. Swarztrauber. "A Fast Method for the Numerical Evaluation of Continuous Fourier and Laplace Transforms". In: *SIAM Journal on Scientific Computing* 15.5 (1994), pp. 1105–1110. DOI: 10.1137/0915067.

[7] D. H. Bailey and P. N. Swarztrauber. "The Fractional Fourier Transform and Applications". In: *SIAM Review* 33.3 (1991), pp. 389–404. DOI: 10.1137/1033097.

[8] A. Bamberger, T. H. Duong, and J. C. Nedelec. "Formulation variationnelle espace-temps pour le calcul par potentiel retardé de la diffraction d'une onde acoustique (I)". In: *Mathematical Methods in the Applied Sciences* 8.1 (1986), pp. 405–435. DOI: 10.1002/mma.1670080127.

[9] L. Banjai and M. Kachanovska. "Fast convolution quadrature for the wave equation in three dimensions". In: *Journal of Computational Physics* 279 (2014), pp. 103–126. ISSN: 0021-9991. DOI: 10.1016/j.jcp.2014.08.049.

[10] L. Banjai and S. Sauter. "Rapid Solution of the Wave Equation in Unbounded Domains". In: *SIAM Journal on Numerical Analysis* 47.1 (2009), pp. 227–249. DOI: 10.1137/070690754.

[11] L. Banjai. "Multistep and Multistage Convolution Quadrature for the Wave Equation: Algorithms and Experiments". In: *SIAM Journal on Scientific Computing* 32.5 (2010), pp. 2964–2994. DOI: 10.1137/090775981.

[12] L. Banjai, C. Lubich, and J. M. Melenk. “Runge–Kutta convolution quadrature for operators arising in wave propagation”. In: *Numerische Mathematik* 119.1 (Sept. 2011), pp. 1–20. ISSN: 0945-3245. DOI: 10.1007/s00211-011-0378-z.

[13] L. Banjai and M. Schanz. “Wave Propagation Problems Treated with Convolution Quadrature and BEM”. In: *Fast Boundary Element Methods in Engineering and Industrial Applications*. Ed. by U. Langer, M. Schanz, O. Steinbach, and W. L. Wendland. Berlin, Heidelberg: Springer Berlin Heidelberg, 2012, pp. 145–184. ISBN: 978-3-642-25670-7. DOI: 10.1007/978-3-642-25670-7_5.

[14] A. Barnett, L. Greengard, and T. Hagstrom. “High-order discretization of a stable time-domain integral equation for 3D acoustic scattering”. In: *Journal of Computational Physics* 402 (Feb. 2020), p. 109047. DOI: 10.1016/j.jcp.2019.109047.

[15] D. Baskin, E. A. Spence, and J. Wunsch. “Sharp High-Frequency Estimates for the Helmholtz Equation and Applications to Boundary Integral Equations”. In: *SIAM Journal on Mathematical Analysis* 48.1 (Jan. 2016), pp. 229–267. DOI: 10.1137/15m102530x.

[16] D. Baskin and J. Wunsch. “Resolvent estimates and local decay of waves on conic manifolds”. In: *Journal of Differential Geometry* 95.2 (2013), pp. 183–214.

[17] A. Bayliss and E. Turkel. “Radiation boundary conditions for wave-like equations”. In: *Communications on Pure and Applied Mathematics* 33.6 (Nov. 1980), pp. 707–725. DOI: 10.1002/cpa.3160330603.

[18] J.-P. Berenger. “A perfectly matched layer for the absorption of electromagnetic waves”. In: *Journal of Computational Physics* 114.2 (Oct. 1994), pp. 185–200. DOI: 10.1006/jcph.1994.1159.

[19] T. Betcke, S. Chandler-Wilde, I. Graham, S. Langdon, and M. Lindner. “Condition number estimates for combined potential integral operators in acoustics and their boundary element discretisation”. In: *Numerical Methods for Partial Differential Equations* 27.1 (Aug. 2010), pp. 31–69.

[20] T. Betcke, N. Salles, and W. Śmigaj. “Overresolving in the Laplace Domain for Convolution Quadrature Methods”. In: *SIAM Journal on Scientific Computing* 39.1 (Jan. 2017), A188–A213. DOI: 10.1137/16m106474x.

[21] E. Bleszynski, M. Bleszynski, and T. Jaroszewicz. “Fast time domain integral equation solver for dispersive media with auxiliary Green functions”. In: *IEEE/ACES International Conference on Wireless Communications and Applied Computational Electromagnetics, 2005.* IEEE. 2005, pp. 711–718.

[22] E. Bleszynski, M. Bleszynski, and T. Jaroszewicz. "AIM: Adaptive integral method for solving large-scale electromagnetic scattering and radiation problems". In: *Radio Science* 31.5 (Sept. 1996), pp. 1225–1251. ISSN: 1944-799X. DOI: 10.1029/96RS02504.

[23] S. Börm and C. Börst. *Hybrid matrix compression for high-frequency problems*. 2018. eprint: arXiv:1809.04384.

[24] S. Börm, L. Grasedyck, and W. Hackbusch. "Introduction to hierarchical matrices with applications". In: *Engineering Analysis with Boundary Elements* 27.5 (May 2003), pp. 405–422. DOI: 10.1016/s0955-7997(02)00152-2.

[25] H. Brakhage and P. Werner. "Über das dirichletsche aussenraumproblem für die Helmholtzsche schwingungsgleichung". In: *Archiv der Mathematik* 16.1 (1965), pp. 325–329.

[26] D. Brunner, M. Junge, P. Rapp, M. Bebendorf, and L. Gaul. "Comparison of the fast multipole method with hierarchical matrices for the Helmholtz-BEM". In: *Computer Modeling in Engineering & Sciences(CMES)* 58.2 (2010), pp. 131–160.

[27] O. Bruno, T. Elling, and C. Turc. "Regularized integral equations and fast high-order solvers for sound-hard acoustic scattering problems". In: *International Journal for Numerical Methods in Engineering* 91.10 (June 2012), pp. 1045–1072. DOI: 10.1002/nme.4302.

[28] O. P. Bruno and P. Laurence. "Existence of three-dimensional toroidal MHD equilibria with nonconstant pressure". In: *Communications on pure and applied mathematics* 49.7 (1996), pp. 717–764.

[29] O. P. Bruno and F. Reitich. "Solution of a boundary value problem for Helmholtz equation via variation of the boundary into the complex domain". In: (1991).

[30] O. P. Bruno and E. Garza. "A Chebyshev-based rectangular-polar integral solver for scattering by geometries described by non-overlapping patches". In: *Journal of Computational Physics* (Aug. 2020), p. 109740. DOI: 10.1016/j.jcp.2020.109740.

[31] O. P. Bruno and L. A. Kunyansky. "A Fast, High-Order Algorithm for the Solution of Surface Scattering Problems: Basic Implementation, Tests, and Applications". In: *Journal of Computational Physics* 169.1 (May 2001), pp. 80–110. DOI: 10.1006/jcph.2001.6714.

[32] O. P. Bruno and M. Lyon. "High-order unconditionally stable FC-AD solvers for general smooth domains I. Basic elements". In: *Journal of Computational Physics* 229.6 (Mar. 2010), pp. 2009–2033. DOI: 10.1016/j.jcp.2009.11.020.

[33] O. P. Bruno and A. Pandey. *Fast, higher-order direct/iterative hybrid solver for scattering by Inhomogeneous media – with application to high-frequency and discontinuous refractivity problems*. 2019. eprint: arXiv:1907.05914.

[34] A. Burton and G. Miller. "The application of integral equation methods to the numerical solution of some exterior boundary-value problems". In: *Proceedings of the Royal Society of London. A. Mathematical and Physical Sciences* 323.1553 (1971), pp. 201–210.

[35] F. Cardoso and G. Popov. "Quasimodes with exponentially small errors associated with elliptic periodic rays". In: *Asymptotic Analysis* 30.3, 4 (2002), pp. 217–247.

[36] S. N. Chandler-Wilde, I. G. Graham, S. Langdon, and M. Lindner. "Condition number estimates for combined potential boundary integral operators in acoustic scattering". In: *Journal of Integral Equations and Applications* 21.2 (June 2009), pp. 229–279. DOI: 10.1216/jie-2009-21-2-229.

[37] S. N. Chandler-Wilde, E. A. Spence, A. Gibbs, and V. P. Smyshlyaev. "High-frequency Bounds for the Helmholtz Equation Under Parabolic Trapping and Applications in Numerical Analysis". In: *SIAM Journal on Mathematical Analysis* 52.1 (Jan. 2020), pp. 845–893. DOI: 10.1137/18m1234916.

[38] S. N. Chandler-Wilde, I. G. Graham, S. Langdon, and E. A. Spence. "Numerical-asymptotic boundary integral methods in high-frequency acoustic scattering". In: *Acta Numerica* 21 (2012), pp. 89–305. DOI: 10.1017/S0962492912000037.

[39] S. N. Chandler-Wilde and P. Monk. "Wave-Number-Explicit Bounds in Time-Harmonic Scattering". In: *SIAM Journal on Mathematical Analysis* 39.5 (Jan. 2008), pp. 1428–1455. DOI: 10.1137/060662575.

[40] Q. Chen, P. Monk, X. Wang, and D. Weile. "Analysis of Convolution Quadrature Applied to the Time-Domain Electric Field Integral Equation". In: *Communications in Computational Physics* 11.2 (2012), pp. 383–399. DOI: 10.4208/cicp.121209.111010s.

[41] Q. Chen and P. Monk. "Discretization of the Time Domain CFIE for Acoustic Scattering Problems Using Convolution Quadrature". In: *SIAM Journal on Mathematical Analysis* 46.5 (Jan. 2014), pp. 3107–3130. DOI: 10.1137/110833555.

[42] H. Childs, E. Brugger, B. Whitlock, J. Meredith, S. Ahern, D. Pugmire, K. Biagas, M. Miller, C. Harrison, G. H. Weber, H. Krishnan, T. Fogal, A. Sanderson, C. Garth, E. W. Bethel, D. Camp, O. Rübel, M. Durant, J. M. Favre, and P. Navrátil. "VisIt: An End-User Tool For Visualizing and Analyzing Very Large Data". In: *High Performance Visualization–Enabling Extreme-Scale Scientific Insight*. Oct. 2012, pp. 357–372.

[43] A. M. Cohen. *Numerical methods for Laplace transform inversion*. Vol. 5. Springer Science & Business Media, 2007.

[44] R. Coifman, V. Rokhlin, and S. Wandzura. “The fast multipole method for the wave equation: A pedestrian prescription”. In: *IEEE Antennas and Propagation Magazine* 35.3 (1993), pp. 7–12.

[45] D. Colton and R. Kress. *Integral Equation Methods in Scattering Theory*. Society for Industrial and Applied Mathematics, Nov. 2013. DOI: 10.1137/1.9781611973167.

[46] M. Costabel. “Boundary integral operators on Lipschitz domains: elementary results”. In: *SIAM journal on Mathematical Analysis* 19.3 (1988), pp. 613–626.

[47] K. Datchev. “Extending Cutoff Resolvent Estimates via Propagation of Singularities”. In: *Communications in Partial Differential Equations* 37.8 (Mar. 2012), pp. 1456–1461. DOI: 10.1080/03605302.2011.626103.

[48] P. J. Davies and D. B. Duncan. “Convolution spline approximations for time domain boundary integral equations”. In: *Journal of Integral Equations and Applications* 26.3 (Sept. 2014), pp. 369–410. DOI: 10.1216/jie-2014-26-3-369.

[49] P. J. Davies and D. B. Duncan. “Convolution-in-Time Approximations of Time Domain Boundary Integral Equations”. In: *SIAM Journal on Scientific Computing* 35.1 (Jan. 2013), B43–B61. DOI: 10.1137/120881907.

[50] P. J. Davies and D. B. Duncan. “Stability and Convergence of Collocation Schemes for Retarded Potential Integral Equations”. In: *SIAM Journal on Numerical Analysis* 42.3 (Jan. 2004), pp. 1167–1188. DOI: 10.1137/s0036142901395321.

[51] A. J. Devaney and G. C. Sherman. “Plane-Wave Representations for Scalar Wave Fields”. In: *SIAM Review* 15.4 (Oct. 1973), pp. 765–786. DOI: 10.1137/1015096.

[52] V. Domínguez, I. G. Graham, and T. Kim. “Filon–Clenshaw–Curtis Rules for Highly Oscillatory Integrals with Algebraic Singularities and Stationary Points”. In: *SIAM Journal on Numerical Analysis* 51.3 (2013), pp. 1542–1566. DOI: 10.1137/120884146.

[53] J. Douglas, J. E. Santos, D. Sheen, and L. S. Bennethum. “Frequency Domain Treatment Of One-Dimensional Scalar Waves”. In: *Mathematical Models and Methods in Applied Sciences* 03.02 (Apr. 1993), pp. 171–194. DOI: 10.1142/s0218202593000102.

[54] J. Driscoll and D. Healy. “Computing Fourier Transforms and Convolutions on the 2-Sphere”. In: *Advances in Applied Mathematics* 15.2 (June 1994), pp. 202–250. DOI: 10.1006/aama.1994.1008.

[55] T. Ha-Duong. "On Retarded Potential Boundary Integral Equations and their Discretisation". In: *Topics in Computational Wave Propagation: Direct and Inverse Problems*. Ed. by M. Ainsworth, P. Davies, D. Duncan, B. Rynne, and P. Martin. Berlin, Heidelberg: Springer Berlin Heidelberg, 2003, pp. 301–336. ISBN: 978-3-642-55483-4. DOI: 10.1007/978-3-642-55483-4_8.

[56] B. Engquist and A. Majda. "Absorbing boundary conditions for the numerical simulation of waves". In: *Mathematics of Computation* 31.139 (Sept. 1977), pp. 629–629. DOI: 10.1090/s0025-5718-1977-0436612-4.

[57] C. L. Epstein, L. Greengard, and T. Hagstrom. "On the stability of time-domain integral equations for acoustic wave propagation". In: *Discrete and Continuous Dynamical Systems* 36.8 (Mar. 2016), pp. 4367–4382. DOI: 10.3934/dcds.2016.36.4367.

[58] G. B. Folland. *Introduction to Partial Differential Equations*. Princeton: Princeton university press, 1995.

[59] L. N. Frazer and J. F. Gettrust. "On a generalization of Filon's method and the computation of the oscillatory integrals of seismology". In: *Geophysical Journal International* 76.2 (Feb. 1984), pp. 461–481. DOI: 10.1111/j.1365-246x.1984.tb05056.x.

[60] M. Fukuhara, R. Misawa, K. Niino, and N. Nishimura. "Stability of boundary element methods for the two dimensional wave equation in time domain revisited". In: *Engineering Analysis with Boundary Elements* 108 (Nov. 2019), pp. 321–338. DOI: 10.1016/j.enganabound.2019.08.015.

[61] A. Gillman, A. H. Barnett, and P.-G. Martinsson. "A spectrally accurate direct solution technique for frequency-domain scattering problems with variable media". In: *BIT Numerical Mathematics* 55.1 (2015), pp. 141–170.

[62] G. H. Golub and C. Van Loan. *Matrix Computations*. 4th ed. The Johns Hopkins University Press, Baltimore, MD, 2013.

[63] A. Gopal and P.-G. Martinsson. *An accelerated, high-order accurate direct solver for the Lippmann-Schwinger equation for acoustic scattering in the plane*. 2020. eprint: 2007.12718 (math.NA).

[64] L. Grafakos. *Classical Fourier Analysis*. Springer New York, 2014. DOI: 10.1007/978-1-4939-1194-3.

[65] L. Greengard, T. Hagstrom, and S. Jiang. "The solution of the scalar wave equation in the exterior of a sphere". In: *Journal of Computational Physics* 274 (Oct. 2014), pp. 191–207. DOI: 10.1016/j.jcp.2014.05.031.

[66] J. Griffith and M. Nakhla. "Time-domain analysis of lossy coupled transmission lines". In: *IEEE Transactions on Microwave Theory and Techniques* 38.10 (1990), pp. 1480–1487. DOI: 10.1109/22.58689.

[67] K. Gröchenig. *Foundations of Time-Frequency Analysis*. Birkhäuser Boston, 2001. DOI: 10.1007/978-1-4612-0003-1.

[68] J. Hadamard. *Lectures on Cauchy's problem in linear partial differential equations*. Yale University Press, 1923.

[69] T. Hagstrom and T. Warburton. "Complete radiation boundary conditions: minimizing the long time error growth of local methods". In: *SIAM J. Numer. Anal.* 47 (2009), pp. 3678–3704.

[70] X. Han and M. Tacy. "Sharp norm estimates of layer potentials and operators at high frequency". In: *Journal of Functional Analysis* 269.9 (Nov. 2015), pp. 2890–2926. DOI: 10.1016/j.jfa.2015.06.011.

[71] W. D. Henshaw. "A High-Order Accurate Parallel Solver for Maxwell's Equations on Overlapping Grids". In: *SIAM Journal on Scientific Computing* 28.5 (Jan. 2006), pp. 1730–1765. DOI: 10.1137/050644379.

[72] P. A. Houseman. "Science in Chaucer". In: *The Scientific Monthly* 38.6 (1934), pp. 561–564. ISSN: 00963771. URL: http://www.jstor.org/stable/15496.

[73] M. Ikawa. "Decay of solutions of the wave equation in the exterior of several convex bodies". In: *Annales de l'institut Fourier*. Vol. 38. 2. 1988, pp. 113–146.

[74] M. Ikawa. "Decay of solutions of the wave equation in the exterior of two convex obstacles". In: *Osaka Journal of Mathematics* 19.3 (1982), pp. 459–509.

[75] D. S. Jones. *The Theory of Electromagnetism*. Pergamon / Macmillan New York, 1964.

[76] M. Kachanovska. *private communication*, ENSTA ParisTech-INRIA-CNRS, France. 04 September 2019.

[77] R. Kress. "On the limiting behaviour of solutions to boundary integral equations associated with time harmonic wave equations for small frequencies". In: *Mathematical Methods in the Applied Sciences* 1.1 (1979), pp. 89–100. DOI: 10.1002/mma.1670010108.

[78] K. L. Kuhlman. "Review of inverse Laplace transform algorithms for Laplace-space numerical approaches". In: *Numerical Algorithms* 63.2 (2013), pp. 339–355.

[79] I. Labarca, L. M. Faria, and C. Pérez-Arancibia. *Convolution quadrature methods for time-domain scattering from unbounded penetrable interfaces*. 2018. eprint: 1809.05084 (physics.comp-ph).

[80] I. Labarca, L. M. Faria, and C. Pérez-Arancibia. "Convolution quadrature methods for time-domain scattering from unbounded penetrable interfaces". In: *Proceedings of the Royal Society A: Mathematical, Physical and Engineering Sciences* 475.2227 (July 2019), p. 20190029. DOI: 10.1098/rspa.2019.0029.

[81] D. Lafontaine, E. A. Spence, and J. Wunsch. "For Most Frequencies, Strong Trapping Has a Weak Effect in Frequency-Domain Scattering". In: *Communications on Pure and Applied Mathematics* (July 2020). DOI: 10.1002/cpa.21932.

[82] P. D. Lax, C. S. Morawetz, and R. S. Phillips. "Exponential decay of solutions of the wave equation in the exterior of a star-shaped obstacle". In: *Communications on Pure and Applied Mathematics* 16.4 (1963), pp. 477–486.

[83] P. D. Lax and R. S. Phillips. *Scattering theory*. Academic press New York, 1967.

[84] J.-F. Lee, R. Lee, and A. Cangellaris. "Time-domain finite-element methods". In: *IEEE Transactions on Antennas and Propagation* 45.3 (Mar. 1997), pp. 430–442. DOI: 10.1109/8.558658.

[85] M. Liebler, S. Ginter, T. Dreyer, and R. E. Riedlinger. "Full wave modeling of therapeutic ultrasound: Efficient time-domain implementation of the frequency power-law attenuation". In: *The Journal of the Acoustical Society of America* 116.5 (Nov. 2004), pp. 2742–2750. DOI: 10.1121/1.1798355.

[86] S. Lin and E. Kuh. "Transient simulation of lossy interconnects based on the recursive convolution formulation". In: *IEEE Transactions on Circuits and Systems I: Fundamental Theory and Applications* 39.11 (1992), pp. 879–892. DOI: 10.1109/81.199887. URL: https://doi.org/10.1109/81.199887.

[87] C. Lubich. "On the multistep time discretization of linear initial-boundary value problems and their boundary integral equations". In: *Numerische Mathematik* 67.3 (Apr. 1994), pp. 365–389. ISSN: 0945-3245. DOI: 10.1007/s002110050033.

[88] R. C. MacCamy. "Low Frequency Acoustic Oscillations". In: *Quarterly of Applied Mathematics* 23.3 (1965), pp. 247–255. ISSN: 0033569X, 15524485. URL: http://www.jstor.org/stable/43635524.

[89] P. A. Martin. *Time-Domain Scattering*. in prep.; draft copy of Oct. 11 2019.

[90] W. McLean. *Strongly elliptic systems and boundary integral equations*. Cambridge University Press, 2000. ISBN: 052166375X.

[91] E. Mecocci, L. Misici, M. C. Recchioni, and F. Zirilli. "A new formalism for time-dependent wave scattering from a bounded obstacle". In: *The Journal of the Acoustical Society of America* 107.4 (Apr. 2000), pp. 1825–1840. DOI: 10.1121/1.428462.

[92] R. B. Melrose and J. Sjöstrand. "Singularities of boundary value problems. II". In: *Communications on Pure and Applied Mathematics* 35.2 (Mar. 1982), pp. 129–168. DOI: 10.1002/cpa.3160350202.

[93] C. S. Morawetz. “Decay for solutions of the exterior problem for the wave equation”. In: *Communications on Pure and Applied Mathematics* 28.2 (Mar. 1975), pp. 229–264.

[94] C. S. Morawetz. “Exponential decay of solutions of the wave equation”. In: *Communications on Pure and Applied Mathematics* 19.4 (Nov. 1966), pp. 439–444.

[95] C. S. Morawetz. “The decay of solutions of the exterior initial-boundary value problem for the wave equation”. In: *Communications on Pure and Applied Mathematics* 14.3 (Aug. 1961), pp. 561–568.

[96] C. S. Morawetz, J. V. Ralston, and W. A. Strauss. “Decay of solutions of the wave equation outside nontrapping obstacles”. In: *Communications on Pure and Applied Mathematics* 30.4 (July 1977), pp. 447–508.

[97] G. Mur. “Absorbing boundary conditions for the finite-difference approximation of the time-domain electromagnetic-field equations”. In: *IEEE transactions on Electromagnetic Compatibility* 4 (1981), pp. 377–382.

[98] L. Muravei. “On the asymptotic behavior, for large values of the time, of solutions of exterior boundary value problems for the wave equation with two space variables”. In: *Mathematics of the USSR-Sbornik* 35.3 (1979), p. 377.

[99] A. I. Nachman, J. F. Smith III, and R. C. Waag. “An equation for acoustic propagation in inhomogeneous media with relaxation losses”. In: *The Journal of the Acoustical Society of America* 88.3 (1990), pp. 1584–1595.

[100] V. Nascov and P. C. Logofătu. “Fast computation algorithm for the Rayleigh-Sommerfeld diffraction formula using a type of scaled convolution”. In: *Appl. Opt.* 48.22 (Aug. 2009), pp. 4310–4319. DOI: 10.1364/AO.48.004310.

[101] M. Pedneault, C. Turc, and Y. Boubendir. “Schur complement domain decomposition methods for the solution of multiple scattering problems”. In: *IMA Journal of Applied Mathematics* 82.5 (2017), pp. 1104–1134.

[102] S. Petropavlovsky, S. Tsynkov, and E. Turkel. “A method of boundary equations for unsteady hyperbolic problems in 3D”. In: *Journal of Computational Physics* 365 (July 2018), pp. 294–323. DOI: 10.1016/j.jcp.2018.03.039.

[103] J. Poudel, Y. Lou, and M. A. Anastasio. “A survey of computational frameworks for solving the acoustic inverse problem in three-dimensional photoacoustic computed tomography”. In: (2019). DOI: 10.1088/1361-6560/ab2017. eprint: arXiv:1905.03881.

[104] J. V. Ralston. “Solutions of the wave equation with localized energy”. In: *Communications on Pure and Applied Mathematics* 22.6 (Nov. 1969), pp. 807–823. DOI: 10.1002/cpa.3160220605.

[105] A. G. Ramm. “Continuity of solutions to operator equations with respect to a parameter”. In: *Int. J. Pure & Appl. Math. Sci. Vol* 1 (2004), pp. 1–5.

[106] J. W. S. Rayleigh. *The Theory of Sound*. 2 vols. Reprinted by Dover (1945). Macmillan, 1877.

[107] F.-J. Sayas. *Retarded Potentials and Time Domain Boundary Integral Equations*. Springer International Publishing, 2016. DOI: 10.1007/978-3-319-26645-9.

[108] I. H. Sloan and W. E. Smith. “Product integration with the Clenshaw-Curtis points: Implementation and error estimates”. In: *Numerische Mathematik* 34.4 (Dec. 1980), pp. 387–401. DOI: 10.1007/bf01403676.

[109] E. A. Spence. “Wavenumber-Explicit Bounds in Time-Harmonic Acoustic Scattering”. In: *SIAM Journal on Mathematical Analysis* 46.4 (Jan. 2014), pp. 2987–3024. DOI: 10.1137/130932855.

[110] L. N. Stoyanov. *Scattering resonances for several small convex bodies and the Lax-Phillips conjecture*. American Mathematical Soc., 2009.

[111] T. L. Szabo. “Causal theories and data for acoustic attenuation obeying a frequency power law”. In: *The Journal of the Acoustical Society of America* 97.1 (Jan. 1995), pp. 14–24. DOI: 10.1121/1.412332.

[112] T. L. Szabo. “Time domain wave equations for lossy media obeying a frequency power law”. In: *The Journal of the Acoustical Society of America* 96.1 (July 1994), pp. 491–500. DOI: 10.1121/1.410434.

[113] A. Taflove. *Computational electrodynamics : the finite-difference time-domain method*. Boston: Artech House, 2000. ISBN: 1-58053-076-1.

[114] M. Taylor. *Partial differential equations II: Qualitative studies of linear equations*. Vol. 116. Springer Science & Business Media, 2011.

[115] B. E. Treeby and B. T. Cox. “Modeling power law absorption and dispersion for acoustic propagation using the fractional Laplacian”. In: *The Journal of the Acoustical Society of America* 127.5 (May 2010), pp. 2741–2748. DOI: 10.1121/1.3377056.

[116] L. N. Trefethen. “Group Velocity in Finite Difference Schemes”. In: *SIAM Review* 24.2 (Apr. 1982), pp. 113–136. DOI: 10.1137/1024038.

[117] L. Wang, J. A. Cox, and A. Friedman. “Modal analysis of homogeneous optical waveguides by the boundary integral formulation and the Nyström method”. In: *Journal of the Optical Society of America A* 15.1 (Jan. 1998), p. 92. DOI: 10.1364/josaa.15.000092.

[118] J. A. C. Weideman. “Algorithms for Parameter Selection in the Weeks Method for Inverting the Laplace Transform”. In: *SIAM Journal on Scientific Computing* 21.1 (Jan. 1999), pp. 111–128. DOI: 10.1137/s1064827596312432.

[119] P. Werner. “Low frequency asymptotics for the reduced wave equation in two-dimensional exterior spaces”. In: *Mathematical Methods in the Applied Sciences* 8.1 (1986), pp. 134–156. DOI: 10.1002/mma.1670080110.

[120] P. Werner. “Randwertprobleme der mathematischen Akustik”. In: *Archive for Rational Mechanics and Analysis* 10.1 (1962), pp. 29–66.

[121] E. T. Whittaker. “On the partial differential equations of mathematical physics”. In: *Mathematische Annalen* 57.3 (1903), pp. 333–355.

[122] C. H. Wilcox. “The initial-boundary value problem for the wave equation in an exterior domain with spherical boundary”. In: *Notices Amer. Math. Soc* 6 (1959), pp. 869–870.

[123] A. Yilmaz, J.-M. Jin, and E. Michielssen. “Time Domain Adaptive Integral Method for Surface Integral Equations”. In: *IEEE Transactions on Antennas and Propagation* 52.10 (Oct. 2004), pp. 2692–2708. DOI: 10.1109/tap.2004.834399.